GEOLOGICAL SURVEY OF CANADA
BULLETIN 508

GOLD METALLOGENY OF THE CAPE RAY FAULT ZONE, SOUTHWEST NEWFOUNDLAND

B. Dubé and K. Lauzière

1997

Natural Resources Canada | Ressources naturelles Canada

Canada

COOPERATION

COOPERATION AGREEMENT ON MINERAL DEVELOPMENT

ENTENTE DE COOPÉRATION SUR L'EXPLOITATION MINÉRALE

Contribution to Canada-Newfoundland Cooperation Agreement on Mineral Development (1990-1994), a subsidiary agreement under the Economic and Regional Development Agreement.

Contribution à l'Entente de coopération Canada-Terre-Neuve sur l'exploitation minérale (1990-1994), entente auxiliaire négociée en vertu de l'Entente Canada-Nouveau-Brunswick de développement économique et régional.

Contribution to Canada-Newfoundland Agreement on Mineral Development (1994-1995), a subsidiary agreement under the Economic and Regional Development Agreement.

Contribution à l'Entente Canada-Terre-Neuve sur l'exploitation minérale (1994-1995), entente auxiliaire négociée en vertu de l'Entente Canada-Nouveau-Brunswick de développement économique et régional.

Canada

Newfoundland
Terre-Neuve

GEOLOGICAL SURVEY OF CANADA
BULLETIN 508

GOLD METALLOGENY OF THE CAPE RAY FAULT ZONE, SOUTHWESTERN NEWFOUNDLAND

B. Dubé and K. Lauzière

1997

Catalogue No. 0-660-17076-0
ISBN M4-508E

Available in Canada from
Geological Survey of Canada offices:

601 Booth Street
Ottawa, Ontario K1A 0E8

3303-33rd Street N.W.
Calgary, Alberta T2L 2A7

101-605 Robson Street
Vancouver, B.C. V6B 5J3

or from

Canadian Government Publishing
Public Works and Government Services Canada
Ottawa, Ontario K1A 0S9

A deposit copy of this publication is also available for reference
in selected public libraries across Canada

Price subject to change without notice

Cover Illustration

Brecciated nature of the C vein showing various compositions of foliated and angular fragments, Cape Ray gold deposit. See Figure 23A. GSC 1996-127C

Critical reviewers

C.D. Anglin
H.S. Swinden

Author' address

Commission géologique du Canada
Centre géoscientifique de Québec
2535 boulevard Laurier
C.P. 7500
Sainte-Foy (Québec)
G1V 4C7

Original manuscript submitted:1996-01
Final version approved for publication:1997-06

ERRATA

GSC BULLETIN 508

GOLD METALLOGENY OF THE CAPE RAY FAULT ZONE, SOUTHWESTERN NEWFOUNDLAND

B. Dubé and K. Lauzière

Catalogue number and ISBN number are incorrect on the colophon page. Please replace colophon page with this page.

Catalogue No. M42-508E
ISBN 0-660-17076-0

Available in Canada from
Geological Survey of Canada offices:

601 Booth Street
Ottawa, Ontario K1A 0E8

3303-33rd Street N.W.
Calgary, Alberta T2L 2A7

101-605 Robson Street
Vancouver, B.C. V6B 5J3

or from

Canadian Government Publishing
Public Works and Government Services Canada
Ottawa, Ontario K1A 0S9

A deposit copy of this publication is also available for reference

Cover Illustration

Brecciated nature of the C vein showing various compositions of foliated and angular fragments, Cape Ray gold deposit. See Figure 23A. GSC 1996-127C

in selected public libraries across Canada

Price subject to change without notice

Critical reviewers

C.D. Anglin
H.S. Swinden

Author' address

Commission géologique du Canada
Centre géoscientifique de Québec
2535 boulevard Laurier
C.P. 7500
Sainte-Foy (Québec)
G1V 4C7

Original manuscript submitted: 1996-01
Final version approved for publication: 1997-06

CONTENTS

Figures

Tables

Appendix

GOLD METALLOGENY OF THE CAPE RAY FAULT ZONE, SOUTHWESTERN NEWFOUNDLAND

Abstract

The Cape Ray Fault Zone, located in southwestern Newfoundland, is a complex reverse-oblique fault zone of Late Silurian to Early Devonian age which forms the boundary between the Windsor Point Group and the Grand Bay and Port aux Basques complexes of the Port aux Basques gneiss. The Cape Ray Fault Zone hosts the Cape Ray gold deposit in which gold occurs mainly in galena and chalcopyrite-rich fault-fill quartz breccia veins hosted by graphitic schists of the Windsor Point Group. Elsewhere along the fault zone, significant mineralized zones occur in pyrite-rich fault-fill quartz breccia veins at the Big Pond showing, in extensional, subhorizontal quartz veins hosted by the Windowglass Hill Granite and as fault-fill quartz veins and strongly pyritized iron-rich sedimentary rocks at or close to the contact between the Cape Ray Igneous Complex and the Windsor Point Group (Isle aux Morts prospect). The development and geometry of the auriferous zones were controlled by a combination of lithological and structural factors including chemical traps such as graphitic schist and iron-rich sedimentary rocks, competence contrast and reverse-oblique ductile shear zones.

The mineralization is post-peak metamorphism (415 Ma), as the gneisses are retrograded to greenschist facies, and pre-386 Ma, the age of the Isle aux Morts Brook Granite which cuts across the structures that host the mineralization.

The study demonstrates that gold mineralization along the Cape Ray Fault Zone is the product of terrane collision and associated metamorphism and magmatism.

Résumé

La zone de failles de Cape Ray, dans le sud-ouest de Terre-Neuve, est une zone complexe de failles à mouvement inverse-oblique du Silurien tardif-Dévonien précoce qui sépare le Groupe de Windsor Point des complexes de Grand Bay et de Port aux Basques du gneiss de Port aux Basques. À la zone de failles de Cape Ray, est associé le gisement d'or de Cape Ray, dont la minéralisation aurifère est principalement contenue dans des filons bréchiformes de quartz riches en galène et chalcopyrite; ces filons forment les matériaux de remplissage de failles et sont encaissés dans les schistes graphitiques du Groupe de Windsor Point. Ailleurs, le long de la zone de failles, des zones minéralisées d'importance sont associées à des filons bréchiformes de quartz riches en pyrite formant les matériaux de remplissage de failles (indice de Big Pond); dans des filons de quartz d'extension subhorizontaux au sein du Granite de Windowglass Hill; et dans des filons de quartz de remplissage de failles et des roches sédimentaires riches en fer fortement pyritisées au contact du Groupe de Windsor Point avec le Complexe igné de Cape Ray, ou près de ce contact (prospect d'Isle aux Morts). La formation et la géométrie des zones aurifères ont été régies par une combinaison de facteurs lithologiques et structuraux incluant des pièges chimiques (p. ex. des schistes graphitiques et des roches sédimentaires riches en fer), des contrastes de compétence et des zones de cisaillement ductile à mouvement inverse-oblique.

La minéralisation est postérieure à l'atteinte des conditions maximales du métamorphisme (415 Ma), puisque les gneiss ont subi les effets d'un métamorphisme rétrograde au faciès des schistes verts, et est antérieure au Granite d'Isle aux Morts Brook (âge de 386 Ma), qui recoupe les structures hôtes de la minéralisation.

La présente étude démontre que la minéralisation aurifère observée le long de la zone de failles de Cape Ray est le produit de la collision de terranes et des processus métamorphiques et magmatiques associés.

SUMMARY

The Cape Ray Fault Zone, located in southwestern Newfoundland is a major Late Silurian to Early Devonian reverse-oblique fault zone which forms the boundary between the Windsor Point Group and the Grand Bay and Port aux Basques complexes of the Port aux Basques gneiss. The Cape Ray Fault Zone hosts the Cape Ray gold deposit, one of the most important vein-type gold deposits in the Appalachians, with mineable reserves of 450 000 t at 10.1 g/t Au. Other significant vein-type gold occurrences within the Cape Ray Fault Zone area include the Big Pond, Isle aux Morts, and Windowglass Hill occurrences.

The Cape Ray Fault Zone records a complex structural evolution. Regionally, six generations of structures have been documented. The first two generations (D_1 and D_2), correspond to amphibolite grade deformation and are restricted to the rocks of the Port aux Basques gneiss. The D_3 to D_6 generations of structures formed at greenschist grade and are recorded in both the Port aux Basques gneiss and the Windsor Point Group rocks. D_3 structures are characterized by a reverse-dextral sense of motion and are younger than 424 Ma. D_4 structures are older than 384 Ma and record essentially dextral strike slip motion. D_4 structures were re-activated as a sinistral strike slip shear zone. Finally, D_5 structures form a conjugate set of cleavages and associated folds. A late stage of brittle faulting, D_6, of post-Mid Devonian age, is indicated by the presence of tectonic and hydrothermal breccias.

Gold mineralization occurs mainly in galena- and chalcopyrite-rich fault-fill quartz breccia veins. These veins are hosted by graphitic schists of the Windsor Point Group at or near their tectonic boundary with the Grand Bay Complex. Other significant mineralized zones occur in extensional, subhorizontal quartz veins hosted by the Windowglass Hill Granite and as fault-fill quartz veins and strongly pyritized iron-rich sediments (Isle aux Morts prospect) at or close to the contact between the Cape Ray Igneous Complex and the Windsor Point Group. These veins are base metal rich and characterized by a low gold/silver ratio.

Gold mineralization hosted by graphitic schist is characterized by complex gold-bearing and barren quartz pods mixed with gouge and fault rocks. Younger deformations, more intensely developed in the graphitic schists, add to the complexity of the distribution of the mineralized zones.

This study demonstrates that the development and geometry of the auriferous zones were controlled by a combination of primary lithological and structural factors. The graphitic schist and the iron-rich sedimentary rocks acted as chemical traps. Layer anisotropy resulting from the rheology of the graphitic schist favoured fluid circulation. The graphitic schist most probably accommodated slippage during deformation, generating open spaces for fluid circulation and gold precipitation. At the Windowglass Hill showing, the competence contrast

SOMMAIRE

La zone de failles de Cape Ray, dans le sud-ouest de Terre-Neuve, est une importante zone de failles à mouvement inverse-oblique du Silurien tardif- Dévonien précoce qui sépare le Groupe de Windsor Point des complexes de Grand Bay et de Port aux Basques du gneiss de Port aux Basques. À la zone de failles de Cape Ray, est associé le gisement d'or de Cape Ray, l'un des plus importants gisements aurifères de type filonien des Appalaches, dont les réserves exploitables s'élèvent à 450 000 t à une teneur en or de 10,1 g/t. D'autres indices aurifères de type filonien d'importance sont présents dans la région de la zone de failles de Cape Ray, dont ceux de Big Pond, d'Isle aux Morts et de Windowglass Hill.

L'analyse de la zone de failles de Cape Ray révèle une évolution structurale complexe. À l'échelle régionale, six générations de structures ont été documentées. Les structures des deux premières générations (D_1 et D_2) témoignent d'une déformation au faciès des amphibolites et sont limitées aux roches du gneiss de Port aux Basques. Les structures des générations D_3 à D_6 se sont formées au faciès des schistes verts et sont observées tant dans le gneiss de Port aux Basques que dans les roches du Groupe de Windsor Point. Les structures de la génération D_3 rendent compte d'un mouvement inverse-dextre et sont postérieures à 424 Ma. Les structures de la génération D_4 sont antérieures à 384 Ma et témoignent essentiellement d'un mouvement de coulissage dextre. Les structures de la génération D_4 ont été réactivées sous la forme d'une zone de cisaillement à mouvement de coulissage senestre. Enfin, les structures de la génération D_5 correspondent à un ensemble de clivages conjugués et aux plis associés. L'existence d'un épisode tardif de fracturation fragile, D_6, postérieur au Dévonien moyen, est indiquée par la présence de brèches tectoniques et hydrothermales.

La minéralisation aurifère se rencontre surtout dans des filons bréchiformes de quartz riches en galène et chalcopyrite qui forment les matériaux de remplissage de failles. Ces filons sont encaissés dans les schistes graphitiques du Groupe de Windsor Point au niveau de leur contact tectonique avec le Complexe de Grand Bay ou à proximité de celui-ci. D'autres zones minéralisées d'importance sont associées à des filons de quartz d'extension subhorizontaux au sein du Granite de Windowglass Hill et d'autres encore sont présentes au contact du Groupe de Windsor Point avec le Complexe igné de Cape Ray, ou à proximité de celui-ci, où elles sont associées à des filons de quartz de remplissage de failles et à des sédiments riches en fer fortement pyritisés (prospect d'Isle aux Morts). Ces filons sont riches en métaux communs et montrent de manière caractéristique un faible rapport or/argent.

La minéralisation aurifère encaissée dans les schistes graphitiques est associée à un agencement complexe de lentilles fusiformes de quartz, aurifères et stériles, mélangées à de la boue de faille et à des roches fragmentées. Des déformations plus récentes, dont les effets sont plus marqués dans les schistes graphitiques, ont contribué à rendre plus complexe la répartition des zones minéralisées.

Il ressort de la présente étude que la formation et la géométrie des zones aurifères ont été régies par une combinaison de facteurs lithologiques primaires et structuraux. Les schistes graphitiques et les roches sédimentaires riches en fer ont joué le rôle de pièges chimiques. L'anisotropie des couches liée au comportement rhéologique des schistes graphitiques a favorisé la circulation des fluides. Les schistes graphitiques ont fort probablement permis qu'un glissement se produise durant la déformation, créant ainsi des ouvertures

between the granitic host and adjacent sedimentary rocks induced strain refraction and is responsible for the north-northeast trend of the shear zone. At the Cape Ray gold deposit and Big Pond showing the oreshoots plunge steeply to the east and Conolly diagrams suggest that this geometry is controlled by primary changes in attitude of the host structures. The geometry of the zones is also strongly influenced by post-mineralization deformation.

The mineralization is post-424 Ma, the age of the Windowglass Hill Granite that is cut by mineralized veins, and must be post-peak metamorphism (415 Ma), as the gneisses are retrograded to greenschist facies within the Cape Ray gold deposit. The mineralization is also pre-386 Ma, the age of the Isle aux Morts Brook Granite which cuts across the structures that host the mineralization at the Cape Ray gold deposit. This time period corresponds to the development of the D_3 structures.

The lode gold mineralization at Cape Ray was probably formed at depths intermediate between the mesothermal and epithermal deposit model end-members (2-5 km, 200-300°C). Mineralization at the Windowglass Hill showing compares more closely to intrusion-related gold mineralization such as that documented in the Republic of Korea (Shelton et al., 1988; So et al., 1988).

The association of gold with graphitic schist has been reported from many Archean and younger gold deposits. One such analogue is the Ashanti gold mine in Ghana, one of the largest gold producers in the world (Appiah et al., 1991).

The tectonic setting of the Cape Ray gold mineralization is analogous to those of Archean and of many younger gold systems. At Cape Ray, the mineralization is spatially and genetically related to a crustal scale high angle reverse fault which forms the suture zone between two continental blocks: Laurentia and Gondwana. Following crustal thickening associated with the reverse faulting event, thermal re-equilibration induced the production of a hydrothermal fluid carrying metals and circulating through the large scale fault system. The Cape Ray gold-bearing quartz vein system and the emplacement of the late tectonic Strawberry and Isle aux Morts Brook A-type granites are probably the direct end-product of collision along the Cape Ray Fault Zone. The gold-bearing fluid moving upward along the Cape Ray Fault Zone reacted with chemical traps, which destabilized Au complexes within the fluid and induced gold precipitation.

The overprinting of thrust-related mylonites by low temperature hydrothermal breccia with some characteristics typical of epithermal style gold mineralization suggests a progression towards extensional and brittle deformation with time and telescoping of near surface alteration style. Crosscutting relationships suggest that the hydrothermal breccia is post 384 Ma, the age of

pour la circulation des fluides et la précipitation de l'or. À l'indice de Windowglass Hill, le contraste de compétence entre les roches hôtes granitiques et les roches sédimentaires adjacentes a provoqué une réfraction de la déformation et est la cause de la direction nord-nord-est qu'adopte la zone de cisaillement. Au gisement d'or de Cape Ray et à l'indice de Big Pond, les zone minéralisées plongent selon un angle très fort vers l'est et les diagrammes de Conolly indiquent que cette géométrie dépend de changements primaires d'attitude des structures hôtes. La géométrie des zones a également été fortement modifiée par la déformation postérieure à la minéralisation.

La minéralisation est postérieure à 424 Ma, soit l'âge du Granite de Windowglass Hill que recoupent les filons minéralisés, et doit être postérieure à l'atteinte des conditions maximales du métamorphisme (415 Ma), étant donné que les gneiss ont subi les effets d'un métamorphisme rétrograde au faciès des schistes verts dans le gisement d'or de Cape Ray. La minéralisation est également antérieure à 386 Ma, soit l'âge du Granite d'Isle aux Morts Brook qui recoupe les structures renfermant la minéralisation au gisement d'or de Cape Ray. Cette période correspond à la formation des structures de la génération D_3.

La minéralisation d'or filonienne au gisement de Cape Ray s'est probablement formée à des profondeurs intermédiaires entre celles des membres extrêmes du modèle des gîtes mésothermaux et épithermaux (2-5 km, 200-300°C). La minéralisation de l'indice de Windowglass Hill se compare davantage aux minéralisations associées à des intrusions, comme celle qui a été documentée en République de Corée (Shelton et al., 1988; So et al., 1988).

Une association de l'or à des schistes graphitiques a été observée dans de nombreux gisements d'or de l'Archéen et de temps plus récents. Un analogue est fourni par la mine Ashanti au Ghana, un gisement dont la production d'or est l'une des plus importantes au monde (Appiah et al., 1991).

Le cadre tectonique de la minéralisation d'or de Cape Ray est analogue à celui de systèmes aurifères de l'Archéen et de nombreux autres de temps plus récents. Au gisement de Cape Ray, la minéralisation est associée, sur les plans spatial et génétique, à une faille inverse fortement inclinée d'échelle crustale qui forme la zone de suture entre deux blocs continentaux : la Laurentie et le Gondwana. À la suite de l'épaississement crustal résultant du jeu de failles inverses, la recherche d'un nouvel équilibre thermique a entraîné la production d'un fluide hydrothermal qui transportait des métaux et qui a emprunté le système de failles à grande échelle. La formation du système de filons de quartz aurifères de Cape Ray et la mise en place des granites tarditectoniques de type A de Strawberry et d'Isle aux Morts Brook sont probablement des conséquences directes de la collision le long de la zone de failles de Cape Ray. Le fluide minéralisé en or qui a remonté le long de la zone de failles de Cape Ray a réagi avec les pièges chimiques, ce qui a déstabilisé les complexes aurifères contenus dans celui-ci et a provoqué la précipitation de l'or.

La superposition de brèches hydrothermales de basse température, possédant certaines caractéristiques typiques des minéralisations aurifères de style épithermal, à des mylonites formées par le jeu de failles de chevauchement, nous incite à proposer une progression dans le temps de la nature de la déformation, qui ultimement s'est produite en régime extensif et dans des conditions fragiles, et le télescopage du style d'altération hydrothermal. Les relations de recoupement nous font supposer que la brèche hydrothermale est

the brecciated Strawberry Granite. These late structures record declining temperature and pressure possibly due to tectonic unloading.

This study demonstrates that gold mineralization along the Cape Ray Fault Zone is the product of terrane collision and associated metamorphism and magmatism.

postérieure à 384 Ma, l'âge du Granite de Strawberry à texture bréchique. Ces structures tardives témoignent d'une baisse de température et de pression probablement causée par une diminution de la charge tectonique.

La présente étude démontre que la minéralisation aurifère observée le long de la zone de failles de Cape Ray est le produit de la collision de terranes et des processus métamorphiques et magmatiques associés.

INTRODUCTION

Most lode gold deposits are genetically related to convergent orogenic settings and are consequently associated with major fault zones (Hodgson and Hamilton, 1989; Kerrich and Wyman, 1990; Barley and Groves, 1992). This report describes one such gold-bearing fault, the Cape Ray Fault Zone. Located in southwestern Newfoundland, the Cape Ray Fault Zone is the record of major reverse-oblique movement during the Late Silurian to Early Devonian and is located within the suture zone between composite Gondwanan and Laurentian terranes (Dubé et al., 1996) (Fig. 1, 2). The Cape Ray Fault Zone hosts the Cape Ray gold deposit, one of the most important vein-type gold deposits in the Appalachians, with mineable reserves of 450 000 t at 10.1 g/t Au (Dolphin Explorations, Annual Reports, 1990). Other significant vein-type gold occurrences are the Big Pond, Isle aux Morts, and Windowglass Hill showings.

This study describes the geological characteristics of gold mineralization along the Cape Ray Fault Zone and focuses on the lithological and structural control of the mineralization and its relationship with the structural evolution of the fault zone. It is based on detailed lithological and structural analyses and U-Pb, ^{40}Ar-^{39}Ar, and K-Ar radiometric ages along a 60 km segment of the Cape Ray Fault Zone as well as on a detailed mineral deposit study of the gold mineralization within the fault zone. Understanding the structural evolution, timing, and tectonic significance of the Cape Ray Fault Zone in relation with the gold mineralization has direct implications for future gold exploration in the area and elsewhere.

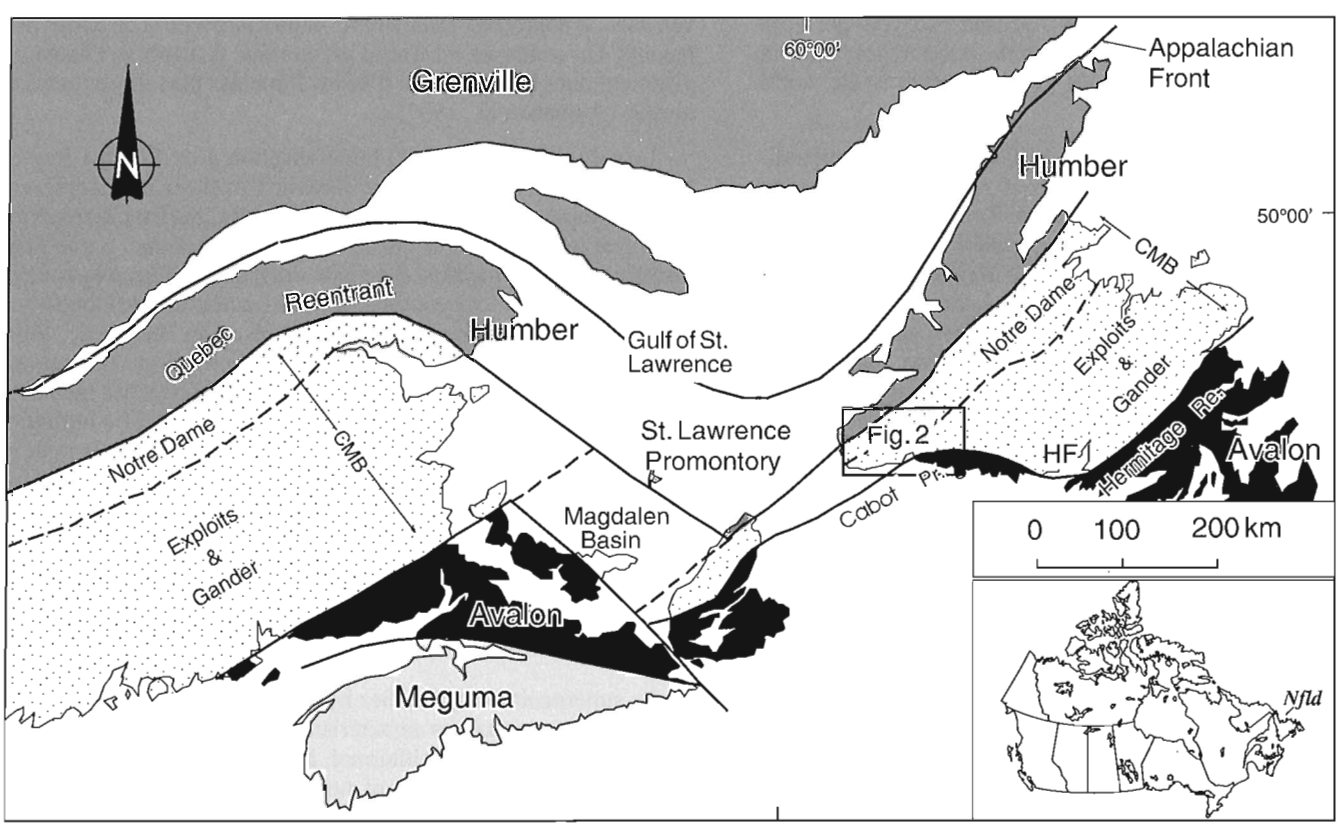

Figure 1. *Tectonostratigraphic zones, promontories and reentrants of the northern Appalachians (simplified after Williams, 1979; Barr and Raeside, 1989). CMB – Central Mobile Belt; HF – Hermitage Flexure; Pr. – promontory; Re. – reentrant; Nfld – Newfoundland. From Lin et al. (1994).*

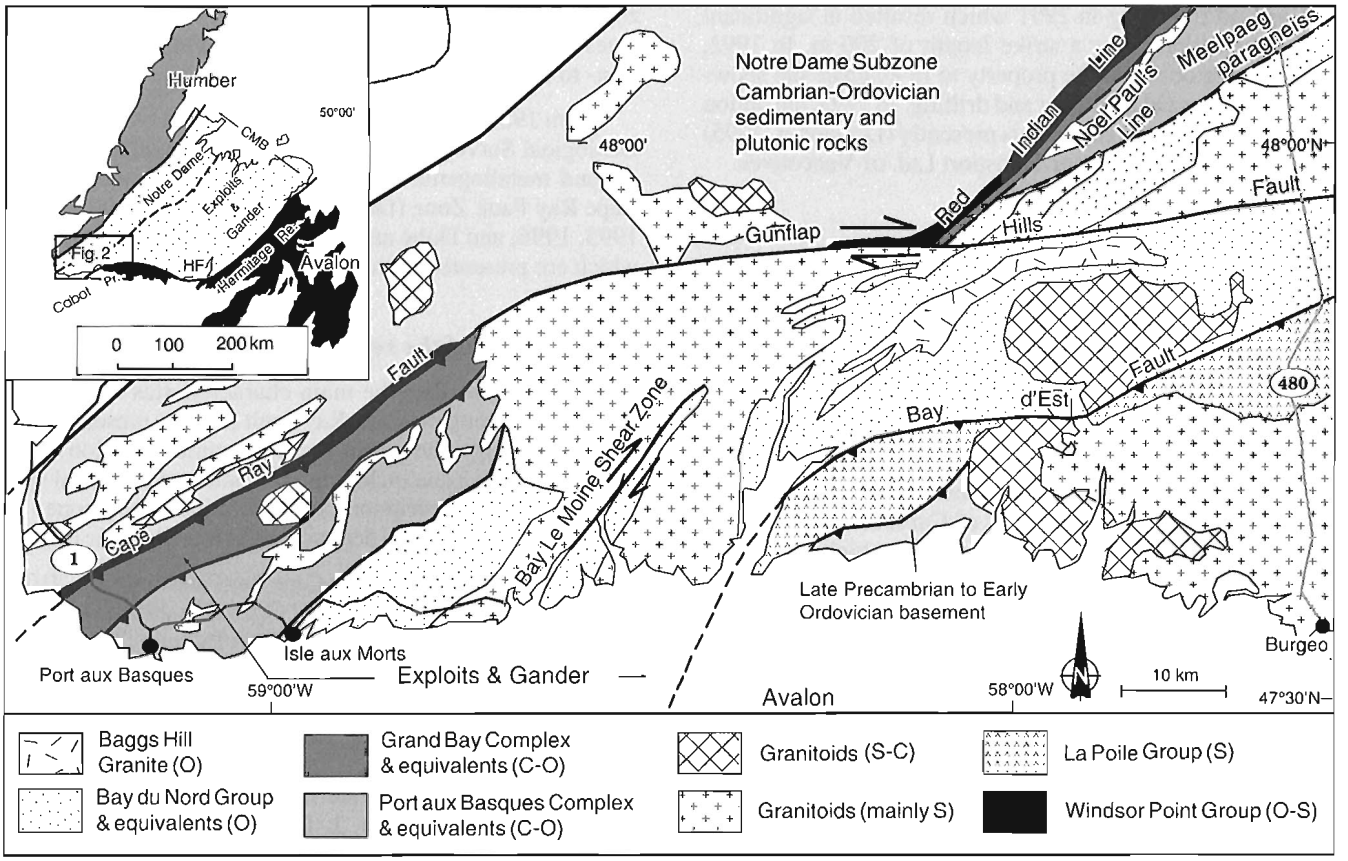

Figure 2. *Geology of southwestern Newfoundland. Modified after Lin et al. (1994). CMB – Central Mobile Belt; HF – Hermitage Flexure; Pr. – promontory; Re. – reentrant; Nfld – Newfoundland.*

The study documents a continuum of deformation from Late Silurian to Early Devonian and demonstrates that gold mineralization along the Cape Ray Fault Zone is the product of terrane collision and associated metamorphism and magmatism and is thus analogous to those of Archean and of many younger gold systems. The development and geometry of the auriferous zones were controlled by a combination of primary lithological and structural factors. The geometry of the zones is also strongly influenced by post-mineralization deformation.

History of exploration and development

The study area lies within a mineral concession granted to Brinex in 1953 by the government of Newfoundland and Labrador. In 1975 and 1976, George Baily, a Newfoundland prospector working for Phillips Management and for Amax Ltd., found several galena-rich quartz veinlets in the strongly altered and strained Windowglass Hill Granite. These are now known as the Gulch, H, and I Brook showings, located near the Cape Ray gold deposit. In 1977, Rio Tinto Canada Exploration Ltd. (Riocannex) optioned the mineral concession and discovered the No. 4 zone of the Cape Ray gold deposit. In 1978, they discovered the No. 41 and 51 zones as well as the Windowglass Hill showing. After four years of exploration, however, they concluded that the potential tonnage of the deposit was insufficient to justify mine development.

In 1984-1985, New Venture Equities Inc. optioned the property, tested the continuity of the mineralized structure via an exploration ramp, and prepared a pre-feasibility study. Subsequently, International Corona Corporation acquired the property. From 1986 to 1989 Dolphin Explorations Ltd., a junior company controlled by Corona, conducted extensive surface and underground exploration programs including more than 30 km of diamond drilling. In 1987 and 1989, they extracted a 330 t bulk sample from the No. 41 zone which analyzed 7.54 g/t Au and 50.7 g/t Ag (Arnold, 1988). In the summer of 1989, Dolphin Explorations discovered the Big Pond showing which was trenched and drilled in the fall of that year. In 1990, Dolphin Explorations established the proven mineable reserves at 450 000 tonnes grading 10.1 g/t Au (Dolphin Explorations, Annual Reports, 1990). Corona, owner of Dolphin Explorations was subsequently bought by Homestake and as of December 1995 the property was owned by American Gem Corporation.

In 1990, the Isle aux Morts showing was found by Fortune Bay Resources Ltd. following discovery of Au-mineralized quartz float in 1988 by Fortune Bay Resources Ltd. and Bay Roberts Resources Ltd. Fortune Bay conducted further

drilling and trenching in 1991 which resulted in significant gold intersections over a strike length of 200 m. In 1992, Placer Dome optioned the property to re-evaluate the showing with additional trenching and drilling. In 1993, the option was not renewed; the showing is presently (December, 1995) owned by Coast Petroleum Transport Ltd. of Vancouver.

Previous geological investigations

The Cape Ray Fault was defined by Gillis (1972) as a prominent lineament separating a mixed plutonic, metavolcanic, and metasedimentary domain of Precambrian to Ordovician age to the northwest from a biotite-quartz-feldspar gneiss and schist domain of Ordovician to Devonian age to the southeast. Brown (1972, 1973, 1976, 1977) mapped much of the area at 1:50 000 scale. He described the Cape Ray Fault as a 1 km wide zone of intense mylonitization and defined the Windsor Point Group as a series of Carboniferous or older metasedimentary and metavolcanic rocks which overlie the Cape Ray Fault. Brown (1973) interpreted the Cape Ray Fault as a Taconian suture representing the trace of the Iapetus Ocean and the Windsor Point Group as having been deposited during exhumation of the fault and subsequently deformed by minor late reactivation. Chorlton (1980, 1983 1984) and Chorlton and Dingwell, (1981) mapped an area including the northeast section of the fault zone. She recognized two stages of faulting within the Cape Ray Fault Zone: 1) pre- to syn-Late Devonian sinistral wrench faulting accompanied by, or followed by deposition of the Windsor Point Group, and 2) post-Late Devonian reverse faulting accompanied by dextral shearing in the east-west splay of the fault (Chorlton, 1983). Chorlton and Dallmeyer (1986) attributed the later complex movements to transpression. Wilton (1983a, b, 1984, 1985) and Wilton and Strong (1986) presented a geological and metallogenic study of the Cape Ray Fault Zone. Based on regional and detailed mapping, Wilton (1983a) defined and traced units within the Windsor Point Group and recognized several generations of structures. He interpreted the Cape Ray Fault Zone as a major Late Devonian, sinistral, ductile shear zone. In an unpublished reconnaissance study in 1989, M.A.J. Piasecki emphasized that the Cape Ray Fault Zone has the character of a major suture and recognized a north-northwest overthrusting followed by post-Mid Devonian overthrusting to the west and northwest. W.A. Barclay (1989) in a structural study of the Cape Ray gold deposit area prepared for Dolphin Explorations, recognized an early episode of ductile deformation, succeeded by intense cataclastic strain restricted to discrete settings within the broader shear zone system.

From a gold metallogenic point of view, Wilton (1983a) and Wilton and Strong (1986) proposed a granite-related model in which gold mineralization slightly predated deformation and was related to an exsolved hydrothermal fluid originating from the Late Devonian Windowglass Hill Granite. Tuach (1986) and Tuach et al. (1988) suggested that the mineralized lodes occur in a late brittle splay of the Cape Ray Fault and that the Windowglass Hill Granite and accompanying mineralization postdate the main movements on the fault zone. Barclay (1989) suggested that the mineralization postdates ductile strain and was emplaced in a high-level setting, post- to late cataclastic deformation.

From 1989 to 1995, the Quebec Geoscience Centre of the Geological Survey of Canada conducted a detailed geological and metallogenic study along a 60 km segment of the Cape Ray Fault Zone (Dubé; 1990; Dubé et al., 1991, 1992, 1993, 1996; and Dubé and Lauzière,1996a, b) the results of which are presented in this report.

Organization of the report

This report describes the main characteristics of the gold occurrences along the Cape Ray Fault Zone by presenting the regional geology, the geology and structural evolution of the Cape Ray Fault Zone including a tectonic and structural synthesis, detailed descriptions of each mineralized zone, an interpretation of the gold deposits, and a metallogenic model.

Four geological maps of the Cape Ray Fault Zone at 1:20 000 scale have been released as GSC Open File 2963 (Dubé and Lauzière, 1996b) and complement this Bulletin. These maps are available separately.

Acknowledgments

Very special thanks are due to J. Thompson (formerly of Dolphin Explorations), J. Dawson, M. Dawson, and L. McNeil of the mining industry for their collaboration, accommodation, and logistic support and for providing access to drill core and underground exposures as well as to unpublished information. The authors express their sincere thanks to C. van Staal, F. Robert, H.K. Poulsen, and G.R. Dunning for thoughtful, stimulating comments and observations in the field and to H.S. Swinden for his help in designing the project, and for sharing his metallogenic and geological knowledge of the Appalachian orogen. M. Brown, Jayanta Guha, J. Winchester, M. Piasecki, and K. Currie are also thanked for discussions in the field. M. Bélanger, P. Carpentier, G. Gosselin, D. Patry, C. Pelchat, S. Pitre, and D. Watanabe provided dedicated and excellent field assistance. David Graham and Gord Watson are thanked for providing satellite images and for their collaboration. Thanks are also due to P. Coté, M. Boutin, and Y. Houde for drafting several diagrams. The manuscript has benefited from the constructive criticism of C.D. Anglin, T.C. Birkett, and H.S. Swinden. Thanks are also due to Placer Dome Canada for permission to publish the section on the Isle aux Morts prospect.

REGIONAL GEOLOGICAL SETTING

The Appalachian Orogen (Williams, 1979) is a late Precambrian to late Paleozoic mountain belt which can be traced from Newfoundland to Alabama in the United States. In Newfoundland, Williams (1979) recognized, from west to east across the orogen, four tectonostratigraphic zonal subdivisions: the Humber, Dunnage, Gander, and Avalon zones. The Humber Zone represents the Cambro-Ordovician sedimentary cover deposited on Grenvillian

rocks which together constitute the continental margin of the eastern North American craton (Laurentia), whereas the Dunnage, Gander, and Avalon zones are interpreted as suspect terranes (Williams and Hatcher, 1983). The Dunnage and Gander zones constitute the Central Mobile Belt of the Canadian Appalachians. It includes the remnants of an early Paleozoic mobile belt (the Dunnage Zone, including the Notre Dame and Exploits subzones) which records the generation and destruction of a Late Precambrian-Early Paleozoic Iapetus Ocean (Harland and Gayer, 1972; Williams, 1979) accreted onto the North American continent during the middle Ordovician Taconian Orogeny (Williams, 1979). The Notre Dame and Exploits subzones are both composed of several distinct volcano-sedimentary belts. The Notre Dame subzone is characterized by a Laurentian fauna in the west whereas the Exploits subzone contains a peri-Gondwana fauna in the east (Williams et al., 1988; Williams et al., 1992). Both subzones are separated by the Red Indian Line which is interpreted as a major terrane boundary (Williams et al., 1988). The Central Mobile Belt also includes the Gander Zone which is characterized by monotonous clastic sedimentary rocks and by a paucity of volcanic rocks in tectonic contact with the Exploits subzone along the Noel Paul's Line (Williams et al., 1988). The Gander Zone represents the continental margin of the Avalon Zone. The Avalon Zone comprises dominantly late Precambrian volcanic and sedimentary rocks and is viewed as an exotic terrane of Pan-African affinity (a rifted-off block of Gondwana) (O'Brien et al., 1983) accreted to the continent during the Silurian orogeny (Dunning et al., 1990; Lin et al., 1994). The Silurian orogeny of Dunning et al. (1990) represents an important mid-Silurian orogenic pulse, postdating the Taconian Orogeny by approximately 30 Ma and accompanied by large scale strike slip and thrust faulting. In summary, the Appalachian orogen on the island of Newfoundland comprises elements of the ancient continental margins of Gondwana and Laurentia, separated by vestiges of the Iapetus Ocean (O'Brien et al., 1993).

The geology of southwestern Newfoundland records the convergence of the rocks of the Humber, Dunnage, Gander, and Avalon tectonostratigraphic zones (Fig. 1, 2). It has been described by Brown (1972, 1976, 1977), Chorlton (1983), Wilton (1983a, b), Chorlton and Dallmeyer (1986), Currie and Piasecki (1989), van Staal et al. (1992a, b), and Lin et al. (1994) and only salient new interpretations and data are summarized here.

Rocks of this area are subdivided into three major geological domains: the Cape Ray Igneous Complex, the Windsor Point Group, and the Port aux Basques gneiss, all of which are intruded by a number of pre- to late-tectonic granitoids (Fig. 3).

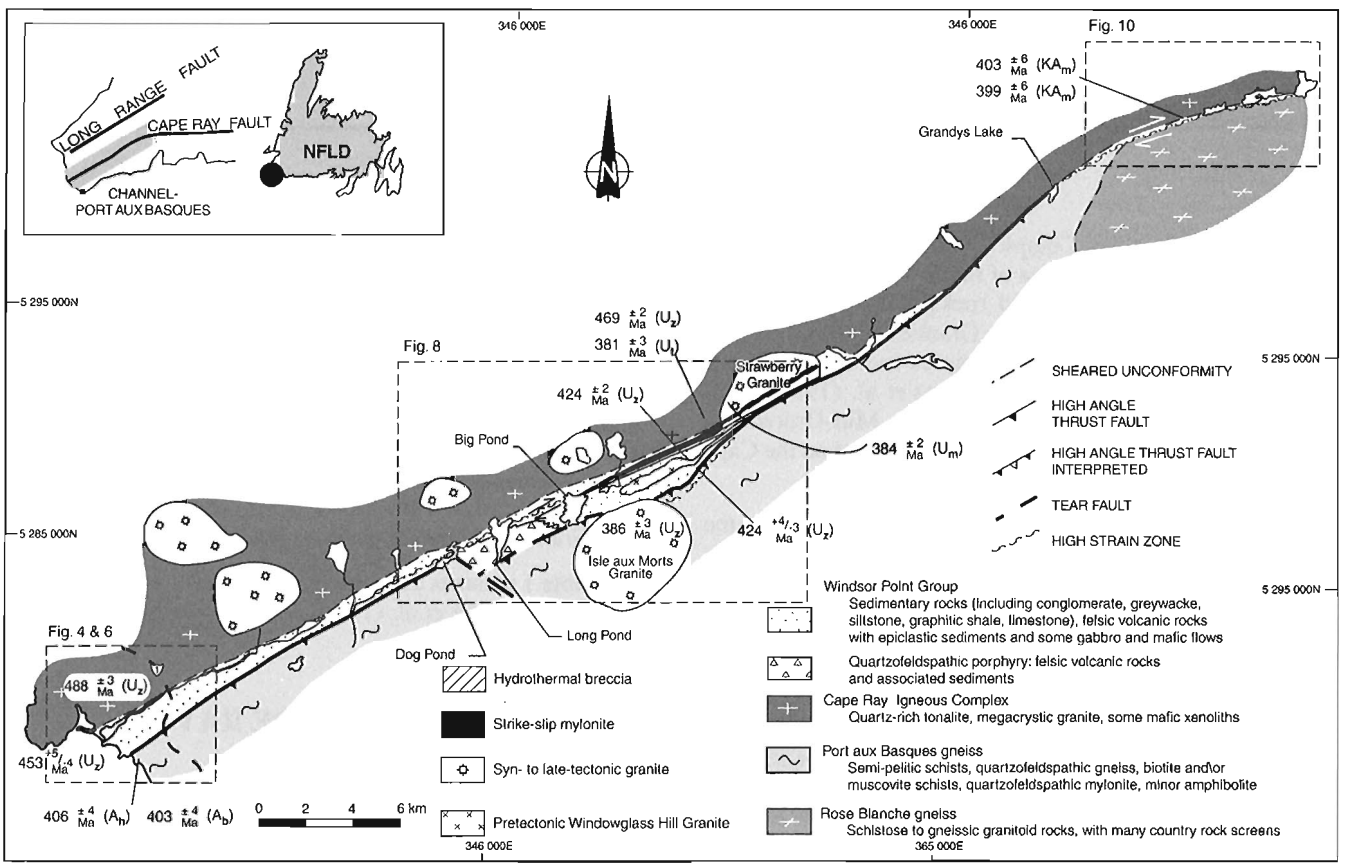

Figure 3. *Compilation map of the Cape Ray Fault Zone showing the main geological units and structural elements. A_h and A_b ($^{40}Ar/^{39}Ar$ on hornblende and biotite respectively), U_z, U_l, U_m (U-Pb in zircon, titanite, and monazite, respectively), KA_m (K-Ar on white mica). From Dubé et al. (1996).*

Table 1. Summary of geochronometry on key rock units in the Cape Ray Fault Zone (Dubé et al., 1996a). A_h and A_b – $^{40}Ar/^{39}Ar$ on hornblende and biotite, respectively; U_z, U_t, U_m – U-Pb in zircon, titanite, and monazite, respectively; KA_m – K-Ar on white mica. GBC – Grand Bay Complex; PABG – Port aux Basques gneiss; WPG – Windsor Point Group; CRIC – Cape Ray Igneous Complex.

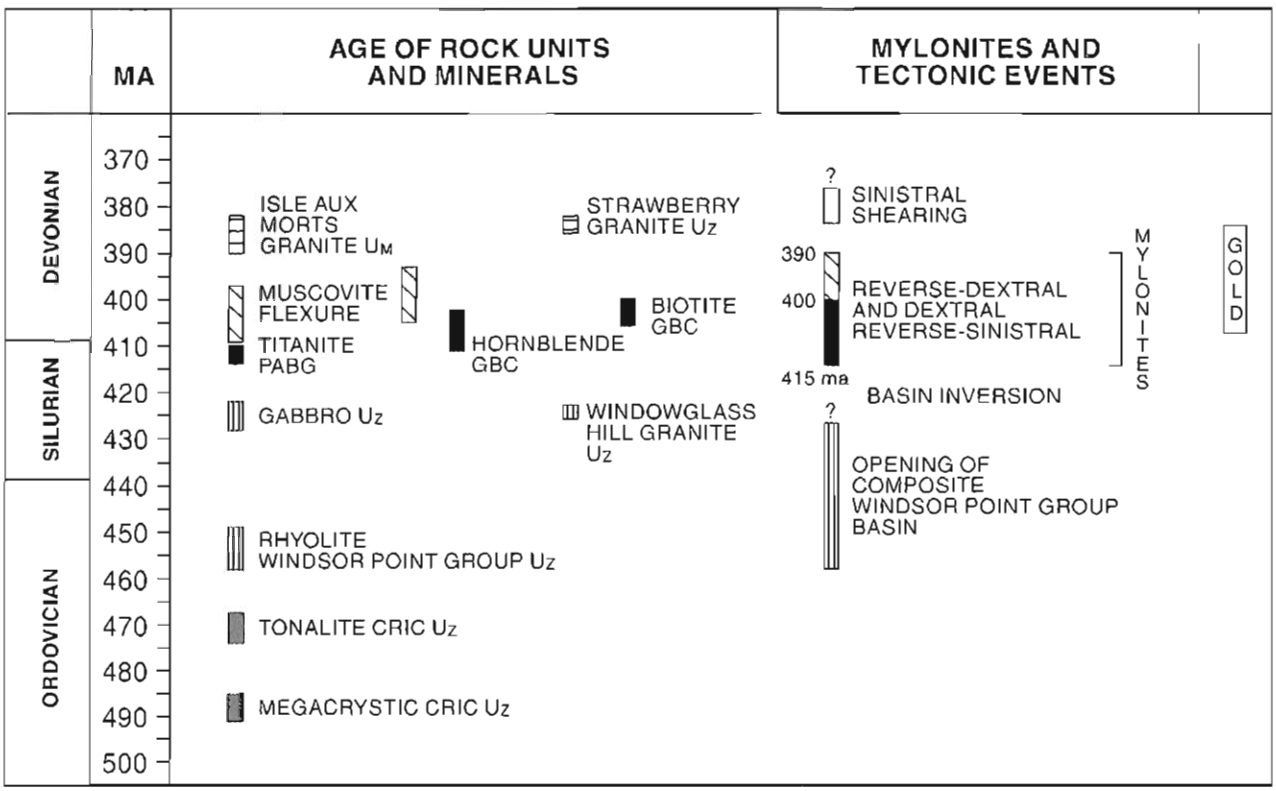

The Cape Ray Igneous Complex (van Staal et al., 1992a) comprises mainly large bodies of mafic to ultramafic intrusive rocks intruded by granitoid rocks (Cape Ray Granite, Cape Ray Tonalite, Red Rocks Granite) (Wilton, 1983b, 1985). The Cape Ray Igneous Complex has been included within the Dunnage Zone by Williams et al. (1988). This interpretation is supported by an Early to Mid-Ordovician U-Pb zircon age (469 ± 2 Ma) recently obtained on the Cape Ray Tonalite (Dubé et al., 1996).

The Windsor Point Group unconformably overlies the Cape Ray Igneous Complex (Brown, 1972; Wilton, 1983b; Chorlton and Dallmeyer, 1986). It is a composite volcanosedimentary package of rocks of Ordovician to ilurian age which has been described in detail by Dubé et al. (1996). The Port aux Basques gneiss (Brown, 1972, 1977) was defined as a series of high grade, kyanite-sillimanite-garnet (see Owen, 1992; Burgess et al., 1993), quartzofeldspathic pelitic and granitic rocks intercalated with hornblende schist or amphibolite and extending from the Cape Ray Fault Zone to Isle aux Morts in the southeast (Fig. 2). Van Staal et al. (1992b), and Lin et al. (1993) subdivided the Port aux Basques gneiss into three distinct lithological packages: Grand Bay Complex, Port aux Basques Complex, and Harbour LeCou Group. Williams (1979) assigned the Port aux Basques gneiss to the Gander Zone.

The Cape Ray Fault Zone is a zone of highly strained rocks 100 km long and several hundred metres wide which separates the Cape Ray Igneous Complex on the northwest, from the Port aux Basques gneiss to the southeast (Brown, 1977; Chorlton, 1983; Wilton, 1983b) (Fig. 3). The Windsor Point Group, located between these two lithological domains, approximately coincides with the trace of the Cape Ray Fault Zone. The Windsor Point Group includes black rhyolite which yielded a zircon age of 453 +5/-4 Ma. It is intruded by Silurian gabbro (U-Pb: 424 +4/-3 Ma) and the Windowglass Hill Granite (U-Pb: 424 ± 2 Ma) (Dubé et al., 1996).

Table 1 presents a summary of the recent geochronological work of Dubé et al. (1996) on key rock units within the Cape Ray Fault Zone.

GEOLOGY OF THE CAPE RAY FAULT ZONE

Lithology

The Cape Ray Fault Zone is well exposed along the coast where a near-complete section through the fault zone is present (Fig. 4). From southeast to northwest, the section includes strongly foliated biotite- and hornblende-rich psammite or garnet-rich metapelite, and quartzofeldspathic mylonite of

the Grand Bay Complex of the Port aux Basques gneiss followed to the northwest by a wide mylonitic zone which separates the Windsor Point Group volcanic-derived conglomerate from the biotite-hornblende psammite (Fig. 4). The mylonite zone is developed in partly to almost completely retrograded Grand Bay Complex rocks, and in rocks of the Windsor Point Group (Fig. 4). Metamorphic minerals defining the mylonitic foliation are typical of greenschist grade and vary from biotite along the southeast margin of the mylonite zone to dominantly chlorite ± sericite along the northwest margin.

The mylonite zone is followed to the northwest by a central sedimentary domain and then by a northern "volcanic" domain; both are assigned to the Windsor Point Group (Fig. 4). The central sedimentary domain is particularly well exposed at Windsor Point and comprises folded and transposed conglomerate, interbedded with tuff, pebbly sandstone, black shale, greywacke, and siltstone. The northern volcanic domain of the Windsor Point Group is formed by a bimodal (mafic and felsic) assemblage of volcanic rocks (Wilton, 1983b). The southeastern part of the volcanic domain is dominated by mafic volcanic rocks, including flows and gabbroic sills well exposed at Jerret Point (Fig. 4) (Dubé et al., 1992). Felsic volcanic rocks are concentrated near the contact with the Cape Ray Igneous Complex and include ignimbrites, rhyolitic flows, and associated pyroclastic, volcaniclastic, and epiclastic rocks. Pillowed basalts are locally intercalated, in stratigraphic contact, with the felsic volcanic rocks. A narrow sedimentary unit consisting of polymictic conglomerate, greywacke, limestone, and graphitic shale underlies the volcanic domain. The mixed volcanic, pyroclastic, and epiclastic felsic subdomain is the most continuous and most typical lithological unit of the Windsor Point Group and is informally termed the Little Barachois formation (Wilton, 1983a, b). It is also characterized by abundant recrystallized magnetite.

The Windsor Point Group is intruded by the pretectonic, Early Silurian Windowglass Hill Granite (Dubé et al., 1996). The Cape Ray Tonalite, Grand Bay Complex, and Windsor Point Group rocks are intruded by the late-tectonic Early to Mid-Devonian Strawberry (384 ± 2 Ma) and Isle aux Morts Brook granites (386 ± 3 Ma) (Dubé et al.,1996) (Fig. 3). These are potassium-rich A-type granites interpreted as partial melts of depleted granulites (Wilton, 1985).

The northwestern boundary of the Windsor Point Group is a quartz-rich tonalite and a megacrystic granitic phase of the Cape Ray Igneous Complex dated respectively at 469 ± 2 Ma and 488 ± 4 Ma (Table 1).

Structural geology

Introduction

The structural geology of the Cape Ray Fault Zone has been described in detail by Dubé and Lauzière (1996a, b) and is summarized here. The various structural elements along the Cape Ray Fault Zone are described on a regional scale in order to understand the nature and the relative timing of the structures hosting the gold mineralization.

The fault exhibits significant across-strike and along-strike variations in strain and in metamorphic grade (Fig. 3). Across strike, these variations are revealed by the generally less-deformed Cape Ray Igneous Complex-Windsor Point Group contact relative to the more-deformed Windsor Point Group-Port aux Basques contact, and by greenschist grade deformation in the Windsor Point Group rocks to the northwest versus amphibolite grade in the Port aux Basques gneiss to the southeast. The Windsor Point Group-Port aux Basques contact generally corresponds to a thick mylonite zone showing reverse-oblique motion in the northeast-oriented segment of the fault and dextral strike-slip motion in the east-west segment. These changes in sense of motion clearly indicate along strike kinematic variations.

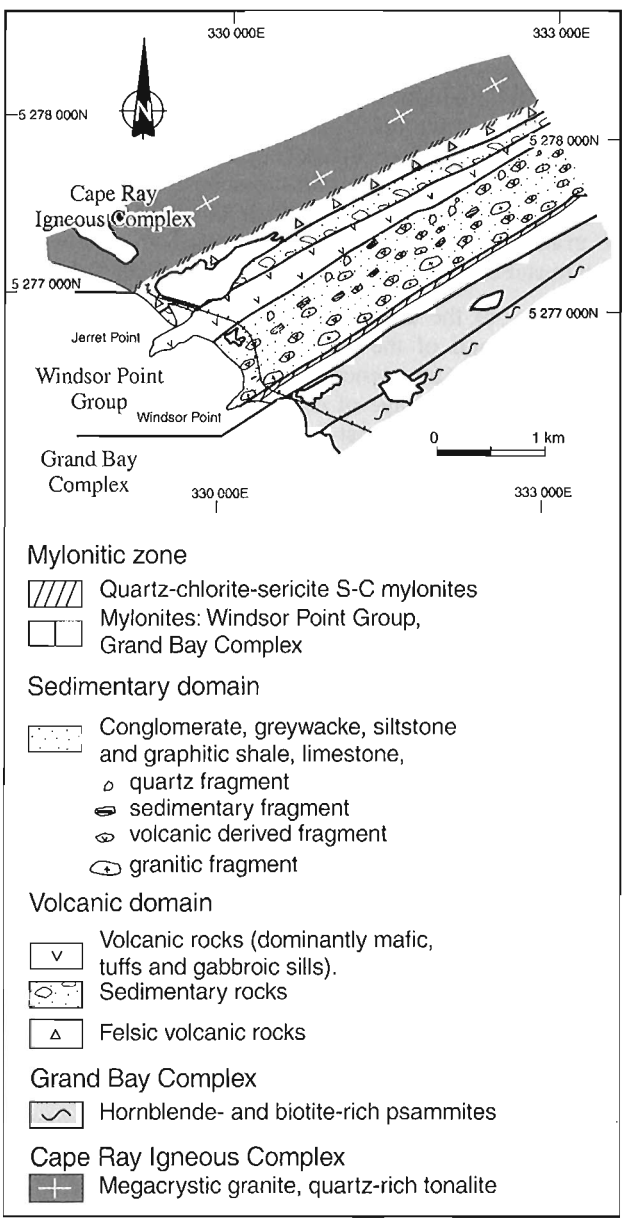

Figure 4. *Geological map of the Cape Ray coastal section showing the lithological domains. From Dubé et al. (1996).*

Based on superposition of planar and linear structures, their relative chronology, metamorphic grade, and age dating by U-Pb and Ar-Ar (Dubé et al., 1993, 1996), six generations of structures have been documented, namely: D_1, D_2, D_3, D_4, D_5, and D_6 that we interpret as resulting from various increments of deformation (Dubé and Lauzière, 1996a). Their corresponding structures are described as: S_1, F_1, etc. This terminology does not, however, necessarily refer to different episodes of deformation. Structures believed to be related are grouped under the same increment of deformation but are temporally distinguished as, for example S_{3a} and S_{3b}. The first two generations of structures, D_1 and D_2, correspond to amphibolite grade deformation and are restricted to the gneissic terranes of the Port aux Basques gneiss. The Windsor Point Group, characterized by greenschist grade metamorphism, records the D_3 to D_6 generations. D_3 is recorded in both Port aux Basques gneiss and the Windsor Point Group rocks and from then on these two units shared a similar structural history. D_3 is younger than 424 ± 2 Ma, the age of the deformed Windowglass Hill Granite as the granite is affected by D_3 structures. D_3 is also older than 386 ± 3 Ma, the age of the Isle aux Morts Brook Granite which cuts D_3 structures. D_4 structures are in part crosscut by the Strawberry Granite and are therefore older than 384 ± 2 Ma the age of the granite. Finally, D_6 structures deform the Strawberry Granite and are consequently younger than 384 ± 2 Ma.

Because of the change in orientation of the Cape Ray Fault Zone, and of the resulting difference in kinematic response, the first four generations of structures, which correspond to the main stage of deformation, will be discussed separately for the northeast-oriented and east-west-oriented portions of the fault zone. Later structures assigned to D_5 and D_6 will be described for the whole length of the fault zone. The right hand rule is applied for all orientations given for planar structures, i.e the orientation is the direction of the plane, the plane dips to the right of this orientation; spherical plots are projections of the lower hemisphere onto equal-area nets.

Main stage of deformation

Northeast-oriented segment

This section of the Cape Ray Fault Zone extends from the coast to Grandys Lake (Fig. 3). In most of the area, the Grand Bay Complex is the dominant unit southeast of the Windsor Point Group, except in the Grandys Lake area where rocks of the Port aux Basques Complex are in contact with the Windsor Point Group. The deformation is described and presented in order of successive generations of structures.

D_1-D_2 structures. The first two generations of structural elements recognized in the area affect rocks of the Grand Bay and Port aux Basques complexes, and reflect deformation that took place at amphibolite grade. At the regional scale, structural elements assigned to the first increment of deformation are recognized throughout the Grand Bay and Port-aux-Basques complexes (van Staal et al., 1992a, b) and are attributed by Burgess et al. (1993) to development of isoclinal F_1 folds. The associated S_1 fabric corresponds to a gneissosity and coplanar quartz veins. In the present study area, this first generation of structures is overprinted and completely transposed by an intense S_2 foliation. As a result, the main fabric recognized in these rocks, is a composite S_{1-2} foliation. Pressure-temperature paths for rocks of the Port aux Basques gneiss area are clockwise in pressure-temperature space with peak metamorphic temperatures of 650 ± 50°C at pressure in the range of 6 to 9 kbar attained during the development of this S_2 fabric (Burgess et al., 1993). Peak metamorphic ages are estimated at 412 ± 2 Ma from titanite in a hornblende-garnet amphibolite layer in the Port aux Basques gneiss (Dunning et al., 1990) and 415 ± 2 Ma obtained from monazite in migmatite (Dunning and van Staal, pers. comm., 1994).

Amphibolite grade mylonitization within the Grand Bay Complex rocks is also attributed to this second increment of deformation (D_2). One such mylonite zone is well exposed along the coast near the contact between the Windsor Point Group and Grand Bay Complex (Fig. 4). It is characterized by a strong planar fabric (S_2) oriented on average at 037°/56°. The S_2 foliation contains well-developed mineral lineations (L_2) plunging moderately to steeply to the south (Fig. 5A), a feature recognized regionally in high strain rocks of the Grand Bay Complex (van Staal et al., 1992a, b). In the study area, these lineations are defined by oriented hornblende crystals. The age of mylonitization estimated at 406 ± 4 Ma by Ar-Ar dating of hornblende (Dubé et al., 1993, 1996) is compatible with the 415-412 Ma peak metamorphic ages cited above.

Kinematic indicators such as back-rotated boudins (Fig. 5B) and C-S type fabrics indicate a southeast-side up reverse sense of shear. Considering the obliqueness of the lineation rake, a sinistral horizontal component of motion is indicated, suggesting north-south-directed shortening.

D_3 structures. D_3 structures within the Cape Ray Fault Zone affect Windsor Point Group, Grand Bay Complex, and Port aux Basques Complex rocks and to a lesser extent Cape Ray Igneous Complex intrusive rocks. The D_3 increment of deformation occurred under greenschist conditions resulting in retrogression and overprinting of the amphibolite grade mylonites and gneisses of the Grand Bay and Port aux Basques complexes, and prograde metamorphism in the Windsor Point Group rocks. Two sets of structures are grouped under D_3. Where only one set is observed, structures are identified as S_3, L_3 and F_3. Where the two sets are present, clear crosscutting relationships are observed and structures are termed S_{3a}, S_{3b}, etc. Because of their similar style of deformation, metamorphic conditions, and orientation of structures, superposition of the two sets is believed to be related to one progressive deformation event (Dubé and Lauzière, 1996a).

From southeast to northwest, there is a general decrease in D_3 deformation in the Windsor Point Group away from the contact with Grand Bay Complex rocks. However, D_3 related structures were recognized in the Cape Ray Igneous Complex tonalites, up to 2 km northwest of the contact between the

Windsor Point Group and the Cape Ray Igneous Complex. Regions of low strain preserved within the Windsor Point Group are relatively uncommon. Where present, they are characterized by one fabric (S_3), defined either by a schistosity, flattened clasts and pebbles or a cleavage, that is oriented northeast, dips steeply to the southeast (026°/85°) and is oblique to east-northeast-striking lithological contacts (Fig. 6A). There is no well-developed L_3 stretching lineation in low strain regions.

Medium strain characterizes most of the Windsor Point Group away from the Windsor Point Group-Grand Bay Complex contact. With increasing strain, the bedding is transposed into the S_{3a} foliation, and both are subsequently folded by the S_{3b} foliation. In most of the area S_{3b} is a penetrative fabric, axial planar to asymmetric, tight, chevron-type to isoclinal F_{3b} folds. Commonly the S_{3a} fabric is transposed into the S_{3b} fabric producing a composite S_{3a-b} foliation. S_{3a} and S_{3b} commonly strike northeast to north-northeast and dip moderately southeast to steeply northwest. Throughout the southeast portion of the Windsor Point Group, L_{3b} lineations, defined by stretching of clasts and pebbles in the conglomerate, are measured on S_{3b} foliation planes. They plunge on average 050° east to east-southeast (Fig. 5C), although south-plunging stretching lineations occur locally. The granitoid clasts have aspect ratios suggesting that most of these rocks can be classified as L>>S tectonites. Generally, F_3 hinges are subparallel with the L_{3b} stretching lineation and plunge steeply to moderately east-southeast.

Increasing deformation during D_3 generated narrow to wide zones of high strain. The most significant of these are developed at the contact between the Windsor Point Group with the Grand Bay Complex and less importantly at the contact between the Cape Ray Igneous Complex and the Windsor Point Group contact. Retrogression of Grand Bay Complex amphibolite grade rocks occurred within these high strain zones and accompanied this D_3 increment of deformation.

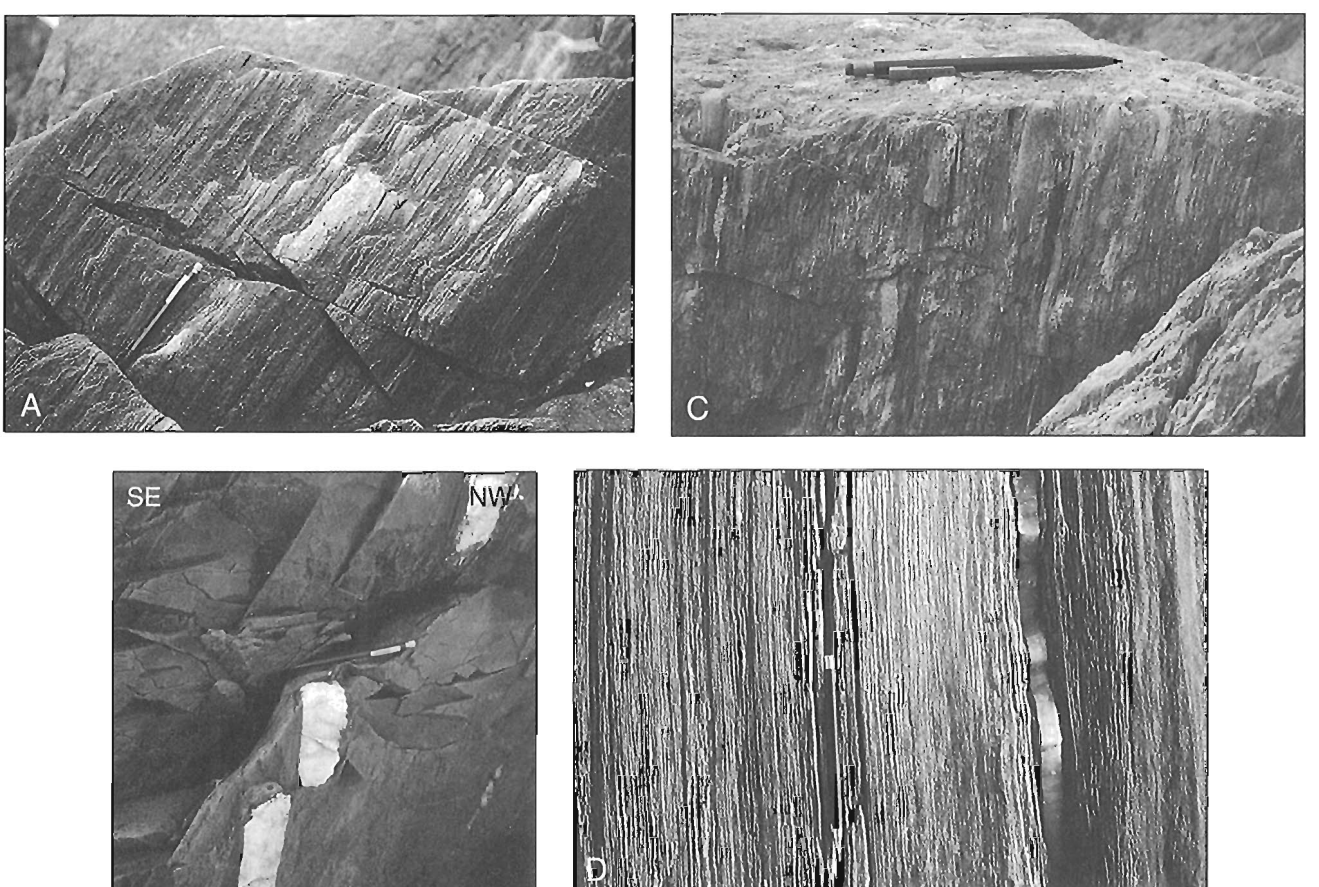

Figure 5. *A) Section view of the S_2 foliation plane showing stretching lineations developed at amphibolite grade, looking northwest. GSC 1996-126A;* ***B)*** *Vertical section view showing back rotated quartz boudins. GSC 1996-126B;* ***C)*** *Vertical section view showing the strong vertical stretching of clasts and pebbles in the conglomerate. GSC 1996-126C;* ***D)*** *Example of the pink mylonite. GSC 1996-126D*

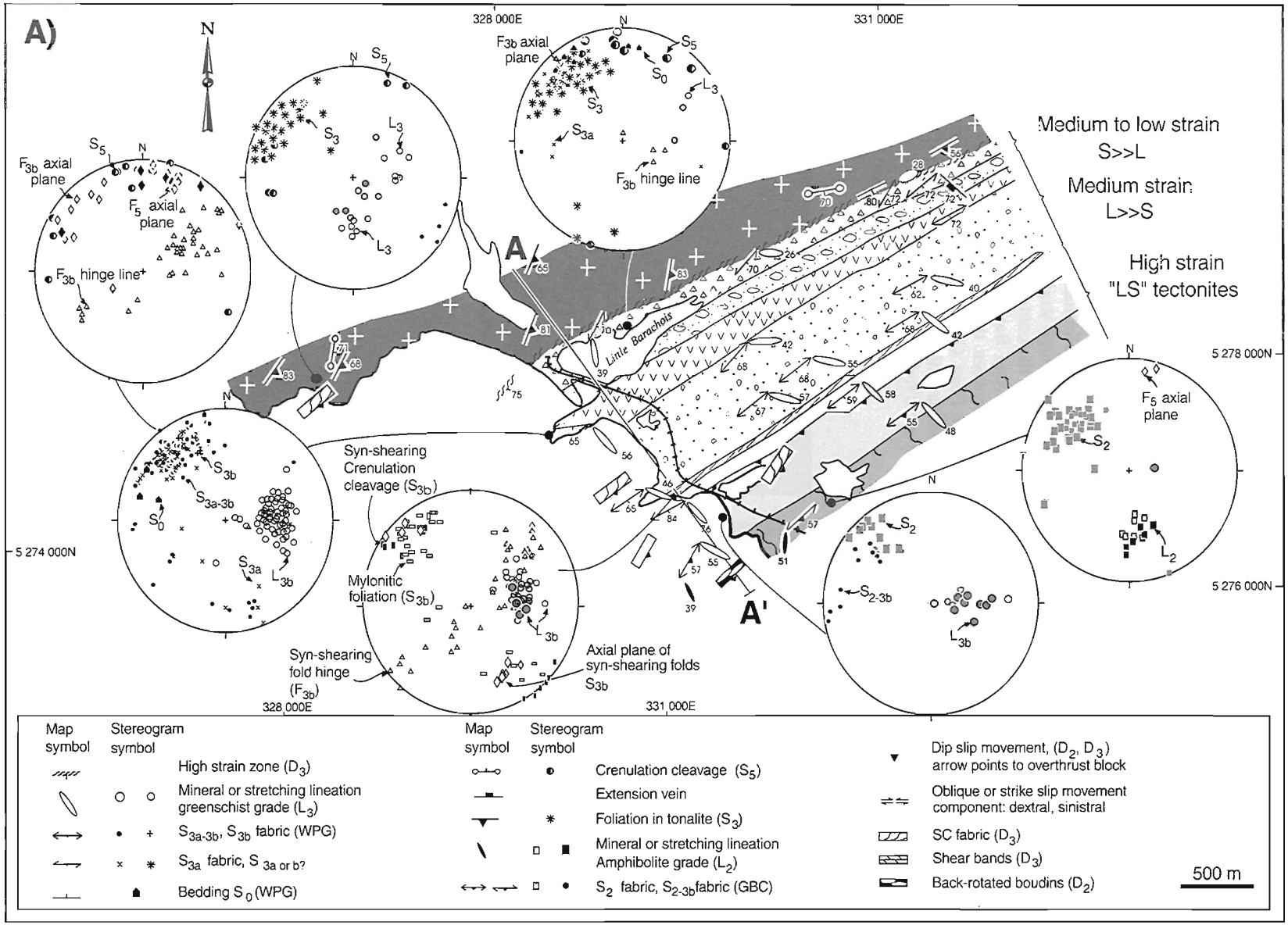

Figure 6. A) *Structural map of the coastal section illustrating the major-elements, kinematics, and a compliation on equal area projections (lower hemisphere).* ***B)*** *Schematic cross-section (AA') of the Cape Ray Fault Zone along the coastal section. Location shown in Figure 6A. CRIC – Cap Ray Igneous Complex; PABC – Port aux Basques Complex. From Dubé and Lauzière (1996a).*

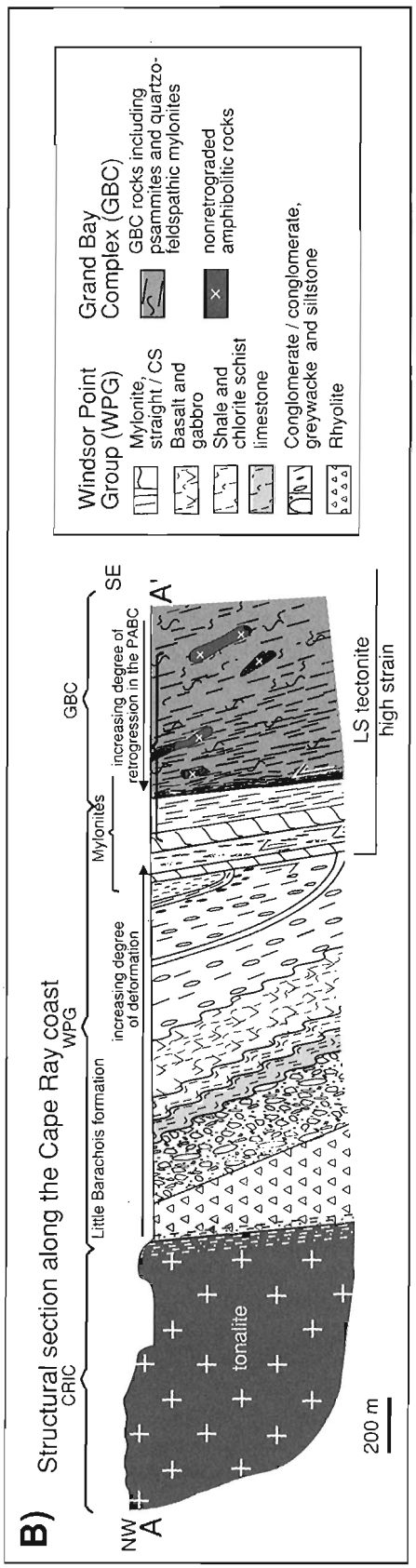

Figure 6. (cont.)

The D_3 mylonite zone at the contact between the Windsor Point Group and Grand Bay Complex is up to 100 m wide (Fig. 3, 6A, B). It is made up of quartzofelspathic mylonites and chlorite and chlorite/sericite schists produced either by retrogression of the Grand Bay Complex gneisses or by shearing of the Windsor Point Group rocks. As observed in drill core in the Isle aux Morts River area, greenschist facies shear zones are more abundant and wider towards the Windsor Point Group contact. This intense shearing has retrograded the original Grand Bay Complex gneisses into chlorite-muscovite schists. Within the mylonites, the dominant rock is a well-developed LS-tectonite characterized by a mylonitic fabric (S_{3b}) which is probably a composite S_{3a-b} foliation or a compositional layering subparallel to the shear zone (Fig. 5D). The mylonitic fabric contains a steeply to moderately easterly plunging stretching lineation (L_3) and parallel intersection lineation (Fig. 6A).

Along the coast, a zone several metres wide characterized by abundant shear bands (Fig. 7A) occurs within the D_3 mylonite zone. These shear bands are oriented on average 062°/60°, slightly oblique to the composite S_3 foliation (045°/75°). They are developed in vertical section view. The intersection between the C-C' planes is perpendicular to the steeply plunging stretching lineation indicating that they can be used as evidence for a reverse-dextral movement. Elsewhere, local CS-type fabrics, shear bands, winged garnet porphyroclasts, and foliation fish are all compatible with the reverse motion (Fig. 7B). The upper time limit of this reverse shearing event is constrained by the intrusion of the Early Devonian Isle aux Morts Brook Granite (386 ± 3 Ma) that cuts the reverse-oblique shear (known as the '50 shear') in the Isle aux Morts River area (Fig. 3).

High strain zones several metres wide related to D_3 are developed within the Windowglass Hill Granite along its contact with enclosing Windsor Point Group rocks and between the Cape Ray Igneous Complex and Windsor Point Group rocks. These zones result from deformation that was probably induced by competency contrast between the granitic rocks and the Windsor Point Group rocks. One such zone along the coast is a metre-wide high strain zone located a few metres from the base of the Windsor Point Group. It contains CS-type fabrics suggesting normal motion. The timing and the structural relationship of this normal sense of motion relative to the D_3 reverse-oblique mylonites are unclear. In addition, a north-to-south trending and steeply dipping high strain zone is present within the Windowglass Hill Granite.

D_4 structures: strike-slip mylonite. Another zone of *mylo*nitic deformation at greenschist facies is developed in the vicinity of the Windsor Point Group and Cape Ray Igneous Complex boundary in the Isle aux Morts River area (Fig. 8). It is difficult to establish the timing of deformation of this zone in relation to the D_3 mylonite as their intersection is not exposed. However, this mylonite zone is clearly discordant to lithotectonic units and to the S_3 fabrics. It is unaffected by F_3 folds and is kinematically incompatible with the vertical sense of motion characterizing the D_3 mylonites. It is thus

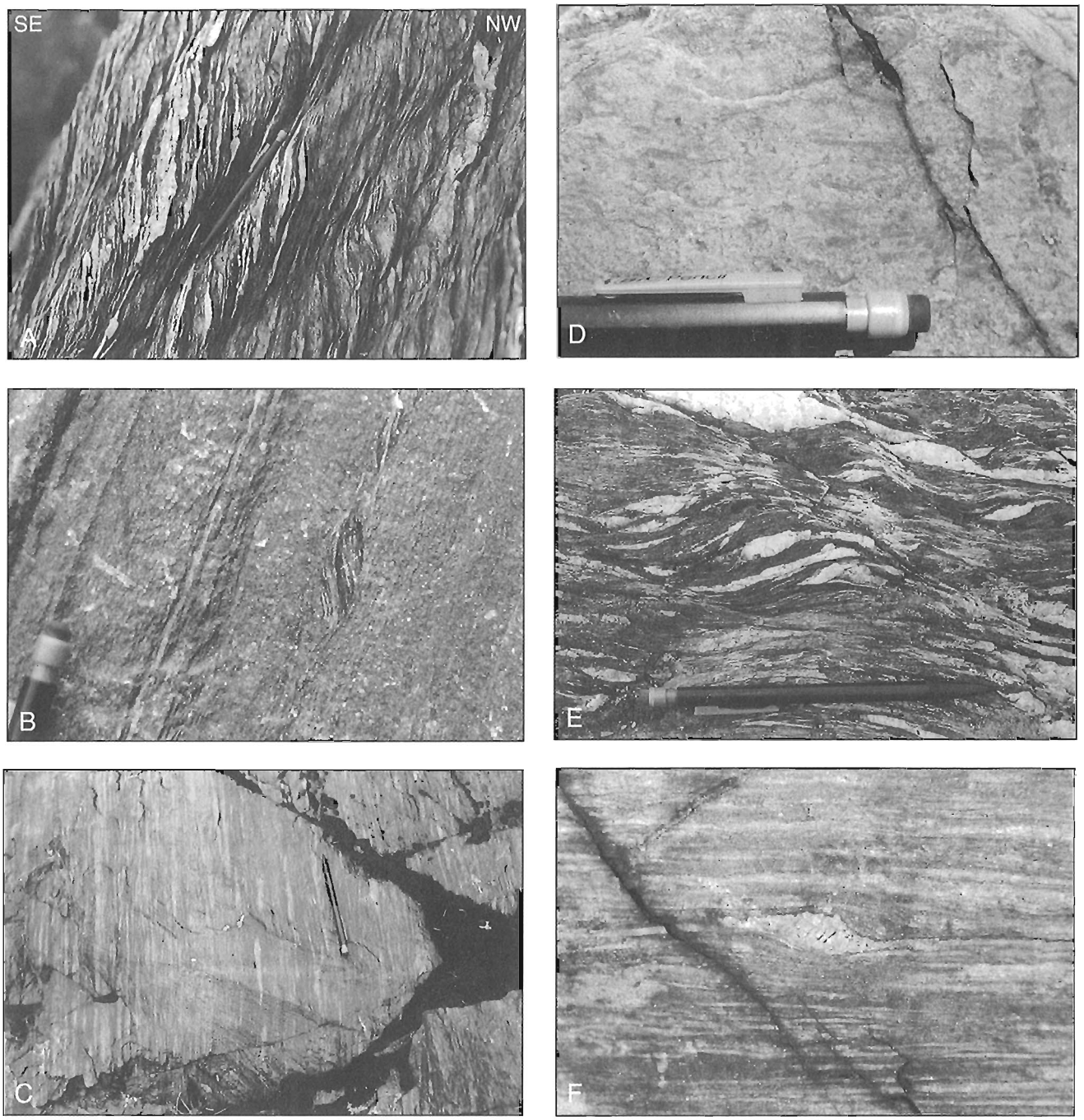

Figure 7.

A) *Vertical section view of shear bands indicating a reverse sense of motion. GSC 1996-126E;*

B) *Vertical section view showing foliation fish. GSC 1996-126F;*

C) *Plan view of the strike slip mylonite derived from Windsor Point Group conglomerate. GSC 1996-126G;*

D) *Longitudinal view showing a subhorizontal stretching lineation. GSC 1996-126H;*

E) *Plane view of C-S type fabric indicating dextral sense of motion. GSC 1996-126I;*

F) *In plane porphyroclast indicating a sinistral movement, compatible with the extension fracture; lower edge of photograph equals 10 cm. GSC 1996-125J*

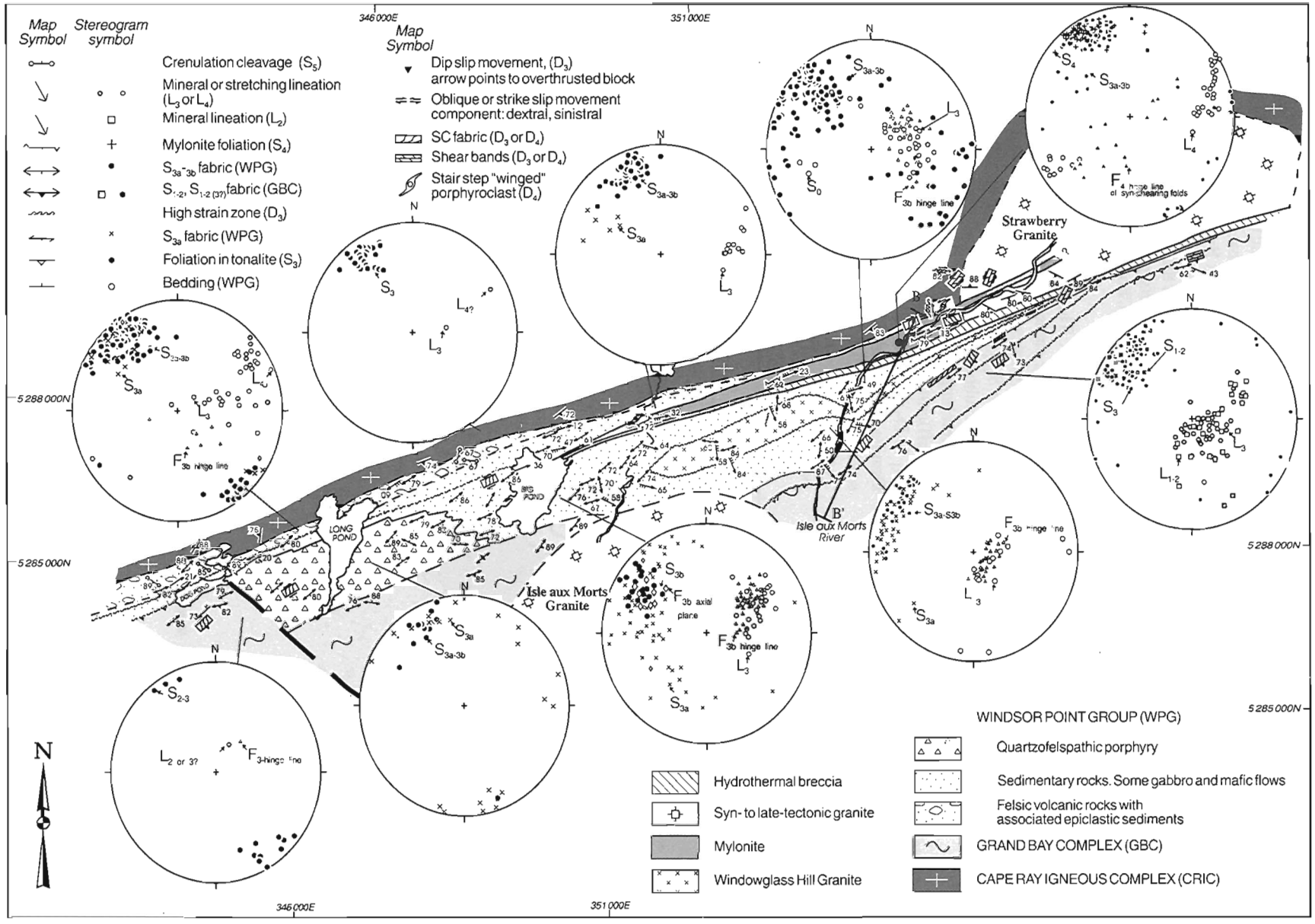

Figure 8. *Geological map of the Isle Aux Morts River area illustrating the main fabric with observed stretching lineations, kinematic indicators, and a compilation of the main structural elements on equal area projections (lower hemisphere). Note the deflection along the Isle Aux Morts River of the Windowglass Hill Granite and of the reverse fault at the Grand Bay Complex-Windsor Point Grove contact resulting from the topographic variation (see cross-section BB1). Modified after the compilation map of Dolphin Explorations, after Wilton (1983a) and work by the company. From Dubé and Lauzière (1996a).*

attributed to a D_4 generation of structures although D_3 and D_4 could well be part of one progressive event (Dubé and Lauzière, 1996a).

This D_4 mylonite is particularly well exposed along Isle aux Morts River where it is up to 250 m wide. It can be traced for up to a few tens of metres northeast of Isle aux Morts River where it is in part cut by the Strawberry Granite (Fig. 8). This mylonite gradually thins west of Big Pond, and it persists as a high strain zone a few metres wide for at least 3 km west of Dog Pond. It is characterized by a foliation (S_4) and compositional layering which strike 064° and dip steeply (80°) south (Fig. 7C, 9). Shallow-plunging to subhorizontal stretching lineations (L_4) are present on S_4 indicating oblique to subhorizontal slip motion (Fig. 7D, 8-stereonets). Kinematic indicators suggest both dextral and sinistral apparent motion along this D_4 mylonite zone (Fig. 7E-F).

East-northeast-oriented segment

The second segment corresponds to an area where the trace of the Cape Ray Fault Zone gradually changes orientation from northeast to east (Fig. 3 - 10). The bend of the Cape Ray Fault Zone is smooth and continuous and is a common feature of many fold-thrust belts (Marshak et al., 1992). This east-northeast-oriented segment is also known as the Gunflap Hills Fault (Chorlton and Dallmeyer, 1986). As in the northeast segment, three lithotectonic units are present: tonalites of the Cape Ray Igneous Complex, Windsor Point Group rocks, and gneisses of the Port aux Basques Complex to the southwest and quartzofeldspathic gneisses of the Rose Blanche Granite which underlie most of the area to the southeast (Chorlton, 1983). Windsor Point Group rocks occur as thin slivers a few hundred metres wide (Chorlton, 1983).

D_1-D_2 structures. The Port aux Basques Complex gneisses experienced the same deformational history as those of the Grand Bay Complex (van Staal et al., 1992a, b). They present a composite S_{1-2} foliation that is defined by gneissic banding. Both subhorizontal and locally steeply plunging mineral and stretching lineations are observed in this unit. However, it is difficult to determine with which period of deformation (D_1 or D_2) the lineations are associated. The Rose Blanche Granite was intruded into Port aux Basques Complex gneisses during D_2 (van Staal et al., 1992a; Lin et al., 1993). Syn-D_2 granites were dated by monazites at 420-414 Ma (van Staal et al., 1994). The presence of screens of Port aux

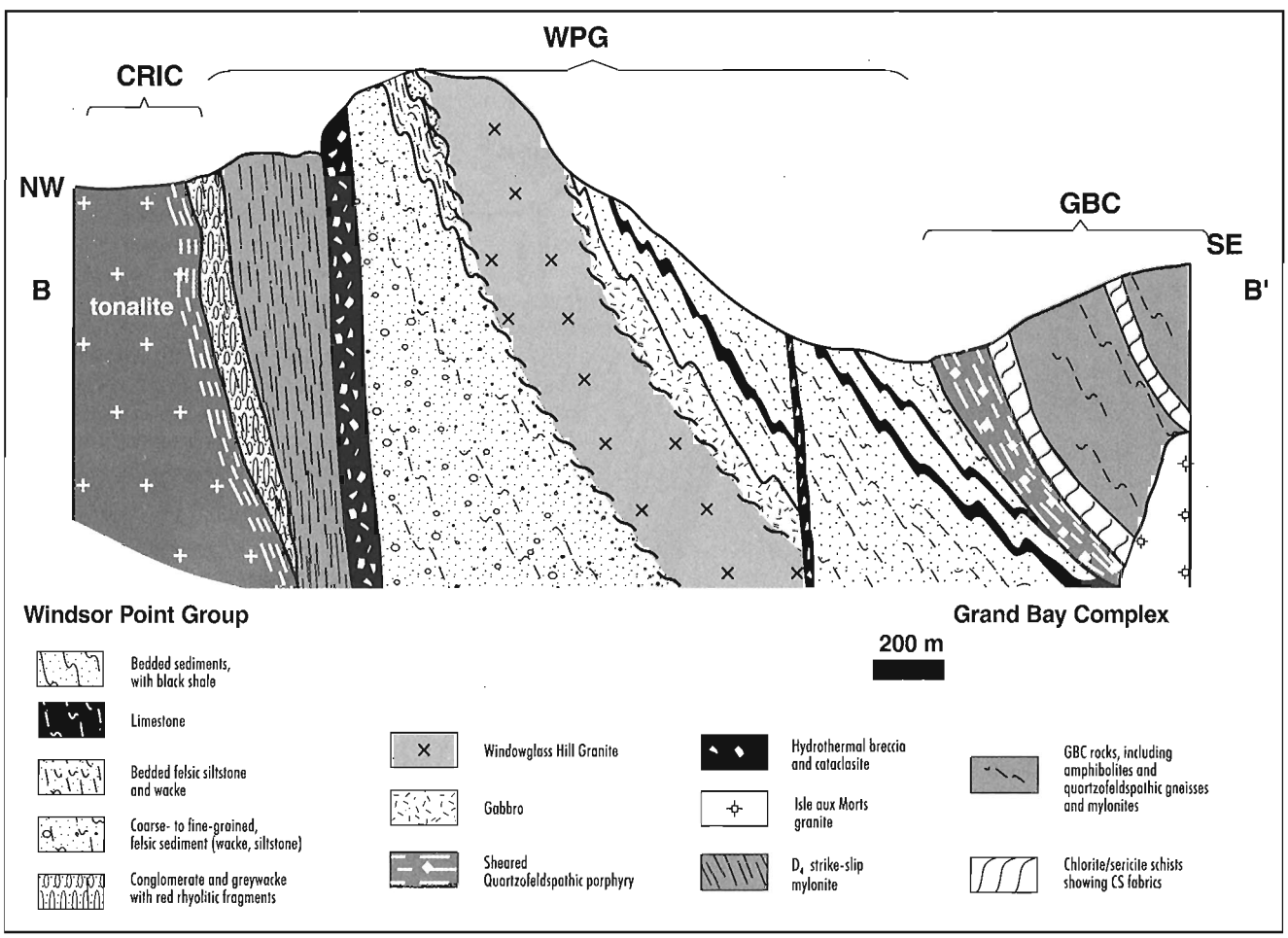

Figure 9. *Cross-section (BB^1) of the Cape Ray Fault Zone in the Isle Aux Morts River area. Vetical and horizontal scales are the same.*

Basques gneiss and pegmatitic dykes injected parallel to the S_2 fabric produce a compositional banding responsible for the gneissic aspect of these granitic rocks.

D_3 structures. Most, if not all of the D_3 deformation occurred at greenschist grade, resulting in retrogression of the amphibolitic gneisses, and prograde metamorphism in the Windsor Point Group rocks.

Within the study area, the orientation of the S_3 foliation varies from northeast to east-northeast as it is dragged by the east-northeast to east segment of the Cape Ray Fault Zone (Fig. 10). The S_3 fabric contains a southwest moderately plunging to subhorizontal stretching lineation defined by stretched quartz or elongate mica aggregates. Local CS fabrics indicating dextral movement are also recognized.

In the Windsor Point Group, two sets of structures are attributed to the D_3 deformation. The earlier fabric (S_{3a}) recorded in the Windsor Point Group varies in orientation from northeast in the southwest part to east-northeast in the northeast part of the study area and dips steeply to the southeast (Fig. 10). Local mineral lineations are shallow plunging to the northeast. The second fabric (S_{3b}) varies from a crenulation cleavage away from the Windsor Point Group-gneiss contact to a mylonitic foliation at the contact. These mylonitic LS tectonites are developed both in the Rose Blanche granitic gneisses and the Windsor Point Group sedimentary rocks.

These highly strained rocks are quartzofeldspathic mylonites, muscovite and chloritic schists including reworked 'granitic' gneisses and sheared Windsor Point Group rocks. This mylonite zone is up to 200 m wide. The S_{3b} fabric is subparallel to the trace of the Cape Ray Fault Zone.

Towards the Windsor Point Group contact, retrogression of the amphibolitic gneisses to upper greenschist grade intensifies.

In the study area, dextral strike-slip to oblique slip motion is indicated by a number of kinematic indicators. First, the trend of foliations south of the flexure clearly indicates dextral dragging of the earlier northeast-oriented S_{1-2} fabric into an east-northeast direction near the Cape Ray Fault Zone (Fig. 10). Dextral shear bands and CS-type fabrics are locally developed approaching the Windsor Point Group contact, especially within the muscovite schists (Fig. 11). These observations are compatible with the dextral-oblique motion described by Chorlton and Dallmeyer (1986) and Lin et al. (1994).

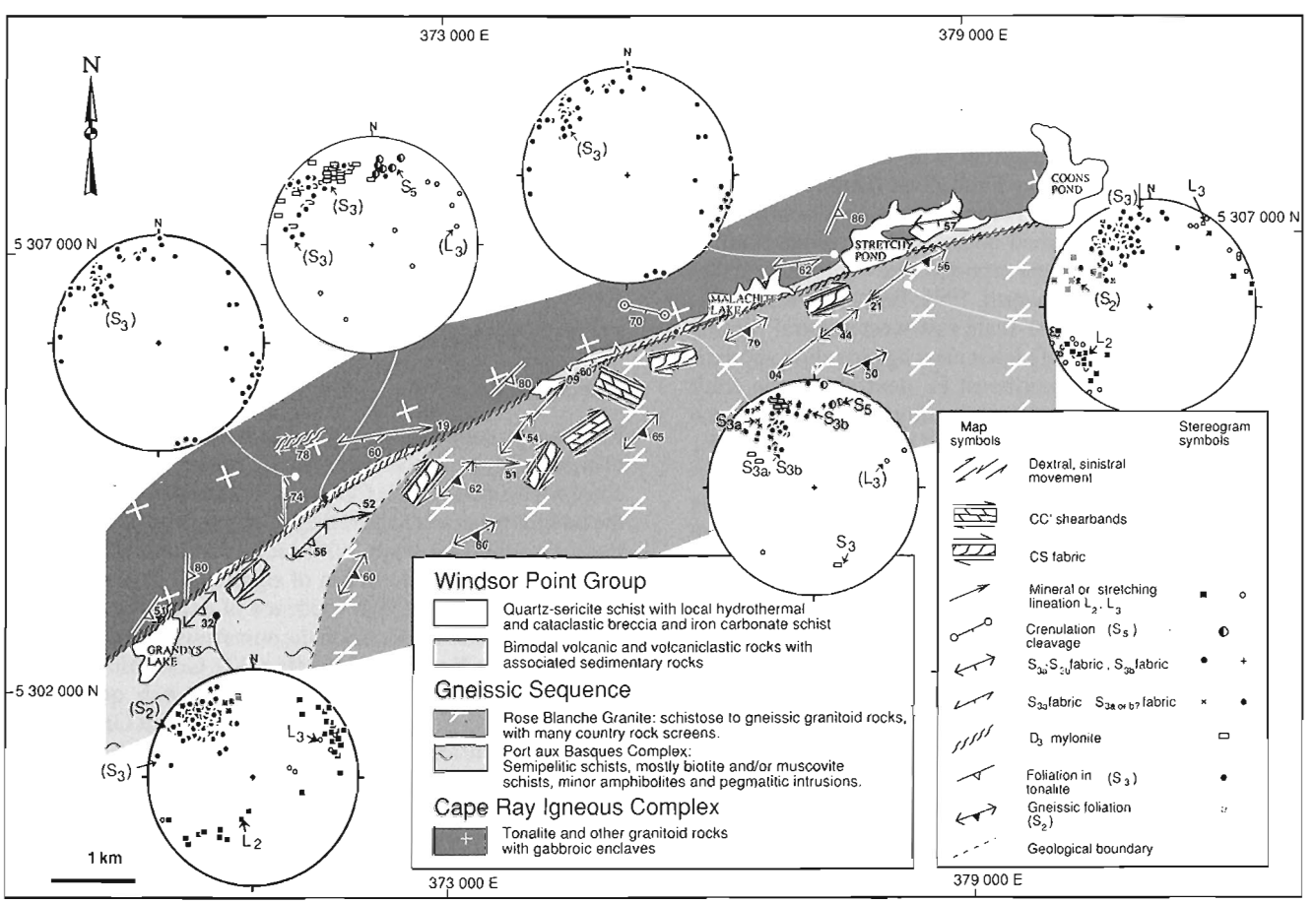

Figure 10. *Geological map of east-west flexure area illustrating the main fabric with observed stretching lineations, kinematic indicators, and a compilation of the main structural elements on equal area projections (lower hemisphere). From Dubé and Lauzière (1996a).*

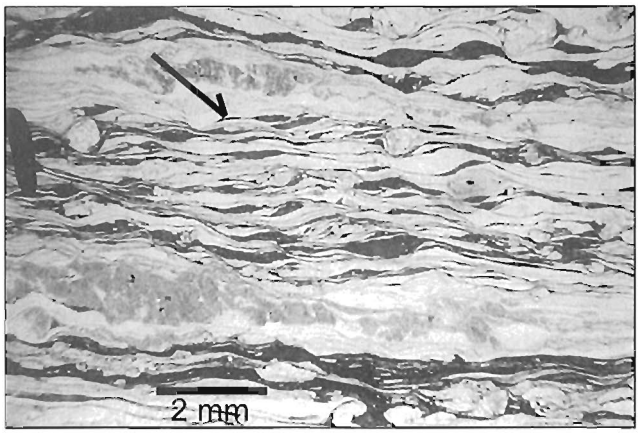

Figure 11. Photomicrograph of dextral CS-type fabric. GSC 1996-126K

Late stage deformation

Late stage phases of deformation are superimposed on the structures described above. They are separated into a ductile-brittle D_5 deformation phase and a late D_6 brittle phase.

D_5: ductile-brittle

As recognized by Wilton (1983b), two sets of "late" axial plane cleavages (S_5, S_5') and associated local folds and kinks (F_5, F_5'), are developed at medium to high angles to the main S_3 fabric along the Cape Ray Fault Zone (Dubé et al., 1992; Dubé and Lauzière, 1996a). These features are observed in all structural domains described above and are postmylonitic. Similar structures have been reported elsewhere along other zones of high strain (Holdsworth, 1991; Bergh and Karlstrom, 1992). Centimetre- to metre-scale east-west sinistral verging folds are related to S_5 axial planar cleavage trending approximately 085°/80°. North-northeast F_5' dextral verging folds plunge moderately to the south-southwest (190°/38°) and have an axial planar cleavage oriented at 025°/80°. These F_5' folds are particularly well developed within units characterized by a strong layer anisotropy. Systematic crosscutting relationships between the two sets of cleavages are not observed but the east-west cleavage is better developed than the north-northeast.

D_6: late brittle faulting

A late stage of post-Mid Devonian brittle faulting, D_6, is indicated by the presence of tectonic and hydrothermal breccias (Wilton, 1983b) along the mylonite zone in the Isle aux Morts River area, especially in the vicinity of the Strawberry Granite (Fig. 8). This zone is characterized by the absence of any consistent planar fabric and by a strong low temperature silicification. The breccia zone, clearly discordant to lithotectonic units, is subparallel to the strike slip mylonite and is preferably developed in its hanging wall (Fig. 9). It can be traced for over 8 km and is a few tens of metres wide. Another manifestation of late brittle deformation is a steeply dipping, barren, extension quartz vein, subparallel to the S_3 fabric in the Windowglass Hill Granite. The vein is up to 8 m wide and extends over tens of metres.

Tectonic and structural synthesis

The tectonic and structural evolution of the Cape Ray Fault Zone can be summarized as follows: between Late Silurian and Early Devonian time a reverse-oblique overthrusting of deeper level, high grade, Port aux Basques gneiss over the lower grade supracrustal Windsor Point Group occurred along the Cape Ray Fault Zone. This event is attributed to major oblique collision between composite Gondwanan and Laurentian terranes (Dubé et al., 1996). The fault recorded early reverse-sinistral thrusting of deeper crustal rocks of the Grand Bay and Port aux Basques complexes at amphibolite grade (D_2), followed by a protracted event (D_3, D_4) characterized by reverse-dextral thrusting and retrogression to greenschist facies of the Grand Bay Complex rocks on top of the supracrustal rocks of the Windsor Point Group (Dubé and Lauzière,1996a). Strain partitioning generated by a combination of pluton-related and tectonic-related strain induced heterogeneity of strain along- and across-strike of the Cape Ray Fault Zone as well as orogen-parallel transcurrent shearing during the later stages of the collision (D_4). The east-northeast- to east-oriented segment of the Cape Ray Fault Zone represents a tear fault accommodating differential displacement between the northeast-oriented segment of the Cape Ray Fault Zone and the correlative fault(s) located farther to the northeast (Dubé et al., 1996). Later stages of deformation include sinistral transcurrent shearing, strike-slip brittle faulting and an extensional event, postdating late tectonic, early Devonian granites (Dubé et al., 1996).

GOLD MINERALIZATION

Introduction

Regionally along the Cape Ray Fault Zone there is evidence of significant hydrothermal activity. An example is along the coast where a 40 m wide CO_2-rich alteration zone is located at the boundary between the retrograded gneiss and the Windsor Point Group. This zone, with rocks containing up to 12% CO_2, is a clear manifestation of significant fluid circulation (Dubé et al., 1992). Other evidence of extensive hydrothermal fluid circulation occurs in the numerous gold occurrences along the Cape Ray Fault Zone (Fig. 12). Gold mineralization occurs mainly in galena- and chalcopyrite-rich quartz veins within shear zones developed in Windsor Point Group rocks. The most significant mineralized zone is the Cape Ray gold deposit. Other significant auriferous quartz veins occur in the Windowglass Hill Granite and at the Big Pond and Isle aux Morts prospects both hosted by Windsor Point Group rocks (Fig. 12). In the following sections, each mineralized zone is described with emphasis on lithological and structural controls on the deposition of gold and sulphides.

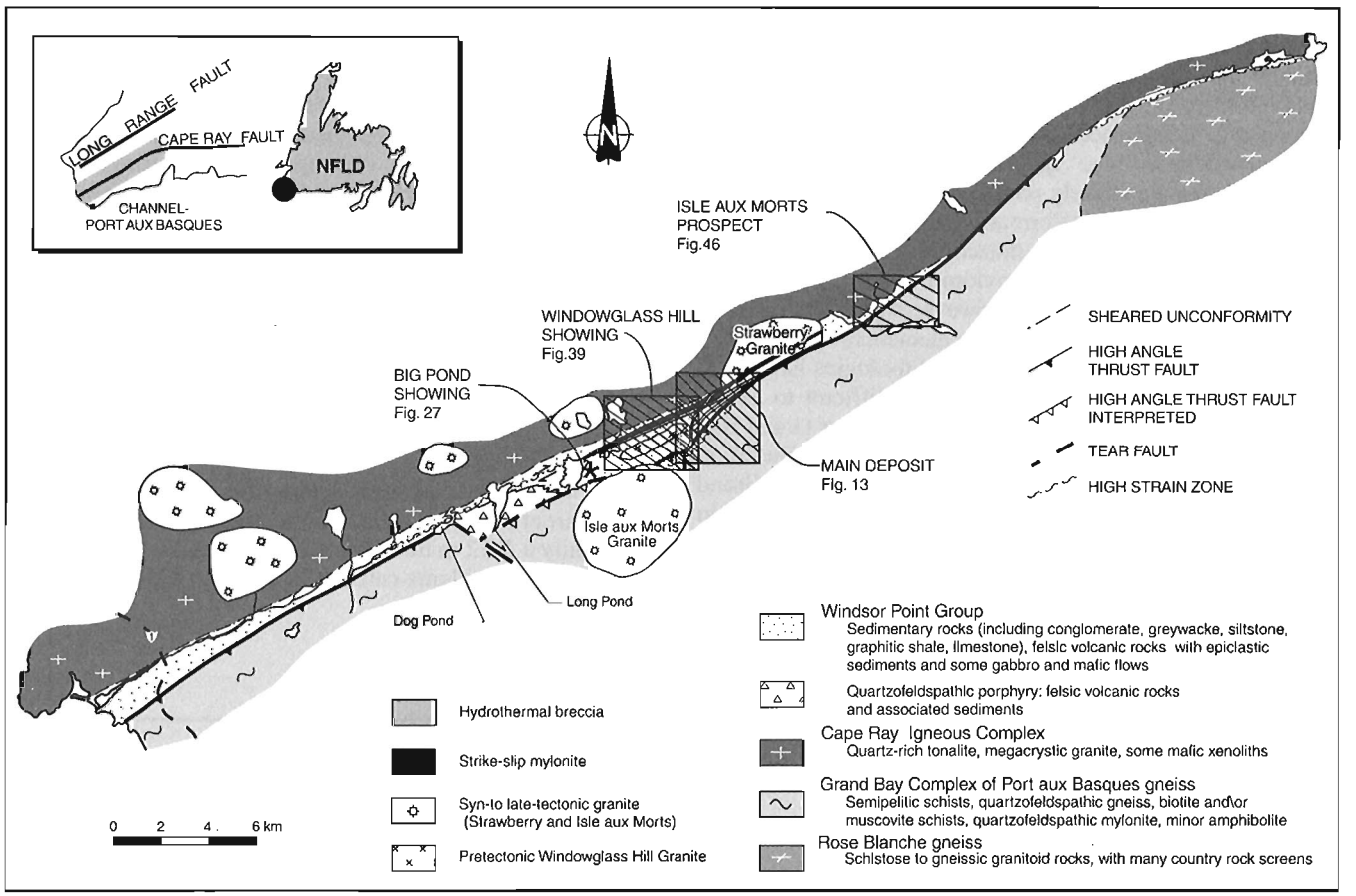

Figure 12. *Location of the mineralized zones along the Cape Ray Fault Zone.*

Geology of the Cape Ray gold deposit

Introduction

The Cape Ray gold deposit contains proven mineable reserves of 450 000 t at 10.1 g/t Au, 32 g/t Ag, 0.25% Cu, 0.69% Zn, and 0.99% Pb, and geological reserves of 886 000 t at 7.54 g/t Au (Dolphin Explorations, Annual Report, 1990). The Cape Ray gold deposit consists of three mineralized lodes (No. 4, 41, and 51) known as the "Main zone" which occupy a 1800 m long segment of the Cape Ray Fault Zone at or near the tectonic boundary between the Windsor Point Group and the Port aux Basques gneiss (Fig. 13).The mineralization at the Cape Ray gold deposit occurs in three lodes, in quartz veins collectively known as the A vein. The A vein is located at, (No. 41 and 51 zones) or near (No. 4 zone), the southeast limit of a sequence of highly deformed and brecciated graphitic schist of the Windsor Point Group. The graphitic schist hosts the mineralization and constitutes its footwall. The graphitic schist is in fault contact with highly strained chloritic schists and quartz-sericite mylonites farther in the hanging wall (Fig. 14). The protolith of these mylonites is difficult to ascertain, but examination of surface exposure suggests that they correspond to partly or totally retrograded (now greenschist facies) Grand Bay Complex rocks. Thus, the A vein is located close to the tectonic boundary corresponding to the Cape Ray Fault *senso stricto*. Other veins (C vein) are present farther in the footwall (Fig. 14). They represent secondary lodes hosted by more competent lithologies.

Nature of the host rocks and alteration

Based on drill cores and surface and underground mapping, a generalized schematic section through the mineralized zone from southeast to northwest includes (Fig. 14): 1) a mylonite zone, 2) chlorite schists, and 3) a graphitic sedimentary sequence. Table 2 presents chemical analyses representative of these three lithotectonic units.

Mylonite zone

The mylonite zone is in the hanging wall of the A vein. It is mainly composed of strongly sheared quartz-feldspar porphyries and by quartzofeldspathic gneisses and banded sediments partly to completely retrograded to greenschist facies. Towards the fault contact with the graphitic units, garnet and hornblende gradually disappear and the porphyries and gneisses are commonly transformed into recrystallized and

highly deformed quartz-sericite and quartz-chlorite-sericite schists with locally up to 5% pyrite. Petrographic studies indicate that the protoliths of most of the mylonites were quartzofeldspathic porphyries. The less deformed porphyries contain up to 35% phenocrysts of euhedral plagioclase (1-3 mm) and recrystallized 'blue' quartz (up to 1 cm). Rhyodacitic flows or dykes are a likely protolith for at least some of the porphyries and despite deformation and metamorphism, the SiO_2 contents of the chlorite-muscovite schist, feldspar porphyry and quartzofeldspathic mylonite (Table 2) are consistent with such an interpretation. However, significant variation in the content of relatively immobile elements such as Al_2O_3, TiO_2, Y, and Zr suggest that various lithologies have been incorporated in the mylonite zone. It is difficult to assign these units to either the Windsor Point Group or Grand Bay Complex due to the intensity of the deformation. Based on similarities with quartzofeldspathic mylonites in the Grand Bay Complex along the coast, the mylonitized porphyries in the hanging wall of the A vein are here interpreted to be derived from the Grand Bay Complex.

Numerous megascopic kinematic indicators such as CS-type fabrics, shear bands, and foliation fish clearly indicate thrusting of the mylonite on top of the Windsor Point Group. In thin sections of the quartzofeldspathic mylonite the shearing plane (C) is locally defined by chlorite and biotite, both replacing hornblende, indicating that shearing occurred under conditions of greenschist facies metamorphism. Elsewhere, the C-S type fabrics are outlined by coarse muscovite and/or chlorite.

Chlorite schists

The contact between the mylonite zone and the graphitic schist is a zone of strong hydrothermal alteration most probably related to the emplacement of the mineralized quartz veins. In No. 41 and 51 zones, this is commonly a 10-25 m thick chlorite±biotite±magnetite schist. Immediately adjacent to the mineralized A vein in the hanging wall, there is typically a 5-12 m thick chlorite-calcite schist. However, in No. 4 zone, the chlorite-calcite schist is much wider (up to 47 m),

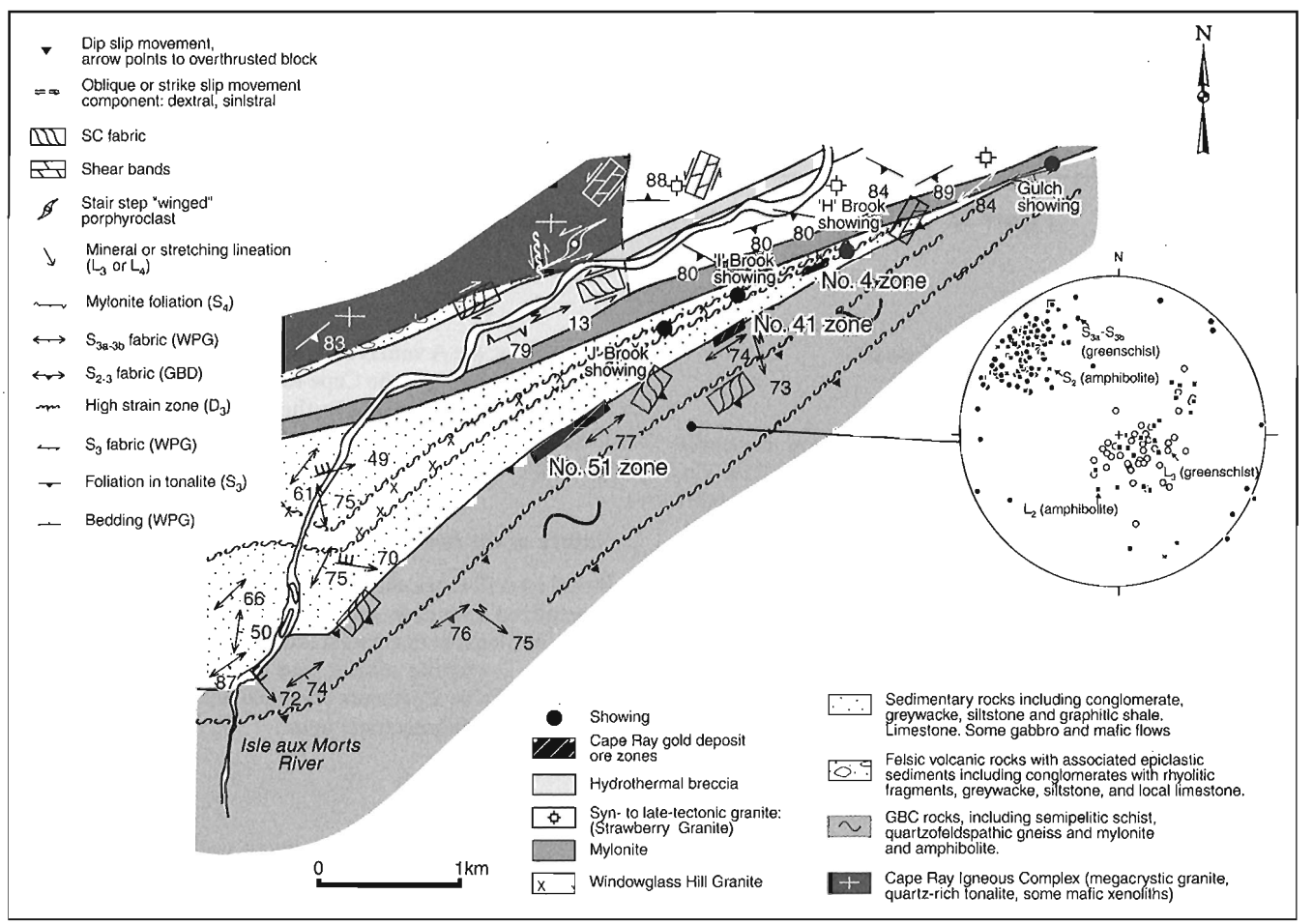

Figure 13. *Geological and structural map of the Cape Ray gold deposit area.*

the chlorite±biotite±magnetite schist zone is not as well defined and graphitic schist units, intercalated with chloritic schists, are present up to 30-40 m in the hanging wall and suggest more structural complexity.

Chlorite±biotite±magnetite schist. This schist is commonly composed of alternating dark brown biotite-rich bands and light green chlorite-rich bands. It is weakly to strongly magnetic and weakly to strongly carbonatized, as shown by several quartz-carbonate veinlets, especially towards the chlorite-calcite schist unit. These two aspects are well illustrated in Table 2 by the Fe_2O_3 and TiO_2 content and the significant increase in CaO and CO_2 in the sample closer to the chlorite-calcite schist. Petrographic studies indicate that biotite is not present everywhere but locally forms up to 15% of the schist. The schist is also composed of up to 35% chlorite, up to 10% secondary magnetite and rutile, muscovite, and less than 10% calcite, in a totally recrystallized matrix of quartz±plagioclase. Traces of garnet and graphite are also locally present.

Chlorite-calcite schist. The chlorite-calcite schist contains up to 50% calcite in layers subparallel to S_3 or in discordant veinlets, and up to 40% chlorite oriented subparallel to the S_3 fabric. The schist also contains muscovite (up to 25%), rutile, and secondary magnetite, as well as local biotite. It is also characterized by locally abundant quartz-calcite veining, subparallel or discordant to the foliation. Elevated CO_2 and CaO contents (up to 8.72% and 11.61% respectively), the H_2O content (up to 5.70%), the high proportion of Fe_2O_3 (up to 18.34%), leaching of silica, indicated by the low concentration of SiO_2, and the presence of As and Zn in samples of this zone are significant indicators of strong hydrothermal alteration (Table 2).

The chlorite-calcite schist is in sharp contact with the brecciated graphitic schist hosting the A vein and is brecciated near the contact with graphitic gouge.

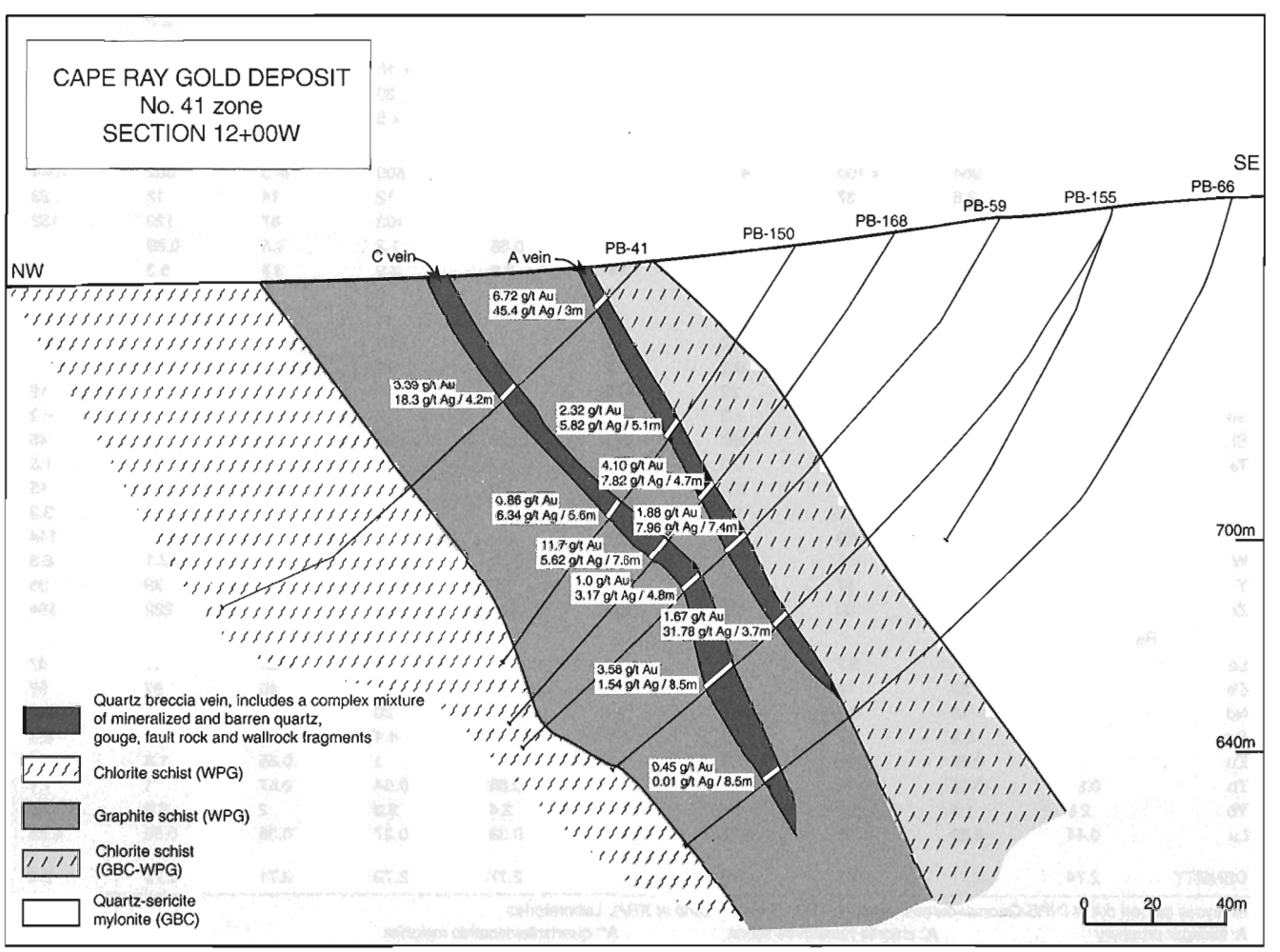

Figure 14. *Cross-section 12+00W of No. 41 zone, Cape Ray gold deposit. Modified from an unpublished diagram from Dolphin Explorations.*

Table 2. Chemical analyses representative of lithotectonic units within the Main zone of the Cape Ray gold deposit.

	Drillhole PB-353-89									
Sample	DB-332 89	DB-351 89	DB-353 89	DB-355 89	DB-356 89	DB-366 89	DB-368 89	DB-371 89	DB-378 89	DB-387 89
location (m)	76.37	147.35	151.51	164.63	169.21	179.15	179.26	186.77	193.6	245.4
lithology	A'	A'		A"	A"	A"	A	A"	A"	A'
SiO_2 %	61.22	73.20	48.39	51.19	59.94	62.99	67.55	65.59	63.80	56.61
Al_2O_3 %	14.49	13.08	17.04	17.00	16.43	15.43	14.62	14.21	17.51	19.72
TiO_2%	0.66	0.37	1.01	0.82	0.88	0.53	0.47	0.47	0.97	0.96
Fe_2O_3(t) %	10.44	2.53	15.17	9.09	8.24	6.31	4.38	4.34	3.76	6.59
MnO%	0.28	0.06	0.22	0.17	0.22	0.15	0.09	0.10	0.08	0.16
MgO%	3.59	2.88	5.33	4.62	3.62	3.02	1.69	1.60	2.37	3.17
CaO%	1.91	1.11	4.52	6.29	2.26	3.43	3.03	3.73	0.81	0.45
Na_2O%	2.75	1.89	2.45	3.44	4.48	4.67	4.63	3.24	3.20	1.24
K_2O%	1.02	1.98	0.48	0.94	0.37	0.49	1.21	2.35	2.95	4.56
P_2O_5%	0.29	0.10	0.23	0.21	0.26	0.14	0.12	0.09	0.19	0.24
LOI%	3.29	2.28	3.54	4.42	2.54	2.69	1.09	3.85	2.68	4.30
S%	0.00	0.00	0.00	0.00	0.00	0.00	0.00	0.00	0.01	0.53
CO_2%	0.56	0.24	0.43	1.80	0.20	0.84	0.31	2.34	0.34	0.15
H_2O+%	3.5	1.8	3.8	2.9	2.7	2.0	0.9	1.5	2.2	3.4
Total	100.75	99.28	99.12	98.53	99.64	100.05	99.05	99.60	98.22	97.29
	Metallic trace elements									
Cu (ppm)	17	25	6	109	64	22	27	15	8	184
Zn (ppm)	118	40	55	97	82	61	54	45	34	93
As (ppm)	< 2	< 2	< 2	< 2	< 2	< 2	< 2	< 2	2.8	7
Mo (ppm)	15	< 2	< 2	< 2	2.2	< 2	< 2	< 2	< 2	2.1
Ag (ppm)	< 10	< 10	< 10	< 10	< 10	< 10	< 10	< 10	< 10	< 10
Pb (ppm)	23	18	12	14	44	24	20	10	5	25
Au (ppb)	< 5	< 5	< 5	< 5	< 5	< 5	< 5	< 5	< 5	7.2
	Trace elements (ppm)									
Ba	666	984	< 100	473	195	206	500	873	802	1044
Co	29	7.6	37	27	17	17	12	14	12	23
Cr	113	89	34	99	60	79	103	87	120	132
Cs	2.2	0.74	0.74	2.4	0.72	0.55	1.2	1.5	0.89	1.6
Hf	4.8	3.6	2.1	3.4	3.9	3.8	3.9	3.9	5.3	4.5
Nb	13	4	3	<2	5	4	6	9	19	19
Ni	161	53	<5	16	<5	<5	<5	<5	34	39
Rb	33	35	12	32	14	14	35	58	95	155
Sb	< .2	< .2	< .2	0.2	< .2	0.3	0.2	0.2	0.3	0.5
Sc	15	11	42	29	29	19	18	17	16	19
Se	< 2	< 2	< 2	< 2	< 2	< 2	< 2	< 2	< 2	< 2
Sr	180	169	355	390	218	328	293	116	69	45
Ta	0.8	0.3	0.3	0.3	0.4	0.7	0.7	0.6	1.3	1.5
Th	9.2	5.8	2.4	6.1	6	8.9	8.6	8.2	13	15
U	3.1	1.5	0.7	1.3	1.3	1.6	1.7	1.6	3	3.3
V	189	70	533	291	202	137	96	95	123	144
W	1.8	4	< 1	< 1	< 1	< 1	1.1	1.7	2.1	6.8
Y	32	21	17	19	24	25	26	22	39	35
Zr	190	145	83	136	159	141	155	153	222	184
	Rare-earth elements (ppm)									
La	38	14	8.7	20	20	28	28	23	47	47
Ce	88	29	18	40	44	56	52	46	97	97
Nd	34	13	9.4	18	21	24	20	15	41	41
Sm	7.1	2.8	2.7	4	4.9	4.6	4.4	3.6	8.1	8.1
Eu	1.9	0.66	0.77	1.2	1.5	1.3	1	0.85	1.8	1.7
Tb	0.93	0.45	0.45	0.62	0.79	0.65	0.64	0.57	1	1.1
Yb	2.8	1.7	1.6	1.9	2.3	2.4	2.3	2	3.6	3.6
Lu	0.44	0.29	0.26	0.31	0.36	0.38	0.37	0.35	0.56	0.56
DENSITY	2.74	2.71	2.87	2.8	2.75	2.77	2.73	2.71	2.73	2.8

Analyses carried out at INRS-Georessources, except for H_2O and CO_2 done at XRAL Laboratories

A: feldspar prophyry — A': chlorite-muscovite schist — A": quartzofeldspathic mylonite

B: chlorite-biotite-magnetite schist — C: chlorite-calcite schist — D: graphite schist

E: quartz vein — E': quartz stockwork — F: basalt

Drillhole PB-353-89									
Sample	DB-391 89	DB-394 89	DB-395 89	DB-399 89	DB-406 89	DB-407 89	DB-411 89	DB-415 89	DB-418 89
location (m)	262.5	270.43	274.39	280.49	294.82	296.04	299.7	301.68	302.68
lithology	A'	A'	B	B	C	C	C	vein	D
SiO_2 %	67.03	54.01	61.00	47.68	43.07	47.97	41.26		52.64
Al_2O_3 %	14.05	15.49	14.08	14.64	11.16	12.28	13.18		18.31
TiO_2%	0.45	0.73	1.23	2.53	2.98	2.80	2.69		0.88
Fe_2O_3(t) %	4.03	7.62	8.50	12.52	12.59	14.79	15.61		7.89
MnO%	0.13	0.16	0.32	0.17	0.38	0.28	0.24		0.23
MgO%	2.24	4.30	3.91	3.76	5.28	4.05	4.39		2.43
CaO%	3.16	5.08	3.88	9.06	11.61	8.38	8.34		3.73
Na_2O%	3.31	3.24	1.86	4.78	1.67	1.68	0.01		0.00
K_2O%	1.46	1.15	1.42	0.41	0.16	0.98	1.70		4.63
P_2O_5%	0.09	0.19	0.18	0.50	0.52	0.84	1.52		0.20
LOI%	2.83	6.20	3.13	5.55	10.64	7.48	9.30		7.36
S%	0.02	0.02	0.00	0.00	0.01	0.23	0.00	12.90	0.22
CO_2%	1.26	3.68	0.68	4.58	8.72	5.36	5.11		3.65
H_2O+%	1.6	3.3	2.8	2.2	0.4	3.7	5.3		3.3
Total	98.86	98.99	99.90	102.88	98.59	103.16	99.39		97.94
Metallic trace elements									
Cu (ppm)	52	40	17	14	30	15	40	15771	81
Zn (ppm)	60	74	87	121	134	138	146	752	129
As (ppm)	2.2	3.7	137	5.2	4.9	8.3	82	226	74
Mo (ppm)	2.1	< 2	2.5	< 2	< 2	3	< 2	45	6
Ag (ppm)	< 10	< 10	< 10	< 10	< 10	< 10	< 10	129	< 10
Pb (ppm)	16	10	10	7	10	13	20	1878	148
Au (ppb)	< 5	< 5	< 5	< 5	< 5	< 5	6.9	590	43
Trace elements (ppm)									
Ba	1191	767	326	< 100	< 100	173	212	229	550
Co	12	22	29	39	35	25	19	29	27
Cr	78	124	176	159	69	25	29	163	163
Cs	0.8	0.57	2	1.7	0.68	4.1	1.4	0.91	2.7
Hf	3.9	3.5	5.2	5.7	5.2	6.3	3.2	1.5	4.1
Nb	7	5	13	22	25	25	16	3	21
Ni	<5	29	50	77	8	<5	13	26	46
Rb	38	27	45	14	5	27	54	48	135
Sb	0.4	1.3	2.3	14	0.9	1.3	0.4	9.1	1.1
Sc	18	25	20	25	25	24	25	6.9	19
Se	< 2	< 2	< 2	< 2	< 2	< 2	< 2	23	2.5
Sr	254	197	112	195	182	118	130	27	95
Ta	0.6	0.3	1	1.3	1.7	1.6	0.7	0.4	1.3
Th	8.5	7	6.5	1.5	2.5	3.9	3.5	4.1	13
U	1.7	1.3	1.7	< .5	0.97	1.6	1.3	6.8	6.8
V	98	251	178	262	354	163	141	311	277
W	1.2	3.6	< 1	< 1	3.6	11	26	17	17
Y	23	20	27	45	39	53	48	15	41
Zr	150	141	221	265	233	276	117	67	168
Rare-earth elements (ppm)									
La	27	17	20	19	24	27	26	16	47
Ce	55	36	45	47	57	66	63	35	103
Nd	20	13	20	30	33	37	40	16	42
Sm	4.3	3.1	4.6	8	8.1	10	11	3.4	8.8
Eu	1.1	0.95	1.3	2.6	2.6	3.2	3.5	0.84	2.1
Tb	0.64	0.4	0.75	1.3	1.2	1.7	1.5	0.44	1.2
Yb	2.4	1.9	2.7	4	3.3	5.4	4.5	1.5	4
Lu	0.36	0.3	0.41	0.6	0.52	0.82	0.67	0.21	0.65
DENSITY	2.74	2.73	2.78	2.86	2.79	2.82	2.8	2.81	2.75

Analyses carried out at INRS-Georessources, except for H_2O and CO_2 done at XRAL Laboratories

A: feldspar prophyry — A': chlorite-muscovite schist — A'': quartzofeldspathic mylonite

B: chlorite-biotite-magnetite schist — C: chlorite-calcite schist — D: graphite schist

E: quartz veln — E': quartz stockwork — F: basalt

Table 2. (cont.)

Drillhole PB-87-198								
Sample	89BD-432	89BD-436	89BD-439	89BD-442	89BD-445	89BD-447	89BD-450	89BD-458
location (m)	296.67	300.91	301.36	303.79	305.30	306.61	315.61	330.61
lithology	C	F	F	D	E	E	E	A'
SiO_2 %	46.64	65.82	65.86	66.76			96.05	55.12
Al_2O_3 %	15.62	16.76	15.82	13.92			0.37	15.27
TiO_2%	0.96	0.65	0.57	0.79			0.01	3.17
Fe_2O_3(t) %	13.59	3.10	2.25	7.94			0.00	13.03
MnO%	0.26	0.08	0.10	0.09			0.00	0.07
MgO%	4.79	0.92	0.76	2.60			0.00	4.96
CaO%	6.38	1.73	3.29	0.64			0.28	0.56
Na_2O%	3.44	4.99	4.07	0.36			0.43	0.47
K_2O%	0.22	1.51	1.74	2.84			0.05	2.55
P_2O_5%	0.09	0.31	0.28	0.19			0.00	0.43
LOI%	7.58	2.85	3.90	4.29	3.49	3.43	1.14	4.87
S%	0.00	0.00	0.00	0.00	4.62	4.22	1.55	0.00
CO_2%								
H_2O+%								
Total	99.57	98.72	98.64	100.42			98.32	100.50
Metallic trace elements								
Cu (ppm)	13	37	21	19	105	509	39	19
Zn (ppm)	67	69	55	103	128523	103179	28929	118
As (ppm)	27	12.9	11.1	43.8	51.1	64.9	11.3	22.7
Mo (ppm)	<2	<2	<2	<2	<2	12.9	2.11	<2
Ag (ppm)	<10	<10	<10	<10	147	119	91.4	<10
Pb (ppm)	11	33	14	173	72642	35344	52256	52
Au (ppb)	<5	<5	<5	118	8840	9470	15700	<5
Trace elements (ppm)								
Ba	<50	242	294	580	<50	<50	<50	<50
Co	34	7	7	19	25	21	8	12
Cr	69	57	86	152	123	168	184	45
Cs	0.48	3.17	1.43	3.3	0.72	0.35	<.2	1.43
Hf	1.8	4.4	4.1	2.7	0.6	0.5	<.2	4.6
Nb	6	8	6	13	<2	<2	<2	22
Ni	<3	<3	<3	38	64	33	12	41
Rb	8	56	55	117	<2	<2	<2	107
Sb	0.59	0.65	0.37	0.66	3.69	3.85	13.4	0.65
Sc	34.9	3.92	3.83	13	3.64	2.47	0.25	30.7
Se	<2	<2	<2	<2	46.6	36.8	26.1	<2
Sr	120	201	284	26	<2	<2	<2	51
Ta	<.1	0.3	0.3	0.6	0.2	0.2	<.1	1.4
Th	1	7	7	9	2	1	<.2	2
U	<.5	2	2	6	1	1	<.5	2
V	430	65	65	278	151	80	13	593
W	2	8	12	18	11	10	4	6
Y	23	18	16	29	<5	<5	<5	66
Zr	66	250	230	123	<2	<2	<2	223
Rare-earth elements (ppm)								
La	3.1	29.9	26.7	31.4	6.4	5.1	0.5	25.2
Ce	7.42	58.4	51.4	64.3	11.6	10.8	<2	56
Nd	<2	21.5	19.8	27	3.33	<2	<2	29.4
Sm	2	4.09	3.67	5.33	1.02	0.85	0.07	7.52
Eu	1.08	1.17	1.15	1.38	0.31	0.26	<.1	2.49
Tb	0.41	0.43	0.38	0.64	0.23	0.17	<.1	1.42
Yb	2.4	0.88	1.14	2.46	0.39	0.56	0.26	5.18
Lu	0.37	0.16	0.14	0.33	0.08	0.08	<.05	0.75
DENSITY	2.75	2.6	2.63	2.36	2.87	2.78	2.71	2.78

Analyses carried out at INRS-Georessources, except for H_2O and CO_2 done at XRAL Laboratories

A: feldspar prophyry — A': chlorite-muscovite schist — A'': quartzofeldspathic mylonite

B: chlorite-biotite-magnetite schist — C: chlorite-calcite schist — D: graphite schist

E: quartz vein — E': quartz stockwork — F: basalt

Drillhole PB-87-198						
Sample	89BD-464	89BD-470	89BD-471	89BD-474A	89BD-474B	89BD-479
location (m)	343.12	354.24	355.15	357.12	357.12	365.61
lithology	C-D	E'	E	C	C	A'
SiO_2 %	58.00	39.73		62.83	53.84	45.41
Al_2O_3 %	14.67	17.99		9.54	18.56	9.15
TiO_2%	3.09	1.72		0.91	1.15	0.49
Fe_2O_3(t) %	12.42	12.16		6.52	6.49	3.44
MnO%	0.23	0.30		0.21	0.12	0.26
MgO%	3.77	5.26		2.76	1.93	0.90
CaO%	0.56	7.57		6.78	4.19	18.77
Na_2O%	0.62	0.43		0.51	0.71	1.20
K_2O%	2.66	3.38		1.81	4.87	1.75
P_2O_5%	0.39	0.19		0.15	0.20	0.12
LOI%	4.68	11.34		7.53	7.52	17.30
S%	0.77	0.00	16.20	1.15	2.15	0.00
CO_2%						
H_2O+%						
Total	101.09	100.26		99.55	99.59	98.79
	Metallic trace elements					
Cu (ppm)	69	62	9037	293	125	35
Zn (ppm)	145	264	637903	2634	236	153
As (ppm)	75.7	15.7	9.66	6.83	10.6	40.3
Mo (ppm)	<2	<2	164	11.3	10	<2
Ag (ppm)	<10	<10	153	<10	<10	<10
Pb (ppm)	26	41	239324	1631	62	102
Au (ppb)	12	6	1960	15	26	<5
	Trace elements (ppm)					
Ba	<50	341	<50	211	622	322
Co	38	16	49	13	19	15
Cr	52	148	39	166	147	42
Cs	1.11	0.46	0.44	0.83	2.51	1.01
Hf	4.6	3.5	1.3	4.9	5.2	2.1
Nb	21	9	<2	12	21	6
Ni	24	51	260	4	40	4
Rb	91	93	<2	53	140	50
Sb	0.83	1.14	42.7	1.66	1.23	1.06
Sc	28.2	32.7	7.62	10.9	17.6	12.1
Se	<2	<2	23.8	<2	<2	<2
Sr	50	167	<2	137	128	312
Ta	1	0.6	0.4	0.9	1.3	0.3
Th	2	2	4	8	12	4
U	1	3	4	2	5	2
V	504	422	552	149	270	82
W	12	23	16	10.3	12.5	2.33
Y	34	30	<5	24	38	28
Zr	218	146	<2	211	233	108
	Rare-earth elements (ppm)					
La	16.9	11.3	15.5	22.8	37.9	14.2
Ce	40.9	27.1	28.5	53.1	87.8	32.8
Nd	21.1	8.63	10.7	22.4	35.8	13.6
Sm	5.97	3.65	1.9	4.52	7.24	3.74
Eu	1.44	1	0.87	1.19	1.7	0.98
Tb	1.03	0.64	0.49	0.66	0.94	0.63
Yb	2.85	2.66	1.07	1.94	2.91	2.16
Lu	0.42	0.42	0.22	0.31	0.47	0.34
DENSITY	2.43	2.6	3.84	2.74	2.82	2.68

Analyses carried out at INRS-Georessources, except for H_2O and CO_2 done at XRAL Laboratories

A: feldspar prophyry — A': chlorite-muscovite schist — A'': quartzofeldspathic mylonite

B: chlorite-biotite-magnetite schist — C: chlorite-calcite schist — D: graphite schist

E: quartz vein — E': quartz stockwork — F: basalt

Table 2. (cont.)

Samples from ramp (underground)										
Sample	89BD-482	89BD-485	89BD-487	89BD-495	89BD-496	89BD-498	89BD-499	89BD-501	89BD-502	89BD-485D*
lithology	A	A''	A''	A''	A''	B	B	A'	C	A''
SiO_2 %	67.56	79.43	76.51	59.13	60.01	81.27	40.27	58.94	47.04	77.60
Al_2O_3 %	14.05	8.35	10.30	15.89	16.49	8.84	15.14	16.59	15.91	8.38
TiO_2%	0.46	0.59	0.63	0.85	0.89	0.44	2.22	1.35	0.75	0.59
Fe_2O_3(t) %	3.42	3.35	4.00	7.98	7.94	2.06	11.72	7.85	18.34	4.14
MnO%	0.09	0.02	0.03	0.17	0.15	0.01	0.29	0.10	0.16	0.03
MgO%	1.98	0.00	1.38	2.76	3.40	0.77	4.50	2.13	3.09	0.74
CaO%	2.77	0.83	0.38	3.45	3.39	0.68	11.22	1.64	3.80	0.79
Na_2O%	4.65	2.88	2.74	4.52	5.45	0.78	1.63	1.29	0.63	3.45
K_2O%	0.64	0.87	1.22	0.67	0.32	2.36	1.57	4.18	2.58	0.95
P_2O_5%	0.11	0.16	0.14	0.37	0.44	0.18	0.33	0.22	0.07	0.10
LOI%	2.83	2.63	2.6	2.59	3.01	1.88	11.31	3.93	7.49	2.23
S%	0.00	2.66	1.96	0.10	0.37	0.37	0.00	0.23	0.00	2.66
CO_2%	1.38	0.43		0.73	1.00	0.15	8.56	1.12	2.85	0.45
H_2O+%	1.5	0.8		0.2	0.2	1.4	4.0	2.8	5.7	0.7
Total	98.66	98.97	96.68	95.16	98.30	98.97	102.70	98.43	101.98	99.00
	Metallic trace elements									
Cu (ppm)	17	25	175	38	58	24	36	31	89	
Zn (ppm)	38	14	42	97	90	262	118	94	117	
As (ppm)	< 2	11	16.7	3	2.6	61	54	16	26	
Mo (ppm)	< 2	4	< 2	< 2	< 2	< 2	< 2	< 2	< 2	
Ag (ppm)	< 10	< 10	< 10	< 10	< 10	< 10	< 10	< 10	< 10	
Pb (ppm)	7	12	24	25	17	82	9	17	25	
Au (ppb)	< 5	< 5	< 5	< 5	< 5	< 5	< 5	< 5	< 5	
	Trace elements (ppm)									
B										
Ba	303	234	461	546	136	662	432	1416	254	345
Co	10	23	9	15	19	8	44	25	27	
Cr	84	142	144	33	41	104	74	111	52	155
Cs	0.6	0.5	0.4	0.5	0.2	1.6	1.2	2.5	1.2	
Ge	18	7	9	22	13	14	16	20	20	
Hf	4	8.2	5.8	3.6	3.5	3.3	4	5.6	1.2	
Ho	0.5	< .5	< .5	0.8	0.8	0.8	0.9	1.1	0.5	
Nb	7	14	13	<2	6	10	21	20	3	< 10
Ni	<5	<5	18	<5	<5	18	38	28	19	
Rb	19	39	37	17	10	74	51	116	80	40
Sb	0.4	0.6	0.5	0.4	0.6	1.3	1.1	1.0	0.5	
Sc	17	3.1	5.5	27	28	8.6	30	23	31	
Se	< 2	2.4	< 2	< 2	< 2	< 2	< 2	< 2	< 2	
Sr	217	47	40	368	263	33	111	41	39	34
Ta	0.7	0.9	0.8	0.4	0.3	0.8	1.4	1.3	0.2	
Th	9.1	9.4	8.4	6.8	6.5	8.1	1.9	11.0	0.5	
Tm	0.32	0.24	< .2	0.31	0.35	0.31	0.3	0.49	< .2	
U	1.9	1.9	2.3	1.7	1.7	2.3	0.9	2.6	< .5	
V	81	52	75	167	198	45	343	209	350	
W	1.2	2.5	4	1.8	2.1	1.8	8.1	13	37	
Y	23	23	24	25	28	28	25	36	12	40
Zr	156	326	245	135	134	137	171	224	51	397
	Rare-earth elements (ppm)									
La	23	51	39.2	21	21	17	18	40	3.5	
Ce	43	98	80.2	44	44	37	43	86	7.4	
Nd	15	34	26.6	20	22	15	23	35	6.6	
Sm	3	5.8	5.2	4.9	4.8	3.6	5.7	7.6	1.7	
Eu	0.75	1.3	1.18	1.5	1.4	0.67	1.8	1.8	0.56	
Tb	0.44	0.59	0.53	0.67	0.73	0.65	0.88	1	0.17	
Yb	2.2	1.6	1.76	2.5	2.5	2.2	2.5	3.6	1.5	
Lu	0.35	0.33	0.28	0.4	0.4	0.34	0.4	0.61	0.24	
DENSITY	2.7	2.72	2.73	2.78	2.76	2.71	2.76	2.78	2.69	2.72

Analyses carried out at INRS-Georessources, except for H_2O and CO_2 done at XRAL Laboratories

A: feldspar prophyry — A': chlorite-muscovite schist — A'': quartzofeldspathic mylonite

B: chlorite-biotite-magnetite schist — C: chlorite-calcite schist — D: graphite schist

E: quartz vein — E': quartz stockwork — F: basalt

* Duplicate sample analyzed at XRAL Laboratories

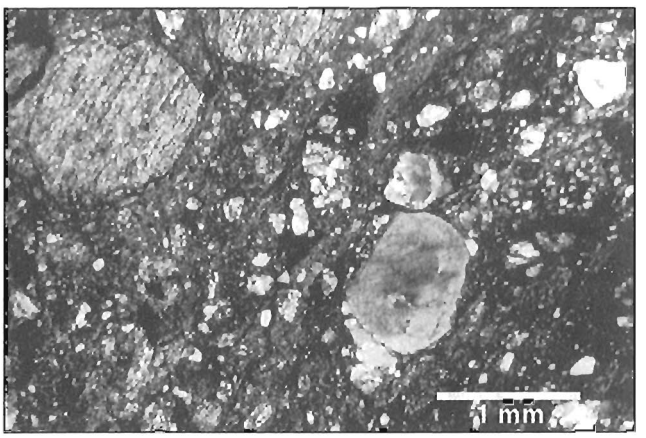

Figure 15. *Photomicrograph of graphitic gouge containing fragments of wall rock, quartz veins, and sulphides in a fine-grained matrix. GSC 1996-127A*

Due to the intensity of the deformation and alteration, it is difficult to determine the protolith of these chloritic schists. Based on their present mineralogy and chemical composition, especially their TiO_2 and Al_2O_3 contents (Table 2), mafic units such as Windsor Point Group basalt and gabbro are likely candidates. The local presence of interlayers of graphitic schists also suggests affiliation with Windsor Point Group rocks.

Graphitic sedimentary sequences

In the deposit area, a continuous sequence of banded, highly contorted, folded and locally brecciated graphitic schist with intercalations of chloritic and sericite-carbonate schists and banded mylonites, constitutes the footwall and host of the A vein (Fig. 14). The banded mylonites are characterized by centimetre-wide siderite-muscovite-quartz-rich bands within graphitic-chlorite-quartz-muscovite schist. The mylonites are commonly spatially associated with local Au-mineralized quartz breccia veins (known as C vein, see below) and stringer zones. Chloritic and carbonatized sheared mafic rocks, and carbonatized pale green metasedimentary rocks are also present. Locally, less altered sections within the sericitic schist of No. 41 zone suggest that the protoliths of at least part of these schists are sills or dykes of Windowglass Hill Granite.

The graphitic schist accommodated much of the D_3 strain and forms a rather chaotic and brecciated unit especially near its upper contact with the chlorite schists and mylonites. There, graphitic gouge zones, up to 6 m wide, which host the A vein, contain centimetre-wide fragments of wall rock, quartz veins, and sulphides in a fine- grained matrix (Fig. 15). A chemical analyses of the graphitic gouge close to the vein indicates anomalous values in As, Cu, Pb, Zn, and Au most probably related to the incorporation of such fragments (Table 2).

This unit becomes strongly to moderately contorted and folded farther in the footwall, but centimetre- to metre-wide graphitic and/or chloritic gouge is still common. The graphitic schist unit contains up to 60% quartz or quartz-carbonate veins. At least three mineralized quartz breccia veins or stockwork zones (a few centimetre to 1 m) are present in the footwall of the No. 41 zone (C vein). They are especially well developed within this zone because of propinquity to the competent Windowglass Hill Granite. These veins or stockwork zones are discontinuous and located above, or below, millimetre-scale brittle faults which were probably induced by competency contrast. The thickness of the graphitic-rich sequence is highly variable from 20 to 70 m but averages 50 to 60 m in the deposit area. To the west of the No. 51 zone, interpretations of ground geophysical surveys suggest that the graphitic horizon extends as a narrow gouge zone (R.W. Arnold, unpublished report for Dolphin Exploration, 1988).

Structure of the deposit

The Cape Ray gold deposit-Main zone mineralization is poorly to not exposed on surface, mainly because of the friable nature of the host graphitic schist. The only available surface exposure is in a trench located on line 14W approximately 100 m west of the economic section (oreshoot) of the No. 41 zone (Fig. 16). Underground work provides a similar section of the No. 41 zone.

Ductile fabric

In the main deposit area, rocks display a penetrative northeast-oriented S_{3b} fabric, steeply dipping southeast and containing relatively steep lineations plunging east-southeast (Fig. 13, 16). This fabric is axial planar to steeply plunging tight F_{3b} folds deforming both the rocks and an earlier bedding-parallel S_{3a} fabric. The rocks are most probably strongly transposed along the S_{3b} fabric. The hangingwall of the mineralized zone is a mylonite zone more than 100 m wide (Fig. 17). Kinematic indicators such as C-S type fabrics and foliation fish developed in vertical section (Fig. 7B), clearly indicate a reverse to oblique sense of motion compatible with down dip to steep southerly plunging stretching lineations present on S_{3b} foliation planes.

Late east and north-trending S_5-S_5' cleavages, dipping steeply south and east, locally cut across the S_{3b} fabric. These cleavages are axial planar to local small scale, steeply plunging, relatively open F_5-F_5' folds. In the surface trench of No. 41 zone , the S_{3b} fabric is folded and the poles of this fabric define a great circle perpendicular to measured F_5 hinges (Fig. 16). These hinges plunge steeply to moderately east (60-70°), coaxial with L_{3b} stretching lineations. These F_5-F_5' folds are typical of those mapped regionally in the Cape Ray Fault Zone area.

Underground, mapping of the 41C crosscut (between 1350-1400W, elevation 790) revealed a large, shallow-plunging (095°-10°) open fold, located in the footwall of the A vein. It affects both lithological units and several mineralized quartz veins (C vein) (Fig. 18). The axial plane of this fold is east-west and steeply dipping. Locally, an axial plane cleavage (080°/87°) is developed. The timing of this fold is poorly constrained but it postdates the S_{3a}-S_{3b} fabrics and could be F_5.

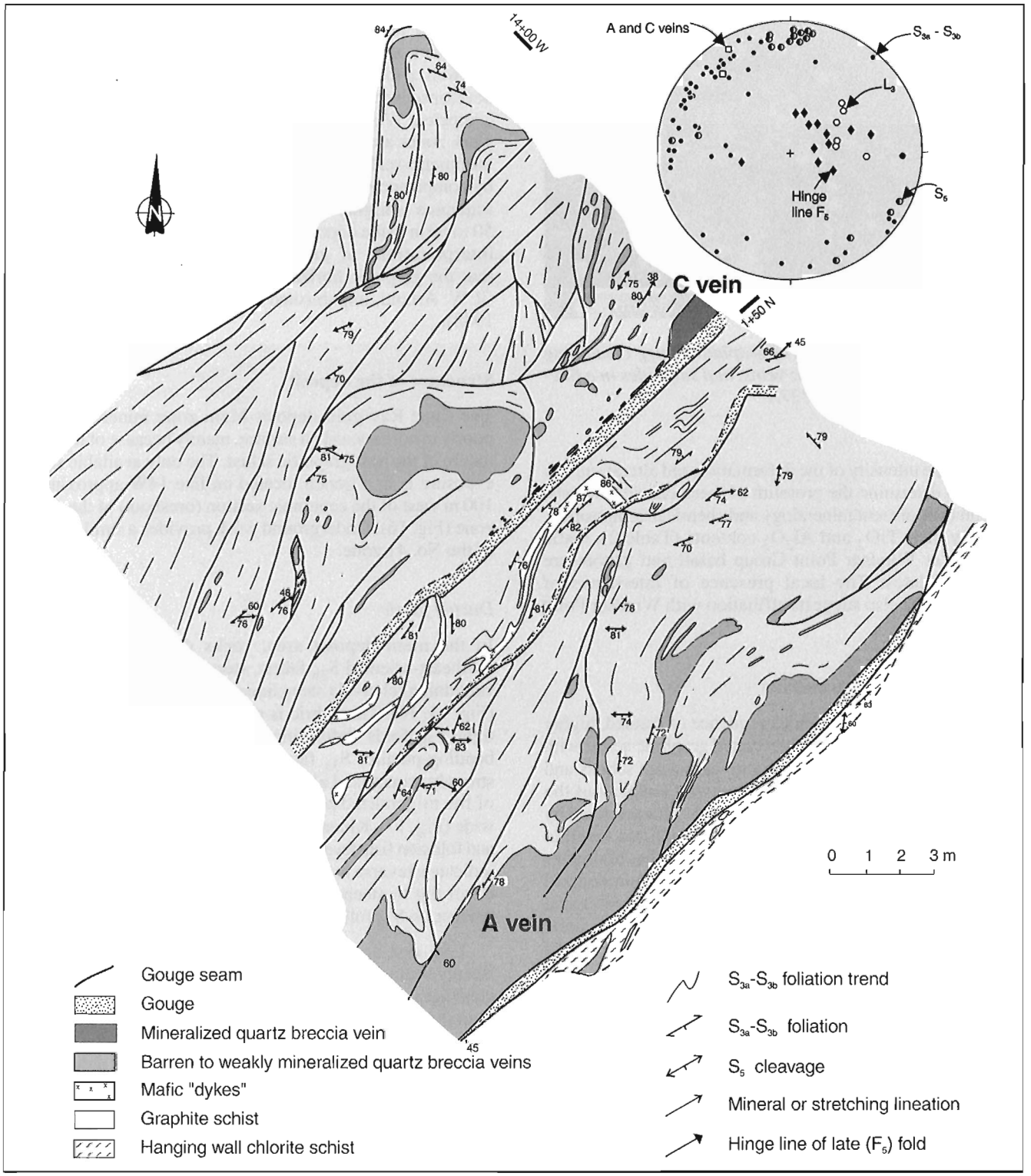

Figure 16. *Geology of the A vein in the surface trench of the No. 41 zone showing main lithotectonic units and structural elements. Modified from an unpublished diagram by Dolphin Explorations.*

However, the fold plunges differently than typical steep-plunging F_5-F_5' folds. A section based on drillholes indicates that this fold is a local feature and that the C vein dips moderately south, overall (Fig. 14).

Brittle deformation

Numerous millimetre- to centimetre-scale gouge seams are developed within the footwall graphitic schist. Underground, a cross-section view shows northeast to east-southeast oriented shallowly dipping fault-gouge with oblique reverse motion of a few centimetres to 1.5 m as indicated by displacement of markers and striations. Some gouge seams correspond to northeast-oriented and southeast-dipping listric thrust faults with stacking producing repetition of units. Other gouge seams cut across the mineralized breccia veins (C vein), or are located along the boundaries between graphitic sedimentary rocks and competent units such as quartz veins or altered Windowglass Hill Granite sills or dykes. Gouge seams locally cut across F_3 folds and several are developed along transposed lithological contacts and are folded by the open subhorizontally plunging folds described above (Fig. 18).

Observations of surface exposure show that the graphitic schist is strongly deformed and is cut by numerous gouge seams (Fig. 16). All these seams represent slip planes within the graphitic schist that delimit metre-wide structural domains, each characterized by a particular S_{3b} orientation. The various gouge seams present conflicting chronological relationships. Some are rectilinear and postdate all other structures whereas others are curvilinear and may be folded. The seams probably developed over a period of time and overprinting relations are incompletely understood because of poor exposures.

The varying aspects of gouge seams could result from: 1) multiple generations of gouge and/or, 2) orientations which are partly controlled by the competency contrast between already deformed graphitic schist and quartz veins or competent dykes. Several gouge zones are marked by sub-horizontal striations indicating strike slip motion.

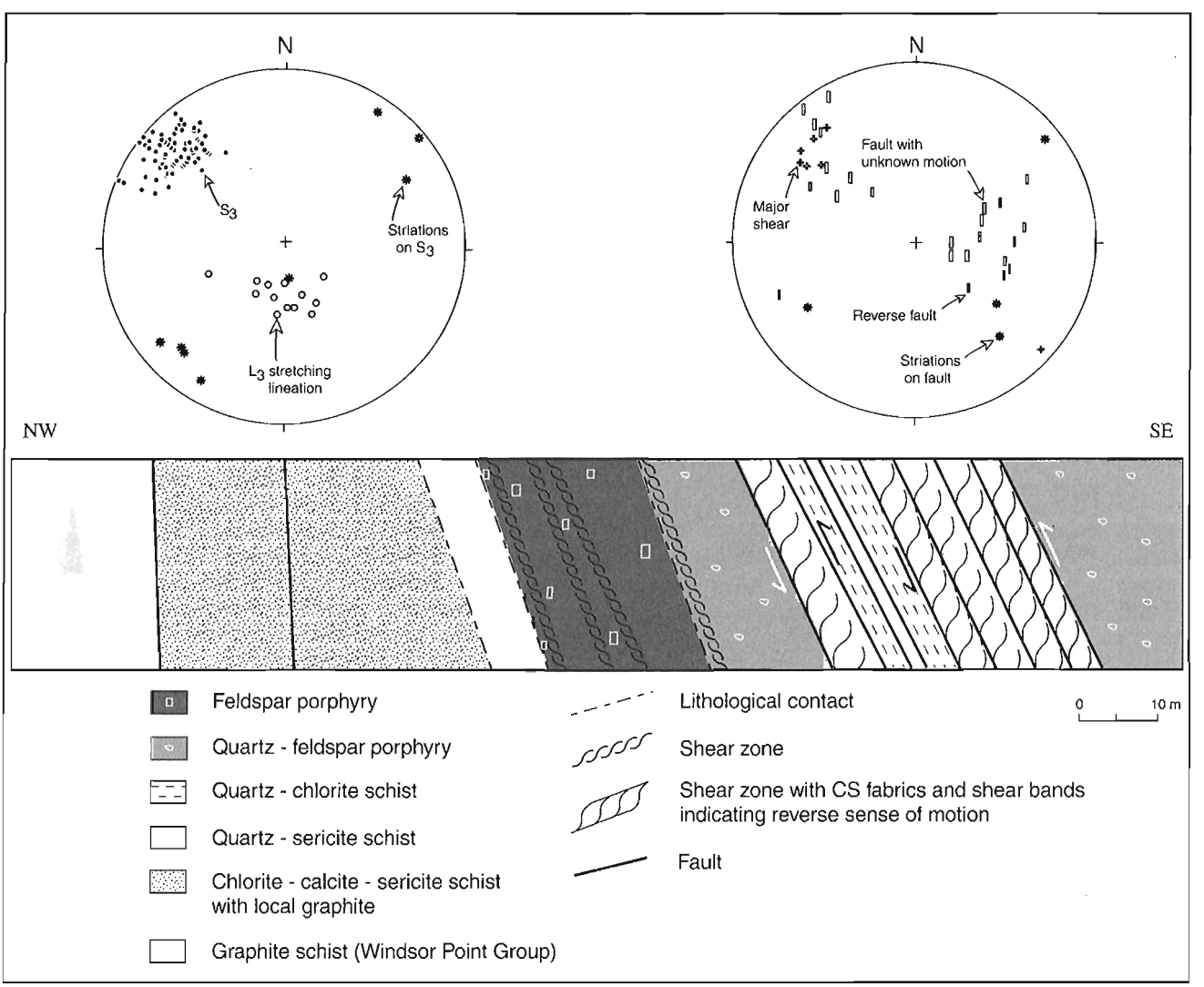

Figure 17. *Schematic cross-section of the hanging wall mylonite zone mapped in the access ramp of the No. 41 zone underground.*

The development of gouge is a characteristic typical of mélange-hosted or sedimentary rock-hosted lode gold deposits (Peters, 1993). Presence of gouge does not necessarily reflect late brittle faulting superimposed on the mineralized quartz veins but may be a manifestation of repeated faulting contemporaneous with mineralization. At the Cape Ray gold deposit, there are several generations of gouge. Some are probably contemporaneous with the mineralized zones but others are definitely late, as indicated by the presence of small fragments of mineralized quartz veins and chloritized and carbonatized rock in fault gouge (≤2 m) which marks the boundary between the mineralized quartz vein with both the hanging wall and the footwall. As well, Figure 19 illustrates that the mineralized A vein is cut and displaced by such a brittle fault. The apparent horizontal sense of motion is sinistral and is not compatible with high angle reverse faulting associated with the mineralizing event.

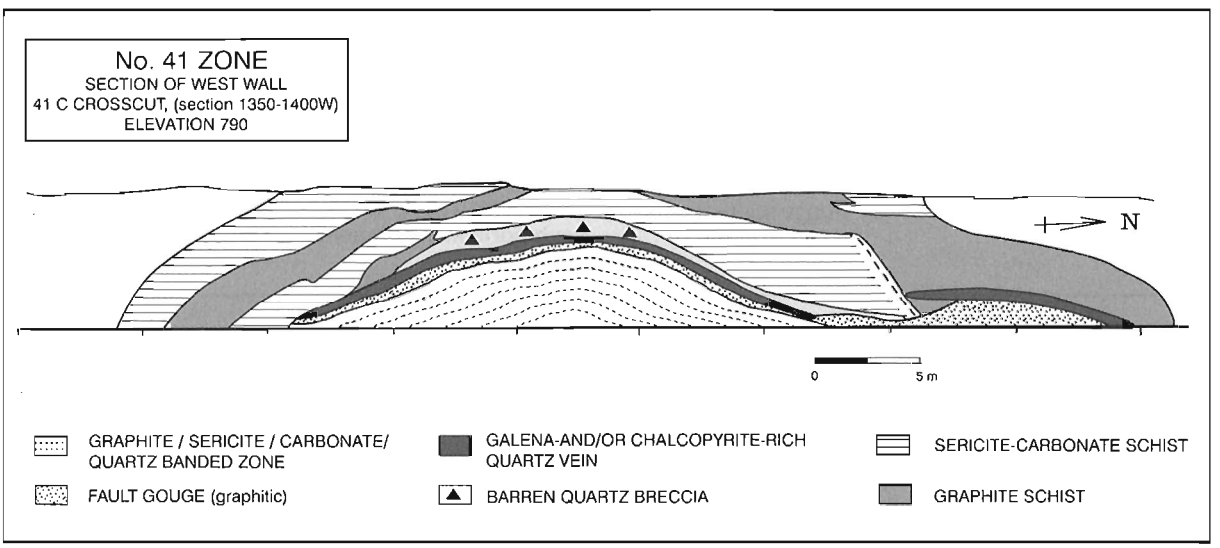

Figure 18. *Shallow-plunging fold mapped underground, C vein, Cape Ray gold deposit.*

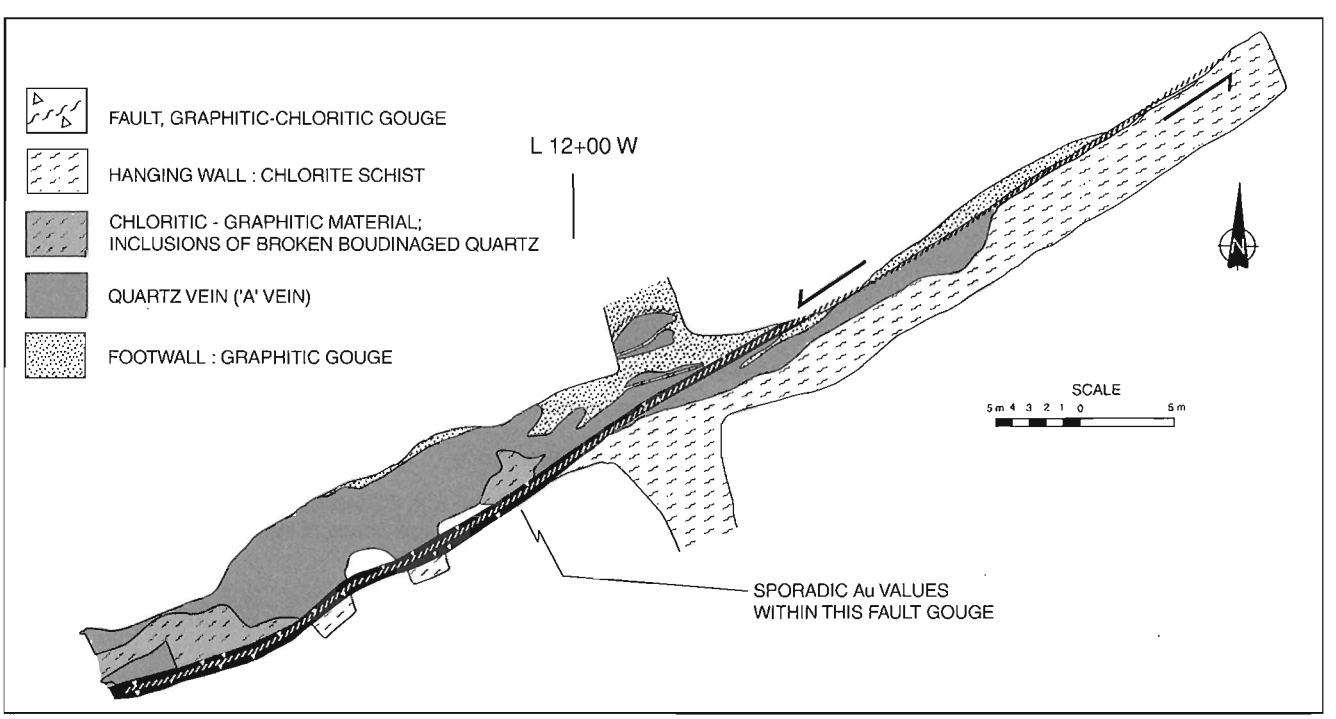

Figure 19. *Geological map from underground showing the A vein crosscut and sinistrally offset by a graphitic and chloritic gouge. Modified from an unpublished diagram by Dolphin Explorations.*

Mineralization

Introduction

The No. 4, 41, and 51 mineralized lodes of the Cape Ray gold deposit are hosted by graphitic schists along a northeast-oriented fault, moderately dipping (50-60°) to the southeast. The lodes consist of complex tabular zones of quartz veins, gouge, and wall rock fragments. They range from several centimetres to a few metres wide and extend laterally from 175 to 700 m. In longitudinal section, the economic zones occur as oreshoots which plunge, in No. 41 and 4 zones, steeply east-southeast to southeast and have a known down-dip extension of up to 300 m (Fig. 20). They are subparallel to the L_3 elongation lineation and to the L_5 intersection lineation with older fabrics. In No. 51 zone, the oreshoot is not as well defined and both subhorizontal and steeply plunging trends may be present (Fig. 20).

Veins

In each of the lodes, there are several mineralized fault-fill quartz breccia veins. The two most significant are the A and C veins. These complex vein systems are composed of several irregular quartz veins or pods mixed with fault gouge, and are hosted by graphitic schist. At the edge of the oreshoots, lower-grade or barren milky quartz-breccia veins were intersected by exploration drilling within the graphitic horizon. Outside the three lodes (4, 41, and 51), neither a vein nor any economic mineralization has been intersected by drilling.

A vein: nature and geometry. The complex geometry of the A vein is presented in a series of cross-sections across a well-mineralized zone (Fig. 21). These cross-sections show the subconcordant (and less commonly slightly discordant) nature of the A vein in relation to the main S_{3b} fabric. The A vein is strongly fractured and deformed. Superimposed brittle deformation on the mineralized veins is indicated by local, centimetre-wide mineralized quartz fragments in the graphitic host.

Within the oreshoot, the A vein typically consists of a breccia vein with various proportions of angular clasts of wall rock (chlorite and graphitic schists) set in a matrix of quartz deposited from hydrothermal solutions and containing up to 40% sulphides (averaging 5-10%). The sulphides are mainly galena and chalcopyrite with lesser sphalerite and pyrite. The A vein is up to 2 m wide with local wider pods. Fault gouge commonly borders the mineralized veins and is

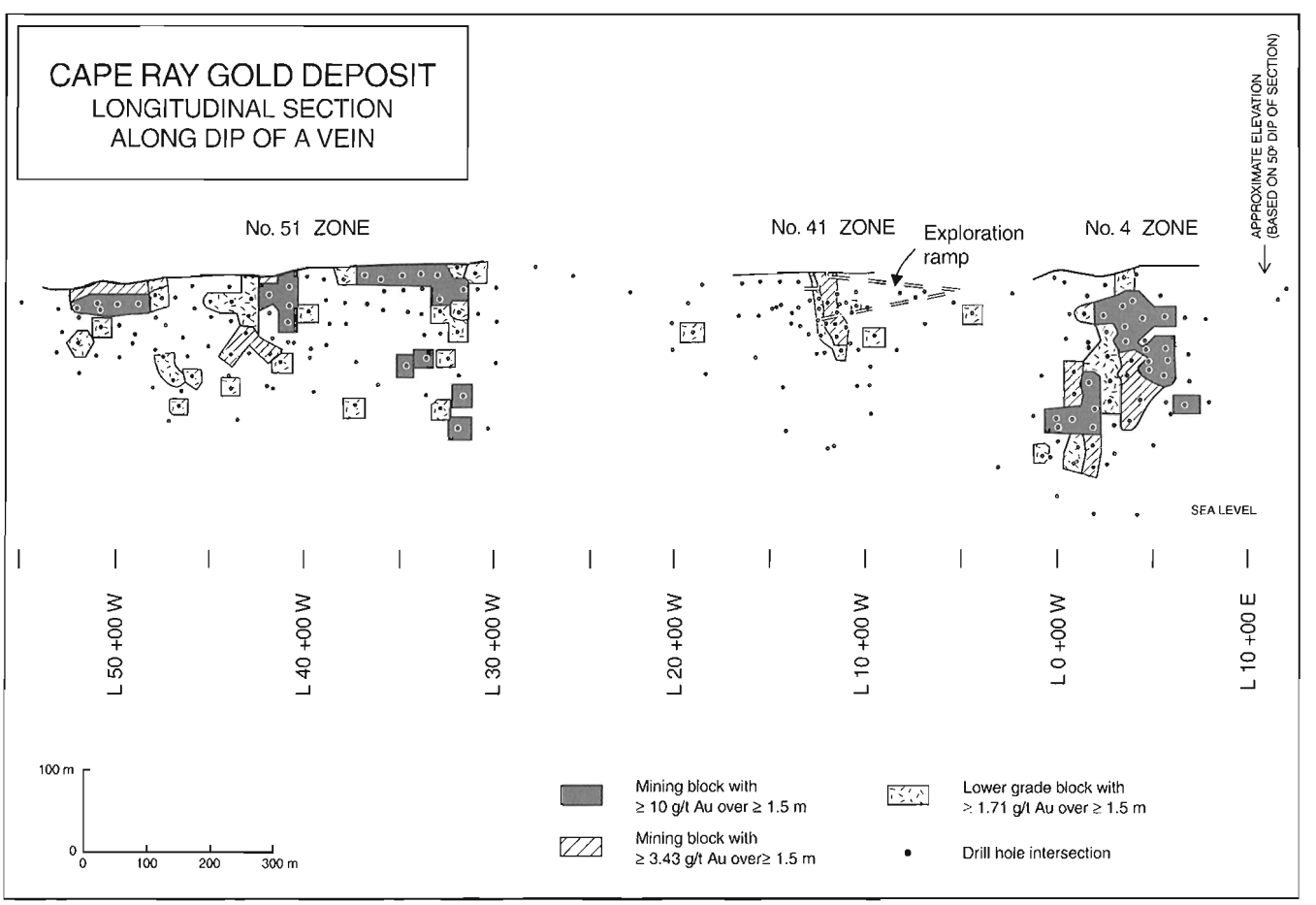

Figure 20. *Longitudinal section of the Cape Ray gold deposit showing the oreshoots. Modified from an unpublished diagram by Dolphin Explorations.*

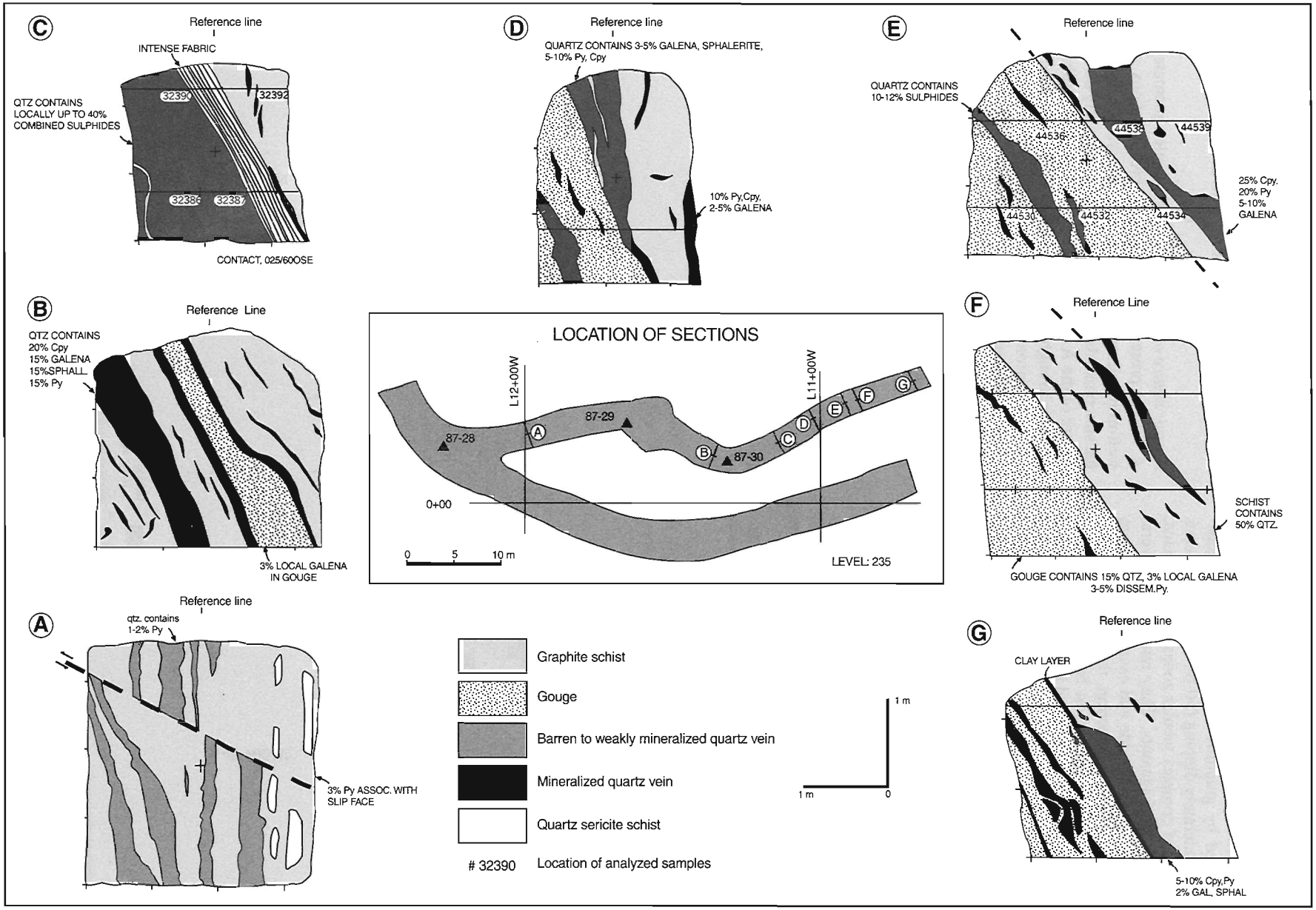

Figure 21. *Cross-sections of the A vein showing the variation in geometry of the mineralized veins, nature of the footwall and hanging wall units, and location of some of the analyses of mineralized samples presented in Table 3. Cpy – chalcopyrite; SPHALL., SPHAL – spalerite; Py – pyrite; QTZ – quartz; GAL – galena; qtz – quartz. Modified from Arnold (1988)*

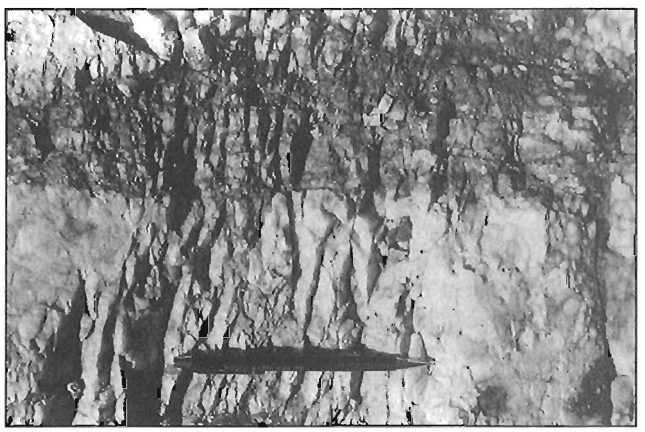

Figure 22. *Cataclastic deformation superimposed on the A vein, surface trench, No. 41 zone. GSC 1996-127B*

superimposed on already highly strained rocks. The nature of the host rocks and superimposed deformation make the mineralized zone complex and variable in terms of vein continuity, width, and grade. Underground mapping done by R.W. Arnold (unpublished report for Dolphin Explorations Ltd., 1988) within the mineralized No. 41 zone indicates that the A vein pinches and swells and commonly branches out into smaller discrete veins or lenses (Fig. 21). Similar observations were made by Wilton and Strong (1986) in a now-filled trench that exposed the A vein within No. 51 zone for over 61.5 m. There, numerous quartz veins that are subparallel to the main fabric pinch and swell extensively. Individual veins are up to 2.4 m thick and 21 m long. They are hosted by brecciated graphitic and chloritic schist and gouge. Wilton and Strong (1986) suggested that the podiform geometry of the veins resulted from boudinage of a formerly more continuous quartz vein. These authors also observed that an east oriented, subvertical cleavage dissects the vein pods. This cleavage is probably the S_5 cleavage recognized regionally.

Laterally outside the oreshoots, the A vein structure consists of either uneconomic quartz veining or fault gouge with little or no veining. In a trench over No. 41 zone, located approximately 30 to 50 m west of the oreshoot, the A vein consists of barren quartz veins with traces of disseminated pyrite (Fig. 16). Megascopically, apart from the lack of sulphides, there is very little difference in the nature and textural aspect of these veins compared to the mineralized zones. Both are milky-looking breccia quartz veins displaying highly irregular contacts with the footwall. These contacts are characterized by pointed terminations invading the graphitic schist. This geometry is typical of "assimilation quartz" produced when fluid pressure is higher than the lithological pressure of the hosting sediments (Peters, 1993). Such a geometry is also more common at the periphery of oreshoots (Peters, 1993). The hanging wall contact with the chlorite-calcite±muscovite schist is rather sharp. Brittle deformation superimposed on the vein by cataclastic features is illustrated in Figure 22.

Underground, a cross-section along section 14W (50-60 m to the west of the oreshoot) intersects the A vein where this structure is a 6 m wide gouge zone in sharp contact with the chlorite-calcite schist on the hanging wall side. The zone is characterized by the absence of any cohesive fabric. It contains numerous millimetre-wide gouge seams, centimetre-wide fragments of quartz vein with traces of chalcopyrite and pyrite, and wall rock fragments showing a penetrative fabric (S_{3b}?). This clearly indicates that at least some gouge development is superimposed on the mineralized veins and on the S_{3b}(?) penetrative fabric. This gouge zone is northeast-trending and moderately dipping and contains shallowly dipping northeast-oriented (040°/33°) thrust faults and listric faults with less than 1 m displacement. Striations, developed on brittle fault planes within the gauge zone as well as at the footwall boundary, are shallow plunging (30°) and suggest an oblique sense of motion. Dragging of the S_3 fabric in plan view suggests a sinistral component of motion compatible with the observed displacement of A vein along a brittle fault (Fig. 19).

Thus, the A vein was definitively subjected to boudinage, and was fragmented, tectonically brecciated, and partly or totally transformed into a gouge zone in which angular quartz fragments are recognized within a dark fine-grained matrix (Fig. 15, 21).

C vein: nature and geometry. The C vein is located up to 30 m into the footwall of the A vein (Fig. 14). Compared to the A vein, it is farther from the reactivated contact between the graphitic and the chlorite-calcite±muscovite schists, and consequently it is better preserved. Underground exposure shows that the C vein is less deformed than the A vein, although in the surface trench over the No. 41 zone, the C vein is strongly boudinaged (Fig. 16).

Drillhole data indicate that the C vein is up to 15 m thick but gold values are not as consistent nor as high as in the A vein. Underground, in No. 41 zone, the C vein corresponds to a series of fault-fill mineralized quartz breccia veins as well as barren quartz breccia, up to 1.5 m thick. The transition between mineralized and barren quartz breccia veins is locally gradual with the barren veins located in the central part of the mineralized quartz breccia. Elsewhere the two vein types are in sharp contact (Fig. 18).

The proportion of fragments in the quartz breccia veins varies from 5% to 80%. The fragments are angular, up to 20-25 cm long and are composed of graphitic schist and sericite-chlorite schist set in a matrix of hydrothermal quartz with local euhedral siderite and ankerite crystals. The barren breccias are mainly composed of sericitic fragments in a matrix of barren quartz whereas the mineralized breccia contains fragments of various compositions. All fragments within the quartz mineralized breccia contain a penetrative fabric interpreted as S_{3a} or S_{3b} (Fig. 23). This fabric, however, is absent in the matrix. These quartz breccia veins are spatially related to strongly altered Windowglass Hill Granite sills or dykes. The high competence of these granitic rocks probably explains this spatial relationship, with brecciation having occurred more readily in the more competent dykes and sills.

In one underground exposure, one quartz breccia vein shows thickening in the lower-pressure hinge zone and thinning along the limbs of an east-oriented, subhorizontally plunging fold (Fig. 18, 24). This geometry resembles a saddle reef-type geometry related to flexural slip folding and thus strongly suggests that, at least locally, a genetic relationship exists between the interpreted folds and some of the quartz breccia veins. Some of the folds, however, may be late relative to the mineralization as some veins appear folded (Fig. 18).

Mineralogy and textures of the mineralized zones

The gold mineralization occurs primarily in the quartz breccia veins, where centimetre- to metre-wide high grade zones, up to 50 g/t Au are encountered (Fig. 21, Table 3). Gold values are also obtained from graphitic gouge of the footwall and hanging wall of the veins, and result from the presence of mineralized quartz veinlets or fragments of mineralized quartz and/or sulphides, crushed and incorporated within the gouge.

The proportion of sulphides in the quartz breccia veins varies over short distances, from traces to 10%. Some veins or veinlets are nearly massive sulphides, and the amount of gold is commonly proportional to the sulphide content. In the A vein, the average proportion of combined sulphides is around 5 to 10%. In the C vein, it is usually less than 2 to 3%. The sulphides are mainly chalcopyrite, pyrite, galena and sphalerite, and locally pyrrhotite and arsenopyrite. They constitute aggregates, veinlets, and disseminations present within a gangue dominated by recrystallized quartz with some carbonate (mainly calcite and ankerite-siderite). The mineralogy of the Cape Ray gold deposit mineralized zones has been described in detail by Wilton (1983a, 1984) and Wilton and Strong (1986), who reported that the sulphides are more abundant in the less deformed portions of the quartz veins where galena, sphalerite, and chalcopyrite with lesser amounts of pyrite, are intergrown in coarse network patches. According to Wilton and Strong (1986), the highest gold values occur in the massive sulphide layers within less deformed quartz pods, suggesting that gold may have been remobilized during deformation. The intense deformation has resulted in

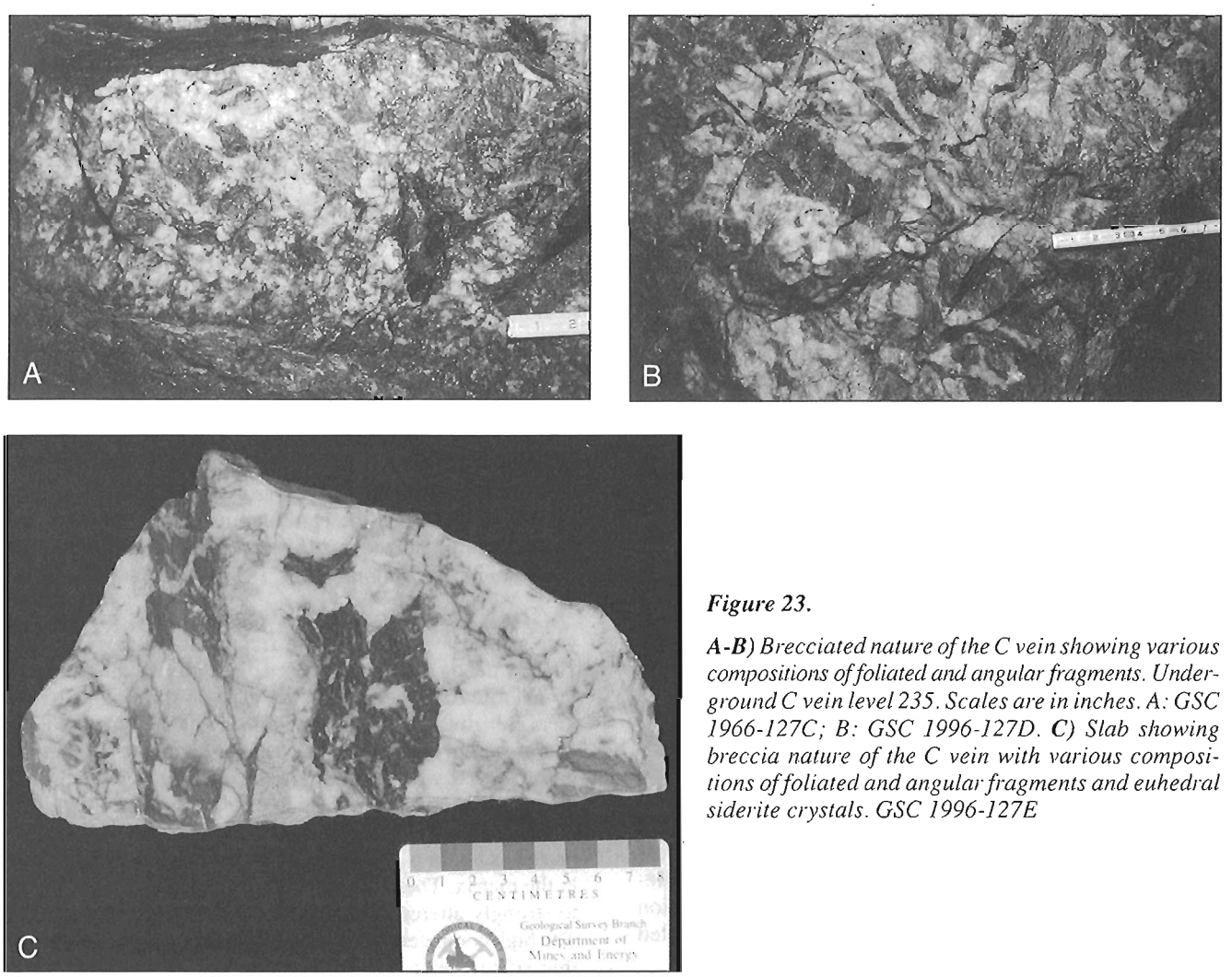

Figure 23.

A-B) *Brecciated nature of the C vein showing various compositions of foliated and angular fragments. Underground C vein level 235. Scales are in inches. A: GSC 1966-127C; B: GSC 1996-127D.* ***C)*** *Slab showing breccia nature of the C vein with various compositions of foliated and angular fragments and euhedral siderite crystals. GSC 1996-127E*

Figure 24. Photograph showing thickening of the C vein in the nose of the sub-horizontal fold in cross-section view. Underground C vein, level 235. GSC 1996-127F

recrystallization of the more ductile galena and chalcopyrite, shattering of pyrite and arsenopyrite, and remobilization of sphalerite (Wilton, 1983a). Microprobe analyses of 13 gold grains indicate that they contain more than 20% Ag and thus correspond to electrum (Wilton and Strong, 1986). Electrum occurs as minute grains intergrown with pyrite, chalcopyrite, galena, and sphalerite, or as solitary grains disseminated through the quartz vein in regions of sulphide concentration (Wilton, 1983a). Native gold found free in quartz and native silver as inclusions in calcite were reported by J.A. McLeod (unpublished report for Dolphin Explorations Ltd., 1988).

Chemical characteristics of mineralized zones

Metallurgical test work by Lakefield Research on a representative sample from the Cape Ray gold deposit gave the following results: 13.4 g/t Au, 30.8 g/t Ag, 0.24% Cu, 1.41% Pb, 1.04% Zn, 5.01% Fe, 0.28% S, and 2.17% C (Dolphin Explorations, unpublished report, 1991). This clearly reflects the abundance of base metals and the higher proportion of Ag compared to Au in the mineralized zones.

Geochemical analyses of 83 samples from the three lodes of the Cape Ray gold deposit-Main zone are presented in Table 4. All the samples but the last six are 0.5 to 1 m wide intersections of quartz veins with variable amounts of wall rock fragments. The others are grab samples of quartz from surface or drillholes. The analyses confirm the high proportion of sulphides with up to 1.5% Cu (mean: 2170 ppm), 63.8% Zn (mean: 13 300 ppm), and 23% Pb (mean: 8850 ppm) as well as anomalous arsenic and molybdenum. Wilton and Strong (1986) also reported very high base metal content in the mineralized zones. Scatterplot diagrams illustrate the high Ag, Pb, and Cu contents of the mineralized zones but do not indicate any positive correlation between the silver or base metal content with gold (Fig. 25). The Au:Ag ratio varies from 1:100 to 40:1 with an average of 1:2.25 if one exceptionally high ratio is removed (ratio 39.13:1, analyses 70376, Table 4). That sample contains visible gold. On

Table 3. Precious metal content of channel samples from underground work, A vein, No 41 zone (from R.W. Arnold, unpublished report for Dolphin Exploration Ltd., 1988).

Sample number	width (m)	Au (g/t)	Ag (g/t)
32386	0.6	22.6	149.0
32387	0.7	28.5	114.0
32388	0.3	1.6	8.6
32389	0.2	2.0	7.2
32390	0.8	8.5	52.5
32391	0.2	0.4	0.7
32391	0.6	0.9	4.5
44530	0.5	11.6	42.5
44531	0.6	51.0	110.0
44532	0.8	1.0	7.2
44533	0.6	6.1	122.0
44534	0.6	13.9	106.6
44535	0.3	25.5	91.9
44536	1	1.5	20.9
44537	0.4	8.4	114.2
44538	0.6	27.9	238.3
44539	0.62	9.5	25.0

the ternary diagram of Au-Ag-base metals (Poulsen, 1996) samples from the Main zone deposit fall in the field of epihermal gold deposits but show a wide distribution (Fig. 26B). High levels of arsenic commonly accompany gold-related carbonaceous lithologies (Wilson and Rucklidge, 1987). Although the number of determinations is limited, the overall level of arsenic is rather low for such vein-type gold mineralization.

Conclusion

In summary, the emplacement of mineralized quartz veins within the graphitic schist close to the tectonic boundary with the retrograded Grand Bay Complex is related to high angle reverse faulting along the Cape Ray Fault Zone and to the rheology and composition of the host graphitic schist.

The breccia texture of the mineralized veins most probably results from a sudden decompression of a supralithostatic gold-bearing silica-rich fluid resulting in fracturing and brecciation of the graphitic host. The mineralized zones define steeply east-southeast to southeast-plunging oreshoots, resulting from the combination of lithological and structural controls. As typically found in mélange-hosted or sedimentary rock-hosted lode gold deposits (e.g. Peters et al., 1990; Peters, 1993), the mineralized zone at the Cape Ray gold deposit is composed of a complex mixture of mineralized and barren quartz, gouge, fault rocks and wall rock fragments showing a complex chronology.

Table 4. Geochemical analyses of the mineralized veins from the Main zone of the Cape Ray gold deposit. (unpublished data from Dolphin Explorations Ltd.).

Analysis	Drillhole	Cu (ppm)	Zn (ppm)	Pb (ppm)	Au (ppm)	Ag (ppm)	Cu+Pb+Zn	Au/Ag	As (ppm)	Mo (ppm)
80034	PB-89-344	300	250	500	1.029	3.430	1050	0.30		
80007	PB-89-344	2500	>10 000	>10 000	2.057	109.700	22 500	0.02		
80010	PB-89-344	1350	2300	5500	1.714	20.570	9150	0.08		
80011	PB-89-344	900	550	7500	5.829	47.990	8950	0.12		
80013	PB-89-344	1900	1600	5300	1.714	13.710	8800	0.13		
80014	PB-89-344	>10 000	2300	10 001	12.343	137.000	22 300	0.09		
80015	PB-89-344	3200	>10 000	>10 000	8.571	92.570	22 200	0.09		
80016	PB-89-344	>10 000	2200	>10 000	5.143	366.860	27 000	0.01		
80017	PB-89-344	7000	>10 000	>10 000	10.971	243.400	27 000	0.05		
80020	PB-89-344	7000	900	3800	10.629	27.430	11 700	0.39		
80021	PB-89-344	1200	175	1000	2.057	10.300	2375	0.20		
80024	PB-89-344	750	180	1300	1.714	3.400	2230	0.50		
80042	PB-89-344	7000	850	5700	14.743	41.100	13 550	0.36		
67329	PB-89-328	2500	4500	>10 000	4.800	17.100	17 000	0.28		
67341	PB-89-328	3200	170	900	4.457	27.400	4270	0.16		
67354	PB-89-328	120	80	480	6.514	13.700	680	0.48		
70675	PB-89-351	220	490	620	1.783	3.400	1330	0.52		
70676	PB-89-351	120	280	320	1.234	3.400	720	0.36		
70677	PB-89-351	6400	>10 000	>10 000	41.486	106.300	26 400	0.39		
69609	PB-89-339	6500	>10 000	>10 000	34.629	65.000	26 500	0.53		
60610	PB-89-339	2900	>10 000	>10 000	26.057	31.000	22 900	0.84		
69611	PB-89-339	120	500	1000	2.160	3.400	1620	0.64		
70604	PB-89-349	440	5300	2700	3.771	6.800	8440	0.55		
70605	PB-89-349	7000	>10 000	>10 000	30.857	103.000	27 000	0.30		
70606	PB-89-349	2600	2900	5000	10.286	34.000	13 100	0.30		
69698	PB-89-340	130	3100	2200	1.543	3.400	5430	0.45		
69699	PB-89-340	74	96	200	1.371	3.400	370	0.40		
69701	PB-89-340	600	>10 000	>10 000	6.171	17.000	20 600	0.36		
69558	PB-89-335	1400	>10 000	>10 000	11.314	13.700	21 400	0.83		
69559	PB-89-335	219	1200	3900	2.331	6.900	5319	0.34		
69487	PB-89-335	270	900	1650	8.914	6.900	2820	1.29		
69421	PB-89-330	1050	1600	3900	1.714	13.700	6550	0.13		
69423	PB-89-330	385	1400	1150	1.131	3.400	2935	0.33		
70428	PB-89-346	4300	1700	3500	1.886	20.600	9500	0.09		
70443	PB-89-346	75	48	120	1.783	3.400	243	0.52		
70452	PB-89-346	175	450	1500	1.714	3.400	2125	0.50		
70453	PB-89-346	750	2300	2600	4.457	3.400	5650	1.31		
70454	PB-89-346	9500	>10 000	>10 000	1.337	92.600	29 500	0.01		
70455	PB-89-346	500	157	1200	1.234	3.400	1857	0.36		
70456	PB-89-346	3200	260	>10 000	14.400	58.000	13 460	0.25		

Analyses carried out by Dolphin Exploration Ltd., except as noted.
*Analyses done at XRAL Laboratories

Analysis	Drillhole	Cu (ppm)	Zn (ppm)	Pb (ppm)	Au (ppm)	Ag (ppm)	Cu+Pb+Zn	Au/Ag	As (ppm)	Mo (ppm)
70470	PB-89-346	400	700	730	3.086	3.400	1830	0.91		
70471	PB-89-346	300	115	1400	3.771	3.400	1815	1.11		
70486	PB-89-347	2900	80	1650	1.474	20.600	4630	0.07		
70508	PB-89-347	36	150	320	1.166	6.900	506	0.17		
70509	PB-89-347	100	100	210	3.154	3.400	410	0.93		
70526	PB-89-347	73	200	480	1.131	3.400	753	0.33		
70366	PB-89-345	500	118	1900	1.337	13.700	2518	0.10		
70376	PB-89-345	110	185	330	133.029	3.400	625	39.13		
70377	PB-89-345	46	70	62	4.800	3.400	178	1.41		
70382	PB-89-345	90	690	3700	1.851	20.570	4480	0.09		
70405	PB-89-345	350	110	310	2.297	3.400	770	0.68		
70409	PB-89-345	210	74	62	7.543	3.400	346	2.22		
70417	PB-89-345	205	120	530	1.131	3.400	855	0.33		
70423	PB-89-345	400	870	4800	4.800	3.400	6070	1.41		
70424	PB-89-345	105	88	450	3.771	3.400	643	1.11		
67439	PB-89-331	2500	2600	5500	2.023	31.000	10 600	0.07		
67446	PB-89-331	2600	1800	145	9.943	20.570	4545	0.48		
67447	PB-89-331	850	47	1250	1.714	13.700	2147	0.13		
67461	PB-89-331	910	2800	6500	7.886	58.300	10 210	0.14		
67467	PB-89-331	450	1300	>10 000	1.234	82.300	11 750	0.02		
67374	PB-89-329	360	110	2600	6.857	10.300	3070	0.67		
67411	PB-89-329	1300	1400	6600	8.229	20.570	9300	0.40		
67414	PB-89-329	2400	6000	>10 000	4.457	41.100	18 400	0.11		
67415	PB-89-329	140	140	140	3.189	3.400	420	0.94		
67605	PB-89-336	500	120	400	5.486	6.900	1020	0.80		
67606	PB-89-336	300	290	1300	1.611	13.700	1890	0.12		
67607	PB-89-336	420	1400	4400	10.629	17.100	6220	0.62		
67608	PB-89-336	180	400	2000	2.434	3.400	2580	0.72		
70757	PB-89-353	2000	1900	1150	16.800	37.700	5050	0.45		
70758	PB-89-353	570	850	1100	1.440	3.400	2520	0.42		
70785	PB-89-353	2200	215	950	3.429	13.700	3365	0.25		
67688	PB-89-338	7300	1000	6100	49.371	281.000	14 400	0.18		
67563	PB-89-334	8400	>10 000	>10 000	14.400	113.000	28 400	0.13		
67566	PB-89-334	800	2500	1800	15.086	6.900	5100	2.19		
67572	PB-89-334	2500	1400	>10 000	1.714	41.100	13 900	0.04		
69943	PB-89-341	550	1250	2000	4.114	10.300	3800	0.40		
70318	PB-89-343	2700	>10 000	>10 000	5.829	17.100	22 700	0.34		
BD-288-91*	trench	1180	16 400	18 300	13.200	30.000	35 880	0.44	5000	3000
BD-415-89*	PB-89-35	15 771	752	1878	59.000	129.000	18 401	0.46	226 000	45 000
BD-445-89*	PB-89-19	105	128 523	72 642	8.840	147.000	201 270	0.06	51 100	1000
BD-447-89*	PB-89-19	509	103 179	35 344	9.470	119.000	139 032	0.08	64 900	12 900
BD-450-89*	PB-89-19	39	28 929	52 256	15.700	91.400	81 224	0.17	11 300	2110
BD-471-89*	PB-89-19	9037	637 903	239 324	1.960	153.000	886 264	0.01	9660	164 000

Analyses carried out by Dolphin Exploration Ltd., except as noted.
*Analyses done at XRAL Laboratories

Based on available information and poor exposure, the relative timing of the gold-mineralizing events is difficult to constrain. The wall rock fragments incorporated within the breccia veins contain a penetrative fabric attributed to S_{3a} or S_{3b} implying that the quartz was introduced after or during the development of the main ductile regional fabric. Surface exposures indicate that quartz veins, similar to the A and C veins, and hosted by the graphitic schist unit, are folded by the F_5-F_5' folds. Thus, the mineralized veins are syn- to late-D_3 and pre-D_5.

The veins are base metal rich and have a low Au:Ag ratio.

Geology of the Big Pond showing

Introduction

The mineralization at Big Pond occurs in sulphide-rich quartz veins that cut a tightly folded sediment-dominated sequence of the Windsor Point Group. The showing is situated in the widest part of the volcano-sedimentary sequence, less than 500 m from the contact between the Windsor Point Group and Grand Bay Complex rocks (Fig. 12). As at the Cape Ray gold deposit, the contact between these two units is interpreted as a high angle reverse fault. At Big Pond, however, thrust-related folding was superimposed on initial reverse shearing while shearing was ongoing along most of the fault zone. This folding is believed to result from less shortening in this portion of the belt. The lack of outcrop, however, makes the exact positioning of the contact difficult.

Windsor Point Group lithologies include complexly folded sedimentary rocks and felsic volcanic rocks characterized by a bedding-parallel foliation (S_{3a}) that is folded about a north-northeast to northeast axial plane cleavage (S_{3b}). Grand Bay Complex rocks comprise highly folded metapelites and psammites that exhibit complex interference patterns defined by an intense fabric and foliation parallel to quartz veins (S_{1-2}), an indication that their deformational history was more complex than that of the Windsor Point Group. The late tectonic, mid-Devonian Isle aux Morts Brook Granite has produced an amphibolite grade metamorphic aureole overprinting regionally deformed Windsor Point Group and Grand Bay Complex rocks.

Nature of the host rocks

The main lithological units in the area are: 1) black graphitic schists, 2) carbonate-rich sericite and/or biotite schists, 3) banded rocks composed of millimetre- to centimetre-wide, white and green layers derived from metasediments, and green chlorite schists, derived in part, from gabbroic rocks and in part from mafic sediments. Fine-grained quartz and quartz-feldspar porphyries, probably related to Windsor Point Group felsic volcanic rocks, are also present. Mylonites occur locally, but represent an insignificant proportion of exposed rocks in the area.

The mineralized zone is located on the long limb of an asymmetric, S-shaped fold deforming Windsor Point Group units (Fig. 27A, B) and an earlier bedding-parallel foliation

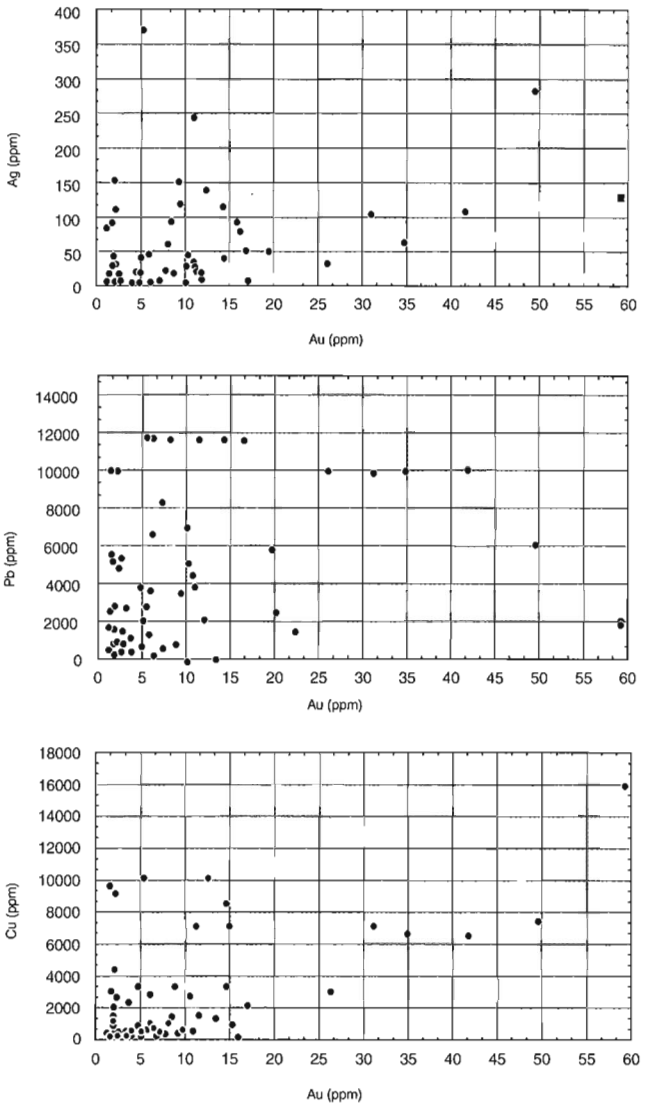

Figure 25. *Variations of Ag, Pb, and Cu with Au in the Cape Ray gold deposit.*

that is correlated with the regionally developed S_{3a} fabric. A cross-section in the hinge area of the fold, from south to north, shows: 1) a highly banded unit, 2) a mafic gabbro, 3) a thin unit of carbonate-rich sericite-biotite schist, 4) graphitic schist, 5) sericite schist, and 6) sericite±biotite schist; the last two are rich in calcite (Fig. 28). These units are briefly described below. In many drillholes and in the trenches, one or more units is missing. It is common for the graphitic schist to structurally overlie the chlorite schist, the carbonate-rich sericite±biotite schist unit being absent. The mineralized quartz vein is slightly discordant to lithological contacts, and commonly occurs at the chlorite and graphitic schist interface (Fig. 27). The chlorite schist generally forms the footwall of the mineralized zone, and the graphitic schist the hanging wall. In certain drillholes, however, the vein is completely hosted in graphitic schist, and in others it occurs in sericite-biotite (and/or chlorite) schist, adjacent to the chlorite schist.

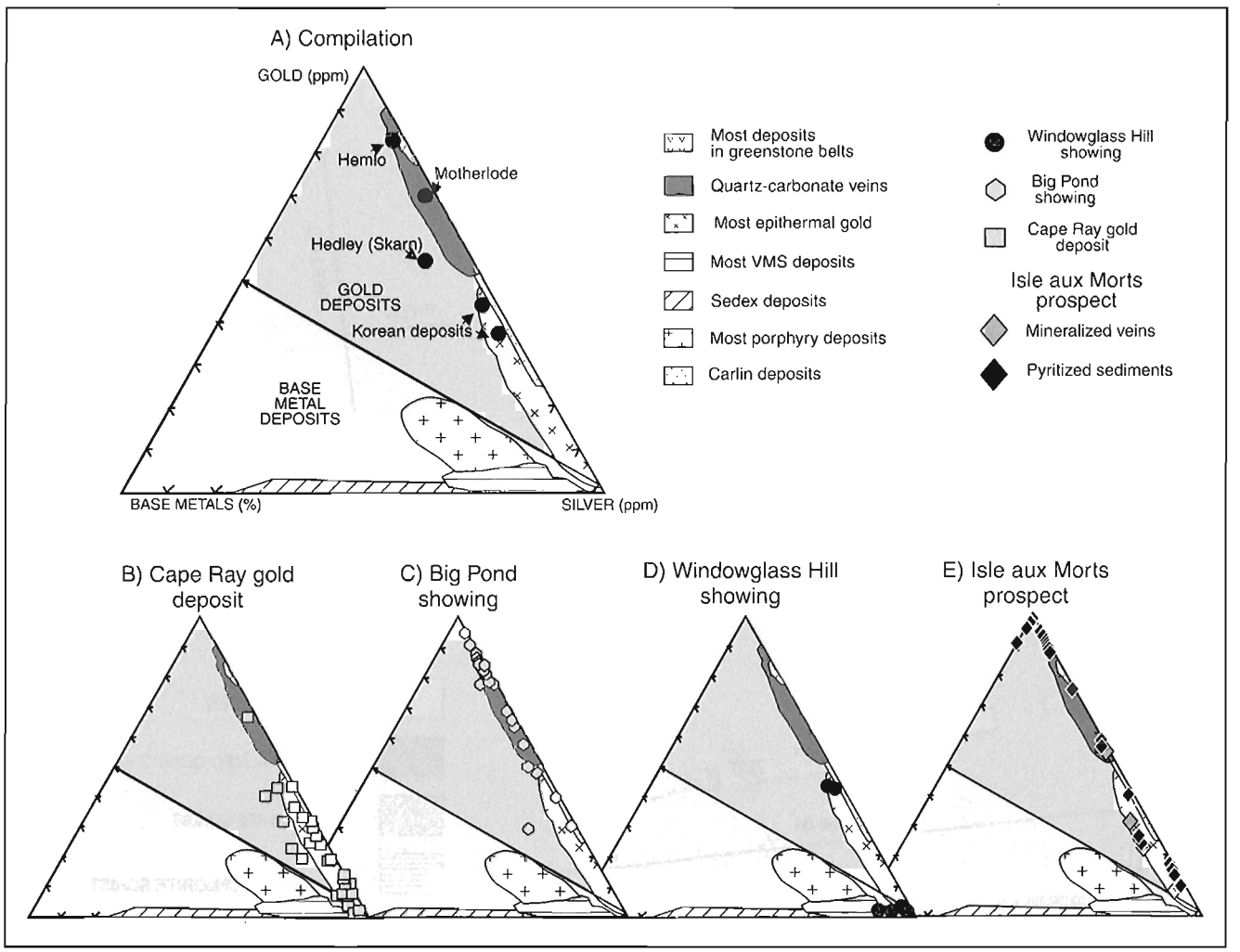

Figure 26. *Ternary diagrams of Au-Ag-base metals (Poulsen, 1996).* ***A)*** *plots for various gold deposits.* ***B)*** *Position of the Cape Ray gold deposit mineralized samples relative to those shown in A.* ***C)*** *Composition of the Big Pond showing mineralized samples relative to those shown in A.* ***D)*** *Composition of the Windowglass Hill showing mineralized samples relative to those shown in A.* ***E)*** *Composition of the Isles aux Morts prospect mineralized samples relative to those shown in A.*

Chlorite schist

Chlorite schist is the term used in Dolphin Explorations drill core logs to describe both homogeneous chlorite schists derived from gabbroic rocks, adjacent to the mineralized zone, as well as highly banded units derived from sedimentary rocks and located farther in the footwall. As these two units were not distinguished in drill core logs, sections of the mineralized zone (Fig. 28) present undifferentiated chlorite schist. No intercalations of graphitic schist are recognized in this unit.

The more homogeneous chlorite schist unit is approximately 3 m thick. It is composed mainly of pale green chlorite, feldspar, quartz, epidote, ±amphibole, and abundant leucoxene. These rocks vary from relatively undeformed to strongly foliated and even mylonitic. The highly banded unit, also described as silicified chlorite schist in drill core is in fact best described as a quartz, muscovite, chlorite±biotite schist. These rocks are composed mainly of muscovite-rich bands with abundant leucoxene and magnetite, epidote and relict greenish amphibole alternating with quartzofeldspathic layers containing chlorite and epidote. In the trenches, this unit was mapped as the highly banded unit (Fig. 27). This compositional layering corresponds to bedding, which is transposed by the main tectonic fabric.

Graphitic schist

Graphitic schists are best exposed in the immediate area of the showing. They are commonly intercalated with chlorite±biotite-sericite, chlorite-biotite and chlorite schists, and vary in thickness from a few metres to over 17 m. The graphitic schists are highly banded as a result of alternating graphitic-rich and quartz±muscovite-rich layers and because

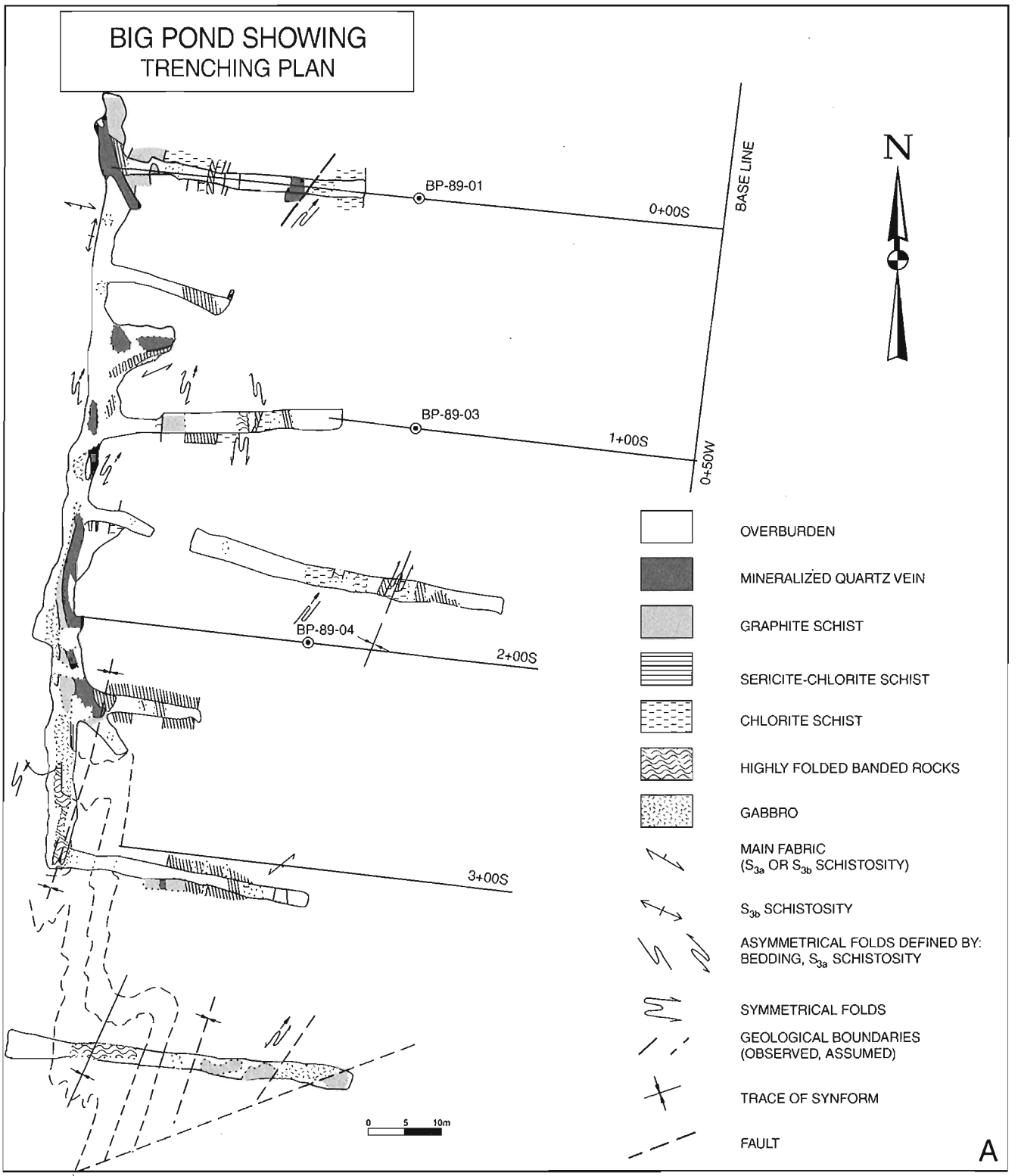

Figure 27. *A) Geological map of the Big Pond showing, illustrating the distribution of the main lithological units.* ***B)*** *Compilation on equal area projections (lower hemisphere) of the structural elements measured at the Big Pond showing.*

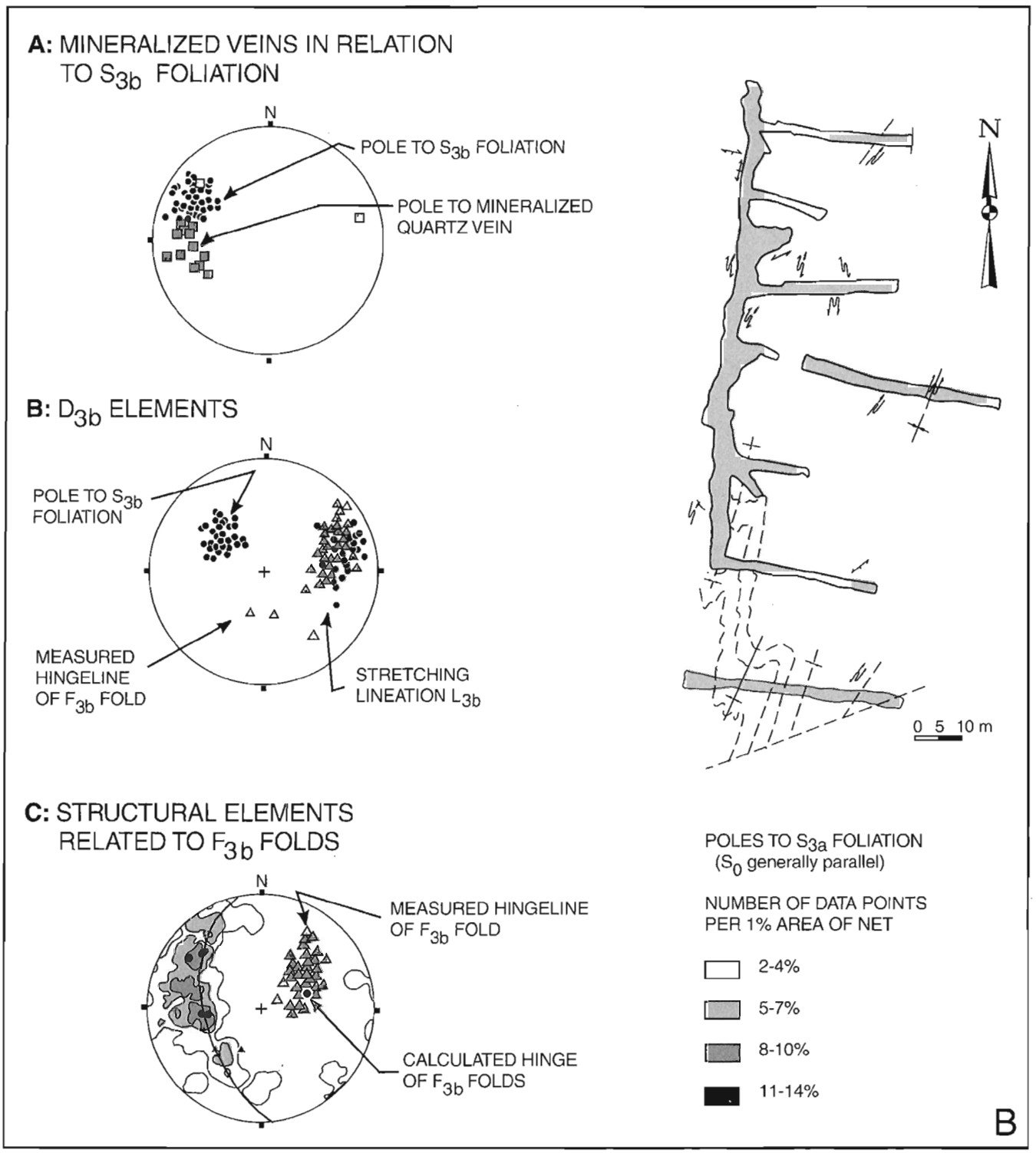

Figure 27. (cont.)

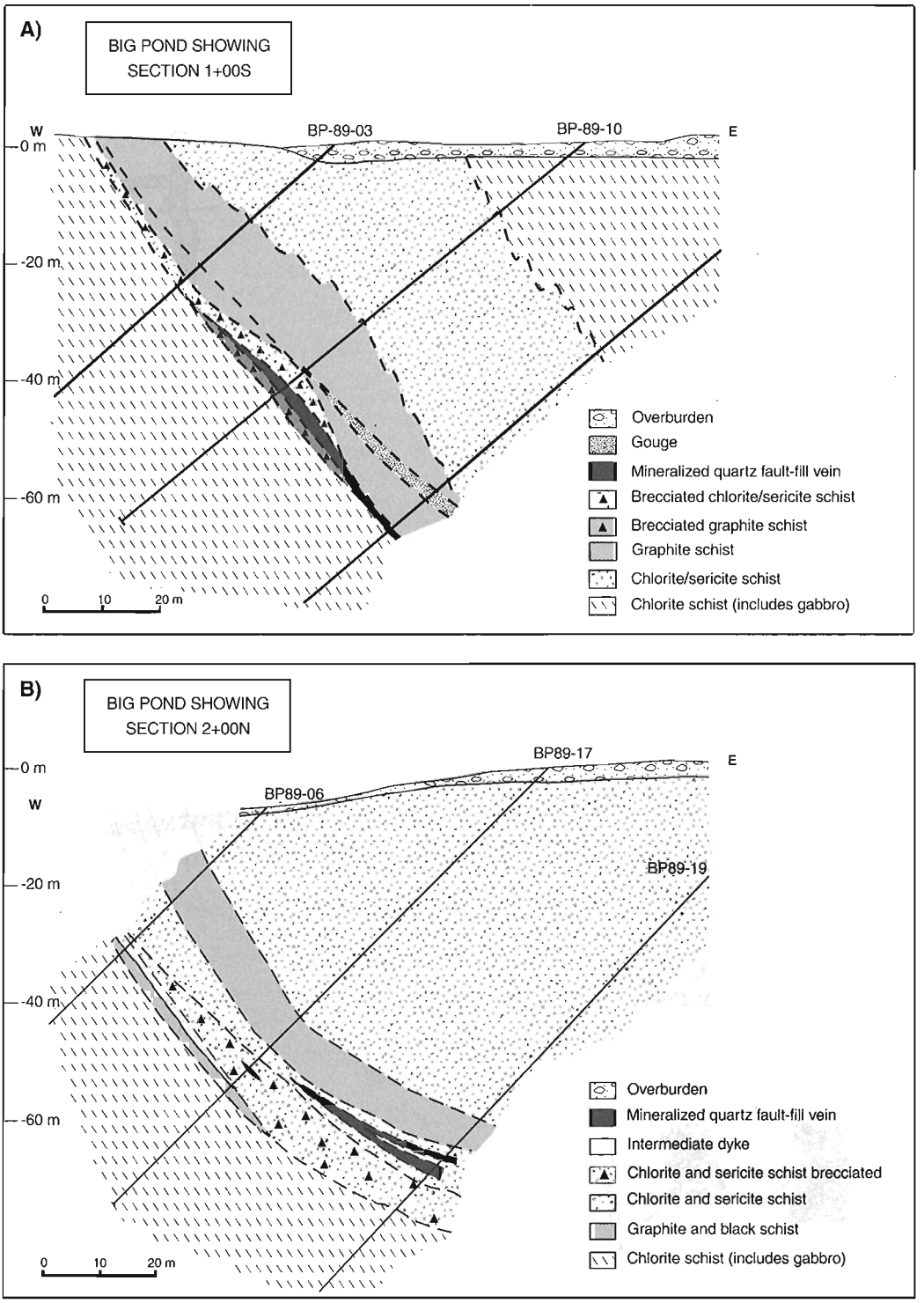

Figure 28. *A) Cross-section 1+00 S at the Big Pond showing.* ***B)*** *Cross-section 2+00 N at the Big Pond showing. Modified from unpublished diagrams by Dolphin Explorations.*

of numerous foliation-parallel quartz and quartz-calcite veinlets that form up to 50% of the rock. Folding is developed throughout the sequence, however the degree of folding increases and the graphitic schist becomes contorted, chaotically folded, and brecciated towards the mineralized veins. Graphitic gouge occurs locally, the widest (30 cm wide), and best developed example, was in the trenches, adjacent to the mineralized vein. The gouge contains mineralized quartz fragments, as well as cataclastically deformed pyritic fragments indicating that gouge development postdates, at least in part, the mineralizing event.

Carbonate-rich sericite-chlorite±biotite and biotite schists

Sericite-biotite(chlorite) and biotite schists structurally overlie and are intercalated with graphitic schists. They are generally carbonate rich, with calcite locally forming up to 70% of the rock. On average, the proportion of carbonates is around 40%. These rocks are beige, buff to brownish. They are composed of millimetre-scale layers rich in muscovite-sericite riddled with stretched opaques. The opaques are composed of elongate aggregates of leucoxene and/or of deformed chalcopyrite±pyrite, alternating with carbonate-rich layers and biotite-carbonate layers. The carbonates are generally recrystallized and equant. Although these rocks are termed carbonatized sericite-chlorite schists in drill core logs, chlorite is never abundant. Biotite is responsible for the darker colour of these rocks. The more biotite-rich schists are termed "brown unit" in drill core logs and are analogous to the chlorite-biotite-magnetite schist present in the hanging wall of the Cape Ray gold deposit. These schists are commonly intercalated with graphitic-rich or quartz- and feldspar-rich layers.

Structure of the deposit

The Big Pond showing is relatively well exposed in a number of trenches adjacent to the eastern shore of Big Pond and in several outcrops south and east of the lake. Folding is the dominant structural feature of this area. There are two main episodes of folding that together cause the complex distribution of stratigraphic units in the area. They are correlated with the D_3 deformation event recognized regionally which includes F_{3a} and F_{3b} folding and associated S_{3a} and S_{3b} fabrics (Dubé and Lauzière, 1996a). Both asymmetrical sinistral and dextral folds occur, but in the immediate vicinity of the mineralized zone the main structural feature is a 50 m scale sinistral F_{3b} fold defined by stratigraphic units and by the S_{3a} fabric (Fig. 27A, B). This S_{3a} fabric, associated with a first folding episode in Windsor Point Group rocks, is commonly penetrative and parallel to bedding. It corresponds to a compositional layering, i.e. quartz-rich and/or muscovite-rich layers, or to a shape oriented fabric, defined by oriented micas and/or by stretched opaque minerals. Angular relationships between the S_{3a} and bedding are locally preserved. This fabric is folded in turn about a north-northeast- to northeast-oriented, northeast-plunging F_{3b} fold, responsible for most of the mesoscopic folding in the area. The average orientation of the S_{3a} fabric on the long limb of the asymmetric S-shaped fold is 019°/65° and on the short limb is 060°/80° (Fig. 27B).

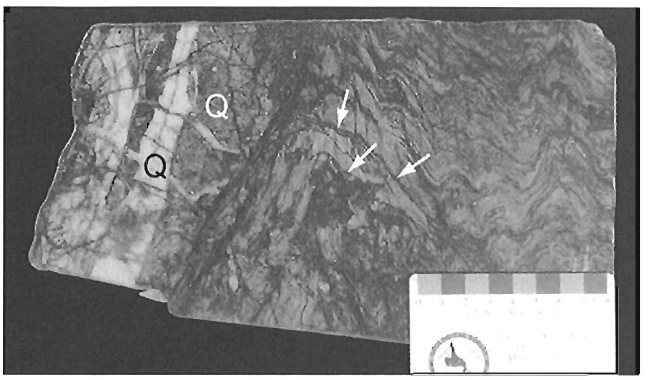

Figure 29. *Wide mineralized quartz vein from Big Pond showing comprising two generations of quartz (Q), an earlier dark grey quartz cut by white quartz veins. Small, dark grey, gold-bearing quartz veinlets (shown by arrows) are folded. GSC 1996-128A*

The intensity of deformation related to the F_{3b} folding event is variable, from that of folding without development of an axial planar cleavage to a composite S_{3a}-S_{3b} fabric in the schist units, producing the layering parallel to the axial surface and anastomosing textures commonly observed in the biotite- and/or chlorite-sericite schists. The orientation of the S_{3b} cleavage varies; this is attributed to fanning of the axial planar cleavage. The average orientation of the axial planar cleavage is 029°/65° which is at an angle with the overall orientation of the Cape Ray Fault Zone. The mean orientation of fold axes is 059°/54°. Mylonitic fabrics associated with this deformation episode were recognized only in the most northerly trench. There, CS-type fabrics suggest reverse movement. Stretching lineations (L_3) are poorly developed throughout the area. Where observed, they plunge on average 50° towards 067°, subparallel to F_{3b} fold hinges. No other major folding episode is recognized in the immediate area of the Big Pond showing, although in thin section, in the more micaceous units, a crenulation cleavage overprints the S_{3b} fabric. It is generally at a 40 to 50° angle to the S_{3b} fabric and could be equivalent to S_5-S_5' recognized at the regional scale.

Late brittle deformation is registered as striated slip planes and millimetre- to centimetre-wide gouge seams. These occur mostly in the graphitic schist but are also present in chlorite schist.

In comparison to other areas along the Cape Ray Fault Zone, deformation in the Big Pond region appears to have been less intense. Angular relationships between bedding/cleavage and S_{3a} and S_{3b} fabrics suggest that these rocks have not been subjected to the same history of deformation as rocks of the Cape Ray gold deposit area. The thickness of the volcano-sedimentary sequence in the Big Pond area and the angle between the S_{3b} foliation and the Cape Ray Fault Zone suggest that shortening was not as significant as in narrower parts of the belt (Fig. 12). The development of tear faults, on either side of the Big Pond area, could be responsible for the preservation of this area from intense shearing and shortening in the later phases of the D_3 increment of deformation.

Mineralization

Detailed mapping at the Big Pond showing, in addition to drillhole data, indicates that the best-mineralized segments of the Big Pond structure occur in two oreshoots, both located on the long limb of the asymmetric S-shaped F_{3b} fold (Fig. 27A). The oreshoots are slightly oblique to contacts and occur mostly at the mafic gabbro/graphitic schist contact (see Fig. 27, 28). The mineralized vein system is oblique to both S_{3a} and S_{3b}. Towards the south, the mineralized zone ends where the lithological units are asymmetrically folded and displaced sinistrally. There, the vein is thickened and its outline describes a hook, suggesting that the vein may also have been affected by F_{3b} folding. A more definite indication that the mineralization is affected by the F_{3b} folding is the presence of gold- bearing quartz veinlets, at a high angle to and folded by F_{3b} folding (Fig. 29).

Veins

As at the Cape Ray gold deposit, the mineralized structure is a complex tabular zone, up to 5 m wide. The longitudinal section shows that the two oreshoots dip steeply to the northeast as do F_{3b} hinges (Fig. 30). The oreshoots are known to extend more than 90 m at depth and 50 m on strike. The mineralized zone typically includes one or more of the following zones: 1) a brecciated zone composed of 2 to 70% quartz veinlets injected in graphitic and/or biotite-sericite schists resulting in a stockwork or breccia vein texture (Fig. 31A); this zone varies in width from 0 to 5 m (Fig. 27, 28); 2) a more massive quartz breccia vein up to 4 m wide, located on either side of the brecciated zone (Fig. 31B-C); and 3) a graphitic gouge containing small rounded millimetre- to centimetre-scale fragments of mineralized quartz (Fig. 31D). The gouge is a local feature, associated with the mineralized vein on either side of it, or on strike in its extension. The proportion of gouge is, however, overall insignificant. No intense fabric was recognized adjacent and parallel to the vein, although the graphitic schist in the hanging wall of the mineralized structure commonly exhibits what is described in drillhole logs as chaotic folding. This structure is probably related to the brittle behavior of the graphitic schist. Folding also increases near the vein in the Big Pond trenches. Lower grade breccia quartz veins and fault gouge occur between and beyond the oreshoots.

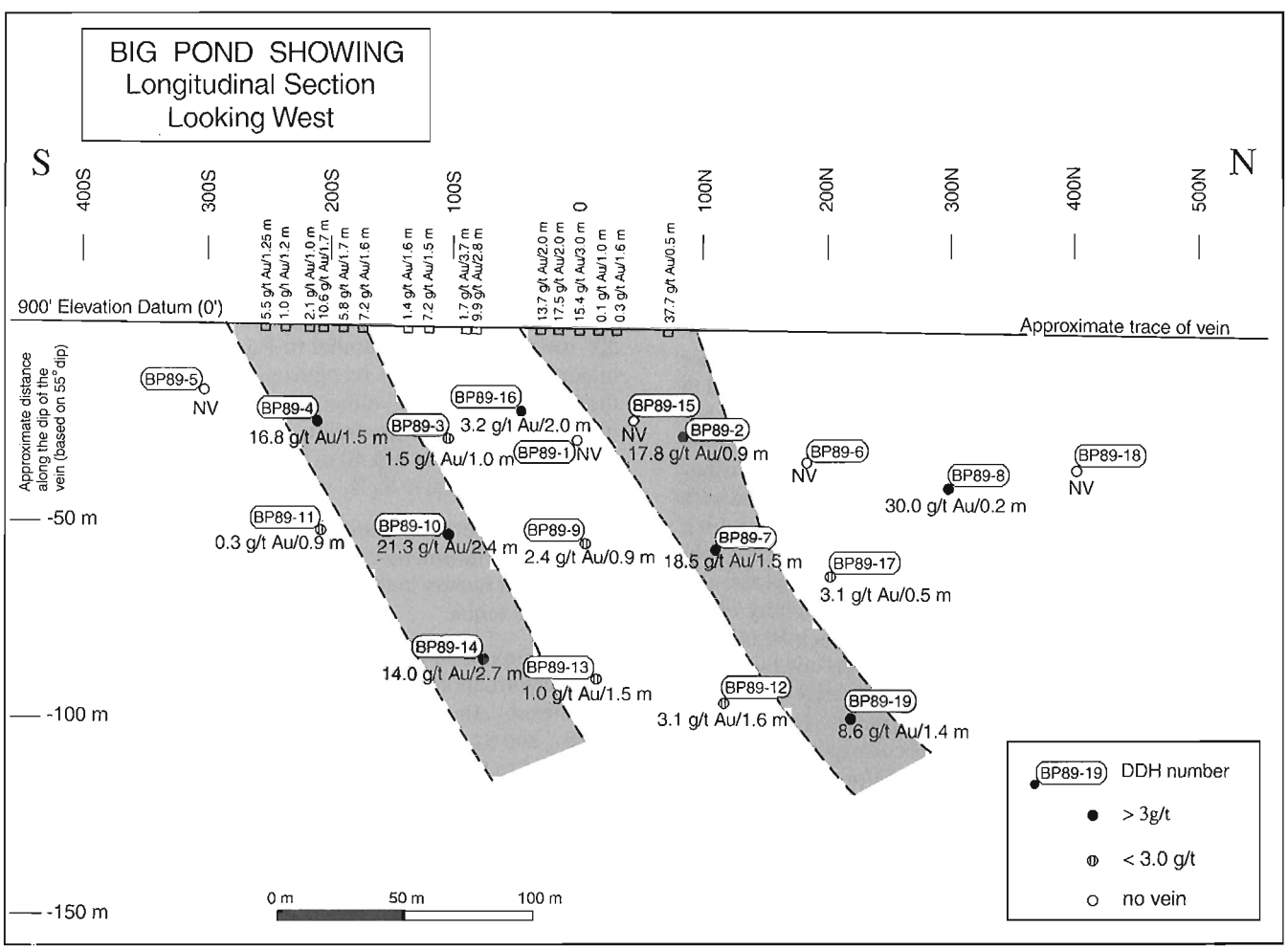

Figure 30. *Longitudinal section of the Big Pond showing. Modified from an unpublished diagram by Dolphin Explorations.*

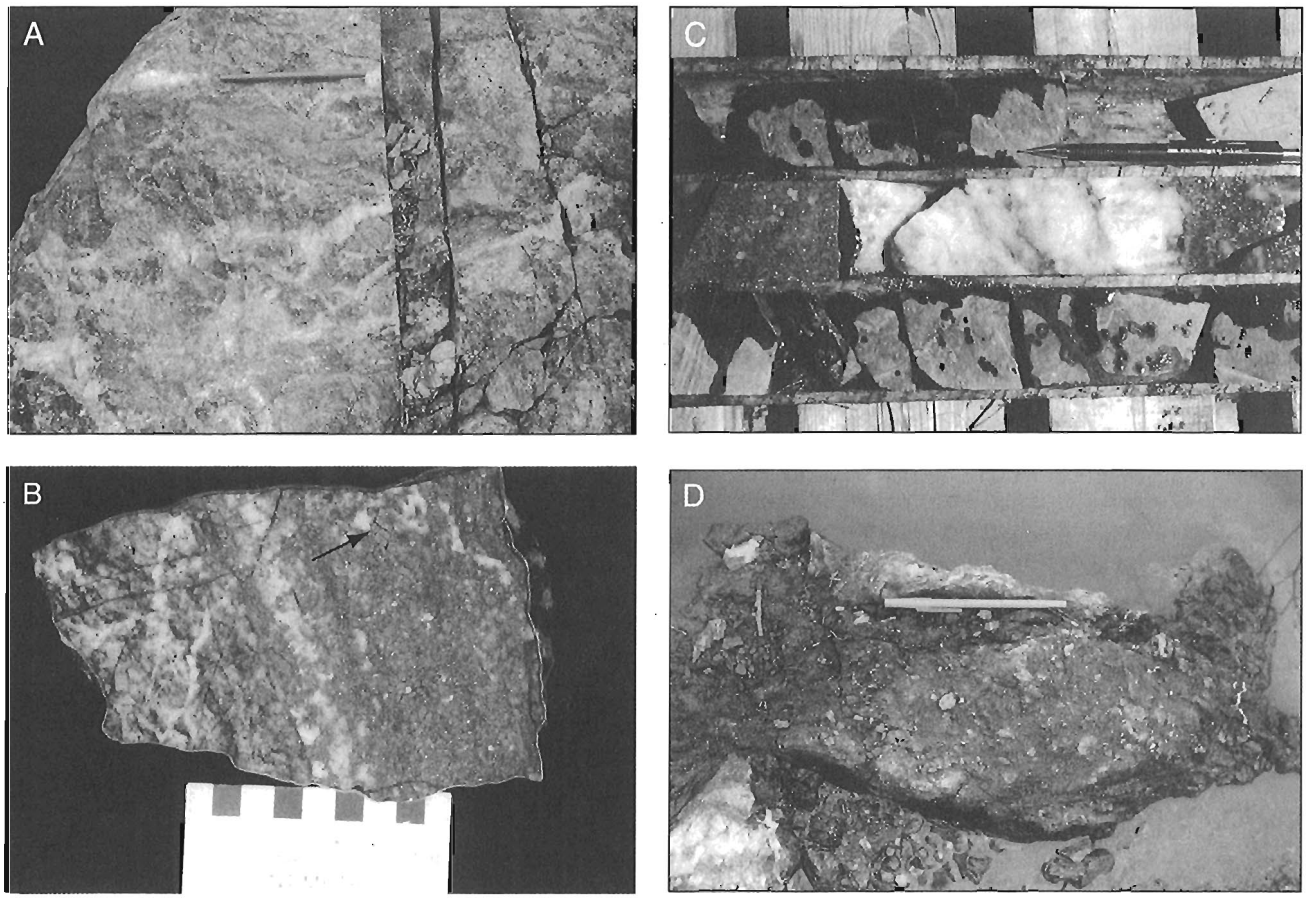

Figure 31. *Various components of the mineralized zone at Big Pond.* ***A)*** *Breccia quartz vein emplaced within highly strained sericite schist. GSC 1996-128B.* ***B)*** *Laminated aspect of the Big Pond quartz vein suggested by near massive pyrite aggregates and veinlets and wall rock slivers. Note the cataclasis of the larger pyrite crystals. GSC 1996-128C.* ***C)*** *Massive quartz vein with pyrite-rich bands on either side of barren quartz. GSC 1996-128D.* ***D)*** *Graphitic gouge at Big Pond showing angular fragments set in a graphitic matrix. GSC 1996-128E*

Figure 32. *Laminated quartz-pyrite vein with veinlets of near massive pyrite. The arrow points to one such veinlet. GSC 1996-128F*

Most of the mineralization occurs in a stockwork arrangement of veins or in a quartz breccia vein. Vein borders are generally difficult to define because of a progressive increase in the proportion of veining. The brecciated aspect of the quartz vein is produced by numerous foliated and unfoliated chloritic zones, by centimetre-scale angular chlorite- and carbonate-rich fragments, as well as intensely foliated sericite schist fragments. In certain parts of the vein, the presence of near-massive pyrite bands, host rock slivers and variable coloured quartz bands, produced by deformation, confer a laminated aspect to the vein (Fig. 32). Locally the vein includes subrounded fragments of nearly massive pyrite, up to 5 cm in diameter, probably produced by brecciation of the more sulphide-rich portions (Fig. 33). Overall the mineralized quartz vein(s) is best described as a fault-fill vein (Robert et al., 1994).

Table 5. Chemical analyses showing the composition of various units of the Big Pond showing based on samples from drillhole BP-89-04.

	Drillhole BP-89-04									
Sample	90BD-204	90BD-206	90BD-207	90BD-210	90BD-212*2	90BD-215*2	90BD-217*2	DB-218 90*2	DB-219 90	DB-220 90*2
location (m)	29	37.5	43	52.5	65.8	80.5	92.4	95.4	98.2	101
lithology*1	A'	A'		A"	A"	A	A"	A"	A"	A'
SiO_2%	39.03	80.36	36.36	44.30	33.80	82.80	37.00	69.60	25.28	79.20
Al_2O_3%	13.38	8.83	16.30	14.47	15.80	6.02	15.54	12.67	12.20	6.62
TiO_2%	2.17	0.24	1.51	1.40	1.44	0.37	1.53	0.48	0.20	0.27
Fe_2O_3(t) %	9.91	1.65	8.18	8.65	4.19	2.09	10.30	3.10	2.35	3.16
MnO%	0.17	0.04	0.12	0.16	0.17	0.02	0.18	0.05	0.11	0.02
MgO%	3.91	0.44	5.06	4.85	2.72	0.72	4.27	1.99	2.35	0.62
CaO%	13.59	1.27	16.37	9.24	19.77	1.83	11.76	0.61	29.07	1.09
Na_2O%	2.39	2.49	1.34	0.55	2.35	0.58	1.30	0.22	0.00	0.14
K_2O%	2.89	1.39	3.39	3.20	2.86	1.70	3.76	3.83	3.16	2.08
P_2O_5%	0.43	0.06	0.34	0.37	0.26	0.15	0.28	0.09	0.29	0.08
LOI%	10.50	1.58	11.25	9.62	15.25	2.82	11.73	4.20	22.17	4.75
S%	0.98	0.05	0.04	2.60	1.15	1.17	1.89	1.34	0.49	2.19
CO_2%	8.85	0.71	10.50	6.27	13.90	1.11	8.11	0.34	21.60	0.67
H_2O+%	1.5	0.8	1.8	3.4	1.7	1.0	3.0	2.0	1.8	1.2
Total	99.20	98.33	101.31	99.46	100.11	99.56	98.92	96.32	98.90	97.34
	Metallic trace elements									
Cu (ppm)	60	8	18	22	19	49	39	15	24	35
Zn (ppm)	151	48	92	112	91	76	234	75	76	24
As (ppm)	697	11	156	342	83	205	586	28	91	17
Mo (ppm)	< 2	< 2	< 2	< 2	< 2	59	< 2	< 2	< 2	34
Ag (ppm)	< 10	< 10	< 10	< 10	< 10	< 10	< 10	< 10	< 10	< 10
Pb (ppm)	31	26	40	60	38	27	39	28	49	58
Au (ppb)	34	43	15	6	42	< 5	110	29	< 5	33
	Trace elements (ppm)									
Ba	1713	374	2810	1414	1445	806	1070	2042	888	497
Co	37	4	33	33	35	15	32	11	24	17
Cr	74	158	92	117	84	195	92	100	121	193
Cs	3.7	1.0	3.6	4.0	2.8	0.9	4.6	3.2	3.5	1.4
Hf	3.9	6.3	2.4	2.5	2.3	1.7	2.1	8	3.1	2.1
Nb	32	16	19	21	18	7	24	17	22	6
Ni	23	<5	19	12	23	62	19	7	17	45
Rb	86	51	91	85	60	37	100	99	74	59
Sb	0.8	0.5	0.5	0.8	0.4	0.4	0.6	0.7	0.5	2.9
Sc	28	8.4	24	22	22	8.3	22	14	22	7.9
Se	< 2	< 2	< 2	< 2	< 2	< 2	< 2	< 2	< 2	2.4
Sr	197	48	236	119	300	47	189	28	325	24
Ta	1.9	0.9	1.3	1.2	1.3	0.4	1.1	1.1	1.6	0.4
Th	3	11	1	2	1	4	1	15	2	5
U	1	3	< .5	2	2	15	< .5	4	2	14
V	302	9	226	221	187	399	238	65	197	102
W	9	2	6	7	5	3	3	3	3	4
Y	26	50	19	22	19	29	18	61	18	32
Zr	162	261	97	106	103	81	102	286	137	90
	Rare-earth elements (ppm)									
La	23	33	16	17	14	19	16	48	18	18
Ce	51	72	34	36	31	41	32	105	42	43
Nd	25	32	18	18	15	19	18	45	20	20
Sm	5.8	7.3	4.3	4.3	3.7	4.1	4.1	10	4.7	4.2
Eu	2	1.3	1.7	1.3	1.4	0.99	1.2	2.2	1.9	1
Tb	0.84	1.2	0.66	0.64	0.58	0.6	0.62	1.6	0.64	0.74
Yb	2.4	4.2	1.6	1.9	1.5	2	1.6	6.3	1.9	2.1
Lu	0.4	0.64	0.24	0.29	0.24	0.35	0.26	0.92	0.32	0.34
DENSITY	2.85	2.66	2.83	2.73	2.74		2.82	2.73	2.74	2.71

Analyses carried out at INRS-Georessources, except for H_2O and CO_2 done at XRAL Laboratories

*1 A: feldspar prophyry A': chlorite-muscovite schist A": quartzofeldspathic mylonite
B: chlorite-biotite-magnetite schist C: chlorite-calcite schist

*2 Analysis carried out at XRAL Laboratories

*3 : duplicate sample analyzed at XRAL Laboratories

	Drillhole BP-89-04							
Sample	DB-224 90	DB-225 90	DB-226 90	DB-227 90	DB-228 90	DB-230 90	SARM 4*2	90BD-206D*3
location (m)	114.3	118	123.6	142.8	148	163.7		37.5
lithology*1	A'	A'	B	B	C	C		A'
SiO_2 %	35.77	45.94	53.00	72.02	69.74	77.96	52.30	78.80
Al_2O_3 %	14.30	14.91	14.29	13.61	14.15	11.10	16.20	9.07
TiO_2%	2.18	1.46	1.37	0.46	0.48	0.38	0.19	0.26
Fe_2O_3(t) %	10.19	10.61	10.64	3.71	3.62	2.78	8.93	2.48
MnO%	0.27	0.20	0.18	0.07	0.08	0.04	0.19	0.06
MgO%	6.23	9.40	6.84	0.76	0.95	0.91	7.15	0.93
CaO%	14.31	6.65	2.55	2.21	3.52	1.85	11.60	1.26
Na_2O%	1.81	2.04	0.63	1.49	0.67	1.48	2.41	3.07
K_2O%	1.56	1.39	2.50	2.95	3.61	3.09	0.30	1.45
P_2O_5%	0.30	0.22	0.22	0.22	0.27	0.23	0.02	0.05
LOI%	13.01	5.32	6.58	3.10	4.22	1.90	0.47	1.31
S%	0.00	0.00	0.01	0.00	0.00	0.00	0.00	0.05
CO_2%	9.78	1.29	1.80	1.23	2.15	0.95	0.03	0.71
H_2O+%	4.0	4.1	5.1	1.8	2.2	1.2	0.1	0.8
Total	100.70	98.21	99.13	100.53	101.43	101.97	99.76	98.74
	Metallic trace elements							
Cu (ppm)		8	75	7	24	17		
Zn (ppm)		104	1298	70	59	34		
As (ppm)		4.2	2.2	2.2	2.3	2.5		
Mo (ppm)		< 2	< 2	3	2	< 2		
Ag (ppm)		< 10	< 10	< 10	< 10	< 10		
Pb (ppm)		195	1128	24	28	25		
Au (ppb)		26	49	< 5	6	< 5		
	Trace elements (ppm)							
Ba		587	1080	850	1362	493	128	
Co		52	48	5	5	3		
Cr		459	370	95	80	98		
Cs		1.7	2.4	2.7	3.4	3.2	24.0	
Hf		2.6	3.5	11	11	8.4		
Nb		11	8	20	19	17	11	
Ni		171	145	13	21	5		
Rb		78	139	150	171	120	18	
Sb		0.8	0.4	0.4	0.7	< .2		
Sc		31	28	11	11	8.4		
Se		< 2	4.1	< 2	< 2	< 2		
Sr		196	49	139	147	112	261	
Ta		0.7	0.9	1.5	1.5	1.1		
Th		1	4	17	18	14		
U		< .5	2	5	5	4		
V		258	276	14	18	6		
W		3	5	2	4	2		
Y		18	24	63	68	53	< 10	
Zr		108	144	422	429	348	< 10	
	Rare-earth elements (ppm)							
La	16	12	26	55	58	45		
Ce	39	28	56	121	129	97		
Nd	20	15	27	52	55	42		
Sm	5.3	3.7	5.9	12	12	9.5		
Eu	1.9	1.4	1.5	1.9	1.9	1.5		
Tb	0.69	0.57	0.81	1.9	1.9	1.4		
Yb	2.3	1.7	2.6	6	6.2	4.8		
Lu	0.35	0.26	0.38	0.89	0.96	0.73		
DENSITY	2.8	2.85	2.66	2.73	2.76	2.72		

Analyses carried out at INRS-Georessources, except for H_2O and CO_2 done at XRAL Laboratories

*1 A: feldspar prophyry A': chlorite-muscovite schist A": quartzofeldspathic mylonite
B: chlorite-biotite-magnetite schist C: chlorite-calcite schist

*2 Analysis carried out at XRAL Laboratories

*3 : duplicate sample analyzed at XRAL Laboratories

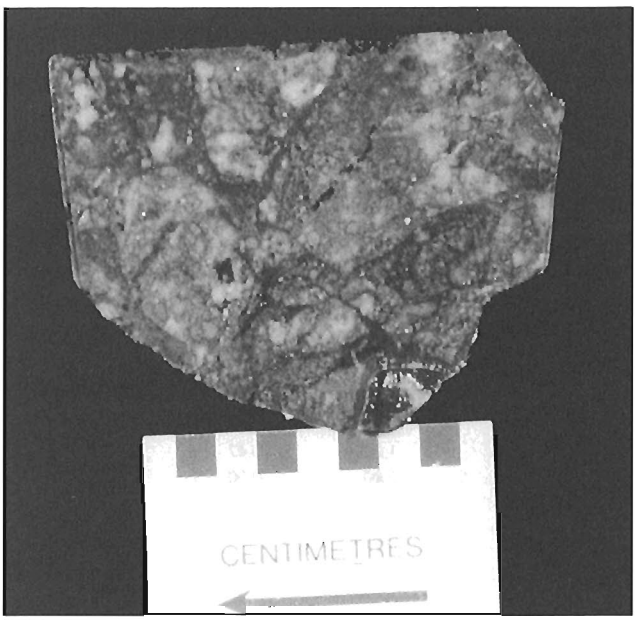

Figure 33. Subrounded fragments of near massive pyrite in the Big Pond vein. GSC 1996-128G

Alteration

Results of chemical analyses of samples from drillhole BP-89-04 are presented in Table 5. Considering the changing nature of lithological units hosting the mineralized zone and the deformation superimposed on the mineralization, a quantitative study of the alteration was not attempted as it was almost impossible to find unaltered equivalents for any of these units.

Visible alteration related to gold mineralization at the Big Pond showing is not extensive, aside from restricted zones of silicification less than 15 cm wide in adjacent graphitic schists. However, numerous quartz veinlets and local calcite veinlets producing a stockwork-like arrangement commonly border the mineralized zone.

Carbonate rocks are abundant in this area, but their spatial distribution and timing indicate that they are not all associated with the mineralizing process. Surface exposures of some of these schists resemble deformed limestone; also calcareous shale occurs adjacent to graphitic schist along Isle aux Morts River. Carbonate rocks occur in bands parallel to the compositional layering. They are recrystallized, generally equant to tabular, and oriented parallel to the S_{3b} fabric. Rocks with abundant carbonate and low proportions of silica are therefore probably sedimentary in origin.

Later carbonate is present either replacing chlorite in chlorite schist or as veinlets. Two generations of veinlets can be recognized. The earlier veinlets are generally discordant to S_{3a} and are folded by the S_{3b} fabric. The carbonate in these veinlets is partially recrystallized, and many show deformation twins. Although no significant gold mineralization is associated with these veinlets, they do contain trace amounts of chalcopyrite and galena, suggesting that they are related to the mineralizing event. Late carbonate veinlets crosscut all fabrics in the rock, postdating all ductile deformation.

Mineralogy and textures of the mineralized zones

The gold mineralization at Big Pond is essentially located in quartz breccia veins. The proportion of sulphides is highly variable, from traces to over 15% in some veins. The sulphides include mainly pyrite, with up to 1% chalcopyrite and traces of galena, pyrrhotite, sphalerite, and arsenopyrite. Pyrite is commonly intergrown with up to 2-3% hematite and trace amounts of magnetite (Fig. 34). The sulphides occur either disseminated or semimassive, in bands or filling fractures. Sulphides also occur bordering host rock fragments indicating that the fragments influenced the precipitation of the sulphides. Gold content generally relates directly to the abundance of sulphides.

Quartz veins are white to dark grey (Fig. 29), and massive to brecciated. Quartz is commonly deformed, showing undulose extinction, polygonization/recrystallization, fibrous quartz, and cataclasis. Recrystallization in bands is in part responsible for the laminated aspect of the vein.

In the more pyrite-rich portions of the vein, banding is defined by alternating fine- and coarse-grained pyrite (0.1 mm to 8 mm) parallel to the vein. The euhedral to subhedral crystals are fractured and cataclastically deformed (Fig. 31B), and contain rare inclusions of pyrrhotite and/or chalcopyrite.

Pyrite occurs in various paragenetic positions. Early precipitation of pyrite is suggested by subhedral crystals bordering host rock fragments. Late pyrite occurs as fracture-filling material in cataclastically deformed quartz (Fig. 35), possibly as a result of a physical remobilization during cataclastic deformation of quartz. At least two generations of pyrite occur in the fracture filling assemblages, shown by poekilitic pyrite rims surrounding euhedral crystals (Fig. 36).

Locally, pyrite is intergrown with radiating aggregates of bladed and needle-like crystals or irregular aggregates of magnetite and hematite (Fig. 34). Pyrite appears to be replacing the oxides, a reflection of the changing fluid composition, probably as a result of wall rock/fluid interaction.

In mineralized offshoots of the main zone, pyrite overgrows and selectively replaces portions of the host rock, producing a highly poikilitic pyrite with numerous inclusions of gangue. Inclusion trails define the folded S_{3a} foliation, suggesting that pyrite growth or recrystallization was late-F_{3b} folding (Fig. 37A, B). The folded aspect of the veinlet, however, confirms that its emplacement was related in time to the F_{3b} folding event (Fig. 29).

Several gold grains were observed under the microscope. More commonly gold occurs as inclusions in pyrite of the earliest generation, as well as in the late coarse pyrite crystals. Free gold is rarely observed but does occur in the cataclastic and polygonized quartz. Therefore it appears that gold was either remobilized or introduced throughout the hydrothermal process. The more gold-rich samples are generally more cataclastically deformed and there appears to be a correlation with the abundance of sulphides. However, the abundance of hematite/magnetite bears no relationship with that of gold.

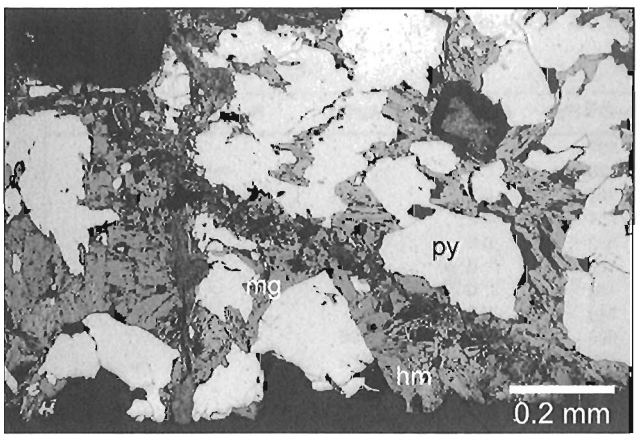

Figure 34. *Photomicrograph of pyrite (py) intergrown with bladed hematite (hm) and magnetite (mg).GSC 1996-128H*

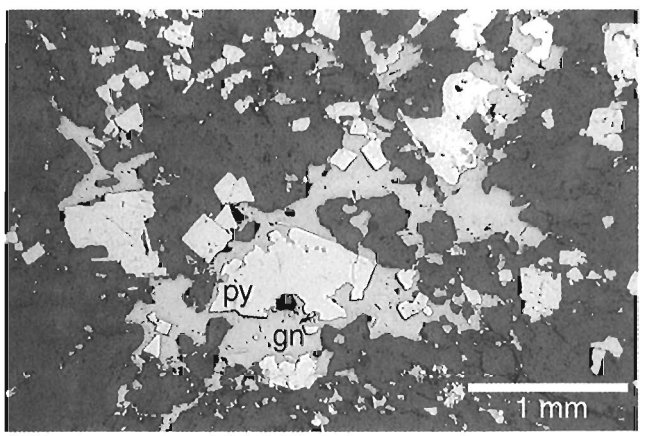

Figure 35. *Photomicrograph of pyrite (py) and galena(gn) filling fractures in cataclastic quartz at Big Pond. GSC 1996-128I*

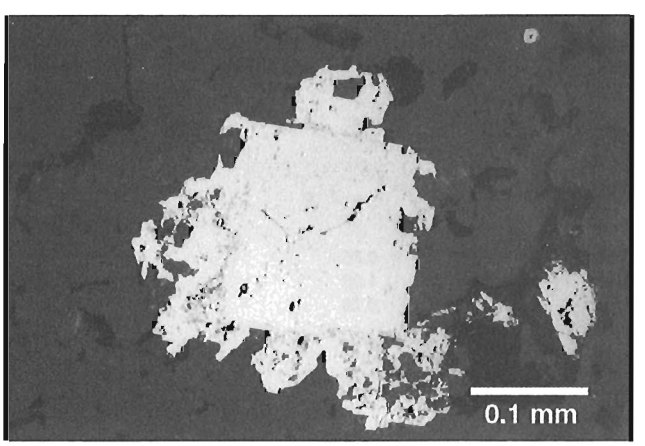

Figure 36. *Photomicrograph showing two generations of pyrite, a first generation of euhedral pyrite surrounded by a rim of second generation of poekilitic pyrite. GSC 1996-128J*

Chemical characteristics of mineralized zones

Chemical analyses of mineralized samples of the Big Pond showing are presented in Table 6. Compared to the Cape Ray gold deposit, the proportion of base metals is much lower although several samples contain elevated proportions of Pb and Zn (>10 000 ppm) and Cu up to 0.42% (4200 ppm). Scatterplot diagrams indicate that there is no direct correlation between base metal and silver contents and gold grade (Fig. 38). The Au:Ag ratios vary from 25:1 to 1:25 and average 5:1. When plotted on a ternary diagram of Au-Ag-base metals where most gold deposits are compiled (Poulsen, 1996), all samples of the Big Pond showing fall in the field that characterizes gold deposits in greenstone belts and of quartz carbonate veins (Fig. 26B).

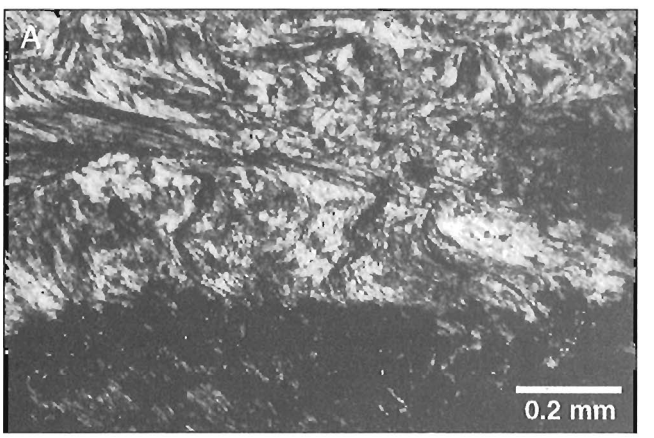

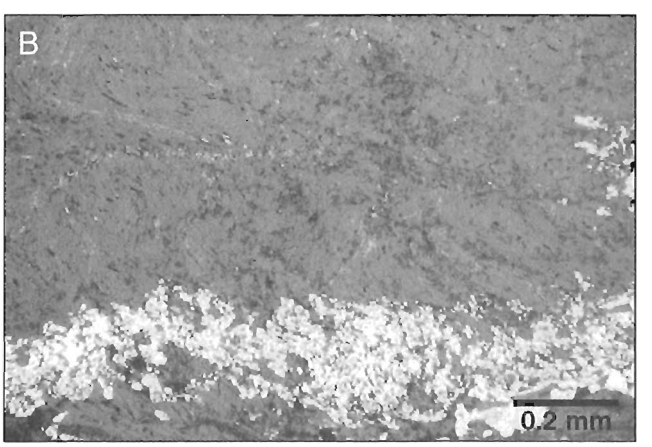

Figure 37. A) *Photomicrograph showing a pyrite-rich vein crosscutting a folded S_{3a} foliation defined by micas. GSC 1996-128K.* ***B)*** *Photomicrograph, in reflected light, showing poekilitic pyrite with inclusion trails defining the folded S_{3a} foliation suggesting that pyrite growth or recrystallization was late-F_{3b} folding. GSC 1996-128L*

Table 6. Chemical analyses of the mineralized veins from the Big Pond showing (unpublished data from Dolphin Explorations Ltd.).

Sample	Zn (ppm)	Pb (ppm)	Au (ppm)	Cu (ppm)	Cu+Zn+Pb	Ag (ppm)	Au/Ag	As (ppm)	Mo (ppm)
67805	8	76	0.48	23	107	0			
67806	5	83	0	240	328	0			
67807	3	40	0	61	104	0.2			
67808	40	24	25.82	690	754	3.2	8.07		
67809	38	40	1.44	260	338	0.6	2.40		
67810	4	110	0	8	122	0			
67818	41	65	0	26	132	0			
67819	0	120	0	28	248	0.3			
67820	19	86	0.21	500	605	0.8	0.26		
67821	22	200	0.38	480	702	0.5	0.76		
67822	19	63	1.71	680	762	0.7	2.44		
67823	216	650	0.17	250	1116	1.9	0.09		
67824	1080	920	1.92	470	2470	6	0.32		
67825	21	250	0	86	357	0			
67826	6	110	0	11	127	0			
67827	7	80	0	29	116	0			
67828	9	86	0	59	154	0			
67963	60	130	0	47	237	0.2			
67964	35	40	0	47	122	0			
67965	35	80	0	46	161	0.2			
67966	120	71	0.48	79	270	0.8	0.60		
67967	170	110	16	480	760	3	5.33		
67968	10 000	900	26.91	3900	14 800	6	4.49		
68969	47	37	0	57	141	0.4			
68970	13	51	0	88	152	0			
70801	42	140	0	63	245	0.2			
70802	11	42	0.34	290	343	0.3	1.13		
70803	11	41	1.1	450	502	0.4	2.75		
70804	8	28	1.99	360	396	0.4	4.98		
70805	8	25	2.26	74	107	0			
70806	20	20	0.31	39	79	0			
70807	8	18	3.98	120	146	0.2	19.90		
70808	8	34	2.5	210	252	0.2	12.50		
70809	250	130	53.01	1000	1380	2.4	22.09		
70810	9	29	1.51	94	132	0			
70811	8	40	0.17	95	143	0			
70812	15	15	0.17	48	78	0			
70813	7	30	0.86	14	51	0			
70839	13	78	0	97	188	0			
70940	9	61	0	136	206	0			
70941	10	66	0	107	183	0			
70942	5	75	0	23	103	0			
70943	11	85	31	2000	2096	1.7	18.24		
70944	8	75	0.17	12	95	0			
70945	13	61	0	115	189	0			
70946	15	56	0.55	182	253	0			
70947	15	81	0.58	108	204	0			
70948	10	70	0	77	157	0			
70949	14	91	5.01	1300	1405	1.4	3.58		
70950	8	54	0	97	159	0			
70951	9	69	0	47	125	0			
70981	290	129	0	69	488	1.3			
70982	41	154	0	50	245	0.2			
70983	108	300	0.21	52	460	0.3	0.70		
70984	530	884	1.99	169	1583	1.9	1.05		
70985	157	276	0.38	92	525	0.5	0.76		
70986	27	97	0	95	219	0.2			
70987	16	118	0	223	357	0			
70988	39	69	2.5	550	658	1.4	1.79		
70989	21	47	0	90	158	0.3			
70990	7	99	0	218	324	0			
71508	17	86	0.21	191	294	0.2	1.05		
71509	27	52	0	206	285	0.4			
71510	23	39	0	48	110	0.4			
71511	74	31	4.39	220	325	0.6	7.32		
71512	21	23	5.79	440	484	0.5	11.58		
71513	5200	91	40.59	930	6221	6	6.77		
71514	260	89	32.3	750	1099	4.1	7.88		
71515	280	124	0	67	471	1.5			

Analyses carried out by Dolphin Exploration Ltd., except as noted
*)Analyses done at XRAL Laboratories

Sample	Zn (ppm)	Pb (ppm)	Au (ppm)	Cu (ppm)	Cu+Zn+Pb	Ag (ppm)	Au/Ag	As (ppm)	Mo (ppm)
71516	18	43	0	87	148	0.3			
71517	17	84	0	98	199	0.2			
71671	220	155	0	41	416	0.8			
71672	250	520	0	67	837	1.1			
71673	182	216	0	76	474	0.9			
71674	310	970	0	160	1440	1.6			
71675	2100	1880	0	160	4140	4.3			
71676	710	5680	0	110	6500	2.6			
71677	1500	10 000	0.24	2500	14 000	6	0.04		
71678	35	85	0	110	230	1.4			
71679	7	130	0	39	176	0			
71686	46	77	0	99	222	0.4			
71687	36	200	0	310	546	0.5			
71688	40	140	0.62	1100	1280	1.5	0.41		
71689	10	84	0.79	65	159	0.3	2.63		
71690	12	120	1.41	39	171	0.3	4.70		
71691	15	80	0	35	130	0			
71695	2	83	0	64	148	0			
71696	13	70	0	120	203	0.2			
71697	9	33	0	190	232	0.3			
71698	19	480	4.08	1000	1499	6	0.68		
71699	21	20	21.46	2000	2041	4.5	4.77		
71700	18	17	8.13	1400	1435	2	4.07		
71701	63	130	31.82	4000	4193	6	5.30		
71702	26	153	5.93	3600	3779	6	0.99		
71703	8	47	0	1100	1155	0.3			
71704	10	55	0	45	110	0			
80079	7	51	0.41	97	155	0			
80080	27	44	0	49	120	0			
80081	27	35	0	36	98	0			
80082	26	55	0	46	127	0			
80083	2000	1200	0.34	1300	4500	6	0.06		
80084	27	70	0	470	567	0.2			
80085	14	44	0	1400	1458	0.6			
80086	23	52	9.6	1300	1375	1.5	6.40		
80087	16	37	0.45	320	373	0.4	1.13		
80088	67	23	6.86	310	400	1.9	3.61		
80089	310	87	11.18	2600	2997	6	1.86		
80090	101	62	0.72	230	393	1.6	0.45		
80091	31	82	1.41	166	279	0.6	2.35		
80092	14	62	0.21	490	566	1.2	0.18		
80093	20	260	0	82	362	0.5			
80094	5	82	0	37	124	0			
80106	19	70	0	40	129	0			
80107	19	48	0.55	84	151	0			
80108	22	83	0.17	60	165	0			
80109	9700	5760	3.19	270	15 730	6	0.53		
80110	820	170	0	55	1045	4.1			
80111	43	151	0	180	374	0.2			
80112	63	312	0.27	440	815	1.2	0.23		
80156	8	79	0.17	69	156	0			
80157	11	70	0	37	118	0			
80158	8	79	0.17	69	156	0			
80159	3	51	0	18	72	0			
80160	1400	1440	8.74	290	3130	6	1.46		
80161	240	312	8.37	820	1372	4.1	2.04		
80162	45	111	0.69	94	250	0.3	2.30		
80163	30	70	0.38	119	219	0.3	1.27		
80164	1	30	0	69	31	0			
80165	0	42	0	68	110	0			
80470	0	61	4.32	190	251	0.2	21.60		
80471	0	69	1.03	47	116	0			
80472	0	73	3.6	160	233	0.9	4.00		
80473	16	41	0.86	160	217	0.3	2.87		
80474	1	41	7.71	14	56	0.3	25.70		
90KL-204*[1]	7.3	63	4.04	964	1034.3	0		290	<1
90KL-205*[1]	46.2	6	3.63	563	615.2	0		6	2
90BD-179*[1]	19.1	30	12.3	1820	1869.1	1.1	11.18	61	5
90BD-180*[1]	8.8	23	11.7	4270	4301	3.5	3.34	0.3	149
90BD-162*[1]	36	0	0.725	175	211	0.5	1.45	0.69	29
90BD-167*[1]	85.3	29	13	143	257.3	1.1	11.82	0.08	1010

Analyses carried out by Dolphin Exploration Ltd., except as noted
*[1]Analyses done at XRAL Laboratories

Discussion and conclusion

The mineralized zone at Big Pond can be summarized as a complex tabular structure composed mainly of a fault fill quartz breccia vein, although mineralization also occurs in more massive quartz veins and stockwork zones. Graphitic gouge is relatively insignificant. The principal sulphide phase is pyrite. Chalcopyrite, galena, pyrrhotite, sphalerite, and arsenopyrite also occur in overall trace amounts. The mineralized zone is hosted in graphitic schist. Like the Cape Ray gold deposit, the role played by the graphitic schist was two-fold: 1) as a structural trap due to its rheology, and 2) as a chemical trap because of its composition. The mineralized zone is defined by two oreshoots that plunge steeply to the northeast.

Mapping of the Big Pond trenches indicates that the mineralization is necessarily late-S_{3a} as it cuts across the S_{3a} fabric and contains strongly foliated fragments in the quartz breccia vein. The timing between the mineralized zone and the S_{3b} fabric is not as clear, as the two structures are nearly parallel. Some observations, however, indicate that the mineralized vein is, at least in part, pre-S_3b. Small scale offshoots of the main mineralized vein, at a high angle to the S_3b fabric, appear to be affected by the F_3b folding event. However, in these same veinlets, microscopic observations indicate that the development of pyrite occurred after some of the F_3b folding was already initiated. Late S_3b mineralization is also indicated by fragments in the vein of graphitic schist with two fabrics, a first layer-parallel fabric folded about a crenulation cleavage. Considering these observations, mineralization at Big Pond was probably emplaced throughout the development of the S_3b fabric. Circulation of the hydrothermal fluid, taking place after the onset of deformation and folding related to S_3b, may explain why the mineralized zone is not completely enclosed in, and folded with, the graphitic schist. Also the subparallelism between the mineralized quartz vein and the S_3b fabric at Big Pond explains why folding of the mineralized zone itself is not evident.

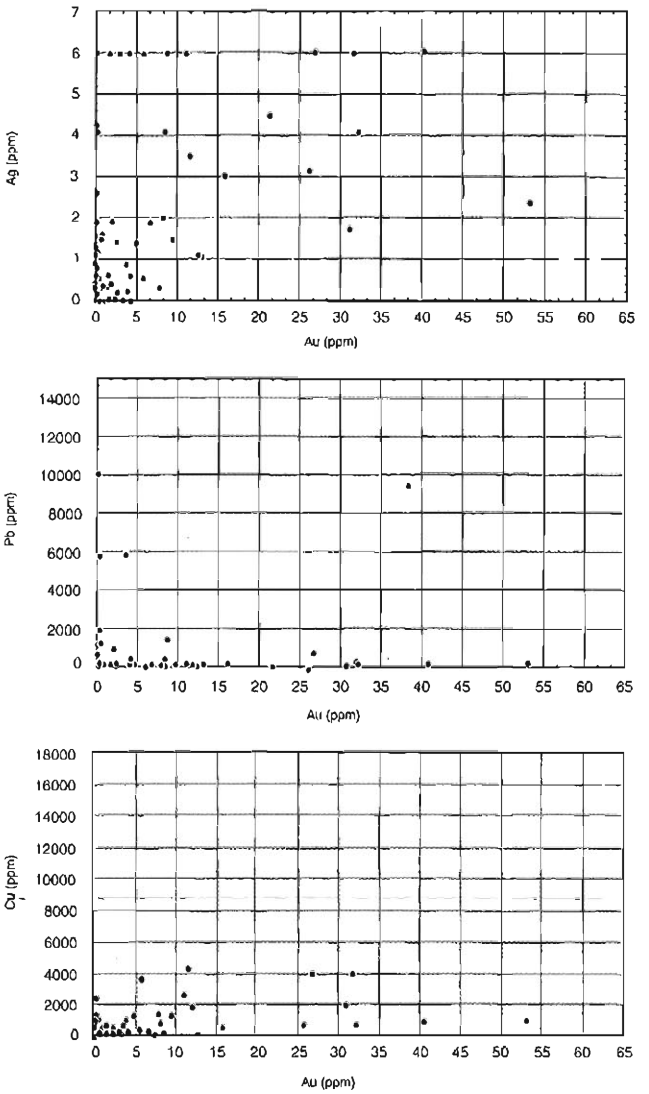

Figure 38. Diagrams showing variations of Ag, Pb, and Cu with Au in the Big Pond showing.

Geology of the Windowglass Hill showing

Introduction

Mineralization at the Windowglass Hill showing occurs predominantly in a set of flat-lying sulphide-rich quartz veins hosted in the relatively undeformed Windowglass Hill Granite (Fig. 12). Figure 39 shows a map of the Windowglass Hill Granite with the approximate extent of the mineralized veins at depth, projected to surface.

The Windowglass Hill Granite is well exposed. It is easily outlined on satellite images or air photos of the area, especially to the southwest side of Isle aux Morts River where it appears as a pale, less vegetated area. It is completely enclosed within Windsor Point Group rocks. The intrusion is elongate to elliptical in plan, and extends 2.7x 0.6 km on the western side of Isle aux Morts River and 100 m wide x 3.4 km long on the eastern side where it is cut across by a strike-slip mylonite zone (D_4) (Fig. 12). Most contacts between the main intrusive body and Windsor Point Group rocks are sheared by D_3 high strain zones, but the granite is clearly intrusive within Windsor Point Group rocks as indicated by a Windowglass Hill granitic dyke in Silurian gabbroic rocks of the Windsor Point Group in the Isle aux Morts River area. There, both units are folded by the main S_{3b} foliation indicating that intrusion and cooling took place prior to F_3 folding.

The intrusion is principally composed of a pink, aphanitic groundmass with minute quartz accompanied locally by alkali feldspar or plagioclase phenocrysts. Biotite is the only mafic silicate present and makes up less than 2% of the rock. Magnetite octahedra are also common but never exceed 2%. Graphic to granophyric textures characterize the Windowglass Hill Granite (Wilton, 1983b, 1985), and are suggestive of a shallow level of emplacement (Barker, 1970). This implies that intrusion took place either during deposition of the Windsor Point Group or late during the deformation history, post-peak metamorphic conditions. The 424 ± 2 Ma age obtained by U-Pb dating on zircon (Dubé et al., 1996) confirms that the intrusion was emplaced prior to peak metamorphic conditions estimated by U-Pb on monazite at 415 Ma (van Staal et al., 1994).

Table 7. Chemical analyses of the Windowglass Hill Granite. From Wilton (1983a).

Sample	WGH-1	WGH-2	WGH-3	WGH-4	W79-112	W79-126	W79-140	W80-148	W80-186	W80-164
SiO_2%	79.10	78.40	77.80	78.20	78.00	77.20	77.20	74.00	79.40	77.00
Al_2O_3%	10.90	12.40	12.20	12.20	12.00	13.00	10.80	14.60	12.40	14.00
TiO_2%	0.00	0.11	0.00	0.00	0.28	0.18	0.24	0.10	0.07	0.00
Fe_2O_3(t)%	0.88	0.79	0.83	0.65	0.34	1.69	0.44	0.98	0.44	0.54
MnO%	0.01	0.02	0.02	0.01	0.01	0.02	0.01	0.02	0.00	0.01
MgO%	0.02	0.06	0.04	0.05	0.01	0.20	0.16	0.20	0.07	0.00
CaO%	0.87	0.99	0.71	0.81	0.50	0.17	0.61	0.81	0.18	0.10
Na_2O%	5.87	6.49	5.25	5.66	6.68	3.82	1.38	4.03	6.92	4.68
K_2O%	0.05	0.39	2.70	1.55	0.20	4.30	7.40	2.55	0.24	3.97
P_2O_5%	0.00	0.00	0.00	0.00	0.05	0.03	0.03	0.00	0.01	0.00
LOI%	1.21	1.07	0.94	1.05	0.70	0.82	1.00	2.15	0.39	0.42
Total	98.91	100.72	100.49	100.18	98.77	101.43	99.27	99.44	100.12	100.72
Metallic trace elements										
Cu (ppm)	14	15	14	15	12	13	14	38	28	15
Zn (ppm)	18	11	13	20	18	36	15	77	21	35
As (ppm)	10	12	18	15	17	30	31	0	23	0
Ag (ppm)	0.71	0.35	0.23	1.62	0.19	0.03		0.12	0.07	
Pb (ppm)	12	9	70	15	37	20	8	166	13	67
Au (ppb)	10	6	19	2	13	10		15	0.6	
Trace elements (ppm)										
Ba	30	32	314	201	27	327	750	662	83	89
Cr	0	7	0	0	0	0	0	0	8	0
Nb	40	39	39	42	38	31	16	31	34	48
Ni	21	15	16	18	14	26	9	3	0	0
Rb	24	11	59	41	5	163	121	79	6	273
Sr	61	83	64	84	85	26	28	64	93	31
Th	30	17	23	27	18	27	10	24	22	42
U	10	5	10	7	0	4	0	6	0	11
V	3	0	4	1	0	4	25	7	7	0
Y	178	146	149	144	133	143	69	140	47	58
Zr	351	352	279	374	314	242	177	328	280	64
Ce	106	127	115	130	104	278	38	103	17	2
La	30	32	314	201	48	107	19	64	1	2

Sample	PB7-10	PB19-25	PB38-2A	PB38-14	PB133-5	W79-74	W79-78B	W79-112	W79-112A
SiO_2%	75.60	76.20	66.70	65.70	72.60	74.70	77.20	76.60	78.60
Al_2O_3%	12.8	13.60	17.00	19.00	13.60	13.30	11.90	11.80	12.00
TiO_2%	0.12	0.10	0.24	0.23	0.18	0.09	0.00	0.16	0.00
Fe_2O_3(t)%	0.98	0.30	2.29	0.30	2.17	1.76	1.80	1.44	0.96
MnO%	0.03	0.01	0.03	0.03	0.01	0.03	0.03	0.02	0.01
MgO%	0.19	0.05	1.12	0.41	0.09	0.40	0.06	0.03	0.00
CaO%	0.93	0.78	3.72	1.42	0.19	0.65	0.03	0.62	0.08
Na_2O%	4.15	7.80	5.27	10.80	8.10	1.55	6.32	4.12	6.56
K_2O%	1.74	0.13	1.02	0.13	0.11	3.58	0.55	3.51	0.28
P_2O_5%	0.02	0.00	0.02	0.07	0.00	0.02	0.00	0.06	0.01
LOI%	1.74	0.69	2.24	1.27	1.09	2.62	1.44	0.85	0.39
Total	98.30	99.66	99.65	99.36	98.14	98.70	99.33	99.21	98.89
Metallic trace elements									
Cu (ppm)	39	23	27	20	30	26	27	9	12
Zn (ppm)	347	36	50	12	22	455	59	23	21
As (ppm)	12	15	0	17	60	34	6	2	21
Ag (ppm)	0.09	0.02	0	0.03	2.9	0.24	0.16	0.06	0.02
Pb (ppm)	105	16	11	19	116	1939	176	8	14
Au (ppb)	23	1	2	5.4	3.5	7	5.8	1.8	12
Trace elements (ppm)									
Ba	664	69	416	57	79	385	59	329	30
Cr	0	1	2	0	10	0	0	0	0
Nb	28	24	2	12	28	31	22	38	43
Ni	0	0	0	0	0	26	27	9	12
Rb	62	1	24	1	4	104	0	117	8
Sr	64	260	553	227	117	10	150	38	29
Th	19	20	2	2	27	28	18	19	27
U	9	2	0	1	7	7	3	5	5
V	4	6	60	42	10	385	59	329	30
Y	111	64	6	21	98	118	92	161	100
Zr	295	328	98	266	269	305	261	266	326
Ce	76	23	25	25	100	99	66	116	3
La	45	4	7	0	52	52	23	104	1

Chemical analyses of the Windowglass Hill Granite, (Table 7), detailed in Wilton (1983a, 1984) indicate that it is anomalously siliceous, commonly rich in either K or Na. These anomalous chemical abundances are common in granophyric granites, some authors interpret them as resulting from crystallization in presence of a vapour phase (Simpson, 1962) whereas others believe that relatively rapid and episodic growth of crystals from a viscous medium is necessary to produce this chemistry (Martin, 1982). The granite was considered by Wilton (1983b, 1985) as a subvolcanic equivalent of the felsic volcanic and volcaniclastic rocks of the Little Barachois formation based on similar chemistry as well as comparable initial Sr ratios. However, the felsic volcanic rocks of the Little Barachois formation yielded a U-Pb zircon age of 453 +5/-4 Ma indicating that they are 30 Ma older than the Windowglass Hill Granite (Dubé et al., 1996) and thus refuting the possibility that these two felsic melts were comagmatic.

Structure of the deposit

Deformation in the Windowglass Hill Granite is generally weak but is very heterogeneous. Strain is most intense in centimetre- to metre-wide zones of shearing that separate relatively undeformed domains characterized by jointing and locally by a northeast- to north-northeast-trending spaced, fracture cleavage. The high strain zones are best developed at the Windowglass Hill-Windsor Point Group contact. The main fabric in these zones is oriented at 040°/75°, concordant with the main S_{3b} fabric (Fig. 39). The mylonitic foliation locally contains a penetrative down-dip stretching lineation defined by elongate quartz. Other metre-wide high strain zones also occur within the intrusion. Most are parallel to the contact, however, some are at a high angle to it (north-northeast- to north-northwest). Specifically, those spatially associated with the mineralization strongly deviate from the typical northeast-trend of the area (Fig. 39). Stretching

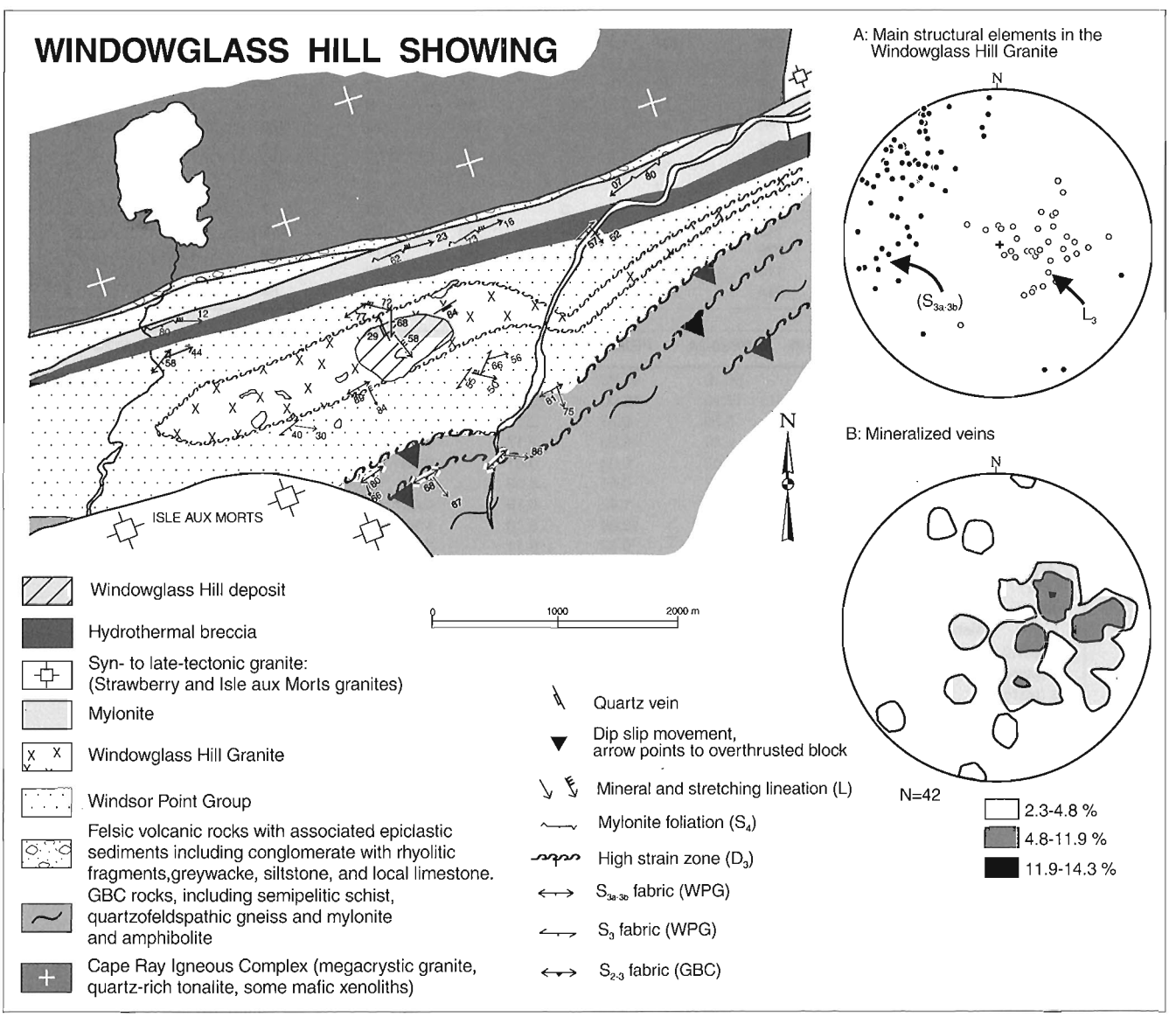

Figure 39. Geological map of the Windowglass Hill showing illustrating distribution of the main lithological units and a compilation on equal area projections (lower hemisphere) of the main structural elements.

Figure 40. *Cross-section view of a gold-bearing subhorizontal extensional quartz vein at the Windowglass Hill showing. GSC 1996-129A*

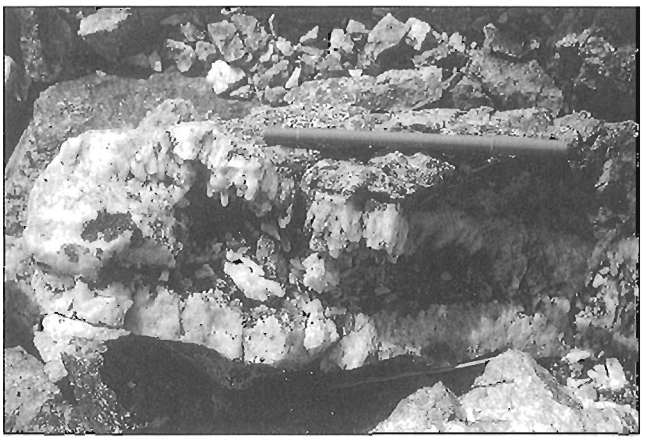

Figure 41. *Barren subvertical extensional quartz vein at Windowglass Hill showing. GSC 1996-129B*

lineations in both concordant (northeast-trending) and discordant (north-northeast- to north-northwest-trending) high strain zones are subparallel and plunge steeply (Fig. 39) and therefore could have resulted from the same deformation event. The north-northeast to north-northwest discordant shear zones most probably result from strain refraction induced by competence contrast between the competent Windowglass Hill Granite and the anisotropic and less competent Windsor Point Group rocks. As demonstrated by Treagus (1983, 1988), the refraction of the principal strain axes orthogonal to the orientation of the layer is proportional to the competence of the unit. The high proportion of quartz and granophyric intergrowth within the Windowglass Hill Granite make it a very stiff unit and could explain the refraction of the strain axes toward northerly trending shear zones at high angle to the orientation of its granitic host. The stretching lineations within these northerly trending shear zones are subparallel to those outside the granite and suggest that despite the variation in orientation these high strain zones are probably related to the same D_3 deformation episode. Similar settings have been described in gold deposits hosted by competent units such as gabbroic sills (Dubé et al., 1989; Robert et al., 1994).

Mineralization

Veins

Two principal sets of veins cut across the Windowglass Hill Granite (Fig. 39) (Wilton and Strong, 1986). The first corresponds to the mineralized set. The veins are flat to moderately dipping, generally to the west. They are millimetre- to centimetre-wide and spaced 1 cm to several tens of centimetres apart (Fig. 40). Granitic wallrock is mostly undeformed, without any penetrative foliation. The veins commonly show open space filling textures, with idiomorphic quartz crystals developed subparallel to the down-dip stretching lineation, suggesting that vein development occurred during the D_3 deformation event. The widest veins observed in the showings are 20-40 cm thick (Fig. 40), but Wilton (1983a) described veins up to 1 m in thickness. They are known to pinch and swell, with the best mineralized areas in zones of maximum thickness (Wilton and Strong, 1986).

A second set of veins, subparallel to the main S_3 foliation, is northeast oriented and steeply dipping. These veins are millimetres to several metres wide and contain no sulphides, nor any gold values, except where they intersect the mineralized veins (Wilton, 1983a; Wilton and Strong, 1986). One of the best examples of this set is a 3 to 7 m wide, white bull quartz vein near the centre of the Windowglass Hill Granite that is about 2 km long. It contains abundant granitic fragments that are mostly undeformed. Also, there is little evidence of deformation in adjacent granitic wall rock. This vein set is characterized by open space filling textures indicating that it is an extensional vein (Fig. 41). These veins are not structurally compatible with the D_3 structures and are most probably post-D_3 deformation. Regionally, late extension is evidenced by the presence of a hydrothermal breccia bordering the strike-slip mylonite zone (D_4) and the Strawberry Granite in the Isle aux Morts River section. The breccia contains fragments of the Strawberry Granite and is thus younger than 384 Ma, the age of the granite. The steeply dipping barren extensional quartz veins within the Windowglass Hill Granite were possibly emplaced at the same time as both are structurally compatible with a southeast extension.

Alteration

Alteration haloes are best developed around the more extensively mineralized veins. Megascopically, evidence of alteration can be recognized several metres away from the mineralized veins. However, intense alteration is restricted to close proximity to the veins. The proximal alteration zone is defined by disseminated pyrite and moderate to intense sericitization of feldspars giving somewhat of an apple green colour and a bleached aspect to the rock. The bleached aspect is only partly attributable to sericitization of feldspars. It is mostly a result of the absence of hematite staining of the feldspars. Sericite alteration occurs in both perthites and plagioclase. Sericite associated with the mineralization is, in

general, coarser grained than the fine sericite that is attributed to regional metamorphism. Chloritization of feldspars is local, and seems to be associated with magnetite-bearing veins (Fig. 42). Chlorite occurs in fine-grained aggregates replacing feldspar in graphic intergrowth with quartz. Hematite in fibro-radial aggregates, leucoxene and/or chalcopyrite and magnetite and euhedral zircon crystals are commonly associated with the dark green chlorite. The extent of chloritization is more restricted than that of sericitization. Although alteration is present, deformation is rather limited and igneous textures are commonly preserved (Fig. 42).

Away from the veins, in more distal zones, the alteration is fracture-controlled, and consists of pyrite disseminations and sericitization along the fractures. In both proximal and distal alteration zones, carbonate minerals are nearly absent, although in some rare veins calcite does occur. In such cases, calcite is intergrown with sericite replacing feldspars. Clay minerals were also observed in several thin sections from the Windowglass Hill showings. They appear to be late in the mineral paragenesis as they fill fractures that crosscut the proximal alteration zone as well as sericite-filled fractures.

Despite the mineralogical transformation, chemical analyses of two samples adjacent to mineralized quartz veins do not indicate significant transformations (Table 8). The CO_2, H_2O, and S variations are very limited. There is no significant variation in major elements. Anomalous Pb and Au values only occur in sample 90BD-189.

Mineralogy and textures of the mineralized zones

The gold-bearing veins commonly display banded textures, produced by alternating quartz-rich and sulphide-rich bands. The veins are mostly asymmetrical with sulphide bands commonly found towards the top part of the vein, suggesting multiple opening and filling of veins. Sulphides also occur throughout the quartz-rich portion, but in less significant proportions. Not all veins exhibit the same mineral paragenesis, some are pyrite-rich, others are chalcopyrite-rich and/or galena-rich (Fig. 43). Locally magnetite-bearing veins are also present. Other metallic phases in these veins are pyrrhotite, sphalerite, electrum, and locally covellite and hematite as late secondary alteration phases. Gangue minerals are principally grey to white quartz with rare calcite and altered granitic wall rock. Quartz is commonly undeformed, forming comb structures. Where deformed, textures range from undulose extinction, to subgrain development, to fibre-like aggregates. The last is most common in the pyrite-rich parts of the veins. Pyrite is the most common sulphide although chalcopyrite and galena are locally abundant. In some sulphide-rich bands, pyrite makes up more that 50% of the rock. It is euhedral to subhedral and individual crystals reach up to 5 mm in section, but size is highly variable. Crystals are typically fractured and cataclastically deformed. Pyrite contains up to 1% inclusions of mostly globular blebs of chalcopyrite and/or pyrrhotite, irregular shaped inclusions of galena, and globular as well as irregular, angular inclusions of gold.

In magnetite-bearing veins, rounded grains as well as euhedral crystals of magnetite occur as inclusions in pyrite. Chalcopyrite and galena commonly occur along grain boundaries of pyrite. Where chalcopyrite is the dominant sulphide phase it occurs as massive aggregates in fractures and along grain boundaries in quartz. The near massive chalcopyrite bands include anhedral grains of pyrite, sphalerite, galena, and locally radiating aggregates of hematite.

Wilton and Strong (1986) reported electron-probe microanalyses of many gold grains, all of which contain significant amounts of silver, with Au:Ag in proportions varying from 0.61 to 0.76 and thus correspond to electrum. Most of the gold in this study is associated with pyrite, as globular inclusions (0.005 mm) (Fig. 44) or filling fractures in pyrite (up to 0.025 mm long). Also electrum grains (0.0025 mm) were observed among quartz fibres.

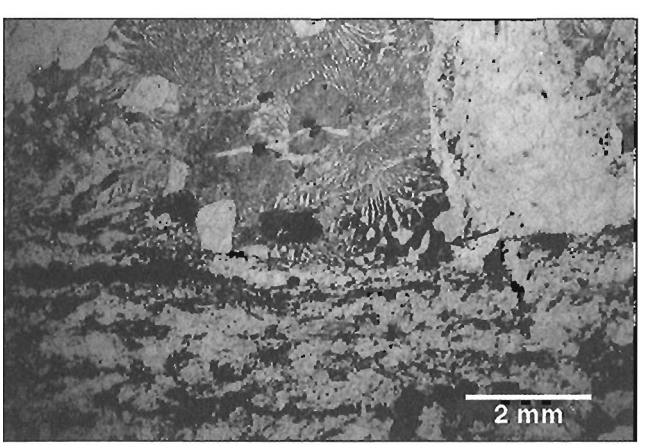

Figure 42. *Photomicrograph showing sericite and chlorite replacing fedspars adjacent to a magnetite-rich quartz vein. Chlorite alteration is not as extensive as the sericite alteration. Note the well-preserved graphic texture. GSC 1996-129C*

Figure 43. *Cross-section view of an auriferous pyrite-rich subhorizontal quartz vein at Windowglass Hill showing. GSC 1996-129D*

Table 8. Chemical analyses of mineralized samples of the Windowglass Hill showing.

Sample	90BD-190 Vein	90BD-191 Vein	90BD-192 Vein	93KL-21 Vein	93KL-23 Vein	93BD-25 Vein	90BD-189 altered wall rock	91BD-111 altered wall rock	93BD-25*3 Vein
SiO_2 %							79	79.3	
Al_2O_3 %							11.9	11.9	
TiO_2%							0.099	0.096	
Fe_2O_3(t) %							0.96	0.63	
MnO%							<0.01	0.01	
MgO%							0.07	0.06	
CaO%							0.83	0.94	
Na_2O%							5.25	5.87	
K_2O%							0.96	0.63	
P_2O_5%							<0.01	<0.01	
LOI%							0.7	0.25	
CO_2%							0.57	0.65	
H_2O+%							0.5	0.3	
S% *2							0.28	<0.01	
Total							99.8	99.8	
	Metallic trace elements (ppm)								
Cu	9430	20 100	1830	7130	3080	6120	20.3	15.2	6250
Zn	251	432	26.6	126	70.5	112	15	19.1	114
As	3	7	15	4	48	4	15	1	<3
Mo	<1	<1	<1	<1	<1	<1	<1	<1	<1
Ag	47.2	177	105	313	9.3	9.3	0.7	1	9
Pb	9680	32 200	1720	28 800	254	706	515	<2	729
Au	0.486	3.58	75.6	0.886	7.27	0.099	0.079	<.001	0.11
	Trace elements (ppm)								
B							<10	14	
Ba							130	116	
Be							5	4	
Br							2	2	
Cd							<1	<1	
Co							2	2	
Cr							<2	20	
Cs							1	<1	
Ge							10	<10	
Hf							12	11	
Nb							35	35	
Ni							<1	<1	
Rb							37	26	
Sb							0.3	0.4	
Sc							1.1	1.3	
Se							<3	<3	
Sr							91	119	
Ta							2	3	
Th							18	18	
U							8.8	5.6	
V							<10	<10	
W							5	3	
Y							107	101	
Zr							303	301	
	Rare-earth elements (ppm)								
La							65.4	71.2	
Ce							121	126	
Nd							58	60	
Sm							12.5	12.3	
Eu							1.7	1.4	
Tb							2.7	2.4	
Yb							8.9	8.4	
Lu							1.3	1.22	

*1 analyses carried out at INRS-Georessources
*2 analyses carried out at Geological Survey of Canada Laboratory
others done at X-RAL Laboratories
*3 duplicate sample analyzed at XRAL Laboratories

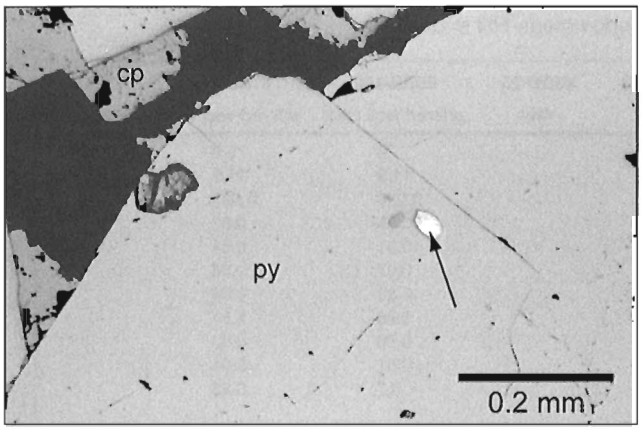

Figure 44. *Photomicrograph showing rounded inclusions of electrum in euhedral pyrite (py). Chalcopyrite (cp) is interstitial. Arrow points to electrum inclusion. GSC 1996-129E*

Some veins contain magnetite in relatively elevated proportions. Magnetite occurs in 1-2 mm wide bands, as fractured euhedral crystal aggregates. It commonly contains small rounded inclusions of pyrite as well as numerous inclusions of chalcopyrite. Magnetite also occurs as rounded inclusions in pyrite. This, and intergrown magnetite and pyrite suggest that they were deposited synchronously. Locally magnetite is partially altered to hematite.

Chemical characteristics of mineralized zones

Geochemical analyses of mineralized grab samples are presented in Table 8. The high grade 75.6 ppm of Au is from a pyrite-rich vein. The veins contain high proportions of base metals in particular Pb (up to 32 200 ppm) and Cu (up to 20 100 ppm) whereas the Zn content is rather low. Similar observations were reported by Wilton and Strong (1986). Scatterplot diagrams do not indicate any correlation between the base metal and silver contents with the gold grade (Fig. 45). Although few samples were analyzed, the Au:Ag ratios vary between 1:1 to 1:353 and average 1:99. On the ternary diagram of Au-Ag-base metals (Poulsen, 1966), all samples of the Windowglass Hill showing fall in the field of epithermal gold deposits, some plot near the granite-related Korean deposits (Fig. 26D).

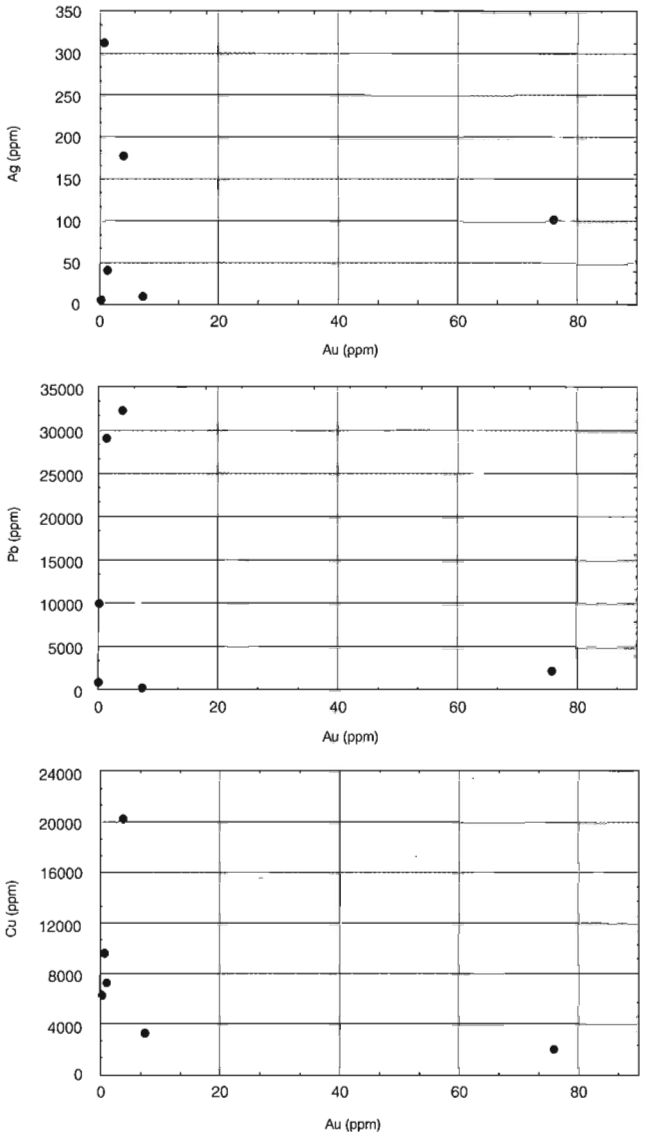

Figure 45. *Diagrams showing variations of Ag, Pb, and Cu with Au in the Windowglass Hill showing.*

Conclusion

Gold mineralization in the Windowglass Hill showing is confined to quartz veins and is essentially structurally controlled. The veins are extensional quartz veins structurally compatible with the L_{3b} stretching lineation developed outside the granite during D_3. They are associated with north-northeast-trending shear zones which deviate from the regional northeast trend due to strain refraction within the highly competent granitic host rock. The relative timing of the mineralization is syn-D_3. Despite their structural relationship with ductile shearing, many characteristics of the gold mineralization at Windowglass Hill are suggestive of emplacement at relatively shallower depth. The average Au:Ag ratio of 1:99, and the abundance of base metal sulphides, especially Pb, are consistent with such an interpretation.

Geology of the Isle aux Morts prospect

Introduction

Gold mineralization at the Isle aux Morts prospect occurs in sulphide-bearing quartz veins, at or close to the Cape Ray Igneous Complex-Windsor Point Group contact and in strongly pyritized magnetite-rich sedimentary rocks of the Windsor Point Group (Little Barachois formation) (Fig. 12, 46). However, as the exposed thickness of the Windsor Point Group is much less than in the Cape Ray gold deposit area, the mineralized zone is less than 200 m from the interpreted position of the boundary between Grand Bay Complex and

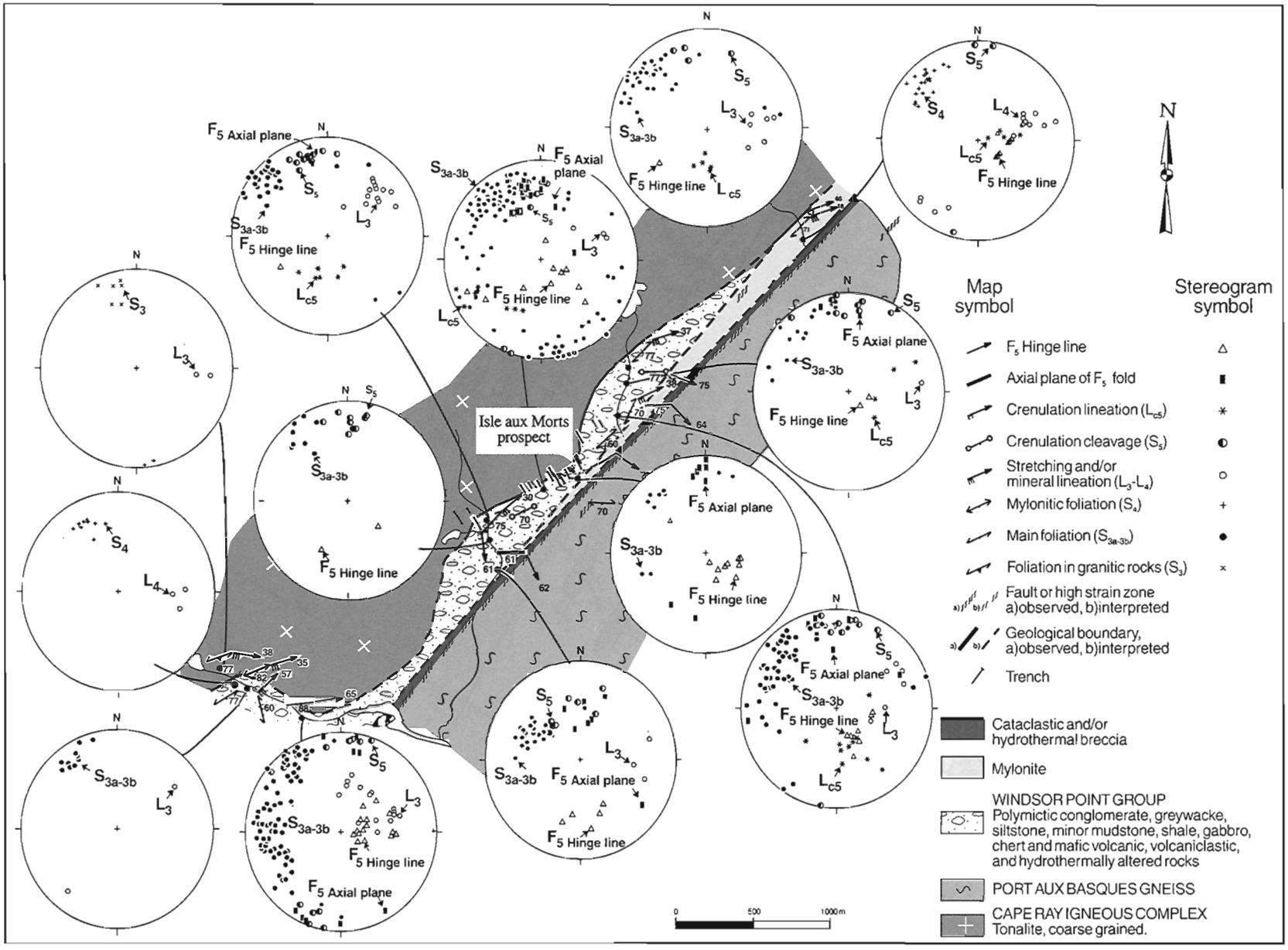

Figure 46. Geological map of the Isle aux Morts prospect illustrating distribution of the main lithological units, trenches, and drillholes and a compilation on equal area projections (lower hemisphere) of the main structural elements.

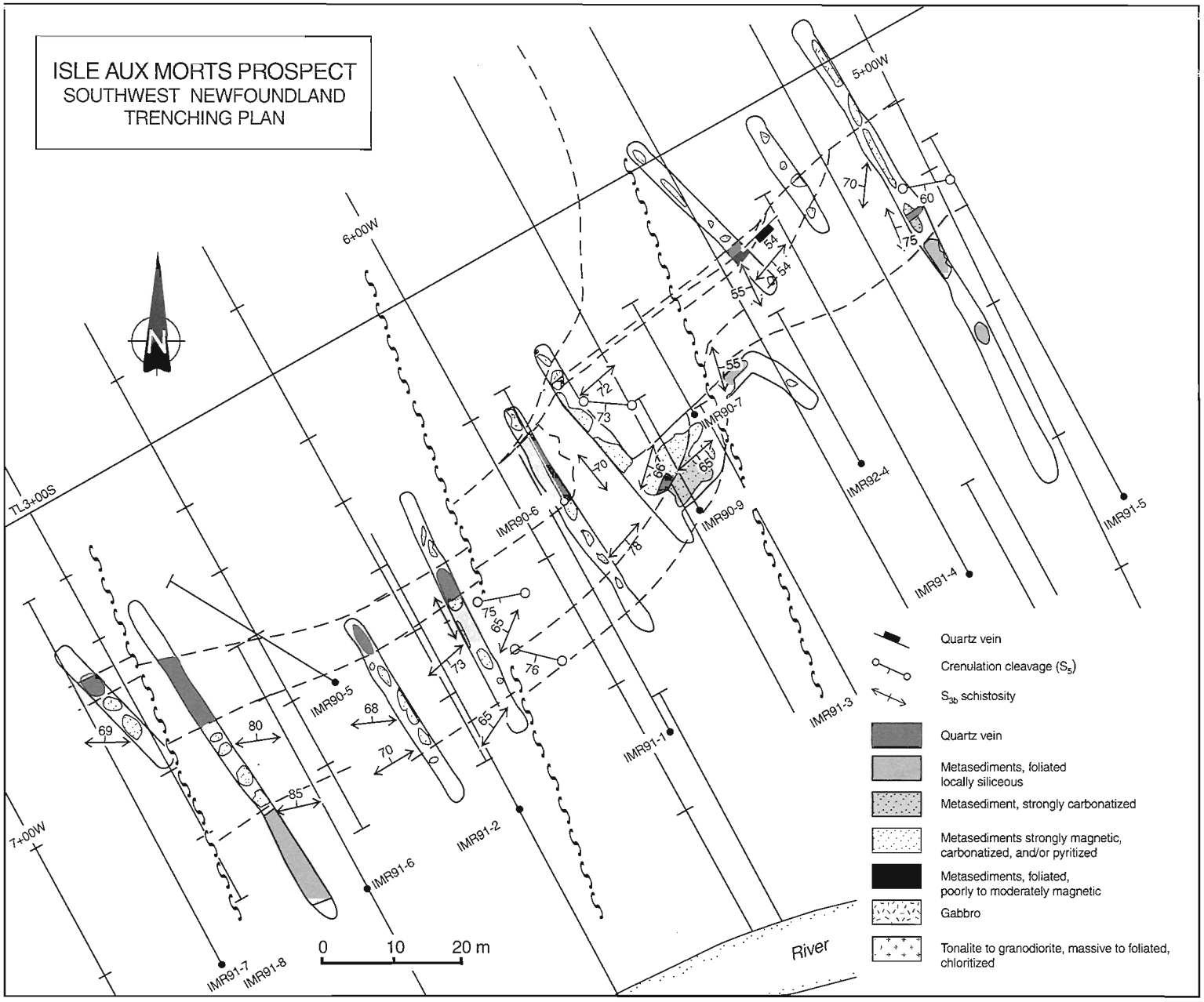

Figure 47. *Detailed geological map of the trenches showing distribution of the geological units. Based on mapping done by Dubé and Lauzière. Modified from an unpublished diagram by Placer Dome.*

Windsor Point Group rocks, i.e. the Cape Ray fault *per se* (Fig. 46). In this area, the fault is not exposed, its location is based on ground geophysics, and reverse motion is interpreted on the basis of observations in the rest of the northeast segment of the Cape Ray Fault Zone.

Drillhole data and mapping of trenches indicate that there are several gold-bearing veins hosted both in the Cape Ray Tonalite and in the Windsor Point Group sedimentary rocks. Gold values were intersected in drillhole (DDH IMR90-9: 9.88 g/t Au over 10.97 m) and on surface (trench 5+90W: 10.54 g/t Au over 13 m). The most significant vein is located at the tonalite-sediment contact. It trends east-northeast on average and is irregular both in orientation and dip (Fig. 47-49). On surface the contact dips steeply to the southeast, becoming locally moderate at depth (Fig. 49). Deformation is also variable. In some areas the contact is marked by a high strain or mylonite zone several metres wide, whereas elsewhere, granitic rocks are undeformed less than a metre away. At the property scale, gabbro is locally present at the contact. The proportion of gabbro increases to the northeast, where the mineralized zone tapers off (Fig. 47). It is not clear to which unit this gabbro belongs. In erratics found in the area, however, tonalitic dykes of the Cape Ray Igneous Complex cut a gabbro suggesting that it is probably part of the Cape Ray Igneous Complex.

Windsor Point Group rocks include those of the Little Barachois Formation and comprise mostly greywacke, siltstone, and banded iron-rich sediments, as well as conglomerate. The conglomerate is characterized by abundant granitic and felsic volcanic clasts, local jasper fragments, and magnetite octahedra disseminated in the matrix and in andesitic fragments. Felsic porphyries, aphanitic rhyolitic rocks, limestone, and gabbro were also identified locally.

Units of the Windsor Point Group are discordant to the Windsor Point Group-Cape Ray Igneous Complex contact. This relationship is evident in section view, as the contact dips moderately whereas units dip steeply. At the contact, the variable nature of rocks in the hanging wall of the main mineralized vein underlines this discordant relationship; in the northeast part, units in the hanging wall contain strongly chloritic and carbonaceous sediments, whereas to the southwest, hanging wall rocks include mostly strongly pyritized iron-rich sediments (Fig. 47).

Nature of host rocks

Lithological units in the footwall of the main mineralized vein include mostly granitic rocks of the Cape Ray Igneous Complex. They vary from tonalite to granodiorite and are grey-green to pink, coarse grained, moderately to strongly foliated. They contain up to 40% quartz, trace amounts of disseminated pyrite, and are locally magnetic. Late, reddish to pink, coarse grained, Strawberry-type granitic dykes cut the Cape Ray Tonalite. Towards the mineralized zone, the Cape Ray Tonalite grades into a highly sheared to strongly foliated green chloritic rock that is weakly to moderately magnetic and weakly carbonatized. Gabbroic rocks are also present in the footwall of the mineralized zone to the northeast. They pinch out at depth (see sections in Fig. 48, 49) and were intersected only in one drillhole. The gabbro is massive or schistose and strongly chloritic and carbonatized. Deformation in the gabbro is similar to that in Windsor Point Group rocks. Near the mineralized zone, localized iron-carbonate alteration is best developed in this unit. Adjacent to the mineralized zone the gabbro contains numerous quartz stringers with chalcopyrite, galena, pyrite, and hematite.

Hanging wall lithological units, all part of the Windsor Point Group, are mainly composed of fine-grained sediments and are subdivided into four groups based on composition reflecting both original and alteration mineral assemblages. From the mineralized zone towards the southeast, these units include: 1) weakly to moderately magnetic metasediments, 2) strongly magnetic siliceous metasediments intercalated with chlorite-rich metasediments, 3) carbonate-rich siliceous metasediments, and 4) siliceous fine-grained metasediments. A number of felsic intrusions, occurring both as dykes and irregular plugs, occur throughout the sequence. The distribution of these units is shown in Figure 47. Geochemical analyses of the different units are presented in Table 9.

Weakly to moderately magnetic metasediments

The weakly to moderately magnetic metasediments are most abundant at the Windsor Point Group-Cape Ray Igneous Complex contact, between lines 6+00W and 5+40W (Fig. 47). They form a 10 m wide unit in the hanging wall of the relatively thin mineralized vein in trenches 5+40W and 5+86W. These rocks are dark to light green to buff orange or red and are best described as chlorite-calcite-magnetite-iron carbonate schists. They are well foliated, weakly to moderately magnetic, and weakly to strongly carbonatized. Carbonatized units contain iron carbonate-rich bands, up to 1 cm. Intense folding of the main foliation is common. Quartz veinlets with up to 3% pyrite cut these rocks.

Strongly magnetic siliceous metasediments

The second sedimentary package, approximately 20 m thick, is characterized by its magnetite content. It constitutes the hanging wall of the mineralized zone between lines 5+75W and 6+50W. Present data suggest that this unit does not extend past line 5+75W to the northeast. Foliation trends indicate that the sediments are most likely folded about an easterly plunging anticlinal fold, explaining the distribution pattern of this unit (Fig. 47).

The rocks are principally composed of dark green to dark grey highly banded magnetite-rich sediments that resemble banded iron-formation (Fig. 50A). The sediments are rhythmically banded and include 1-2 cm wide magnetite-rich bands alternating with 4-5 cm wide sericite-rich and/or chlorite-rich bands and local pyrite-rich bands. Some sections are more chloritic and carbonate rich (pure calcite and an iron-bearing calcite). Pyrite-rich veinlets both concordant and discordant to the banding also occur. Pyrite can represent up to 20% of the rock. Numerous, discontinuous quartz veinlets crosscut all bands. Magnetite-rich conglomerates occur

throughout the sequence (Fig. 50B). They are characterized by abundant subrounded elongate felsic volcanic fragments. Magnetite occurs as disseminations and in veinlets.

Geochemical analyses of magnetite-rich metasediments are identified as lithology A in Table 9. Fe_2O_3 content for most magnetite-rich samples (91BD-303A, 91BD-217, 91BD-220, 91BD-222) averages 11%, except for two samples from trench 5+86W with 19.6 and 28.2% Fe_2O_3 (samples 92BD-104A, 91BD-306A). Pyritized samples present a wide range of Fe_2O_3 content between 9 and 22%.

Carbonate-rich siliceous metasediments

Carbonate-rich siliceous metasediments constitute a third mappable unit. The unit is 10 m thick, and occurs east-southeast of the magnetite-rich sediments. It comprises cream to buff to light grey to light green, slightly magnetic to nonmagnetic metasediments, characterized by wispy calcite and iron carbonate parallel to the main fabric. These rocks are typically laminated. Laminations, in the order of 1 mm to 1 cm, are composed of iron carbonate layers alternating with quartz-carbonate layers and sericite+rutile-leucoxene layers with some magnetite and pyrite. These rocks are cut by quartz-iron carbonate veinlets with local concentrations of sulphides. This unit is characterized by a high CO_2 content. Fe_2O_3 abundances are comparable to those of magnetite-rich sedimentary rocks but here are related to the abundance of ankerite (lithology B in Table 9, samples 91BD-30, 91BD-314, 91BD-315).

Silicified

The fourth recognizable unit on the property is composed mainly of fine-grained siliceous metasediments. They are dark grey green, chloritic, finely laminated and foliated, with numerous banded, siliceous intervals, locally cherty. Some

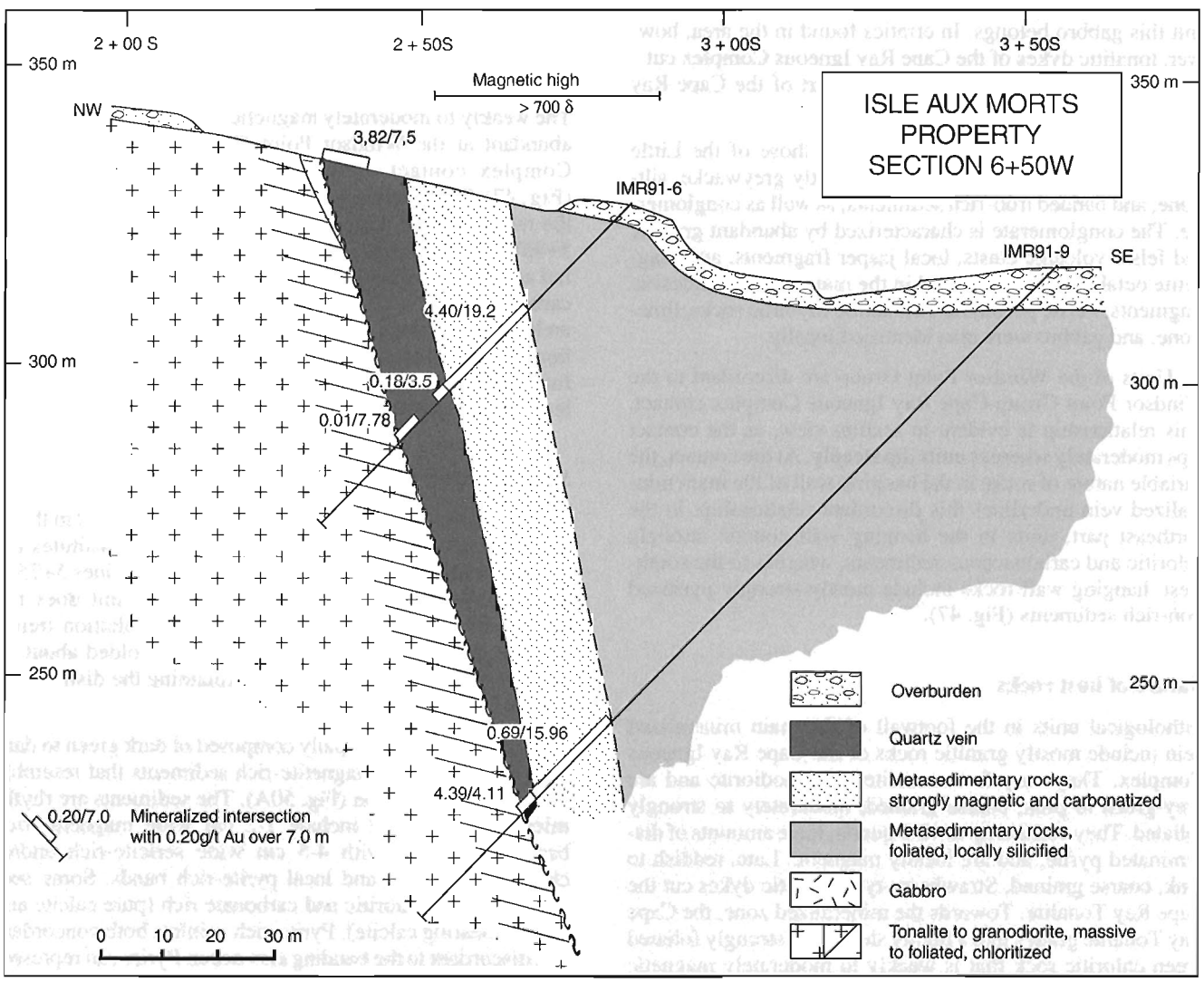

Figure 48. *Cross-section 6+50W, Isle aux Morts prospect. Modified from an unpublished diagram by Placer Dome.*

felsic dykes intrude the sediments. This unit also contains weakly to moderately calcareous sections with wispy calcite parallel to the main fabric. The rocks in this unit are generally nonmagnetic.

Geochemically, this unit is characterized by low Fe_2O_3 content (less than 6%), and silica generally greater than 60%, but varying between 49.6 and 77% (lithology C in Table 9).

Gabbro was also recognized in drill core to the southeast of this unit. The gabbro is typically chloritized and carbonatized. A gabbro sample (lithology D) was analyzed and results are presented in Table 9 (sample 91BD-201).

Origin of magnetite

Magnetite is ubiquitous in the deposit area. It also characterizes most rocks of the Little Barachois formation where it occurs as massive deformed veins that crosscut felsic and mafic volcanic rocks and as disseminations in conglomerates and in felsic volcanic units. The origin of all this magnetite is poorly constrained. A small part of the magnetite occurs as elongate aggregates surrounded by rutile and leucoxene and results from the transformation of primary titanomagnetite during greenschist metamorphism. However most of the magnetite occurs as scattered euhedral crystals, 0.4 mm in size, overprinting the main foliation. This magnetite probably results from recrystallization of iron-rich sediments.

Compared to the other gold occurrences in the area, magnetite is much more abundant in the Isle aux Morts prospect area. The highly magnetic nature of the sediments, their banded aspect, the presence of red cherty units and iron carbonates are all features typical of iron-formations, referred to as ironstones in Phanerozoic rocks. By definition ironstones contain over 21.3% Fe_2O_3 (James, 1966; Pettijohn, 1975) and the main oxide phase is hematite. Only two samples analyzed (Table 9) contain enough iron to be categorized as such, also

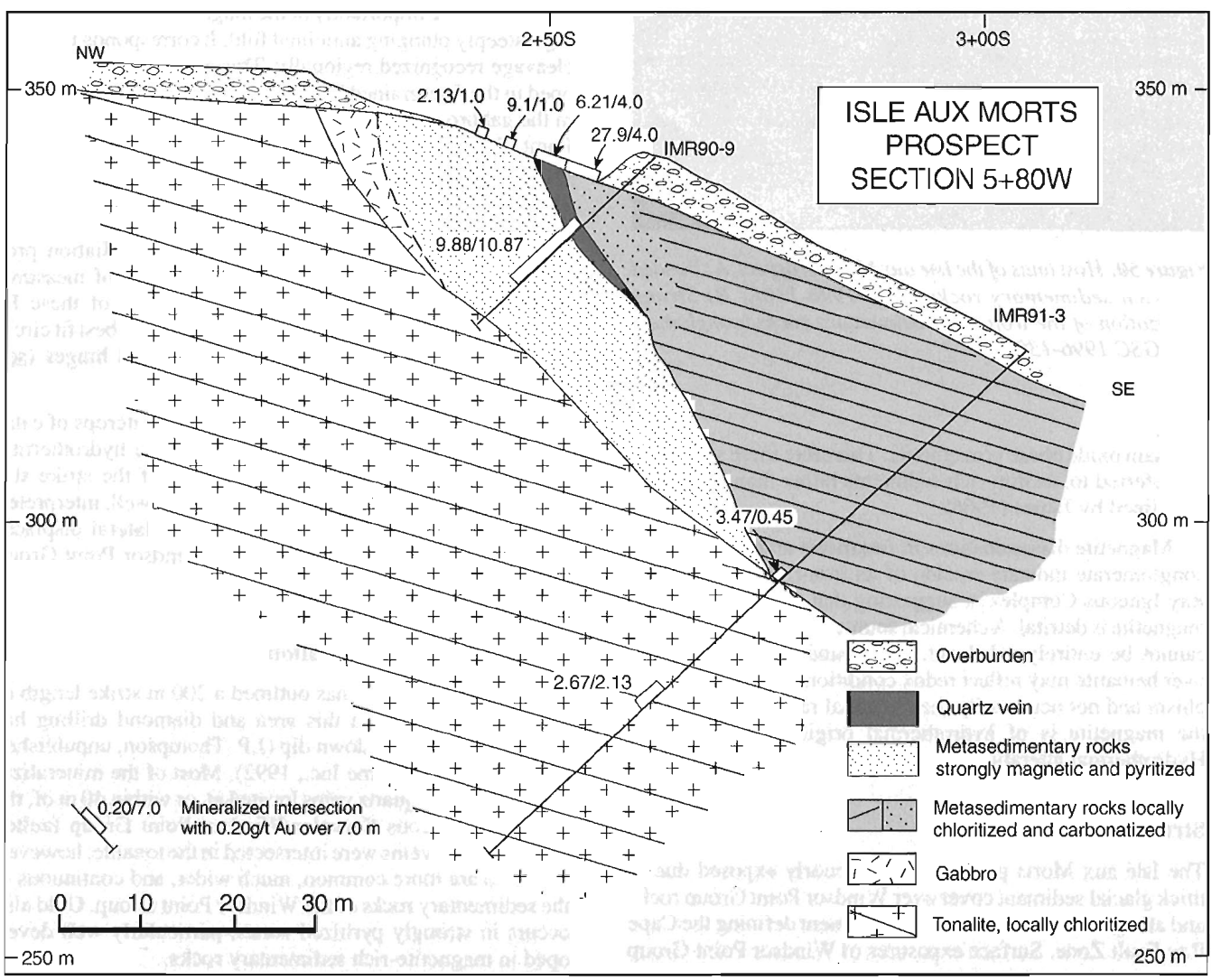

Figure 49. Cross-section 5+80W, Isle aux Morts prospect. Modified from an unpublished diagram by Placer Dome.

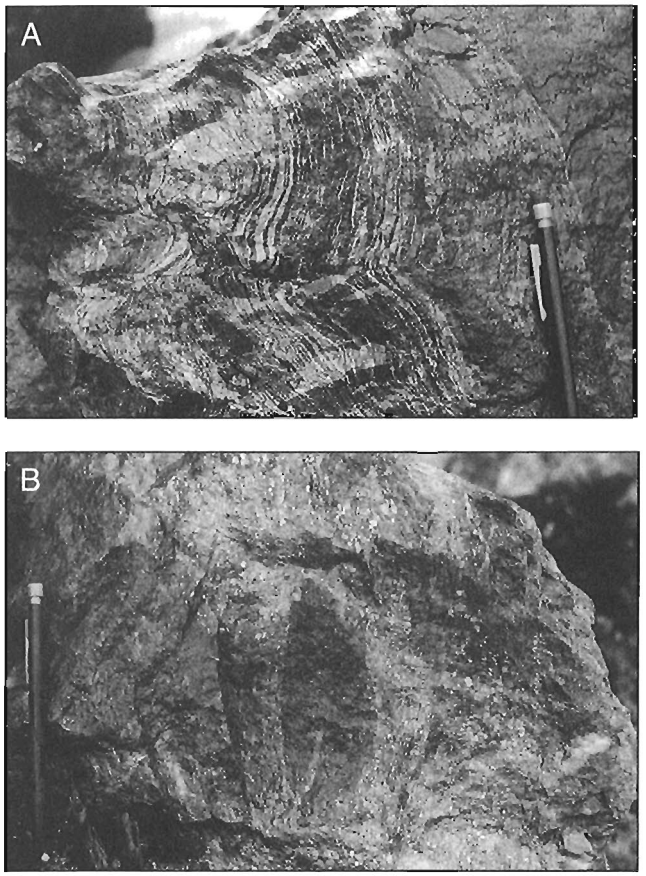

Figure 50. *Host units of the Isle aux Morts prospect.* ***A)*** *Banded iron-rich sedimentary rocks. GSC 1996-130A;* ***B)*** *Strong pyritization of the iron-rich sedimentary rocks (conglomerate). GSC 1996-130B*

the main oxide phase is magnetite. Therefore these sediments are referred to, as iron-rich sediments rather than ironstones as defined by James (1966).

Magnetite disseminations in fragments and matrix of the conglomerate indicate erosion of an iron-rich source (Cape Ray Igneous Complex?), suggesting that at least part of the magnetite is detrital. A chemical source for the iron, however, cannot be entirely ruled out. The abundance of magnetite over hematite may reflect redox conditions during metamorphism and not necessarily their original ratio. Also, some of the magnetite is of hydrothermal origin (see section on Hydrothermal alteration).

Structure of the deposit

The Isle aux Morts prospect area is poorly exposed due to thick glacial sediment cover over Windsor Point Group rocks and along the trace of the surface lineament defining the Cape Ray Fault Zone. Surface exposures of Windsor Point Group rocks are mostly restricted to streams and trenches in the vicinity of the mineralized zone. Aside from some outcrops of cataclastic breccia, the fault itself is not exposed.

Windsor Point Group units are complexly distributed as a result of a long history of folding, transposition, and faulting. The main penetrative fabric in this part of the fault zone is a bedding parallel northeast-oriented foliation (Fig. 46). It is a composite foliation correlated with the S_{3a-3b} defined at the regional scale. It contains a moderate to shallow dipping, moderately to poorly developed stretching lineation, best defined in the conglomerate by elongate clasts. In a stream northeast of the prospect area, a mylonitic zone that projects on strike with the strike slip mylonite southwest of the Strawberry Granite marks the Cape Ray Igneous Complex-Windsor Point Group contact (Fig. 46). It is characterized by poorly developed subhorizontal mineral lineations and is assigned to the D_4 deformation event.

The most notable structural feature of this area is the easterly crenulation cleavage that produces metric to decametric (20 m) scale sinistral folding of the composite S_{3a-3b} foliation, and more importantly of the magnetite-rich units, forming a steeply plunging anticlinal fold. It corresponds to the S_5 cleavage recognized regionally. This cleavage is best developed in the fine-grained banded sediments, but is also present in the gabbro near the Cape Ray Igneous Complex-Windsor Point Group contact. Structural elements are compiled in Figure 46. The S_5 crenulation cleavage, with an average orientation of 084°/65°, is responsible for the dispersion of the S_{3a-3b} foliation. F_5 folds are open to tight and plunge steeply southeast. Compilation of the S_{3a-3b} foliation produces a relatively wide girdle, with a maxima of measurements around 048°/78°. The calculated hinge of these F_5 folds (082°/70°), determined with the pole of the best fit circle of S_{3a-3b} foliations, is close to measured fold hinges (see measured F_5 fold hinges in Fig. 46).

Late brittle deformation occurs in some outcrops of cataclastic breccia that project on strike with the hydrothermal breccia (D_6) located in the hanging wall of the strike-slip mylonite in the Isle aux Morts River area. As well, interpreted east-northeast faulting is suggested by the lateral displacement of Cape Ray Igneous Complex-Windsor Point Group contact (Fig. 47).

Mineralization and alteration

Trenching and drilling has outlined a 200 m strike length of gold mineralization in this area and diamond drilling has traced it up to 100 m down dip (J.P. Thompson, unpublished report for Placer Dome Inc., 1992). Most of the mineralization is hosted in quartz veins located at, or within 40 m of, the Cape Ray Igneous Complex/Windsor Point Group faulted contact. Some veins were intersected in the tonalite, however, the veins are more common, much wider, and continuous in the sedimentary rocks of the Windsor Point Group. Gold also occurs in strongly pyritized zones, particularly well developed in magnetite-rich sedimentary rocks.

Table 9. Chemical analyses showing the composition of various units at the Isle aux Morts prospect.

				Trench 5+86W						
Location (m)	91BD-300	91BD-301	91BD-303A	91BD-303B*	91BD-304	91BD-305	91BD-307A	91BD-307B	91BD-311A	91BD-312b
	A·	A	A1	A1	A2	A1	A1	A1	A2	Q
lithology	py-mg	se-py	mg-py-se	mg-se	mg-se	mg-se-py	py-mg	mg	py-mg	py
SiO_2 %	54.10	52.80	54.70	49.51	67.30	52.50	60.40	68.00	45.80	
Al_2O_3 %	13.20	12.60	15.10	17.01	11.20	14.00	5.35	9.59	13.40	
TiO_2%	1.37	0.32	2.00	2.10	0.37	2.67	0.89	1.45	0.44	
Fe_2O_3(t) %	9.33	19.90	11.30	7.50	14.20	16.40	20.80	13.50	24.50	
MnO%	0.21	0.02	0.12	0.31	0.03	0.03	0.01	0.02	0.02	
MgO%	0.76	0.37	1.85	1.99	0.42	0.82	0.26	0.42	0.55	
CaO%	6.83	0.01	3.92	5.93	0.04	0.67	0.25	0.42	0.04	
Na_2O%	2.35	0.05	0.08	0.41	0.29	0.06	0.04	0.04	0.07	
K_2O%	3.21	4.33	4.99	5.90	3.75	4.94	1.91	3.31	4.84	
P_2O_5%	0.25	0.04	0.49	0.32	0.07	0.54	0.21	0.29	0.09	
LOI%	3.62	9.85	4.62	7.96	1.93	7.31	9.93	2.70	10.50	
CO_2%	5.48	0.04	2.69		0.05	0.04	0.05	0.08	0.04	
H_2O+%	1.1	0.9	2.2		1.2	1.4	0.7	1.3	1	
S% *2	4.31	13.00	2.98	0.65	0.63	8.42	14.60	2.10	13.91	3.25
Total	102.50	104.38	102.42	99.59	99.55	102.49	105.47	100.52	104.70	
	Metallic trace elements									
Cu (ppm)	169	43	38	69	25	22	23	46	66	965
Zn (ppm)	62	76	109	93	129	89	33	71	75	6
As (ppm)	2	2	2	<2	2	2	2	2	2	3
Mo (ppm)	5	27	5	<2	10	18	7	5	5	1
Ag (ppm)	0.9	1.8	0.5		0.5	1.1	1.5	0.5	1.7	29.8
Pb (ppm)	12	3	9	13	25	9	7	15	80	25 400
Au (ppb)	8100	19 000	4000	681	680	17 000	20 000	1600	26 000	10 000
	Trace elements (ppm)									
B	12	23	29		33	27	16	21	27	
Ba	563	960	893	541	1270	1190	709	1240	1540	4220
Be	4	6	5		4	6	4	4	7	0.5
Br	3	3	3		2	2	2	1	4	
Cd	1	1	1		1	1	1	1	1	4
Co	21	4	18	23	2	15	8	3	19	11
Cr	41	35	91	144	26	66	28	42	38	16
Cs	1	1	2	1.88	2	3	1	1	1	
Ge	10	10	10	23	10	10	10	10	10	
Hf	7.1	3.9	6.1	3.2	3.7	5.5	1.6	4.3	5.6	
Nb	26	23	23	16	10	20	30	32	19	
Ni	23	30	30	47	11	20	9	10	18	8
Rb	94	149	195	211	155	192	59	134	202	
Sb	8.5	3.4	20	12.8	4.2	31	12	21	4.4	<5
Sc	19.8	6.2	30.2	34.0	7.2	34.2	11.1	18.6	9.1	0.5
Se	3	3	3	<2	3	3	3	3	3	
Sr	140	12	116	114	26	27	10	20	27	142
Ta	1	1	1	0.5	1	1	1	1	1	
Th	8.9	14	5.9	0.9	12	4	2.1	4	19	
U	2.7	1.7	2.9	19.6	1.8	4.2	1.5	2.5	3.7	
V	129	69	165	264	58	249	81	145	76	3
W	110	24	58	39	20	100	36	61	32	10
Y	39	23	26	31.3	25	28	17	15	10	0.2
Zr	319	157	248	139	124	249	111	177	198	2
	Rare-earth elements (ppm)									
La	39.5	28.6	23.7	13.6	78.1	20.9	11.1	21.1	34	
Ce	77	45	50	32	96	43	22	35	53	
Nd	36	16	27	21.5	32	23	11	23	15	
Sm	7.3	2.4	6	5.08	4	5.3	2.4	4.9	2	
Eu	1.8	0.6	2.5	1.7	1.2	2.5	0.7	1.2	0.9	
Tb	1	0.6	0.8	0.8	0.7	1	0.5	0.9	0.8	
Yb	3.5	2.5	3.1	2.54	2.2	3.5	1.3	2	3.3	
Lu	0.47	0.36	0.46	0.38	0.32	0.5	0.17	0.27	0.44	

All analyses carried out at XRAL Laboratories except as noted
*1 analyses carried out at INRS-Georessources
*2 analyses carried out at Geological Survey of Canada Laboratory

A: magnetite-rich sediments	A1: banded	A2: conglomerate		
B: carbonate-rich sediments	C: siliceous metasediments	D: gabbro	F: mylonite	Q: quartz vein
E1: tonalite and granodiorite	E2: granite	E3: aplite		
se: sericite	py: pyrite	mg: magnetite	cl: chlorite	carb: carbonate

D*3: Duplicate sample

Table 9. (cont.)

	Trench 5+86W						
Sample	91BD-306A	91BD-306B	91BD-306C	92BD-104A	92BD-104B	92BD-104C	91BD-306AD*3
	A2	A2	A2	A2	A2	A2	A2
Ilthology	mg	mg-se	py-se	mg	mg-se	py-se	mg
SiO_2 %	44.00	44.5	39.5	40.2	40.8	46.1	43.90
Al_2O_3 %	14.9	21.6	16.4	20.2	20.8	17.6	14.9
TiO_2%	3.14	4.71	3.69	4.28	4.45	3.89	3.12
Fe_2O_3(t) %	28.2	14.6	21.6	19.6	19.00	15.1	28.00
MnO%	0.04	0.03	0.02	0.05	0.04	0.02	0.04
MgO%	0.72	1.05	0.74	1.28	1.25	0.84	0.70
CaO%	0.89	1.25	1.02	1.14	1.24	1.03	0.88
Na_2O%	0.11	0.12	0.11	0.14	0.15	0.13	0.11
K_2O%	5.36	7.87	6.10	7.64	7.81	6.73	5.40
P_2O_5%	0.60	0.84	0.67	0.79	0.82	0.70	0.60
LOI%	1.90	3.20	10.4	3.50	3.75	7.90	1.80
CO_2%	0.03	<0.01	0.02	0.01	0.01	0.03	0.03
H_2O+%	1.8	2.3	1.1	2.2	2.2	1.1	1.7
S%*2	0.02	0.32	11.9	0.78	0.75	7.61	0.02
Total	100.1	100.2	100.6	99.1	100.4	100.4	99.70
	Metallic trace elements						
Cu (ppm)	64.3	36.5	27.5	146	107	19.3	71
Zn (ppm)	69.3	82.7	60.5	109	113	67.5	73.3
As (ppm)	2	1	3	2	2	4	2
Mo (ppm)	<1	<1	<1	<1	<1	<1	<1
Ag (ppm)	1.9	1.2	2.4	1.4	1.4	2.2	0.9
Pb (ppm)	2	<2	3	6	<2	2	4
Au (ppb)	35	223	18 300	220	159	20 300	40
	Trace elements (ppm)						
B	27	25	18	21	22	21	22
Ba	1830	2520	2180	1990	2100	2130	1840
Be	6	6	4	7	7	6	5
Br	2	2	2	2	2	2	2
Cd	<1	<1	<1	<1	<1	<1	<1
Co	7	3	8	<1	1	13	8
Cr	69	97	57	82	90	78	72
Cs	2	2	3	4	3	<1	1
Ge	<10	<10	<10	<10	<10	<10	<10
Hf	5	8	7	8	7	7	6
Nb	14	18	15	17	16	17	11
Ni	8	9	7				1
Rb	181	269	198	278	279	230	185
Sb	36	71	54	27	37	57	38
Sc	34.1	47.8	41.5	47.5	47.9	43.5	35.7
Se	<3	<3	<7	<3	<3	<9	<3
Sr	71	99	80	102	99	90	71
Ta	1	1	<1	1	1	<1	1
Th	3	4	3	4	4	3	3
U	2.9	5.1	4.6	5.4	4.6	4.1	3.1
V	358	334	256	302	316	250	352
W	87	150	140	83	95	130	89
Y	56	67	58	60	60	52	55
Zr	270	372	296	346	361	305	266
	Rare-earth elements (ppm)						
La	33.9	39.2	43	27.8	29.5	37.7	34.5
Ce	72	84	83	62	65	72	71
Nd	35	42	37	30	30	33	34
Sm	7.6	9.0	7.5	7.1	7.5	6.9	7.8
Eu	2.0	1.9	3.0	1.7	1.7	2.6	2
Tb	1.3	1.6	1.2	1.4	1.2	0.8	1.3
Yb	5.1	6.8	5.4	6.1	6.4	5.5	5.3
Lu	0.78	0.99	0.89	0.95	1.01	0.97	0.78

All analyses carried out at XRAL Laboratories except as noted
*1 analyses carried out at INRS-Georessources
*2 analyses carried out at Geological Survey of Canada Laboratory

A: magnetite-rich sediments	A1: banded	A2: conglomerate		
B: carbonate-rich sediments	C: siliceous metasediments	D: gabbro	F: mylonite	Q: quartz vein
E1: tonalite and granodiorite	E2: granite	E3: aplite		
se: sericite	py: pyrite	mg: magnetite	cl: chlorite	carb: carbonate

D*3 : Duplicate sample

Trench 5+20W							
Sample	91BD-20*[1]	91BD-21	91BD-30	91BD-314	91BD-315*	91BD-319	91BD-318a
	C	C	B	B	B	F	Q
lithology		cl				se	py
SiO_2%	76.42	64.50	36.60	38.10	41.83	47.10	
Al_2O_3%	12.12	13.70	17.30	18.40	18.15	11.70	
TiO_2%	0.54	0.57	0.71	0.84	0.91	2.75	
Fe_2O_3(t)%	1.09	4.23	13.00	9.59	10.24	11.80	
MnO%	0.06	0.18	0.47	0.45	0.45	0.22	
MgO%	1.24	2.15	4.04	2.62	2.98	0.85	
CaO%	0.85	4.18	9.23	10.40	9.37	10.90	
Na_2O%	4.60	3.98	0.13	0.15	0.00	2.55	
K_2O%	1.60	2.48	5.11	5.61	5.71	2.62	
P_2O_5%	0.15	0.10	0.23	0.24	0.22	1.45	
LOI%	1.50	3.70	13.40	13.80	10.25	8.23	
CO_2%		4.19	13.3	11.1		7.39	
H_2O+%		1	2.1	2.3		1.1	
S% *[2]	0.00	0.03	0.15	1.31	1.36	0.02	5.78
	100.16	101.29	102.37	101.11	100.11	100.45	
	Metallic trace elements						
Cu (ppm)	203	4	271	132	127	16	58
Zn (ppm)	34	61	120	115	135	53	8
As (ppm)	2.83	2	6	5	8.91	6	3
Mo (ppm)	<2	5	5	15	6.65	6	40
Ag (ppm)		0.5	0.5	0.7		0.5	3.8
Pb (ppm)	208	8	6	11	23	19	564
Au (ppb)	56	41	85	1000	887	5	5110
	Trace elements (ppm)						
B		16	22	30		12	
Ba	416	538	814	929	869	568	127
Be		3	5	5		5	0.9
Br		2	2	3		2	
Cd		1	1	2		1	1
Co	4	14	23	30	35	15	19
Cr	103	71	19	52	52	20	17
Cs	0.44	2	1	2	1.79	1	
Ge	10.32	10	10	10	18.16	10	
Hf	5.8	6	1.9	2.4	1.3	6.7	
Nb	9	11	13	18	12	31	
Ni	17	40	13	23	14	20	2
Rb	38	80	131	147	164	77	
Sb	3.3	2.5	0.5	0.5	0.4	9.5	<5
Sc	7.7	12.3	37.2	49.3	48.5	28.3	0.6
Se	<2	<2	<2	<2	<2	<2	
Sr	75	88	168	206	243	107	3
Ta	<1	<1	<1	<1	<1	<1	
Th	7.3	8.3	0.8	1.3	2.7	3.4	
U	2.4	2.3	<0.5	<0.5	0.6	1.5	
V	56	94	283	379	409	184	12
W	23	<3	16	4700	1420	9	124
Y	23.6	36	20	31	28.6	48	0.6
Zr	179	225	62	48	39	269	2
	Rare-earth elements (ppm)						
La	33.4	26.8	12.7	13.6	12.9	35	
Ce	66	49	30	46	32.2	86	
Nd	28.3	17	14	20	17	58	
Sm	5.43	4.4	3.4	4.1	4.47	10.7	
Eu	1.14	0.7	1.1	1	1.13	4.3	
Tb	0.59	0.7	0.5	0.9	0.57	1.7	
Yb	2.18	3	1.5	2.1	2.13	4.1	
Lu	0.34	0.47	0.25	0.29	0.3	0.65	

All analyses carried out at XRAL Laboratories except as noted
*[1] analyses carried out at INRS-Georessources
*[2] analyses carried out at Geological Survey of Canada Laboratory
A: magnetite-rich sediments A1: banded A2: conglomerate
B: carbonate-rich sediments C: siliceous metasediments D: gabbro F: mylonite Q: quartz vein
E1: tonalite and granodiorite E2: granite E3: aplite
se: sericite py: pyrite mg: magnetite cl: chlorite carb: carbonate
D*[3]: Duplicate sample

Table 9. (cont.)

Drillhole IMR-91-9												
Sample	91BD-201*[1]	91BD-203*[1]	91BD-205*[1]	91BD-206*[1]	91BD-209*[1]	91BD-212*[1]	91BD-213*[1]	91BD-215*[1]	91BD-216*[1]	91BD-217	91BD-218	91BD-219
location (m)	13.9	24.2	33.3	44.5	57.0	81.8	89.7	98.8	103.0	108.8	110.0	113.3
	D	C	C	C	C	C	C	C	C	A1	A1	A1
lithology										mg	se-mg	se-mg
SiO_2%	44.73	54.93	49.60	51.83	66.87	75.20	76.84	61.30	68.48	66.30	50.20	48.50
Al_2O_3%	13.65	17.48	19.76	18.72	14.64	10.77	9.03	17.03	11.00	13.30	12.40	13.10
TiO_2%	3.23	1.05	1.29	1.35	0.70	0.74	1.15	0.97	0.75	0.84	2.73	2.89
Fe_2O_3(t)%	13.84	4.77	4.48	4.13	2.99	1.56	1.33	2.33	5.86	6.00	10.60	13.80
MnO%	0.28	0.13	0.28	0.36	0.06	0.06	0.10	0.06	0.07	0.13	0.22	0.17
MgO%	6.65	3.22	3.22	3.32	1.77	1.46	1.48	1.72	2.38	1.69	2.72	2.78
CaO%	7.05	4.81	6.60	5.93	1.88	2.40	2.44	2.67	2.10	2.40	6.99	6.26
Na_2O%	3.35	5.88	5.47	6.67	1.99	2.05	3.34	5.01	2.41	5.30	2.90	2.67
K_2O%	1.67	4.51	3.23	1.97	3.76	2.56	1.18	5.95	2.29	1.46	2.48	3.07
P_2O_5%	0.38	0.21	0.20	0.23	0.16	0.14	0.19	0.18	0.21	0.18	0.63	0.61
LOI%	6.97	4.46	7.03	6.08	3.36	2.97	2.60	2.26	3.16	1.39	8.23	5.77
CO_2%										1.66	8.53	6.42
H_2O+%										1.1	1	1.1
S%*[2]	0.00	0.00	0.00	0.00	0.00	0.00	0.00	0.00	0.80	0.03	0.38	0.06
Total	101.80	101.44	101.16	100.59	98.19	99.90	99.68	99.49	98.72	100.55	101.95	101.61
Metallic trace elements												
Cu (ppm)	21	<4	9	<4	<4	<4	<4	5	10	57	266	18
Zn (ppm)	299	119	124	98	78	65	58	68	125	95	139	151
As (ppm)	<2	<2	<2	<2	<2	<2	<2	<2	<2	<2	<2	<2
Mo (ppm)	<2	<2	<2	<2	<2	<2	<2	<2	<2	<5	<5	<5
Ag (ppm)										<0.5	<0.5	<0.5
Pb (ppm)	17	7	13	13	11	10	34	14	11	7	6	8
Au (ppb)	<5	<5	<5	<5	<5	<5	22	<5	168	29	79	14
Trace elements (ppm)												
B										<10	<10	11
Ba	677	1157	787	586	959	444	379	1713	755	492	731	878
Be										5	4	5
Br										4	3	3
Cd										<1	1	1
Co	42	12	4	5	6	5	5	8	7	5	16	19
Cr	72	103	118	115	110	154	160	105	70	<6	38	35
Cs	1.71	1.8	1.57	0.84	1.1	5.21	2.27	2.46	2.52	3	<2	3
Ge	18.15	11.88	22.36	19.31	19.78	10.24	8.5	10.21	18.81	<10	<10	11
Hf	4	13.2	17.8	18.2	8.07	12.5	25.6	16.4	9.63	9.4	7.3	7.1
Nb	19	19	22	22	12	12	15	15	22	38	13	26
Ni	41	38	36	22	19	10	<3	30	7	6	22	26
Rb	63	165	96	56	116	103	45	238	85	71	88	106
Sb	3.7	0.2	1.9	3	1.1	3.6	3.4	0.3	0.9	1.1	9.4	11
Sc	32.4	13.4	15.5	13.6	10.8	8.1	8.7	8.6	28.1	48.7	30.9	34.5
Se	<2	<2	<2	<2	<2	<2	<2	<2	<2	<3	<3	<3
Sr	224	187	325	273	114	123	102	151	99	106	170	139
Ta	0.6	1	1.5	1.5	0.8	0.9	1.3	1	1.3	<1	<1	<1
Th	1	15.1	18.4	18.2	9.9	117	16.8	13.5	7.2	7.4	3.6	2.9
U	<0.5	3.4	4.3	4.6	2.5	2.9	5.4	3.4	2	1.5	5.1	3.9
V	408	79	110	88	83	52	38	55	32	<10	102	124
W	8	8	19	15	14	15	14	7	10	11	45	34
Y	35.7	39.9	63.1	49.7	26.8	37.8	54.8	42.3	68.8	87	45	42
Zr	167	409	590	552	248	479	912	620	434	494	355	332
Rare-earth elements (ppm)												
La	16.8	49.6	55.6	77.6	40.9	43.3	53.7	44.6	43.8	46.2	33.4	32.9
Ce	41.3	108	119	166	86.4	92.9	115	95.6	98.7	99	70	65
Nd	23.1	44.6	47.2	64.4	35.2	39.6	45.5	38.5	47.2	50	36	35
Sm	6.49	8.66	9.68	12.1	6.81	7.9	9.12	8.2	11.7	11.7	8.9	7
Eu	2.33	2.01	2.26	2.36	1.39	1.62	1.97	1.82	4.01	6	3.5	2
Tb	0.966	1.05	1.51	1.35	0.701	0.978	1.26	1.05	1.76	2.7	1.3	<0.5
Yb	3.07	3.77	5.82	5.12	2.52	3.62	4.59	4.16	6.46	8.4	4.3	4.2
Lu	0.469	0.587	0.931	0.794	0.389	0.555	0.76	0.63	1.05	1.31	0.61	0.6

All analyses carried out at XRAL Laboratories except as noted
*[1] analyses carried out at INRS-Georessources
*[2] analyses carried out at Geological Survey of Canada Laboratory
A: magnetite-rich sediments A1: banded A2: conglomerate
B: carbonate-rich sediments C: siliceous metasediments D: gabbro F: mylonite Q: quartz vein
E1: tonalite and granodiorite E2: granite E3: aplite
se: sericite py: pyrite mg: magnetite cl: chlorite carb: carbonate
D*[3]: Duplicate sample

	Drillhole IMR-91-9											
	91BD-220*[1]	91BD-221	91BD-222	91BD-223	91BD-224	91BD-225*[1]	91BD-226	91BD-228	91BD-229*[1]	91BD-230*[1]	91BD-231	91BD-232*[1]
Location (m)	117.0	117.0	121.2	126.7	130.0	131.8	133.3	136.7	138.5	140.6	144.2	147.9
	A1	A1	A1	E	E	E	E	E	E	E2	E2	E3
lithology	mg	mg-py	mg	cl	cl	cl		cl	cl			
SiO_2%	41.65	45.70	47.60	61.60	59.90	62.77	56.20	59.30	61.60	74.57	76.50	
Al_2O_3%	14.06	13.00	14.90	14.30	14.60	15.03	15.20	15.70	14.51	12.80	12.90	
TiO_2%	1.99	1.43	1.75	0.39	0.45	0.43	0.44	0.49	0.43	0.13	0.12	
Fe_2O_3(t)%	10.94	9.83	11.20	6.08	7.46	4.50	6.95	7.34	5.31	0.13	0.70	
MnO%	0.35	0.31	0.26	0.25	0.26	0.22	0.39	0.29	0.26	0.05	0.06	
MgO%	5.90	4.20	5.86	1.87	2.06	1.92	2.72	2.44	2.47	0.62	0.48	
CaO%	8.11	8.39	5.82	5.36	5.23	3.83	6.43	4.52	4.59	1.63	1.38	
Na_2O%	1.66	3.50	2.28	2.55	1.28	2.03	0.45	1.99	2.94	4.15	4.94	
K_2O%	4.37	2.36	2.72	3.01	3.60	3.96	4.16	3.32	3.25	2.13	1.61	
P_2O_5%	0.23	0.22	0.23	0.13	0.12	0.13	0.16	0.12	0.16	0.09	0.04	
LOI%	12.32	9.93	6.47	3.16	3.85	4.73	6.16	4.00	5.17	2.21	1.54	
CO_2%		11.2	4.35	4.22	4.09		5.01	3.28			0.99	
H_2O+%		1.1	3.4	1.6	2		2.3	2.1			0.7	
S %*[2]	0.03	0.20	0.00	1.05	1.24	0.73	0.53	0.03	0.23	0.02	0.01	2.15%
Total	101.56	101.58	100.52	102.61	102.48	99.54	101.18	101.04	100.70	98.49	100.68	
	Metallic trace elements											
Cu (ppm)	8	41	5	77	24	28	254	15	25	6	12	<4
Zn (ppm)	255	204	397	129	126	80	172	131	70	18	18	20
As (ppm)	<2	<2	<2	<2	<2	<2	<2	<2	<2	<2	<2	<2
Mo (ppm)	<2	<5	5	<5	<5	<2	<5	<5	<2	<2	<5	<2
Ag (ppm)		<0.5	<0.5	0.6	<0.5		1	<0.5			<0.5	
Pb (ppm)	10	6	9	16	15	13	14	9	6	13	7	15
Au (ppb)	144	120	190	420	99	48	66	<5	8	<5	<5	887
	Trace elements (ppm)											
B		19	<10	22	22		21	26			18	
Ba	747	559	725	1240	1160	1390	1580	661	601	1855	1830	1153
Be		2	4	4	4		3	5			2	
Br		2	3	3	2		2	1			2	
Cd		2	1	1	1		1	<1			<1	
Co	44	39	48	15	23	11	15	16	12	3	2	10
Cr	86	68	73	9	11	58	9	13	41	75	3	78
Cs	3.55	2	5	3	2	1.76	3	1	1.43	1.03	<1	1.21
Ge	17.91	<10	<10	<10	14	16.14	<10	<10	12.94	9.41	<10	8.55
Hf	3.34	4.1	3.9	2.3	2.5	2.89	1.9	3	2.75	3.57	2	2.45
Nb	19	12	20	-10	17	8	<10	17	9	2	24	11
Ni	64	53	76	9	9	<3	9	10	<3	<3	4	<3
Rb	128	73	106	100	112	108	134	117	117	67	53	72
Sb	1.2	1.1	0.7	0.6	0.3	0.4	0.2	0.5	0.7	0.3	0.2	0.3
Sc	32.1	23.8	30.0	19.6	18.6	21.1	27.0	33.9	22.9	3.0	3.5	5.0
Se	<2	<3	<3	<3	<3	<2	<3	<3	<2	<2	<3	<2
Sr	256	343	248	349	175	146	275	140	104	123	229	81
Ta	0.6	<1	<1	<1	<1	0.3	<1	<1	0.2	0.1	<1	1.5
Th	0.8	2.7	2.3	2	2.4	5.1	0.7	0.9	4.2	7.4	4	18.6
U	<0.5	0.9	0.8	0.7	0.9	<0.5	0.7	1.3	<0.5	1.1	0.9	7.2
V	294	135	201	127	150	99	139	160	126	25	<10	34
W	14	11	11	10	16	15	20	3	<5	<5	<3	<5
Y	29.5	23	29	21	34	18.1	27	39	39.1	8.1	16	23.7
Zr	183	163	175	88	110	97	84	104	124	133	87	77
	Rare-earth elements (ppm)											
La	11.9	14.4	14.4	15.5	13	23.8	9.4	7.2	30.1	40.1	15.9	22.6
Ce	30.4	32	32	32	30	48.7	22	21	67.4	73.7	24	43.9
Nd	17.6	17	17	15	15	18.8	13	15	32.6	19.9	7	16
Sm	4.75	4	4	3.3	3.8	3.62	3.3	4.7	7.88	2.15	1.2	3.2
Eu	1.64	1.6	1.7	0.9	0.7	0.843	0.8	0.9	1.37	0.852	0.7	0.668
Tb	0.711	<0.5	0.7	0.7	1	0.447	<0.5	0.7	1.07	0.132	<0.5	0.531
Yb	2.47	2	2.2	2	2.8	1.95	2	3.9	3.61	0.665	0.5	1.5
Lu	0.334	0.35	0.32	0.28	0.4	0.251	0.31	0.64	0.517	0.109	0.09	0.26

All analyses carried out at XRAL Laboratories except as noted
*[1] analyses carried out at INRS-Georessources
*[2] analyses carried out at Geological Survey of Canada Laboratory

A: magnetite-rich sediments	A1: banded	A2: conglomerate		
B: carbonate-rich sediments	C: siliceous metasediments	D: gabbro	F: mylonite	Q: quartz vein
E1: tonalite and granodiorite	E2: granite	E3: aplite		
se: sericite	py: pyrite	mg: magnetite	cl: chlorite	carb: carbonate

D*[3]: Duplicate sample

Table 9. (cont.)

Sample	91BD-03	91BD-28	91BD-320	92BD-108	91BD-321*[1]
	Others				
	F	E	Q	Q	F
lithology	carb				
SiO_2%	57.90	71.00			69.18
Al_2O_3%	12.70	13.70			12.61
TiO_2%	0.74	0.24			0.51
Fe_2O_3(t)%	5.42	3.08			2.91
MnO%	0.13	0.09			0.11
MgO%	3.05	1.14			1.72
CaO%	6.01	1.63			2.53
Na_2O%	2.15	3.84			3.32
K_2O%	2.96	2.36			2.09
P_2O_5%	0.15	0.07			0.07
LOI%	7.62	1.93			3.93
CO_2%	8.14	1.25			
H_2O+%	1.3	1.3			
S %*[2]	0.46	0.07			0.73
Total	101.23	99.95			98.98
Metallic trace elements					
Cu (ppm)	18	41	10 200	6570	4
Zn (ppm)	136	81	93	13	50
As (ppm)	7	<2	4	<3	3.31
Mo (ppm)	<5	<5	16	<1	<2
Ag (ppm)	<0.5	<0.5	41	51	
Pb (ppm)	10	78	8290	36 700	38
Au (ppb)	<5	5	4460	26 300	<5
Trace elements (ppm)					
B	39	20			
Ba	496	1100			282
Be	2	2			
Br	2	3			
Cd	1	<1			
Co	16	7			4
Cr	96	8			64
Cs	2	1			1.2
Ge	<10	<10			8.69
Hf	5.7	2.6			3.2
Nb	19	19			5
Ni	112	5			26
Rb	105	96			62
Sb	0.5	0.6	<5	<5	0.4
Sc	11.3	9.3			13.5
Se	<3	<3			<2
Sr	104	265			122
Ta	<1	<1			<1
Th	8.6	8.1			7.4
U	2.5	1.1			<0.5
V	76	35			21
W	3	7			<5
Y	23	<10			24.8
Zr	270	107			120
Rare-earth elements (ppm)					
La	32	29.2			18.8
Ce	62	50			39.3
Nd	27	19			16.8
Sm	5.2	3.1			3.8
Eu	1.7	0.8			1.01
Tb	0.7	0.7			0.58
Yb	2.4	1.6			2.21
Lu	0.35	0.22			0.38

All analyses carried out at XRAL Laboratories except as noted
*[1] analyses carried out at INRS-Georessources
*[2] analyses carried out at Geological Survey of Canada Laboratory
A: magnetite-rich sediments; A1: banded; A2: conglomerate
B: carbonate-rich sediments; C: siliceous metasediments; D: gabbro
F: mylonite; Q: quartz vein
E1: tonalite and granodiorite; E2: granite; E3: aplite
se: sericite; py: pyrite; mg: magnetite; carb: carbonate
D*[3]: Duplicate sample; cl: chlorite

The widest and most continuous gold-bearing vein is located at the granite-sedimentary rock contact and is hosted in the sediments. It extends from line 6+85W up to 5+80W (Fig. 47). Its average orientation is 060° and dips moderately to steeply south. It varies in width from 1 to 8 m. The vein, almost 8 m wide in trench 5+95W, is nearly absent only 10 m away in trench 5+86W. There, mineralization occurs in several veins less than 1 m wide and in over 10 m of strongly pyritized coarse sediments. A similar setting occurs in trench 5+86W where a mineralized quartz vein terminates abruptly against felsic sedimentary rocks and interbedded pyrite- and magnetite-rich sediments (Fig. 47).

Type 1 mineralization: mineralized quartz veins

The mineralized veins comprise white and greyish quartz with up to 8% sulphides. No shear fabric subparallel to the vein is present in the host rocks. The veins are best described as fault-fill. They are massive, devoid of any banding or fabric. The sulphides, mostly pyrite with lesser amounts of chalcopyrite and galena, are disseminated or in aggregates, filling fractures. Rare wall rock tonalitic enclaves were recognized. The veins typically contain two generations of quartz. The first includes deformed and recrystallized grey quartz, the second is whitish and comprises slightly deformed euhedral to subhedral crystals up to 1-2 cm (Fig. 51A).

Type 2 mineralization: alteration zones in magnetite-rich sediments

Significant gold mineralization is also present in wall rock alteration zones that extend up to 10 m from the main mineralized vein in the hanging wall of the mineralized zone (Windsor Point Group). The gold is concentrated in pyrite-rich alteration zones (Fig. 51B). The gold values in this zone range up to 5.18g/t of gold over 24.1 m (DDH IMR-91-6, J.M. Dawson, contract report to Fortune Bay Resources Ltd., 1991). There is a direct correlation between gold values and the abundance of sulphur in the rock (Table 9), indicating that sulphide complexes played an important role in the transport and deposition of gold.

Alteration

The distribution of alteration zones is variable according to host lithology. The wider and more significant alteration zones occur in magnetite-rich conglomerates. Pyritization is extensive, relatively homogeneously distributed throughout the matrix and related to a stockwork arrangement of quartz-pyrite veinlets (Fig. 51B). In banded sediments, pyritization is less extensive and has produced pyrite-rich layers intercalated with quartz-rich, sericite-rich, and magnetite-rich bands (Fig. 51C).

The study of alteration can be best documented in the magnetite-rich conglomerates, as magnetite is somewhat more evenly distributed than in banded rocks. In the conglomerates, visible alteration surrounding quartz-pyrite veinlets can be more than four times the width of the associated mineralized vein. The veinlets generally consist of pyrite-rich

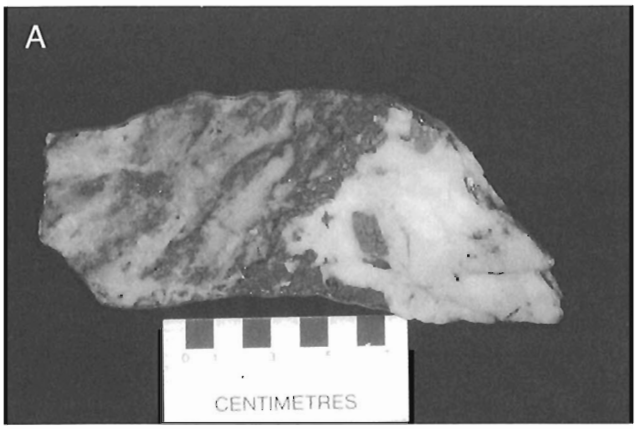

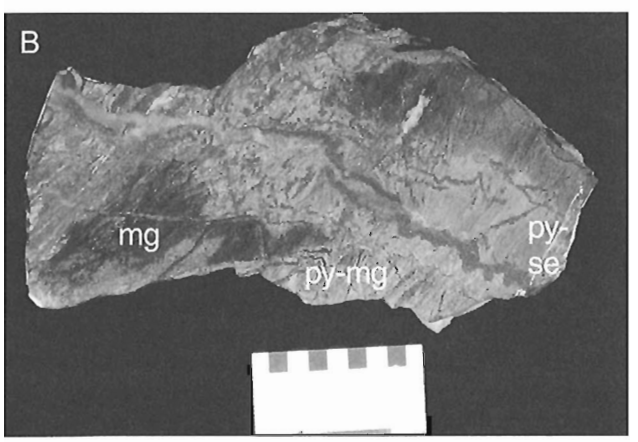

Figure 51. *Mineralization at the Isle aux Morts prospect.* ***A)*** *Two types of quartz present in the auriferous vein. GSC 1996-130C;* ***B)*** *Strong pyritization of the iron-rich sediments. Note quartz-pyrite veinlets and associated symmetric pyritization developed in the adjacent iron-rich host rock. Pyrite in the veinlets occurs at the borders. py-se refers to the pyrite-sericite alteration zone, mg to the magnetite-rich zone, and py-mg to the pyrite-magnetite zone. GSC 1996-130D;* ***C)*** *Pyritization is developed parallel to banding; rusty pyrite-rich layers are intercalated with quartz-rich, sericite-rich, and magnetite-rich bands. GSC 1996-130E*

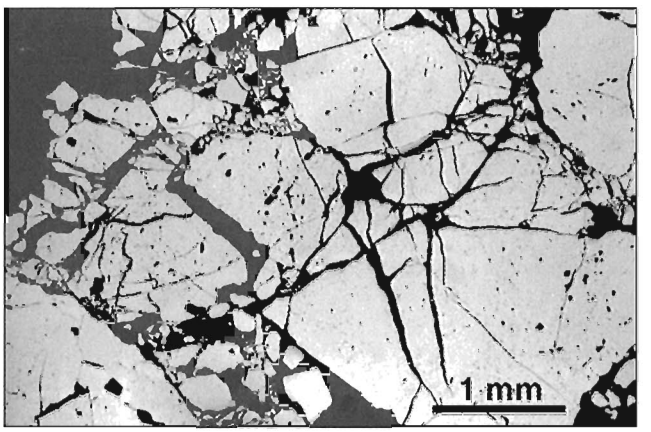

Figure 52. *Photomicrograph showing cataclastic deformation in pyrite. GSC 1996-130F*

margins and quartz-rich centres (Fig. 51B). The visible, proximal alteration zone is one of intense sericitization conferring a beige-yellowish colour to the rock. This zone is divided into two subzones: the first is characterized by the near complete absence of magnetite and presence of discontinuous, millimetre-scale pyrite veinlets that crosscut the main S_{3a-3b} fabric and are folded by the S_5 crenulation cleavage; the second is more distal and contains disseminated fine-grained (less than 1 mm) magnetite with little or no pyrite (Fig. 51B). Gold mineralization is restricted to the pyrite-rich zone. The visible alteration zone is in sharp contact with what can be termed the distal alteration zone that also comprises magnetite, and much lesser proportions of sericite.

Chemical analyses of the various alteration zones are presented in Table 9. The more significant chemical variations occur within the visible alteration zone, between the magnetite-sericite and pyrite-sericite zones. Changes in chemical composition are limited to an increase in sulphur and gold content in samples from the pyrite-sericite alteration zone. Little other variation is observed between the pyrite-sericite and magnetite-sericite zones.

Mineralogy and textures of the mineralized zones

In type 1 mineralization, most of the pyrite is located at the contact between the two quartz generations. It is found in both generations but is more abundant in the grey quartz. Pyrite constitutes up to 6% of the vein, occurring as euhedral crystals, 2-3 mm, mostly clear and devoid of gangue inclusions. Many crystals exhibit cataclastic deformation textures (Fig. 52). Galena or chalcopyrite is locally abundant and occurs predominantly in the white quartz, filling fractures in relatively undeformed quartz. Galena and chalcopyrite also occur as rounded inclusions in pyrite. Most of the gold is present as free grains, varying in size from 0.02 to 0.05 mm, in white quartz locally bordering galena. Carbonate (calcite) crystals, as well as sericite and chlorite clots representing incorporated wall rock fragments, occur locally.

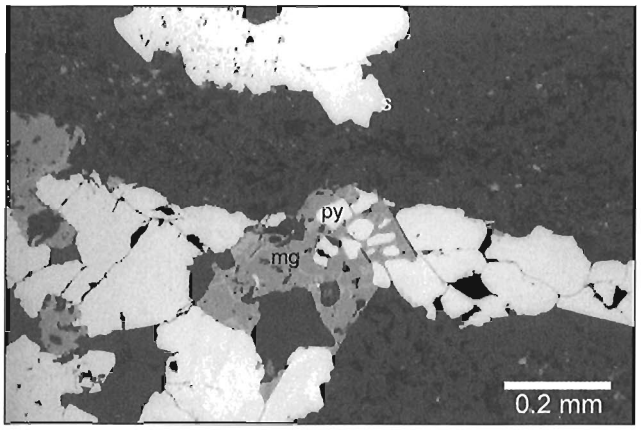

Figure 53. Photomicrograph showing magnetite (mg) with rounded inclusions of pyrite (white), suggesting that some of the magnetite is late in the paragenetic sequence. GSC 1996-130G

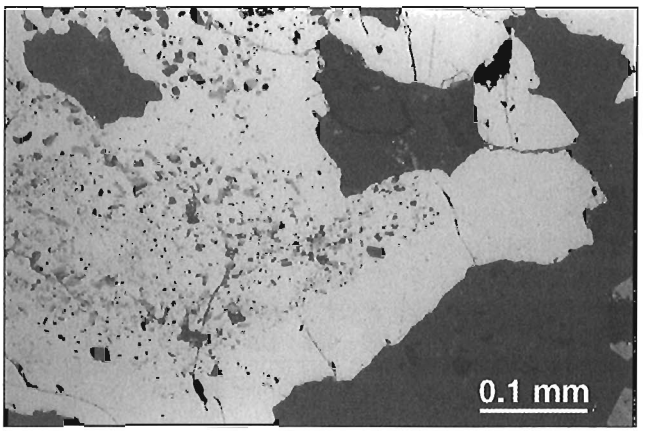

Figure 54. Photomicrograph showing pyrite with poekilitic cores and inclusion-free rims. Inclusions consist of leucoxene and quartz. GSC 1996-130H

In type 2 mineralization, quartz-pyrite veinlets vary in width from several millimetres to up to 1 cm. Pyrite occurs in aggregates along vein margins. Pyrite grains are fractured and some contain inclusions of galena and gold. Locally magnetite is also present in the veinlets. It is generally in contact with pyrite, mostly at grain boundaries and along fractures. Rounded inclusions of pyrite may occur within magnetite indicating the secondary origin of at least part of the magnetite (Fig. 53). Magnetite is partially altered to hematite along fractures and grain boundaries. The quartz within these veinlets typically presents deformation textures such as undulose extinction, polygonization, and seriate grain boundaries.

In the pyrite-rich visible alteration zone, sericite is abundant, and occurs as unoriented and lesser oriented leaflets, associated with seams of rutile and/or leucoxene. Pyrite, mostly in veinlets, represents up to 20% of this zone. It occurs mainly as coarse aggregates up to 5 mm, with lesser euhedral crystals less than 1 mm in size. Pyrite crystals are fractured. They commonly contain numerous inclusions of quartz and locally rutile/leucoxene in the core region, whereas rims are clear (Fig. 54). This textural relationship suggests that part of the pyrite replaced primary titanomagnetite. Gold occurs both as inclusions in pyrite (0.025 mm) and filling fractures in cataclastically deformed pyrite. Subhedral to euhedral crystals of magnetite are present in trace amounts within aggregates of pyrite, but convincing replacement textures of magnetite by pyrite were not observed under the microscope. Furthermore, where magnetite is locally abundant, some of the magnetite is secondary after pyrite. Although microscopic textures do not demonstrate replacement of magnetite by pyrite, the proximity of intensely pyritized zones to veins, the concentration of pyrite at the borders of these veins (Fig. 51B) as well as chemical analyses of altered and unaltered zones, all point to the addition of sulphur to an already iron-rich rock.

In the more distal sericite-magnetite zone, pyrite aggregates and veinlets are absent. Magnetite is more abundant and can represent 10% of the rock, occurring principally as allotriomorphic crystals up to 0.4 mm. Most crystals are disseminated and evenly distributed but some occur in bands.

Rocks of the Little Barachois formation typically contain abundant magnetite. For this reason, much of the magnetite is considered to be a residual phase, i.e magnetite that was present in the host rock prior to mineralization and alteration. However the presence of hydrothermal magnetite cannot be completely ruled out. Coarse magnetite occurs with quartz± pyrite and carbonates in veins, mostly parallel to the main fabric and locally crosscutting it (Fig. 55). The veinlets are affected by the late D_5 deformation event. Other indications that some of the magnetite is a late phase are locally abundant inclusions of pyrite, and chalcopyrite within certain magnetite crystals (Fig. 56). As in the pyrite-sericite zone, it is also common, although not systematic, to observe magnetite replacing pyrite. These textures indicate that some of the magnetite is definitively an alteration phase related to the circulation of the hydrothermal fluid. The same case can be made for calcite and iron carbonate. As limestone is present in the Isle aux Morts prospect area, part of the recrystallized carbonates in banded carbonate-rich rocks may be of sedimentary origin. However, numerous observations suggest that some of the carbonates were introduced as an alteration product as is surely the case in the carbonatized gabbro. Furthermore, the presence of carbonates in mineralized veinlets suggests that some are clearly related to the mineralizing process.

Chemical characteristics of the mineralized zones

Chemical analyses of the mineralized veins and auriferous pyrite-rich alteration zones from the Isle aux Morts showing are presented in Table 9. Similar to the Cape Ray gold deposit, the auriferous veins contain significant amounts of Pb (up to 3.67%) and Cu (up to 1.02%), whereas the concentration of Zn is rather low (<120 ppm). Overall, the increase

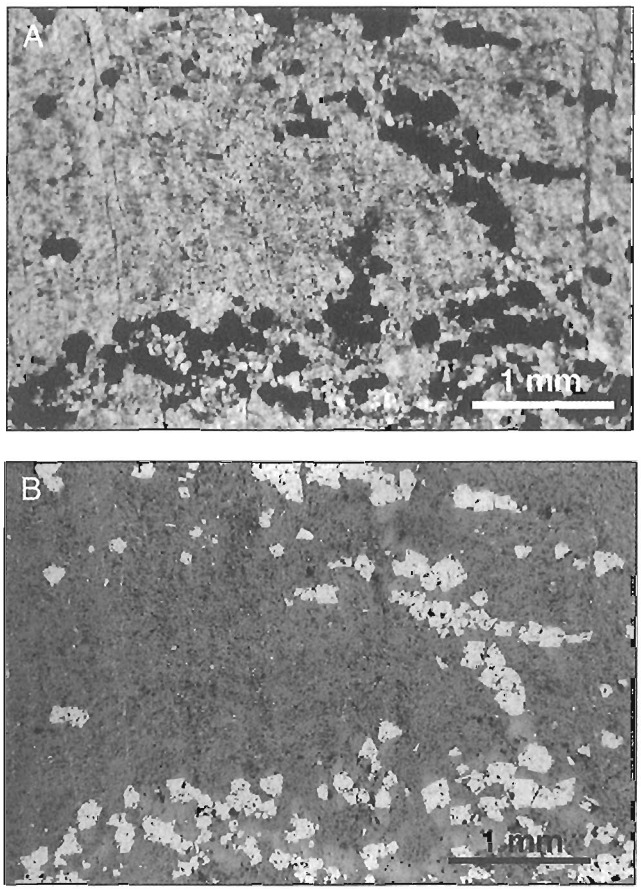

Figure 55. Photomicrograph showing coarse magnetite with quartz±pyrite and carbonates in veins, subparallel or discordant to layering. A) transmitted light, GSC 1996-130I; B) Reflected light. GSC 1996-130J

in base metal content, especially Pb, in the veins correlates with an increase of the gold content (Fig. 57). The proportions of As and Mo are very low. The silver content is high (up to 51 g/t) and the Au:Ag ratio varies between 1.3:1 to 1:9 with an average around 1:4. On the ternary diagram of Au-Ag-base metals (Fig. 26E) the mineralized vein samples for the Isle aux Morts prospect are somewhat scattered but most fall in the epithermal gold deposit field.

In contrast to the veins, the mineralized pyrite-rich alteration zones contain significantly lower levels of base metals (Fig. 57). The Au content is directly related to the amount of sulphur present, and bears no relation to the amount of Fe_2O_3 (Fig. 57). The direct correlation between S and Au confirms the megascopic relationship between pyrite and gold. The concentrations of As and Mo are very low. The Au:Ag ratio varies between 33:1 to 1:9 with an average around 1:1, all but one are greater than 3:1. The last ratio is more typically found in mesothermal style gold deposits. The very low silver content of these mineralized altered zones contrasts with the adjacent mineralized veins. On the ternary Au-Ag-base metals diagram, samples of the mineralized, pyritized wall rock for the Isle aux Morts prospect are scattered although most fall in the field of gold deposits in greenstone terranes and of quartz carbonate veins (Fig. 26).

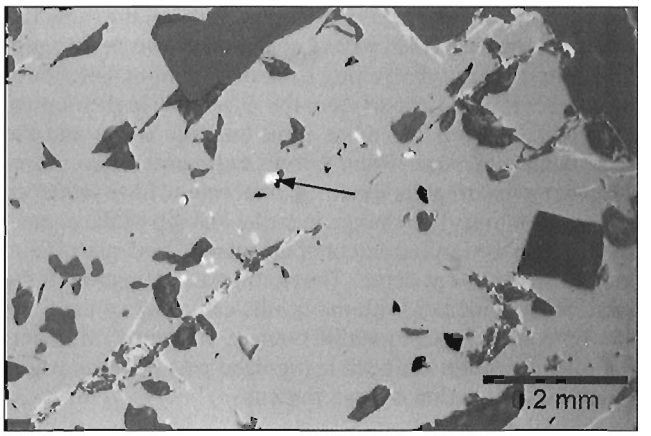

Figure 56. Photomicrograph showing inclusions of chalcopyrite (arrow) in magnetite. GSC 196-130K

Conclusion and discussion

The gold mineralization at the Isle aux Morts prospect occurs both in a massive fault fill quartz vein and in strongly pyritized zones in adjacent magnetite-rich sediments. Many aspects that characterize the latter type of the gold mineralization resemble gold mineralization in banded iron-formations. The concordant gold-bearing pyrite-rich strata in banded magnetite-rich rocks are very similar to those described in the literature for Archean greenstone belts around the world (Fyon et al., 1983; Macdonald, 1983; Phillips et al., 1984; Groves et al., 1987; Oberthur et al., 1990). The chemical control of iron-rich rocks on the precipitation of gold has been the subject of many discussions concerned with gold in banded iron-formations, and is evidently an important control on the mineralization in the Isle aux Morts prospect. The correlation between gold and sulphur in these rocks, as well as the common occurrence of inclusions of gold in pyrite, suggests that the gold was transported as reduced bisulphide complexes $Au(HS)^-_2$. Reaction with iron-rich wall rock caused H_2S from the fluid to be consumed to produce pyrite in the wall rock of the fluid conduit (Phillips and Groves, 1984):

$$Fe_3O_4 + 6H_2S + O_2 = 3FeS_2 + 6H_2O$$

The loss of H_2S from the fluid resulted in the decrease of sulphur activity in the residual hydrothermal fluid inducing gold precipitation (Romberger, 1986). The bisulphide complex could also be the source of sulphur and gold and thus gold coprecipitates with the pyrite (Romberger, 1986):

$$Au(HS)_2^- + Fe^{2+} + 1/4\ O_2 = Fe(Au)S_2 + 1/2H_2O + H^+$$

The widest mineralized intersections in magnetite-rich sediments occur in coarse-grained conglomerate. The conglomerates were probably more permeable, and provided increased access, favouring the circulation of the mineralizing fluid more readily than the fine-grained sediments. A primary structural control was also important in the localization

of the principal mineralized quartz vein at the tonalite-sediment contact. This contact appears to have been a preferred site of dilation resulting from deformation. Dilation at the contact resulted in part from the difference in rheological behaviour between the more rigid tonalitic rocks and the more ductile Windsor Point Group sediments. Also movement along the irregular tonalite contact could have produced zones of dilation. The change in strike and dip of the contact may explain the limited extent of the mineralized quartz vein, both on strike and at depth. The northeast termination of the quartz vein coincides with the northwest swing of the Cape Ray Igneous Complex tonalite contact. At depth, no important mineralization has been recognized past the zone where the dip of the tonalite contact flattens.

The superposition of the S_5 fabric on the mineralization is also responsible, in part, for the distribution of the mineralized zone. The quartz vein does not appear to be folded by the S_5 cleavage, but pyrite-rich veinlets and the magnetite-rich sedimentary rocks are folded by east-trending F_5 folds. Therefore the mineralization is pre-S_5. High competency and subparallelism between the main quartz vein and the S_5 cleavage are probably the reasons why the quartz vein does not appear folded by F_5 folds. Therefore, the correspondence between the plunge of the best mineralized section of the mineralized zone and measured fold plunges may not be fortuitous and probably reflects the superposition of the later D_5 deformation event on the mineralization (Fig. 58). The apparent limited vertical extension of the mineralized zone may be due to the disappearance of the iron-rich sediments at depth. Thus, the mineralization is pre-D_5 and syn- to post-D_3, as the S_{3a-3b} fabric is crosscut by some of the auriferous quartz veinlets.

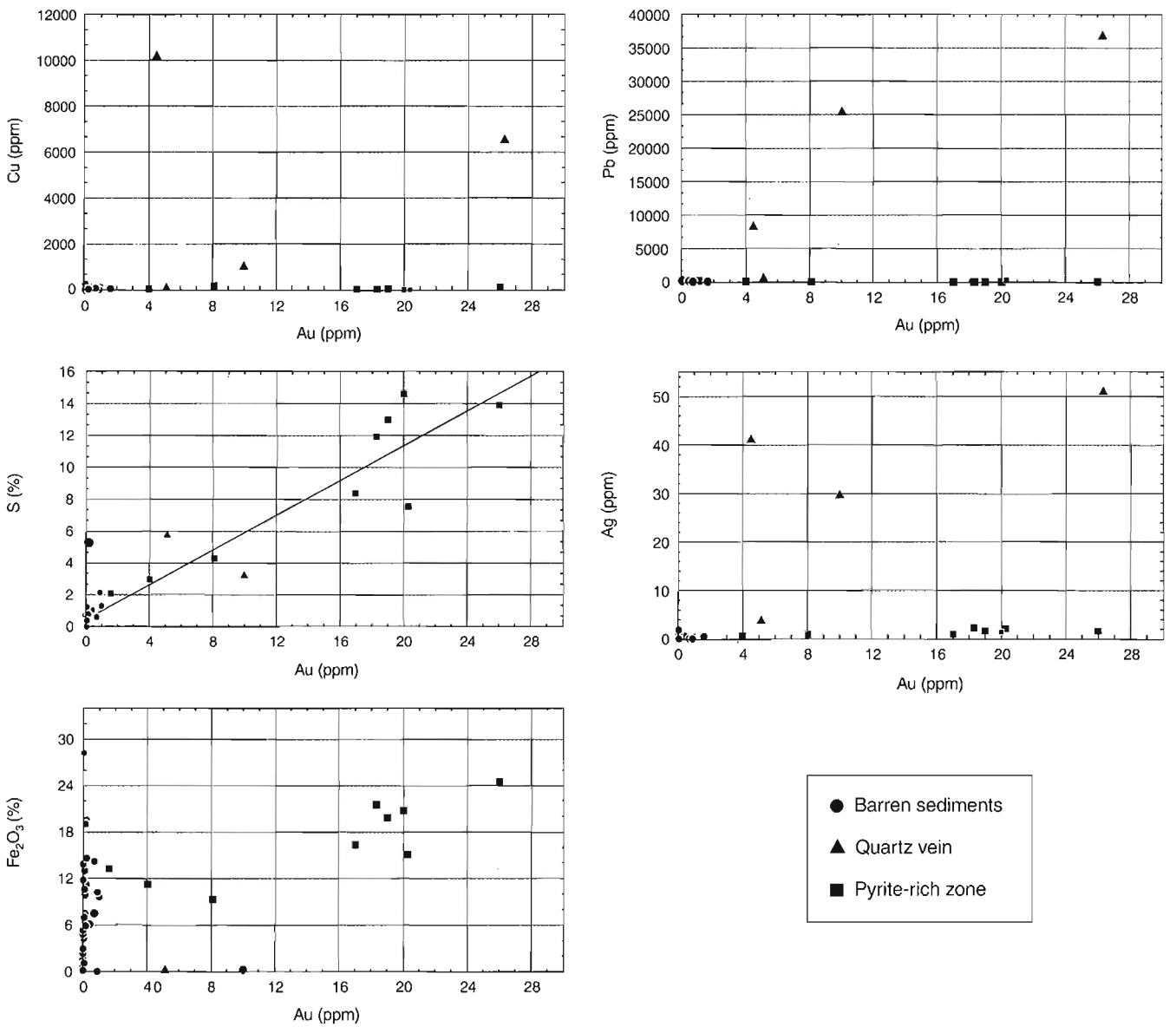

Figure 57. Diagrams showing variations of Ag, Pb, Cu, S, and Fe_2O_3 with Au in the Isle aux Morts prospect.

The veins are locally base metal rich and have a low Au:Ag ratio. The pyritized altered zones contain low base metal concentrations and their silver content is commonly inferior to that of gold.

Other mineralization-alteration zones

Several other gold occurrences are present along the Cape Ray Fault Zone. Among them, the most significant are the I, J, and H Brook showings, the first gold showings discovered in the area, and the Gulch showing (Table 10). All are located close to the Main zone of the Cape Ray gold deposit (Fig. 12), and are hosted by the Windowglass Hill Granite. They occur on the east side of the Isle aux Morts River where the granite is thinner and mylonitized. The mineralization occurs in stockworks of galena-rich quartz veinlets averaging 1-2 cm in width but never more than 6 cm (Fig. 59). The veins are composed of white quartz with proportions of galena and chalcopyrite that vary from trace amounts to semimassive, as aggregates or filling fractures. Most of the mineralized veinlets are discordant to the strong fabric interpreted as S_{3b}. Locally some appear folded, suggesting that the mineralization is early to syn-S3b fabric. At the H Brook showing, however, the veinlets are perpendicular to both the strong planar S3b fabric as well as to the down-dip L3 stretching lineation suggesting emplacement as extension veinlets during the reverse movement along the Cape Ray Fault Zone. Sericite-rich alteration haloes border the veinlets and are comparable to those associated with mineralization at the Windowglass Hill showing (Fig. 59).

Mineralization at the Gulch showing occurs in strongly deformed granitic rocks of the Windowglass Hill Granite hosted by graphitic schists. This showing is adjacent to the hydrothermal breccia located in the footwall of the strike-slip mylonite. Host rocks are intensely deformed, and strong cataclastic deformation is superimposed. Mineralization occurs in millimetre- to centimetre-scale veinlets. Galena occurs in clots and is locally almost massive. The veinlets are discontinuous, show no preferred orientation, and are locally strongly brecciated. Breccias consist of angular fragments of quartz and sericite schist in a matrix of sericite-pyrophyllite and locally of gouge material. Some of the fragments contain galena and/or pyrite indicating that the mineralization is definitely earlier than the D_6 brittle deformation event.

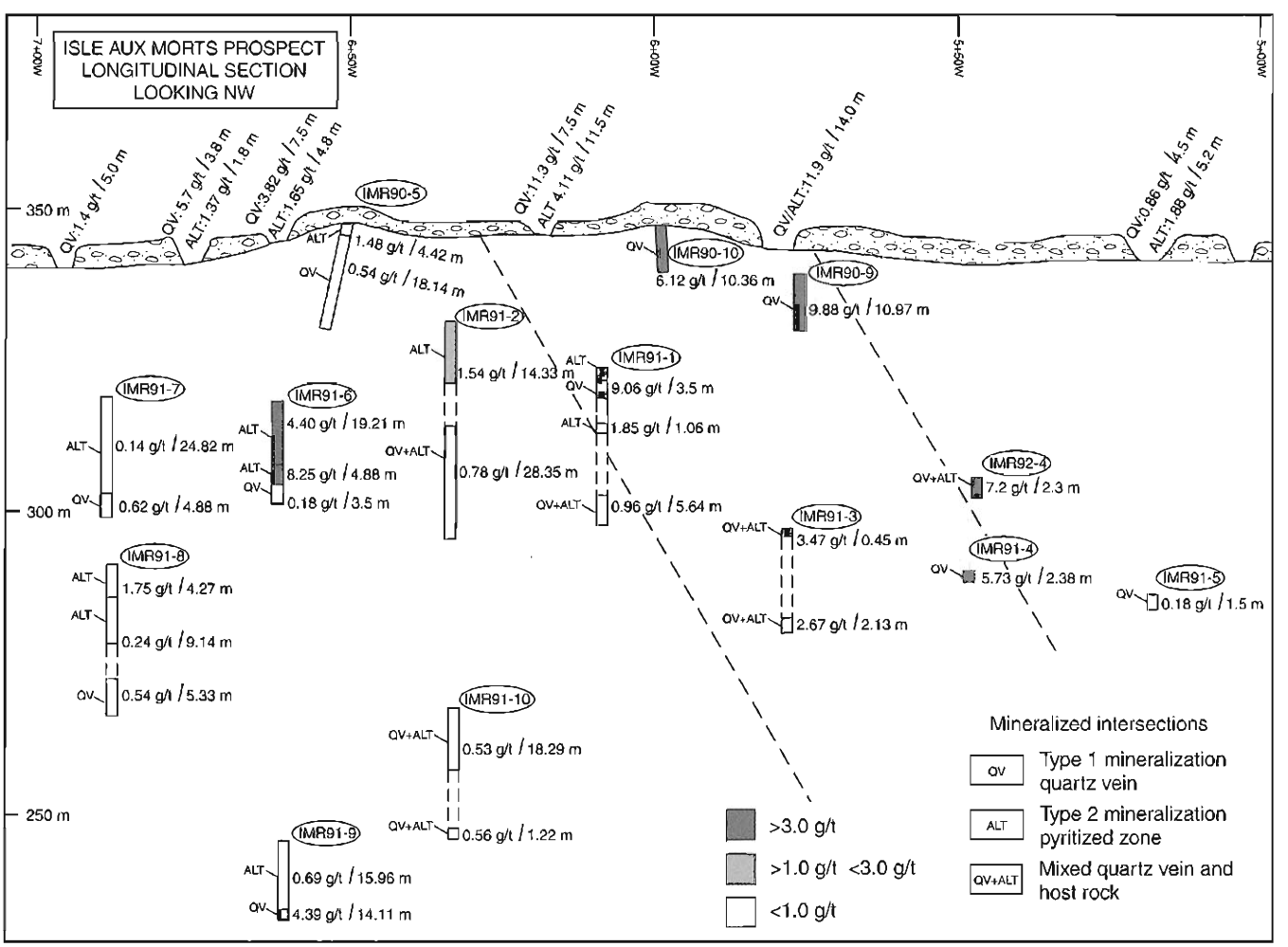

Figure 58. Longitudinal section for the Isle aux Morts prospect. Modified from Thompson (1992).

Table 10. Chemical analyses of various gold occurrences.

Sample	90KL-219B	90KL-219C	90KL-219a	91BD-140	91BD-138A	92BD-125	91BD-10
location	H Brook	H Brook	H Brook	Gulch	Gulch	Grand Bay River area	Isle aux Morts Prospect area
lithology	A(c)	A(a)	V	V	V	P(t)	P(v)
SiO_2%	75.80	77.00					75.6
Al_2O_3%	15.00	13.40					7.91
TiO_2%	0.18	0.16					0.25
Fe_2O_3(t)%	0.79	1.32					7.65
MnO%	< .01	< .01					0.02
MgO%	0.20	0.19					0.64
CaO%	0.09	0.33					< 0.1
Na_2O%	3.54	4.74					0.03
K_2O%	2.87	1.73					2.77
P_2O_5%	0.02	0.02					0.06
LOI%	1.75	1.30					4.62
S%	0.10	0.53	0.89			1.60	5.27
CO_2%	0.03	0.20					0.03
H_2O+%	1.1	0.7					1.2
Total	100.75	99.28					99.55
	Metallic trace elements						
Cu (ppm)	187	76	962	75	95	959	97.2
Zn (ppm)	339	386	10 500	16 100	9520	28	30.7
As (ppm)	< 2	< 2	< 3	6	20	48	150
Mo (ppm)	< 2	< 2	< 1	< 1	3	724	8
Ag (ppm)	1.2	1.3	6.1	3	25.5	1.8	0.9
Pb (ppm)	497	369	8100	2440	17 800	32	2
Au (ppb)	163	201	1030	1400	5210	137	170
	Trace elements (ppm)						
Ba	252	175	73	178	77	220	415
Co	2	2	3	2	3	16	17
Cr	< 2	< 2	8	5	3	9	8
Cs	1	1					7
Hf	10	10					
Nb	30	29					< 10
Ni	1	1	1	1	3	8	10
Rb	91	64					160
Sb	0.8	0.7	< 5	< 5	< 5	< 5	25
Sc	2.5	2.3	0.8	0.7	< .5	6.2	14.4
Se	6	3					< 3
Sn	< 10	< 10	< 10	< 10	< 10	< 10	
Sr	67	86	14.5	37.9	9.1	43.6	< 10
Ta	1	1					< 1
Th	21	20					0.5
U	4.3	4.6					1.1
V	18	< 10	5	< 2	< 2	42	76
W	5	4	< 10	< 10	< 10		6
Y	87	79	4.5	8.4	4	7.8	43
Zr	325	306	41.6	51.6	17.2	5	82
	Rare-earth elements (ppm)						
La	33.4	38	7.2	16.9	10.5	7	5.1
Ce	78	84					18
Nd	37	37					12
Sm	8.8	8.6					3.9
Eu	1.4	0.7					0.7
Tb	1.9	1.6					1
Yb	7.1	6.9					4.2
Lu	1.05	1.02	0.26				0.64

Analyses carried out at XRAL Laboratories
V: mineralized quartz vein in sericitized Windowglass Hill Granite
A(c): sericitized granite close to the vein
A(a): sericitized granite away 5 cm from the vein
P(t): pyritized sericite schist in tonalite
P(v): pyritized sericite schist in felsic volcanic rocks

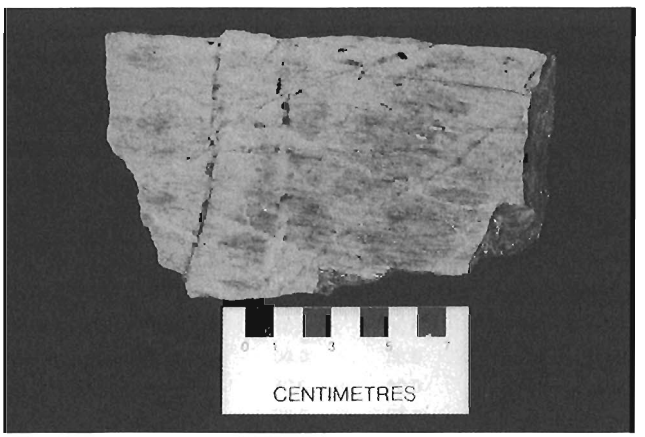

Figure 59. Extensional galena-bearing quartz veinlets in sericitic mylonitic Windowglass Hill Granite. GSC 1996-131A

Hydrothermal alteration zones are locally developed at the sheared contact between Windsor Point Group felsic volcanic rocks and the Cape Ray Tonalite. One such alteration zone is especially well developed in exposures in a northwest-trending river southwest of the Isle aux Morts prospect. There, sheared felsic volcanic rocks and tonalite are sericitized, silicified, and pyritized (up to 5%). Chemical analyses of one altered sample from this zone indicates up to 5.27% S with an anomalous gold value (170 ppb) (Table 10). Despite low gold values, the abundance of pyrite and strong sericitization make it an interesting alteration zone for further prospecting.

Along the Cape Ray Fault Zone, there is also evidence of a near-surface hydrothermal system of post-Mid Devonian age, associated with the D_6 brittle deformation event. It occurs in a zone of intense brecciation bordering the strike slip mylonite on the hanging wall side. The zone can be traced for more than 8 km and is a few tens of metres wide (Fig. 12). It consists of various types of breccias and silicified zones, and variations in texture and mineralogy occur along and across strike. The zone is characterized by the absence of any consistent planar fabric and by a low temperature silicification consisting of chalcedony. The widest section of breccia and most exposures are southeast of the Strawberry Granite in the Gulch area. Cataclastic rock flour breccia and open space breccias are common. Fragments of the Strawberry Granite can be recognized in the cataclastic breccias, confirming that brecciation is a late feature (post 384 Ma) in the tectonic history of the area. Intense silicification characterizes most of this zone. Multiple stages of brecciation and silicification can be demonstrated. The best examples of vuggy breccias contain angular to subangular fragments, between 1-30 cm, rimmed with chalcedonic silica (Fig. 60) and overgrown by fine-grained quartz and pyrophyllite or kaolinite. Chalcedonic bands vary from dark grey to white. Most fragments are typically silicified and massive; their colour varies from red, to purple, to apple green, to grey. Some fragments were previously brecciated (Fig. 60B), containing angular fragments of massive silicified rocks, as well as banded

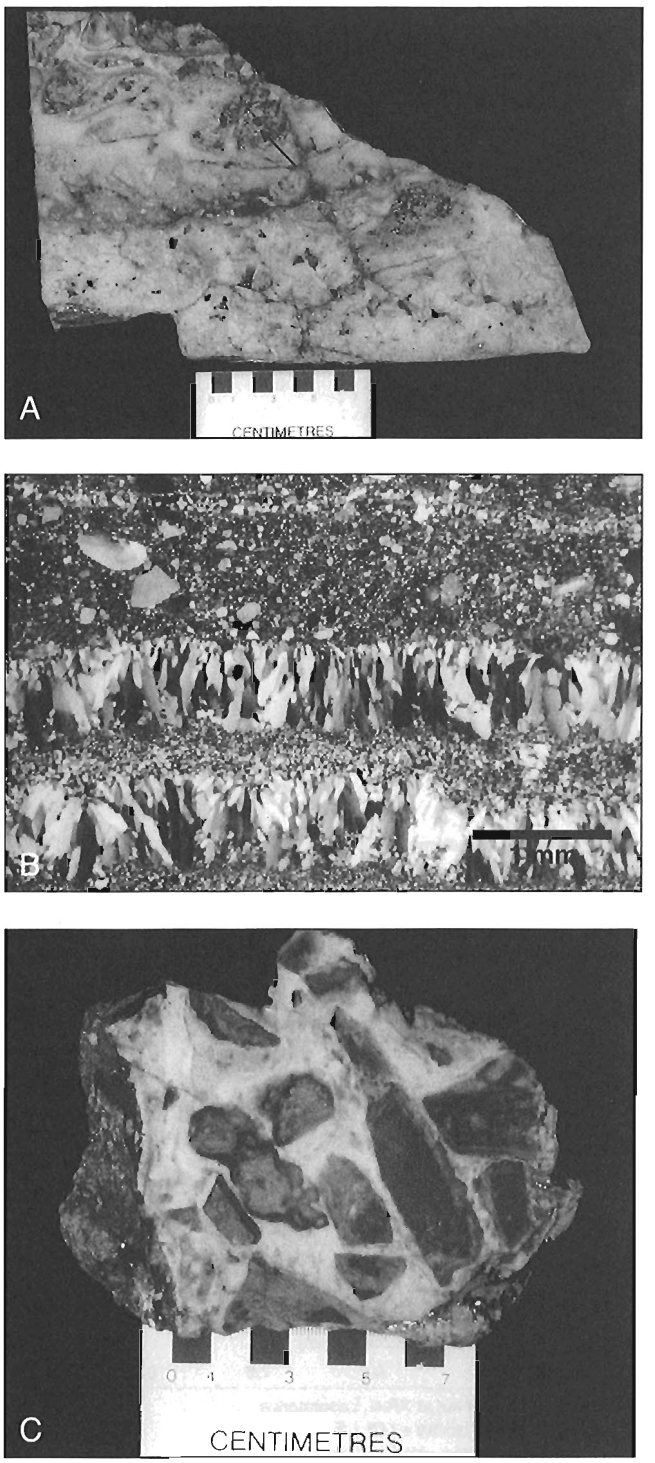

Figure 60. ***A)*** *Hydrothermal breccia showing angular fragment set in a chalcedonic matrix. Note coarse-grained fragments are Strawberry Granite (arrow). GSC 1996-131B;* ***B)*** *Hydrothermal breccia showing chalcedonic bands bordering a silicified cataclasite. GSC 1996-131C;* ***C)*** *Hydrothermal breccia – note fragments with chalcedonic bands set in a cataclastic matrix. GSC 1996-131D*

Table 11. Chemical analyses of the hydrothermal breccia.

Sample	92KL-132	90KL-88	92KL-155	92BD-56	92BD-58	92BD-57	92KL-131	92BD-39A	93BD-39B	92KL-132*[4]
SiO_2%	29.70	87.20	93.40	86.30	86.90	85.50	36.50	63.10	16.70	29.60
Al_2O_3%	0.96	6.35	3.18	7.06	4.27	6.58	1.39	3.44	0.53	0.94
TiO_2%	< .001	0.12	0.17	0.32	0.23	0.25	0.01	0.13	< .001	< .001
Fe_2O_3(t)%	0.21	0.86	0.72	1.60	4.27	2.93	0.32	0.53	0.08	0.23
MnO%	< .01	0.02	0.02	0.02	0.02	0.02	< .01	< .01	< .01	< .01
MgO%	0.07	0.21	0.19	0.37	0.23	0.31	0.01	0.11	0.08	0.06
CaO%	53.10	0.73	0.34	0.33	0.27	0.26	46.60	24.50	62.60	53.30
Na_2O%	0.09	0.12	0.10	0.19	0.21	0.10	0.06	0.07	0.07	0.08
K_2O%	0.20	2.65	0.26	1.36	1.22	1.28	0.35	0.90	0.09	0.21
P_2O_5%	0.04	0.05	0.05	0.05	0.05	0.05	0.04	0.05	0.03	0.04
LOI%	1.25	1.15	1.25	2.00	2.60	3.20	1.40	2.25	1.35	1.35
S%	0.02	0.23	0.01	0.05	2.92	1.83	0.03	0.02	0.02	
F%	34.6	0.3					30	14.6	40.6	34.8
CO_2%	0.02	< .01	< .01	< .01	< .01	< .01	0.01	< .01	< .01	0.02
Total*[2]	120.22	99.76	99.68	99.60	100.27	100.48	116.68	109.68	122.13	120.61
O equivalent of F	14.57						12.63	6.15	17.1	14.57
Total*[3]	105.70	99.76	99.68	99.60	100.27	100.48	104.10	103.50	105.00	106.04
Metallic trace elements										
Cu (ppm)	2	3	5	2	9	77	4	4	2	2
Zn (ppm)	1	3	1	8	33	16	1	3	<.5	<.5
As (ppm)	< 3	8	< 3	211	35	166	21	7	< 3	3
Mo (ppm)	4	2	6	2	< 1	7	4	3	1	4
Ag (ppm)	< .1	0.3	< .1	0.2	0.9	1	< .1	< .1	< .1	< .1
Pb (ppm)	< 2	3	< 2	13	8	634	8	< 2	< 2	< 2
Au (ppb)	6	10	21	60	6	128	38	4	4	5
Trace elements (ppm)										
Ba	22	217	54	238	83	276	38	42	9	22
Co	27	17	17	12	14	12	23	12	22	<1
Cr	143	22	23	35	20	21	19	30	29	127
Hg	< 5	< 5	8	122	998	423	21	11	< 5	< 5
Nb	13	27	25	18	18	21	<10	20	11	
Ni	3	2	5	5	4	18	2	6	2	4
Rb	<10	159	20	50	32	74	12	80	16	
Sb	<5	<5	<5	21	7	16	<5	<5	<5	<5
Sc	0.8	2.3	2.4	8.7	5	9.9	1.2	2.5	0.7	0.8
Se										
Sn	<10	<10	<10	<10	<10	<10	<10	<10	<10	<10
Sr	39.9	33	19.4	229	4.8	20.7	35	24	38.6	39.7
Ta	< 1	1	< 1	< 1	< 1	< 1	< 1	< 1	< 1	< 1
V	10	13	23	79	25	96	18	28	5	11
W	< 10	< 10	< 10	< 10	< 10	< 10	< 10	< 10	< 10	< 10
Y	57.9	5.4	2	8.1	10.2	22	56.6	36	52	57.2
Zr	4.8	30	10.2	33.5	91.9	27.4	10.1	26	4.6	5.5
Rare-earth element (ppm)										
La	6.2	7.6	0.7	7.6	7.6	13.8	6.3	8.6	5.3	6.4

Analyses carried out at XRAL Laboratories
*[2] Total includes oxides + LOI + F
*[3] Total recalculated with O equivalent of F
*[4] Duplicate

Summary of the characteristics of the auriferous zones along the Cape Ray Fault Zone.

MINERALIZED ZONE	RESERVES OR BEST INTERSECTIONS	TYPE OF OCCURRENCE	HOST ROCK	ORIENTATION AND GEOMETRY OF THE ORE ZONE	ORE MINERALOGY	Au:Ag RATIO	ALTERATION	RELATIVE TIMING
CAPE RAY GOLD DEPOSIT (Main zone) □	Proven reserves: 454 000 t/ 10.1 g/t Au Geological reserves: 890 000t/ 7.54 g/t Au	3 mineralized ore shoots (No. 4, 41, 51 zones) quartz breccia fault fill veins (A and C veins)	WINDSOR POINT GROUP: Graphitic schist	3 mineralized ore shoots in a northeast fault, dips moderate southeast (50-60°) 04 and 41 zone oreshoots plunge steeply ESE-SSE	5-10% sulphides chalcopyrite, galena, pyrite, sphalerite and lesser amounts of electrum, pyrrhotite and arsenopyrite	40:1 to 1:100 Average 1:2.25	Moderate Chlorization Carbonatization	Syn to late- D_3 Pre-S_{5}-' folds
BIG POND SHOWING ⬡	Channels: 14.4g/t Au/3.0m DDH: 16.0 g/t Au/1.6m 21.1 g/t Au/2.4m	2 mineralized ore shoots quartz breccia fault-fill veins	WINDSOR POINT GROUP: graphitic schist, chlorite schist, and sericite chlorite schist ± calcite	2 NE plunging oreshoots: in N-S/65° E fault-fill veins on limb of an S-shaped F_3 fold	Trace to 15% sulphides pyrite, chalcopyrite and minor galena, pyrrhotite, sphalerite, magnetite, arsenopyrite, and gold	25:1 to 1:25 Average 5:1	Limited Carbonatization Silicification	Early- to late D_3
WINDOWGLASS HILL SHOWING ●	Best DDH: 4.6g/t Au/12.5m incl: 14g/t Au 4.0m	Extension quartz veins Simple, multiple stages Vein-filling Veins up to 1m banded structures comb structures	Windowglass Hil Granite (alaskite) U-Pb age: 424 ±2 Ma	N-S veins shallow W dipping, associated with N-trending shear	pyrite, chalcopyrite and galena, with minor sphalerite, magnetite, pyrrhotite and electrum	1:1 to 1:350 Average 1:99	Moderate Pyritization, Sericitization and Local chloritization	Syn- to Late D_3
ISLE AUX MORTS PROSPECT ◆	DDH: 9.88 g/t Au/11m 5.1 g/t Au/15.9m 9.6 g/t Au/7.7m 6.2 g/t Au/7.0m 5.1 g/t Au/7.2m Channels: 10.54 g/t Au/11m	a) Massive fault-fill quartz veins	CAPE RAY tonalite WINDSOR POINT GROUP: Magnetite-rich sediments	ore zone strikes NE steep S plunge 200 m long, 120 m deep 2-40 m wide	pyrite, galena, chalcopyrite and gold	1:1 to 1:9 Average 1:4	Extensive in magnetite-rich sediments: Pyritization Sericitization Carbonatization (Fe) ±magnetite	syn- to late D_3 pre-D_5
		B) Pyritized alteration zone in magnetite-rich sediments	WINDSOR POINT GROUP: Magnetite-rich sediments	oreshoots plunge 60-70° NE	5-20% disseminated pyrite with or without magnetite, gold	33:1 to 1:9 Average 1:1		

chalcedonic silica. Along the Isle aux Morts River, fluorite occurs in veins and as the cement of certain breccias. As well, chemical analyses of samples taken along strike of the zone show moderate to elevated concentrations of F throughout (up to 40.6%), indicating that the hydrothermal fluid was F rich (Table 11). The widespread occurrence of quartz as both pervasive replacement of fragments and as cement to fragments in a fine-grained or chalcedonic form is one of the dominant features that characterizes epithermal breccias (Sillitoe, 1985). As well, fluorite and amethyst are minerals that are commonly found in hydrothermal systems developed at shallow depth. An epithermal hydrothermal model is further supported by elevated concentrations of Ba, Hg, and As in chemical analyses of some samples (Table 11). Although, no significant Au mineralization was found in breccias of the Isle aux Morts River and Gulch areas, sulphide mineralization does occur in float of brecciated, silicified material found 600 m northeast of Big Pond on strike with this same hydrothermal breccia. There it consists of a more massive, dark grey, somewhat vuggy, cataclastic and partially silicified rock, with up to 5% pyrite as fine disseminations or filling fractures. These rocks also contain anomalous gold values (92BD-57) (Table 11). The mineralized float occurs in close proximity to the hydrothermal breccia and could have been derived from it. This zone has been relatively unexplored in the past and should be considered a good target in future exploration programs.

DISCUSSION AND CONCLUSION

Introduction

In this section we focus on the key parameters responsible for the formation of the mineralized zones along the Cape Ray Fault Zone. Analogies are drawn with Archean and younger gold deposits, some exploration tools are suggested, and a metallogenic model is presented.

Table 12 presents a summary of the main characteristics of the zones studied and shows the various structural and lithological settings of the mineralized zones.

Controls on the mineralization

Our study demonstrates that the development and geometry of the auriferous zones were controlled by a combination of primary lithological and structural factors. The geometry of the zones is also strongly influenced by postmineralization deformation described below as an overprinting deformation.

Lithological factors

Two lithologies have a strong chemical influence on the precipitation of gold and associated minerals: the graphitic schists and the iron-rich sediments (Table 12). At the Cape Ray gold deposit and at the Big Pond showing, the mineralized zones are hosted in graphitic schists. Wilton (1984) first

Table 13. $\delta^{13}C$ isotopic values of graphitic schists host of the mineralized zones at the Cape Ray gold deposit.[1]

Sample	Description	$\delta^{13}C$
68805	Graphite	-23.8
68806	Graphite	-26.6
68807	Graphite	-26.1
68808	Graphite	-27.7
68809	Graphite	-27.8
68810	Graphite	-27.3
68811	Graphite	-27.4

[1]Analyses were done by Krueger Enterprises Inc. (Geochron Laboratories Division) for Dolphin Explorations Ltd. Standard used was PDB.

recognized this spatial association and its implications at the Cape Ray gold deposit. As indicated by McKeag et al. (1985), the first step in determining the link between graphitic schist and mineralization is to determine whether the graphite formed by metamorphism of carbonaceous horizons or whether it is of hydrothermal origin, and introduced during the mineralizing event. Stable isotopic analyses done by Krueger Enterprises Ltd. for Dolphin Explorations, on the graphitic schists hosting the mineralized zone in the Cape Ray gold deposit gave $\delta^{13}C$ values between -23.8 to -27.8 which are typical of carbon from graphite derived from organic matter (Ohmoto and Rye, 1979) (Table 13). Thus, the graphitic schists are derived from recrystallization and redistribution of carbon in deformed black argillites (Springer, 1986). According to Springer (1986), sulphur reactivity of carbon is enhanced by shearing, explaining why freshly milled carbonaceous mineralized zones are notable gold precipitants. Thus, graphitization by shearing not only induced the mechanical permeability which directed the flow of incoming hydrothermal fluids, but also activated the partly crystalline carbon and induced gold precipitation (Springer, 1986). As well, as indicated by Cox et al. (1991), the carbon present within the schists could have reacted with the H_2O transported in the fluid to produce CO_2 and methane as shown by the following reaction:

$$2C + 2H_2O = CO_2 + CH_4$$

The production of methane causes a reduction of the oxygen fugacity and thus destabilizes the gold-complex inducing gold precipitation (Cox et al., 1991). Furthermore, if the reduced methane-rich fluid mixes with the "fresh", and thus relatively more oxidized, hydrothermal fluid circulating through the system, the reaction will induce gold precipitation much more efficiently (Cox et al., 1991).

Because of their reducing properties, the graphitic schists have clearly acted as a preferential site for gold precipitation.

Iron-rich sediments hosting gold mineralization at the Isle aux Morts prospect have also played a key role in the precipitation of gold. The iron reacted with the sulphur transported by the hydrothermal fluid to produce pyrite. Such pyritization resulted in the reduction of the sulphur activity and destabilization of the gold complexes, allowing gold precipitation spatially and genetically associated with the pyrite zone (Romberger, 1986). This mechanism of gold precipitation is well recognized elsewhere in deposits hosted by iron-rich rocks such as Archean banded iron-formation (Groves et al., 1987) and in gabbro sills in Newfoundland (Kirkwood and Dubé, 1992; Ramezani, 1993) and elsewhere (Dubé et al., 1987).

Structural factors

The layer anisotropy induced by the graphitic schist due to its rheology favoured fluid circulation as most of the strain was accommodated by the schist. The graphitic schist most probably allowed slippage during fault movement generating open space for fluid circulation and auriferous lode precipitation. It is clear that the graphitic schist acted as a permeable horizon for fluid circulation as numerous quartz veins are hosted by these schists.

Layer anisotropy and competence contrast also played a key role at the Isle aux Morts showing in localizing the strain. There, deformation zones, which developed at the boundary between the Windsor Point Group sediments and the tonalite, host the mineralization. Most of the strain was accommodated in the sediments due to their incompetent nature and anisotropy compared to the competent tonalite. The veins and auriferous altered rocks are thus mainly hosted by the Windsor Point Group sediments although local gold-bearing veins are found in the tonalite.

At the Windowglass Hill showing, the competent nature of the granitic host is responsible for the north-northeast-trend of the shear zone. The competency of the granite induced refraction of the strain at a high angle to the trend of the granite, explaining the unusual orientation of these shear zones, compared to the overall northeast trend of the D_3 structures in most of the Windsor Point Group. As well, the development of subhorizontal extensional quartz veins confined to the granite resulted from the combination of reverse motion along the thrust zone and the competent nature of the granite.

Overprinting deformation

The original distribution and geometry of the various mineralized zones have been modified by postmineralization deformation. For example, at the Isle aux Morts showing, F_5 folds overprint the mineralized zones. As well, at Big Pond, the vein has most probably been folded by F_3 folds. In both cases the oreshoots, which resulted from the combination of lithological and structural traps, are now controlled by the east-northeast-oriented steep plunge of these younger folds.

Late brittle deformation, especially developed in the graphitic schist of the Cape Ray gold deposit, resulted in post-mineralization faulting with brecciation, boudinage and sinistral lateral displacement of the mineralized zone over at least a few metres (Fig. 19).

Geometry of the mineralized zones: oreshoot control

The simple presence of favourable structures and quartz veins in the study area are not sufficient to indicate economic mineralization. Oreshoots characterized by higher metal contents than the adjacent parts of the host conduit, are outlined within favourable structures. Most of the oreshoots plunge relatively steeply to the east-southeast or south-southeast (Table 12), as at the Cape Ray gold deposit Main zone and at Big Pond. There appears to be a similar trend at the Isle aux Morts prospect, although, the database is insufficient to test it (Fig. 58). Determination of the factors controlling the orientation and geometry of these oreshoots is of pratical importance for exploration and is addressed below.

Cape Ray gold deposit

In the surface exposure of No. 41 zone (Fig. 16), the A vein is barren to weakly mineralized and is relatively undeformed. The barren nature of the A vein adjacent to mineralized portions suggests that primary geometric or kinematic factors were important in controlling the precipitation of sulphides and gold during vein formation, with well mineralized segments adjacent to barren ones. A Conolly diagram (Conolly, 1936) was prepared to test whether the variation in grade and thickness of the mineralized zone is related to an original change in the attitude of the veins. This diagram helps to discern slight variations difficult to appreciate on maps or sections. It illustrates curvature of a vein surface, using as datum of reference an arbitrarily chosen plane. Such a diagram presents the relation between oreshoot and vein attitude and helps in evaluating the link between the geometry of a vein and its gold content. The diagram is constructed by selecting an inclined plane of reference and contouring the distance between the vein and the selected plane. The reference plane is subparallel to the average strike and dip of the mineralized zone, in this case the A vein. No. 41 zone was selected as it is the best defined oreshoot (Fig. 61). To construct the diagram seven drillhole sections, from 950W to 1400W, and the surface trench on Line 1400W were used. The contours represent the vertical distances between the hanging wall boundary of the zone and the reference plane oriented at 040°/60°. As recommended by Conolly (1936), the gold content corresponds to the grade (in g/t) multiplied by the width of the intersection (in metres). The diagram clearly indicates the geometrical relationship between the oreshoot and the attitude of the vein. The oreshoot is located between 40 and 55 m from the reference plane with the best intersections located at 50 to 55 m from it. The orientation of the A vein varies both with depth, where the vein approaches the reference plane, and laterally, where the A vein departs from it. These geometric variations may explain why, in No. 41 zone, the A vein becomes weakly mineralized to barren to the southwest. The surface trench is located between lines 14+00 and 14+40W and there, the vein is oriented differently, as indicated by increasing distances (>55 m) from the theoretical plane. The oreshoot location is thus probably controlled by areas of structural dilation within the host structures. These dilatant zones resulted from changes in attitude of the host structures.

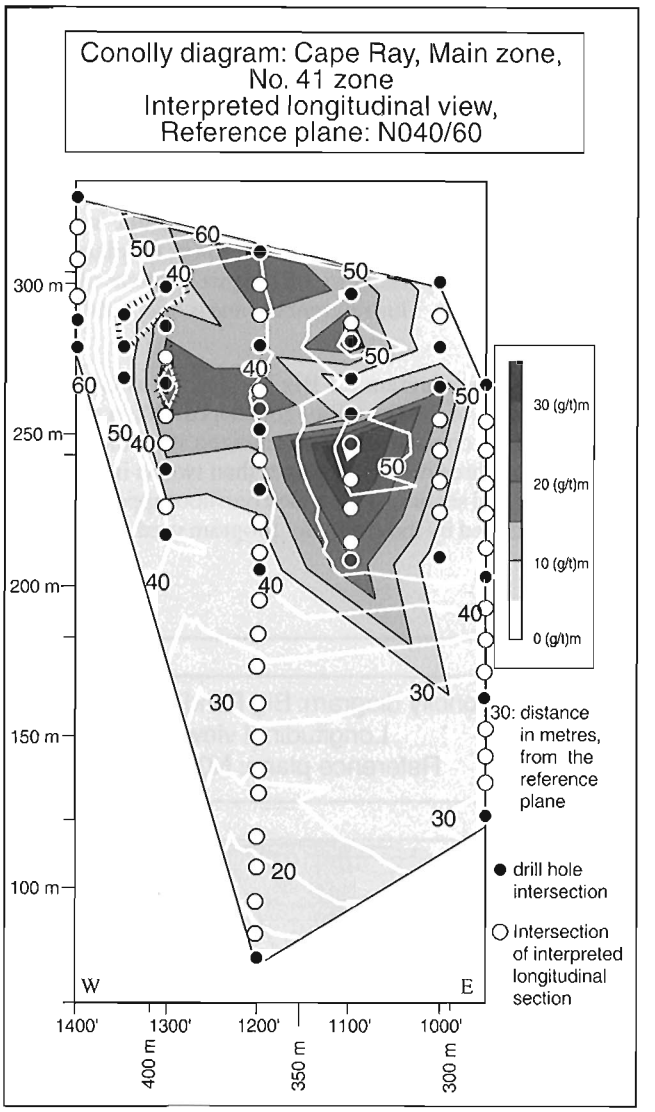

Figure 61. *Conolly diagram for the Cape Ray gold deposit, 41 zone.*

The vertical and lateral variations in the geometry of the vein have obviously had a critical influence on fluid flow and more importantly, the precipitation of sulphides and gold. As the mineralized quartz veins are syn- to late-D_3, the down-dip linear fabric characterizing this phase of deformation could have controlled fluid circulation and pressure fluctuations within dialation zones within the graphitic schist along the S_3 fabric. Strike slip brittle deformation (see above) is superimposed on the oreshoot, producing displacement and boudinage of the veins and could also be responsible for the location of the mineralization in three lodes, in steep oreshoots (at least for the No. 4 and 41 zones), subparallel to the intersections between D_3 and D_5 generations of structures. Postmineralization deformation alone will not explain the distribution of well-mineralized and adjacent barren quartz lodes. Instead, we believe that the three mineralized oreshoots are related to primary factors that produced increased

dilation and precipitation of metals in localized zones. The adjacent barren zones are dominated by gouge and represent areas where the strain was most probably higher.

Big Pond showing

The mineralized structure at Big Pond is presented on a Conolly diagram (Fig. 62). Because of the change in attitude of the oreshoots on surface, the orientation of the plane of reference was chosen parallel to the longest segment of mineralization on surface. This reference plane is oriented 013° and dips north 47°.

The resulting diagram for Big Pond is not as clear cut as for No. 41 zone of the Cape Ray gold deposit Main zone. The contoured gold content of the mineralized structure suggests that there are three oreshoots rather than two as indicated by the longitudinal section. This added oreshoot appears to be an artifact produced by the computer program used to create this diagram (deltagraph), and is caused by a lack of information between sections 200S and 100S. The best mineralized segment is parallel to the reference plane and located approximately 15 m from it. The gold content of the zone appears to decrease as the structure changes orientation towards the north. This change in gold content reflects a change in grade, rather than a change in vein thickness. Farther north, no vein was intersected. The gradual change in grade suggests that the oreshoot results not only from superimposed deformation and boudinage on the vein system but may also be influenced by primary geometric or kinematic factors. The northern oreshoot is oriented differently than the southern one; it is slightly discordant to the reference plane, both in plan and section views. This observation indicates that 013°/47° may not be the only favourable orientation for gold mineralization. Although the gold content of the northern oreshoot is less significant than that of the southern one, this variation is mostly due to the thickness of the zone rather than to grade. Grades in both oreshoots are comparable.

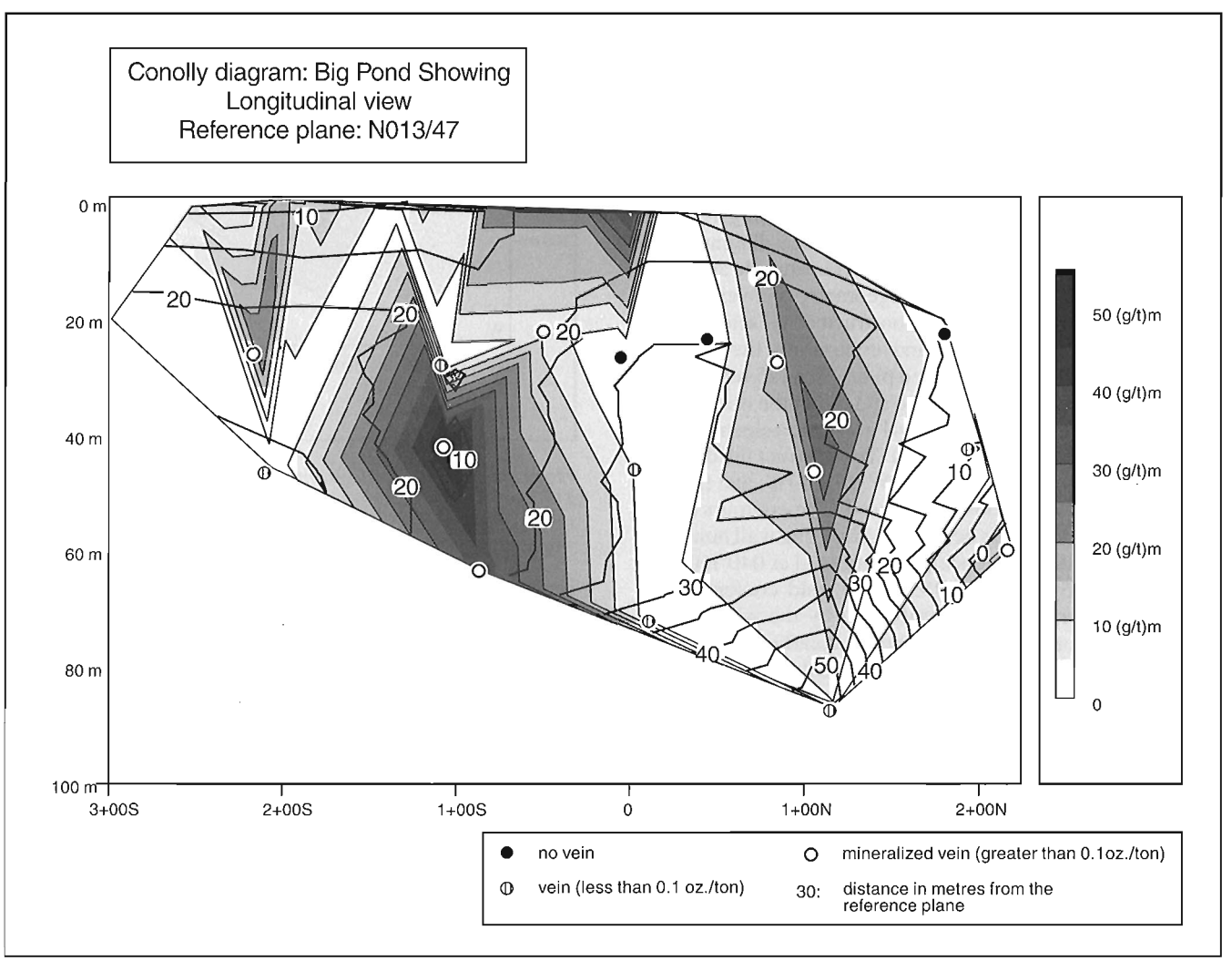

Figure 62. *Conolly diagram for the Big Pond showing.*

Table 14. K-Ar data for muscovite concentrates associated with gold at the H Brook showing.

Sample number/ Lab number	Wt.% K	% Atmos. Contam.	^{40}Ar (Rad.) $10^{-6}cm^3$ STP/g	Apparent age Ma ± 2 sigma	Location
BD135-91/ KAR4386/ GSC 95-21	8.14	0.9	134.3	381 ± 6	H Brook showing
BD137-91/KAR 4387/ GSC 95-20	8.19	0.7	135.6	383 ± 5	H Brook showing

Table 15. K-Ar data (integrated ^{40}Ar-^{39}Ar) for muscovite samples associated with gold at the Windowglass Hill prospect.

Sample number/ Lab number	BD113-91 KAR 4409/GSC 95-23	BD115-91 KAR 4410/GSC 95-22
Mineral	muscovite	muscovite
Location	Windowglass Hill prospect	Windowglass Hill prospect
wt. % K	7.74	8.17
% Atmos contam.	Ar = 1.4	Ar = 2.5
Ages of two steps heating + % gas	380 ± 1 Ma(53%), 381 ± 1 Ma(42%)	383 ± 1Ma (62%), 383 ± 1Ma (33%)
Preferred age: 95% gas plateau age	381 ± 3 Ma	383 ± 4 Ma
Integrated ^{40}Ar-^{39}Ar age	381 ± 3 Ma	383 ± 4 Ma

Timing of the mineralization

The mineralization is post-424 ± 2 Ma, the age of the Windowglass Hill Granite that is cut by mineralized veins; post-peak metamorphism in the Port aux Basques gneiss (415 Ma), and post-407 ± 4 Ma, the cooling age of the hornblende as both the gneisses and the hornblende are retrograded at greenschist facies within the structure hosting the Cape Ray gold deposit. The mineralization must be pre-386 ± 2 Ma, the age of the Isle aux Morts Granite which cuts across the Main zone shear of the Cape Ray Fault Zone, and hosts the gold mineralization at the Cape Ray gold deposit. This time period corresponds to the development of the D_3 structures. Such an interpretation is also compatible with the structural setting of the mineralization within the Windowglass Hill showing. There, the subhorizontal quartz veins that host mineralization are structurally compatible with the L_3 lineations. As well, at Big Pond, the vein has been modified by an F_{3b} fold. Highly strained wall rock fragments enclosed within a mineralized quartz breccia vein in the Cape Ray gold deposit clearly indicate that the mineralizing event is syn- to late-D_3 ductile deformation (Table 12).

We attempted to directly date the age of mineralization, using muscovite-sericite concentrates from the sericite schist bordering the mineralized vein at the Windowglass Hill and the H Brook showings. Dating was done by C. Roddick of the Geological Survey of Canada using Ar-Ar and K-Ar dating techniques. Details of the analytical technique are presented in Appendix 1, the results in Tables 14 and 15 (see also Hunt and Roddick, 1996). The age obtained (383-381 Ma) corresponds to that of the late tectonic Strawberry Granite (384 ± 2 Ma). The H Brook and Windowglass Hill showings are respectively located at 300 and 1200 m from the Strawberry Granite. These results suggest either that the mineralization is the same age and possibly related to the Strawberry Granite or that the age of the sericite was reset by this younger intrusion. Results from dating of samples BD-113-91 and BD-115-91 indicate that the initial step of several per cent gas gave the same age as the two heating steps, suggesting no excess argon was present. As the integrated age is the same for the two steps, this strongly supports interpretation that these ages have not been reset (C. Roddick, pers. comm., 1994).

As presented above, however, field relationships indicate that the ductile structures hosting the mineralization are crosscut by the Isle aux Morts Granite dated at 386 Ma. Thus, the hosting structures are pre-emplacement of the Strawberry and/or Isle aux Morts intrusions. The mineralization could still have been emplaced in already developed older structures. Because of these conflicting relationships there is at present no unique interpretation of the age of the mineralizing event. It is thus constrained to be post-407 ± 4 Ma and pre- or syn-384 Ma.

Type of mineralization

The lode gold mineralization at Cape Ray has a number of characteristics in common with mesothermal gold deposits. The relationship of the different zones with a major ductile fault zone, the nature of quartz veins, grade of metamorphism, and alteration are all compatible with classic mesothermal lode gold deposits (Roberts, 1987). As well,

temperatures of mineralized zone formation, or equilibration, estimated from arsenopyrite and other sulphide intergrowths appear to be around 300°C (Wilton and Strong, 1986) and are in accord with such an interpretation. However, the mineralogical assemblages within the mineralized zone, in particular the abundance of base metals, differ from typical mesothermal assemblages. Furthermore, the abundance of galena suggests a lower temperature of formation.

The concentrations of Ag (see Au:Ag ratios, Table 12) are characteristic of gold deposits formed at shallower depths. As indicated by Figure 26, samples from all mineralized zones with the exception of Big Pond and the pyrite-rich alteration zones of the Isle aux Morts prospect have elevated Ag contents, and fall in the field of epithermal deposits. Otherwise, the Cape Ray mineralized zones present few of the critical geological characteristics of epithermal deposits such as the alteration and an extensional tectonic environment. Their structural and lithological environments are analogous with most deposits in greenstone belts (mesothermal) although the limited amount of hydrothermal carbonate in the veins or the wall rocks contrasts with typical mesothermal deposits.

Consequently, the auriferous zones studied were probably formed at depths intermediate between these two end members (2-5 km depth, 200-300°C). A similar conclusion was proposed by Peters et al. (1990) for mélange-sediment-hosted (slate to turbidite-hosted) gold deposits at Hodgkinson goldfield, Australia. There the high Ag content could mainly reflect the dominantly sedimentary nature of the rocks through which the fluid circulated. A similar interpretation may be proposed for this study.

Mineralization at the Windowglass Hill showing compares more closely to intrusion-related gold mineralization documented in the Republic of Korea (Shelton et al., 1988; So et al., 1988). The intensity and type of alteration, the banded structure of veins, and some of the Au:Ag ratios are features that are similar to Korean-type gold-silver deposits (1:3 to 2:1) (So et al., 1988) and to more silver-rich epithermal deposits (1:10 to 1:200). The only differences with the Korean-type are the presence of abundant base metal sulphides and the more elevated silver content of some of the veins. Korean-type deposits are genetically associated with Early-Late Cretaceous granites, and are characterized by a general paucity of sulphide minerals (mineralization occurred at T = 270°C in response to boiling and cooling at depths of 1.25 km). Silver-rich epithermal deposits associated with Late Cretaceous to Tertiary granites are characterized by different alteration (advanced argillic, silicification, adularia) and an extensional tectonic setting (deposition at <240°C in response to boiling at depths of <0.75 km).

Analogy with Archean and younger gold deposits

The association of gold with graphitic schist has been reported from Archean gold deposits such as the Hollinger (Jones, 1948) and the Moneta Porcupine mines (Buffam, 1948) where gold has precipitated at quartz vein margins injected within graphitic zones (Springer, 1986). One of the best analogues to the Cape Ray gold deposit is the Owl Creek deposit in the Timmins camp, Abitibi greenstone belt, where auriferous quartz veins are hosted by sheared graphitic schists, interpreted as critical in the formation of the deposit (Springer, 1985; Wilson and Rucklidge, 1987).

The Cape Ray gold deposit also shares many similarities with the Ashanti gold mine in Ghana, one of the largest gold producers in the world, with a recorded output of 25 000 000 oz of gold and an annual production of about 500 000 oz (Appiah et al., 1991). Gold mineralization there occurs in a major shear system in early Proterozoic rocks interpreted as a thrust fault juxtaposing tightly folded and metamorphosed metasedimentary rocks and less deformed and metamorphosed metavolcanic rocks (Appiah et al., 1991). The mineralization occurs in shear zones characteristically associated with carbonaceous schists (Oberthur et al., 1991). Most of the mineralization is hosted by quartz veins containing a distinct suite of base metals including galena, chalcopyrite, and sphalerite. Silver contents of gold range from 7 to 26.5 wt.%. The orebodies pinch and swell along both strike and dip. What appears unique at Ashanti is the 7.5 km length and 1.6 km depth of the mineralized shear zones (Appiah et al., 1991).

In younger terranes, the gold-graphite association is also recognized in the Ballarat goldfield, Australia. There, auriferous quartz lodes are restricted mainly to an Ordovician stratigraphic horizon rich in graphitic slates (Cox et al., 1991). The area has produced up to 58 000 kg of gold. In most deposits a close association exists between high gold grades and proximity of carbonaceous slates.

The Otago schist in New Zealand hosts numerous Au-W deposits, comprising shear zone-hosted quartz veins cross-cutting Otago schist (McKeag et al., 1985). Gold vein mineralization resulted from interaction of hot (350 ± 20°C) metamorphogenic fluids and cooler (about 250°C) country rock where a low-angle thrust system intersected graphitic schist. The graphite is metamorphic in origin, and caused gold deposition by reaction with the fluids, leading to reduction of the dissolved metals and sulphur.

Gold bearing quartz veins in the Hodgkinson gold field in Australia are hosted by Siluro-Devonian metasediments and mélange, including carbonaceous shale. They are similar to the veins in the Cape Ray gold deposit although they are not as sulphide-rich and arsenopyrite is the most common sulphide (Peters et al., 1990). Multiple injections of quartz and multiple shear zone movements have produced complex mineralized zones. Quartz veins pinch and swell or occur in pods mixed with gouge within the host shear zones. Gold mineralization accompanied brittle deformation and is interpreted as contemporaneous with regional plutonism which took place late in the evolution of the mélange (Peters et al., 1990).

Exploration guidelines

Based on the results of this study, guidelines are proposed to help define exploration targets. The graphitic sedimentary horizon near the top of the Windsor Point Group has played a key role in localizing strain and allowing gold precipitation. This horizon is easily traced with ground geophysics and further tested by trenching and/or drilling. The Big Pond area is

an example of a gold-bearing zone where the presence of graphitic sediments was also critical. This area is poorly exposed and remains relatively unexplored. Graphitic sediments are present elsewhere in the Windsor Point Group; along the coast, a horizon occurs near the contact with the Cape Ray Igneous Complex, the gold potential of which remains unknown.

Iron-rich sedimentary rocks are present all along the base of the Windsor Point Group near the contact with the Cape Ray Igneous Complex. They represent a good target, as shown at the Isle aux Morts prospect, because of their capacity to destabilize the hydrothermal fluid carrying the metals and induce gold precipitation. As well, untested high magnetic anomalies present to the south-southwest of the known auriferous zones at the Isle aux Morts prospect represent interesting exploration targets (J.P. Thompson, unpublished report for Placer Dome Inc., 1992).

In most cases, oreshoots are geometric resulting from the combination of structural and lithological control. Overall, the oreshoots are steeply plunging east-southeast to south-southeast. The orientation of the known gold bearing structures varies from east-northeast to north-northeast. Near the tectonic boundary between the Windsor Point Group and Grand Bay Complex, the host structures are subparallel to this crustal scale fault zone. As well, at the Isle aux Morts showing strain was localized at the Windsor Point Group-Cape Ray Igneous Complex contact most probably due to competence contrast. Within the Windsor Point Group, however, the structures could be at high angles to the northeast-oriented structural trend as at the Big Pond and Windowglass Hill showings. In the latter, the mineralized veins are associated with north-trending shear zones. Their orientation results from strain partitioning in a highly competent unit in response to horizontal shortening.

The late hydrothermal breccia (D_6) presents analogies from a textural and alteration viewpoint, to epithermal systems and could represent the surface expression of a near-surface hydrothermal system. Further study is needed to test this hypothesis and verify the gold potential of the zone.

Considering the size of the overall system, and the various host rocks and structural settings, the Cape Ray Fault Zone has a good exploration potential for gold. The strong similarities with the giant Ashanti deposit in Ghana demonstrate that graphitic schist-hosted gold deposits have important economic potential. At Cape Ray, however, the superimposed deformation and the state of preservation of the mineralized zones make it more difficult to define orebodies. Smaller deposits along the Cape Ray Fault could be related to the emplacement of the ore zone within the fault system instead of within third order structures oblique to, and up to 5 km away from the main break, as is the case in the Cadillac Break in the Abitibi greenstone belt (Robert, 1990). At Cape Ray, the auriferous zones are within a major fault, and the hydrothermal system and mineralized zones are thus not as well preserved. Consequently, the size of the known mineralized zones at Cape Ray could be due both to the size of the greenstone belt (Windsor Point Group) and to the state of preservation of the system.

Conclusion: tectonic-metallogenic model

The Windowglass Hill showing is a key for definition of the timing and genesis of the mineralization along the Cape Ray Fault Zone. Unlike other mineralized structures in the area, the mineralized zone at the Windowglass Hill showing has been protected from younger superimposed deformation. Wilton (1983a) and Wilton and Strong (1986) proposed a genetic model in which the Windowglass Hill Granite exsolved a base and precous metal-rich vapour phase. The exsolution of this phase raised the internal pressure within the cooling magma and country rocks and hydraulically fractured brittle horizons such as the graphitic schists which offered a structural and possibly a geochemical trap for gold precipitation from the auriferous fluids slightly before this deformation. The mineralization in the Cape Ray area was believed to be Late Devonian, the age of the Windowglass Hill Granite (Wilton and Strong, 1986). For the reasons detailed below, the gold and silver mineralization of the Windowglass Hill showing is unlikely to be genetically related to its granitic host. Textural features of the Windowglass Hill Granite indicate that emplacement took place relatively high in the crust, in a subvolcanic environment, prior to deformation related to the major thrusting event along the Cape Ray Fault Zone. It is unlikely coincidental that the veins are perpendicular to the stretching lineation interpreted as those produced during the thrusting (L_3), strongly suggesting that the mineralization is associated with this deformation. The Windowglass Hill Granite, acting as a rigid body, would have been a preferential site for fracturing and extension, while surrounding Windsor Point Group rocks underwent ductile deformation, accommodating most of the strain. These fractures could have been the site of fluid circulation during the main episode of ductile deformation or during later phases of deformation. The gold mineralizing event in the Cape Ray area is contemporaneous with the development of the ductile fabric produced by motion along the Cape Ray Fault Zone. The syn-S_{3b} emplacement of mineralization at Big Pond supports this conclusion.

The large-scale tectonic setting of the Cape Ray gold mineralization is rather analogous to those of Archean and of many younger gold systems, interpreted as resulting from collision between terranes. Late- to post-peak metamorphic emplacement of gold-bearing quartz vein systems and alkaline magmas along a crustal scale fault system is a direct end-stage and deeper product of the collision (Hodgson and Hamilton, 1989; Kerrich and Wyman, 1990; Kerrich and Feng, 1992; Kerrich and Cassidy, 1994). At Cape Ray, the mineralization is spatially and genetically related to a crustal scale fault zone (Cape Ray Fault Zone) which represents the suture zone between two converging continental blocks: Laurentia and Gondwana (Dubé et al., 1993, 1996). The Cape Ray Fault Zone marks the boundary between high grade deeper crustal rocks of the Port aux Basques gneiss (Gondwana) thrust over lower grade supracrustal rocks of the Windsor Point Group (Laurentia). Following crustal thickening associated with the thrusting event, thermal re-equilibration induced the rise of isotherms through the thickened crust and subcreted rocks (e.g. Fyfe and Kerrich, 1985; Kerrich, 1989a, b) and deep partial melting. This thermal re-equilibration resulted in the production of a hydrothermal fluid, as a result of prograde

devolatilization reactions that are related to the breakdown of hydrous minerals, and of calc-alkaline to alkaline magmas circulating through the large-scale fault system. Fluids released from this breakdown and critical melts produced at the bottom of the crust follow the prevailing pressure gradient and travel upwards (Stuwe et al., 1993). The Cape Ray gold quartz vein system and the emplacement of the late tectonic Strawberry and Isle aux Morts A-type granites are thus most probably the direct end-product of collision along the Cape Ray Fault Zone. Our study indicates that gold mineralization is post-peak metamorphism (415 Ma) whereas the upper time limit is given by the late tectonic Strawberry and Isle aux Morts granites which cut across gold hosting structures. These granites are 30 Ma younger than peak metamorphism. This time interval is similar to the intervals established for the same geological sequences for some important Archean and Phanerozoic gold provinces (compiled by Stuwe et al., 1993). The timing relationships of many greenschist facies metamorphic terranes hosting mesothermal gold deposits show that fluid infiltration and granitoid emplacement are roughly coeval and occur late in the metamorphic history, separated from the metamorphic peak by up to 40 Ma (Stuwe et al., 1993). These authors demonstrated that time intervals up to several tens of millions of years may separate metamorphism from granitoid emplacement at shallow depth and emplacement of gold-bearing quartz veins, such a time gap being the natural consequence of the diachroneity of metamorphism with depth. The K-Ar dating on muscovite associated with the Windowglass Hill and H Brook showings suggests an age indistinguishable from the late tectonic granites. Such time and space relationships between gold mineralization and late-kinematic intrusives are characteristic of mesothermal gold mineralization (Kerrich and Cassidy, 1994). However, structural and metamorphic field relationships do not agree with the mineralization ages as the structure hosting the Cape Ray gold deposit is crosscut by the Isle aux Morts Granite. This may imply that the muscovite ages were reset by the thermal event associated with the emplacement of the late tectonic granites.

Thus, as proposed by Kerrich and Feng (1992), devolatization and anatexis, resulting from tectonic thickening, may continue at deep crustal levels well after peak metamorphism, whereas cooling, uplift, and erosion occur at higher levels. Deposition of gold has been promoted by stratigraphically and structurally controlled fluid-rock interactions. The gold-bearing fluid moving upward along the Cape Ray Fault Zone reacted with chemical traps such as the iron-rich and the graphitic sediments and allowed gold to precipitate. In the latter lithology, carbon activated by the hydrothermal fluids provided a site for fixing the gold in the graphitic schists (Springer, 1985). These reactions have governed the coincidence of structural and geochemical traps. Multiple periods of mineralization are suggested by various settings, several generations of quartz veins, various parageneses and relative timing relationships of mineralization with the deformation history. As observed elsewhere by Hodgson and Hamilton (1989), the relationship of veins to the foliation and lineation, and variations in the intensity of deformation of veins, was a function of the location and orientation of the host structures. They also indicate that gold mineralization was initiated during, but continued after the cessation of, ductile deformation. Because of its rheology the graphitic schist has accommodated much of the strain along the Cape Ray Fault Zone. Similar to observations made elsewhere by Peters (1990, 1993), gold mineralization hosted by graphitic schist at the Cape Ray gold deposit is characterized by complex mineralized and barren quartz pods mixed with gouge and faulted rocks. Furthermore, the graphitic schists were reactivated during younger deformations, adding complexities to the distribution of the mineralized zones.

The quartz breccia veins share characteristics with fault breccias and likely result from hydraulic fracturing. They probably represent implosion breccias (see Sibson, 1986) produced by multiple faulting events of wall rock and existing vein material (Robert et al., 1994). The hydrothermal matrix of these breccias strongly suggests that faulting was an integral part of the mineralizing process (Robert et al., 1994).

The overprinting of thrust-related mylonites by low temperature hydrothermal breccia of epithermal style and cataclasite suggests a progression towards more extensional and brittle deformation with time and telescoping of near surface alteration style. Crosscutting relationships suggest that the normal faulting is post-384 Ma, the age of the brecciated Strawberry Granite. These late structures record declining temperature and pressure possibly due to tectonic unloading in a thick-skinned tectonic system.

REFERENCES

Appiah, H., Norman, D.I., and Boadi, I.
1991: The geology of the Prestea and Ashanti goldfields: a comparative study; in Proceedings of the symposium Brazil Gold'91: the Economics, Geology, Geochemistry and Genesis of Gold Deposits, (ed.) E.A. Ladeira ; A.A. Balkema, Rotterdam, p. 247-255.

Arnold, R.W.
1988: Surface diamond drilling and underground exploration on the Cape Ray project. Unpublished report by Mascot Gold Mines Limited, prepared for Dolphin Explorations Ltd., 65 p.

Barclay, W.A.
1989: Assessment of the structural setting of the Cape Ray Project, Isle aux Morts, Newfoundland; Confidential contractual report for Dolphin Explorations Ltd., 80 p.

Barley, M.E. and Groves, D.I.
1992: Supercontinent cycles and the distribution of metal deposits through time; Geology, v. 20, p. 291-294.

Barker, D.S.
1970: Composition of granophyre, myrmekite and graphic granite; Geological Society of American Bulletin, v. 81, p. 3339-3350.

Barr, S.M. and Raeside, R.P.
1989: Tectono-stratigraphic terranes in Cape Breton Island, Nova Scotia: implications for the configuration of the Northern Appalachian orogen; Geology, v. 17, p. 822-825.

Bergh, S.G. and Karlstrom, K.E.
1992: The Chaparral shear zone: Deformation partitioning and heterogeneous bulk crustal shortening during Proterozoic orogeny in central Arizona; Geological Society of America Bulletin, v. 104, p. 329-345.

Brown, P.A.
1972: The structural and metamorphic history of the Port aux Basques region, Newfoundland; M.Sc. thesis, Department of Geology, Memorial University of Newfoundland, St. John's, Newfoundland, 113 p.

1976: Ophiolites in southwest Newfoundland; Nature, Physical Science, v. 245, no. 140, p. 9-10.

1977: Geology of the Port aux Basques map area (110/11) Newfoundland; Newfoundland Department of Mines, Report 77-2, 11 p.

Buffam, B.S.W.
1948: Moneta Porcupine Mine; in Structural Geology of Canadian Ore Deposits; Canadian Institute of Mining and Metallurgy, Special Volume, p. 457-464.

Burgess, J.L., Brown, M., and van Staal, C.R.
1993: Pressure-temperature conditions and a P-T path for the Port aux Basques area, southwest Newfoundland; in Current Research, Part D; Geological Survey of Canada, Paper 93-1D, p. 47-55.

Cassidy, K.F. and Bennett, J. M.
1993: Gold mineralization at the Lady Bountiful Mine, Western Australia: an example of a granitoid-hosted Archean lode gold deposit; Mineralium Deposita, v. 28, p. 388-408.

Chorlton, L.B.
1980: Grandys Lake, west half; in Current Research, (ed.) C.F. O'Driscoll and R.V. Gibbons; Newfoundland Department of Mines and Energy, Mineral Development Division, Report 80-1, p. 74-78.
1983: Geology of the Grandys Lake area (11O/15), Newfoundland: part I: geology of the southern Long Range Mountains; Newfoundland Department of Mines, Report 83-7, p. 1-116.
1984: Geological development of the southern Long Range Mountains, southwest Newfoundland: a regional synopsis; Ph.D. thesis, Memorial University of Newfoundland, St. John's, Newfoundland, 580 p.

Chorlton, L.B. and Dallmeyer, R.D.
1986: Geochronology of Early to Middle Paleozoic tectonic development in the southwest Newfoundland Gander zone; Journal of Geology, v. 94, p. 67-89.

Chorlton, L.B. and Dingwell, D.B.
1981: Grandys Lake (110-15), Newfoundland; in Current Research, (ed.) C.F. Driscoll and R.V. Gibbons; Newfoundland Department of Mines and Energy, Mineral Development Division, Report 81-1, p. 57-69.

Conolly, H.J.C.
1936: A contour method of revealing some ore structures; Economic Geology, v. 31, p. 259-271.

Cox, S.F., Wall, V.J., Etheridge, M.A., and Potter, T.F.
1991: Deformational and metamorphic processes in the formation of mesothermal vein-hosted gold deposits – examples from the Lachlan Fold Belt in central Victoria, Australia; Ore Geology Reviews, v. 6, p. 391-423.

Currie, K.L. and Piasecki, M.A.J.
1989: Kinematic model for southwestern Newfoundland based upon Silurian sinistral shearing; Geology, v. 17, p. 938-941.

Dawson, J.M.
1991: Report on drilling, trenching and prospecting on the Isle aux Morts River property, Cape Ray district, Newfoundland. Confidential report prepared for Fortune Bay Resources Ltd., 21 p.

Dubé, B.
1990: A preliminary report on contrasting structural styles of gold-only deposits in Western Newfoundland; in Current Research, Part B; Geological Survey of Canada, Paper 90-1B, p. 77-90.

Dubé, B. and Lauzière, K.
1996a: Structural evolution of a major fault zone: the Cape Ray Fault Zone, southwest Newfoundland; Canadian Journal of Earth Sciences, v. 33, no. 2, p. 199-215.
1996b: Geological maps of the Cape Ray Fault, southwest Newfoundland; Geological Survey of Canada, Open File 2963, 4 maps, 1:20 000 scale.

Dubé, B., Dunning, G.R., Lauzière, K., and Roddick, J.C.
1993: The Gondwanan-Laurentian suture: timing of deformation on the Cape Ray Fault, Newfoundland Appalachians; Geological Society of America, Annual meeting, Abstracts with Program, p. A-421.
1996: New insights into the Appalachian orogen from geology and geochronology along the Cape Ray Fault, southwest Newfoundland; Geological Society of America Bulletin, v. 108, no. 1, p. 101-116.

Dubé, B., Guha, J., and Rocheleau, M.
1987: Alteration patterns related to gold mineralization and their relation to CO_2/H_2O ratios; Mineralogy and Petrology, v. 37, p. 267-291.

Dubé, B., Lauzière, K., and Tremblay, A.
1991: Observations on the structural control and tectonic setting of gold mineralization in the Cape Ray Fault Zone, southwestern Newfoundland; in Current Research, Part D; Geological Survey of Canada, Paper 91-1D, p. 135-145.
1992: Structural geology of a crustal scale fault zone: the Cape Ray Fault coastal section, southwestern Newfoundland; in Current Research, Part D; Geological Survey of Canada, Paper 92-1D, p. 199-209.

Dubé, B., Poulsen, K.H., and Guha, J.
1989: The effects of layer anisotropy on auriferous shear zones: the Norbeau mine, Quebec; Economic Geology, v. 84, p. 871-878.

Dunning, G.R., O'Brien, S.J., Colman-Sadd, S.P., Blackwood, R.F., Dickson, W.L., O'Neill, P.P., and Krogh, T.E.
1990: Silurian Orogeny in the Newfoundland Appalachians; Journal of Geology, v. 98, p. 895-913.

Fowler, T.J. and Lennox, P.G.
1992: Low-pressure deformation of a small high-level pluton: the syntectonic Davys Creek Granite from the southeastern Lachlan Fold Belt, N.S.W; Tectonophysics, v. 214, p. 293-309.

Fyfe, W.S. and Kerrich, R.
1985: Fluids and thrusting; Chemical Geology, v. 49, p. 353-362.

Fyon, J.A., Crocket, J.H., and Schwarcz, H.P.
1983: The Carshaw and Malga iron-formation-hosted gold deposits of the Timmins area; in The Geology of Gold in Ontario, (ed.) A.C. Colvine; Ontario Geological Survey, Miscellaneous Paper 110, p. 98-110.

Gillis, J.W.
1972: Geology of the Port-Aux-Basques map area, Newfoundland; Geological Survey of Canada, Paper 71-42, 6 p.

Glasson, M.J. and Keays, R.R.
1978: Gold mobilization during cleavage development in sedimentary rocks from the auriferous slate belt of Central Victoria, Australia: some important boundary conditions; Economic Geology, v. 73, p. 496-511.

Groves, D.I., Phillips, G.N., Falconer, L.J., Houstoun, S.M., Ho, S.E., Browning, P., Dahl, N., and McNaughton, N.J.
1987: Evidence for an epigenetic origin for BIF-hosted gold deposits in greenstone belts of the Yilgarn Block, Western Australia; in Recent advances in understanding Precambrian Gold Deposits, (ed.) S.E. Ho and D.I. Groves; Geology Department and Extension Service, University of Western Australia, Publication 11, p. 167-179.

Hanes, J.A.
1991: K-Ar and $^{40}Ar/^{39}Ar$ geochronology: methods and applications; in Applications of Radiogenic Isotope Systems to Problems in Geology, (ed.) L. Heaman and J.N. Ludden; Mineralogical Association of Canada; v. 19, p. 27-58.

Harland, W.B. and Gayer, R.A.
1972: The artic Caledonides and earlier oceans; Geological Magazine, v. 109, p. 289-314.

Hodgson, C.J. and Hamilton. J.V.
1989: Gold mineralization in the Abitibi greenstone belt: end-stage result of Archean collisional tectonics?; in The Geology of Gold Deposits: The Perspective in 1988; Economic Geology Monograph 6, p. 86-100.

Holdsworth, R.E.
1991: The geology and structure of the Gander-Avalon boundary zone in northeastern Newfoundland; Newfoundland Department of Mines and Energy, Geological Survey Branch, Report 91-1, p. 109-126.

Hunt, P.A. and Roddick, J.C.
1994: A compilation of K-Ar and ^{40}Ar-^{39}Ar ages: Report 24; in Radiogenic Age and Isotopic Studies: Report 8; Geological Survey of Canada, Current Research 1994-F, p. 125-155.
1996: A compilation of K-Ar and ^{40}Ar-^{39}Ar ages: Report 25; in Radiogenic Age and Isotopic Studies: Report 8; Geological Survey of Canada, Current Research 1995-F, p. 57-67.

James, H.L.
1966: Chemistry of iron-rich sedimentary rocks: United States Geological Survey, Professional Paper 440-W, 61 p.

Jones, W.A.
1948: Hollinger Mine; in Structural Geology of Canadian Ore Deposits; Canadian Institute of Mining and Metallurgy, Special Volume, p. 469-481.

Kerrich, R.
1989a: Geodynamic setting and hydraulic regimes: shear zone hosted mesothermal gold deposits; Geological Association of Canada, Short Courses Notes, v. 6, p. 98-128.
1989b: Geodynamic evidence on the sources of fluids and solutes for shear zone hosted mesothermal Au deposits; Geological Association of Canada, Short Courses Notes, v. 6, p. 129-198.

Kerrich, R. and Cassidy, K.F.
1994: Temporal relationships of lode gold mineralization to accretion, magmatism, metamorphism and deformation - Archean to present: a review; Ore Geology Reviews, v. 9, p. 263-310.

Kerrich, R. and Feng, R.
1992: Archean geodynamics and the Abitibi-Pontiac collision: implications for advection of fluids at transpressive collisional boundaries and the origin of giant quartz vein systems; Earth-Science Reviews, v. 32, p. 33-60.

Kerrich, R. and Wyman, D.
1990: Geodynamic setting of mesothermal gold deposits: an association with accretionary tectonic regimes; Geology, v. 18, p. 882-885.

Kirkwood, D. and Dubé, B.
1992: Structural control of sill-hosted gold mineralization: the Stog'er Tight gold deposit, Baie Verte Peninsula, northwestern Newfoundland; in Current Research, Part D; Geological Survey of Canada, Paper 92-1D, p. 211-221.

Lin, S., van Staal, C.R., and Dubé, B.
1994: Promontory-promontory collision and tear faulting in the Canadian Appalachians; Geology, v. 22, p. 897-900.

Lin, S., van Staal, C.R., and Lee, C.
1993: The Harbour le Cou Group and its correlation with the Bay du Nord Group, southwestern Newfoundland; in Current Research, Part D; Geological Survey of Canada, Paper 93-1D, p. 57-64.

Macdonald, A.J.
1983: The iron formation-gold association, Evidence from the Geraldton area; in The Geology of Gold in Ontario, (ed.) A.C. Colvine; Ontario Geological Survey, Miscellaneous Paper 110, p. 75-83.

Marin, R.F.
1982: Quartz and the feldspars; in Short Course in Granitic Pegmatites in Science and Industry, (ed.) P. Cerny; Mineralogical Association of Canada, Short Course Handbook, Volume 8, p. 41-62.

Marshak, S., Wilkerson, M.S., and Hsui, A.T.
1992: Generation of curved fold-thrust belts: Insight from simple physical and analytical models; Thrust Tectonics; (ed.) K.R. McClay; Chapman and Hall, London, p. 83-92.

McDougall, G.J. and Hancock, R.D.
1981: Gold complexes and activated carbon; Gold Bulletin, v. 4, p. 138-153.

McDougall, I. and Harrison, T.M.
1988: Geochronology and thermochronology by the $^{40}Ar/^{39}Ar$ Method; Oxford University Press, Oxford, 272 p.

McKeag, S.A., Craw, D., and Norris, R.J.
1985: Origin and deposition of a graphitic schist-hosted metamorphogenic Au-W deposit, Macraes, East Otego, New Zealand; Mineralium Deposita, v. 24, p. 124-131.

McLeod, J.A.
1988: Microscopic report for Mascot gold mines Ltd on Dolphin Explorations Ltd, Cape Ray Project, Unpublished report, 11p.

Oberthur, T., Saager, R., and Tomschi, H.P.
1990: Geological, mineralogical and geochemical aspects of Archean banded iron-formation-hosted gold deposits: some examples form Southern Africa; Mineralium Deposita, 25[suppl], S125-S135.

Oberthur, T., Vetter, U., Schwartz, M.O., Weiser, Th., Amanor, J., and Gyapong, W.
1991: Gold mineralization at the Ashanti mine, Obuasi, Ghana: preliminary mineralogical and geochemical data; in Proceedings of the Symposium Brazil Gold'91: The Economics, Geology, Geochemistry and Genesis of Gold Deposits, (ed.) E.A. Ladeira; A.A. Balkema, Rotterdam, p. 533-537.

O'Brien, S.J., Wardle, R.J., and King, A.F.
1983: The Avalon Zone: a Pan-African terrane in the Appalachian Orogen of Canada; Geological Journal, v. 8, p. 195-222.

O'Brien, B.H., O'Brien, S.J., Dunning, G.R., and Tucker, R.D.
1993: Episodic reactivation of a Late Precambrian mylonite zone on the Gondwanan margin of the Appalachians, southern Newfoundland; Tectonics, v. 12, no. 4, p. 1043-1055.

Ohmoto, H. and Rye, R.O.
1979: Isotopes of sulfur and carbon; in Geochemistry of Hydrothermal Ore Deposits, (ed.) H.L Barnes; 2nd edition, Wiley-Interscience, p. 509-567.

Owen, J.V.
1992: Comparative petrology of gneissic rocks in southwestern Newfoundland; Canadian Journal of Earth Sciences, v. 29, p. 2663-2676.

Pearce, J.A, Harris, N.B.W., and Tindle, A.G.
1984: Trace element discrimination diagrams for the tectonic interpretation of granitic rocks: Journal of Petrology, v. 25, p. 956-983.

Peters, S., Golding, S.D., and Dowling, K.
1990: Mélange- and sediment-hosted gold-bearing quartz veins, Hodgkinson GoldField, Queensland, Australia; Economic Geology, v. 85, p. 312-327.

Peters, S.G.
1993: Formation of oreshoots in mesothermal gold-quartz vein deposits: examples from Queensland, Australia; Ore Geology Reviews, v. 8, p. 277-301.

Pettijohn, F.S.
1975: Sedimentary rocks; Harper and Row Publ. Inc., 628 p.

Phillips, G.N., Groves, D.I., and Martyn, J.E.
1984: An epigenetic origin for Archean banded iron-formation-hosted gold deposits; Economic Geology, v. 79, p. 162-171.

Phillips, G.N. and Groves, D.I.
1984: Fluid access and fluid-wall rock interaction in the genesis of the Archean gold-quartz vein deposit at Hunt Mine, Kambalda, Western Australia; in Gold'82: The Geology, Geochemistry and Genesis of Gold Deposits, (ed.) R.P. Foster; Proceedings of the symposium Gold'82, University of Zimbabwe, Special Publication 1, p. 389-416.

Poulsen, K.H.
1996: Lode gold; in Geology of Canadian Mineral Deposit Types, (ed.) O.R. Eckstrand, W.D. Sinclair, and R.I. Thorpe; Geological Survey of Canada, Geology of Canada, No. 8, p. 323-328. (*Also* Geological Society of America, The Geology of North America, v. P-1).

Ramezani, J.
1993: The geology, geochemistry and U-Pb geochronology of the Stog'er Tight gold prospect, Baie Verte, Newfoundland; M.Sc thesis, Memorial University of Newfoundland, St. John's, Newfoundland, 312 p.

Robert, F.
1990: Structural setting and control of gold-quartz veins in the Val d'Or area, southeastern Abitibi Subprovince; in Gold and Base Metal Mineralisation in the Abitibi Subprovince, Canada, with Emphasis on the Quebec Segment, compiled by S.E. Ho, F. Robert, and D.I Groves; University of Western Australia, Pubication 24, p. 164-209.

Robert, F., Poulsen, K.H., and Dubé, B.
1994: Structural analyses of lode gold deposits in deformed terranes; Geological Survey of Canada, Open File 2850, 140 p.

Roberts, R.G.
1987: Ore deposit models #11. Archean lode gold deposits; Geoscience Canada, v. 14, no. 1, p. 37-52.

Roddick, J.C.
1983: High precision intercalibration of ^{40}Ar-^{39}Ar standards; Geochimica et Cosmochimica Acta, v. 47, p. 887-898.

Roddick, J.C. (cont.)
1990: $^{40}Ar/^{39}Ar$ evidence for the age of the New Quebec Crater, northern Quebec; in Radiogenic Age and Isotopic Studies, Report 3; Geological Survey of Canada, Paper 89-2, p. 7-16.

Roddick, J.C. and Souther, J.G.
1987: Geochronology of Neogene volcanic rocks in the northern Garibaldi Belt, B.C.; in Radiogenic Age and Isotopic Studies: Report 1; Geological Survey of Canada, Paper 87-2, p. 25-32.

Romberger, S.B.
1986: The solution chemistry of gold applied to the origin of hydrothermal deposits; in Gold in the Western Shield, (ed.) L.A. Clark and D.R. Francis; Canadian Institute of Mining and Metallurgy, Special Volume 38, p. 168-186.

Samson, S.D. and Alexander, E.C. Jr.
1987: Calibration of the interlaboratory ^{40}Ar-^{39}Ar dating standard, MMhb-1; Chemical Geology (Isot. Geosc. Sec.), v. 66, p. 27-34.

Shelton, K.L., So, C.-S., and Chang, J.-S.
1988: Gold-rich mesothermal vein deposits of the Republic of Korea: geochemical studies of the Jungwon Gold area; Economic Geology, v. 83, p. 1221-1237.

Sibson, R.H.
1986: Brecciation processes in fault rocks: inferences from earthquake rupturing; PAGEOPH, v. 124, p. 159-175.

Siegel, E.A. and Soto, A.M.
1984: Microscopic observations on adsorption of metallic gold on activated carbon; Institution of Mining and Metallurgy, Transactions Section C: Mineral Processing and Extractive Metallurgy, v. 93, p. C90-C92.

Sillitoe, R.H.
1985: Ore-related breccias in volcanoplutonic arcs; Economic Geology, v. 80, no. 6, p. 1467-1514.

Simpson, D.R.
1962: Graphic granite form the Ramona pegmatite district, California; American Mineralogist; v. 47, p. 1123-1138.

So, C-S., Chi S-J, and Choi, S-H.
1988: Geochemical studies on Au-Ag hydrothermal vein deposits, Republic of Korea: Jinan-Jeongeup mineralized area, Japanese Association of Mineralogists, Petrologists and Economic Geologists, v. 83, p. 449-471.

Springer, J. S.
1985: Carbon in Archean rocks of the Abitibi belt (Ontario-Quebec) and its relation to gold distribution; Canadian Journal of Earth Sciences, v. 22, p. 1945-1951.
1986: Gold in carbon-rich rocks: improbable protores; in Gold in the Western Shield, (ed.) L.A. Clark and D.R. Francis; Canadian Institute of Mining and Metallurgy, Special Volume 38, p. 104-112.

Steiger, R.H. and Jäger, E.
1977: Subcommission on Geochronology: convention on the use of decay constants in Geo- and Cosmo-chronology; Earth and Planetary Science Letters, v. 36, p. 359-362.

Stuwe, K., Will, T.M., and Zhou, S.
1993: On the timing relationship between fluid production and metamorphism piles: some implications for the origin of post-metamorphic gold mineralization; Earth and Planetary Science Letters, v. 114, p. 471-430.

Thompson, J.P.
1992: Report on geology, geochemistry, geophysics and diamond drilling programs on the One island Pond property, licence 4220, and Isle aux Morts property, licences 3360 and 4052, southwest Newfoundland, NTS 110/15. Confidential report prepared for Placer Dome Inc. Volume 1, 35 p.

Treagus, S.H.
1983: A theory of finite strain variation through contrasting layers and its bearing on cleavage refraction; Journal of Structural Geology, v. 5, p. 351-368.
1988: Strain refraction in layered systems; Journal of Structural Geology, v. 3, p. 517-527.

Trendall, A.F. and Morris, R.C. (ed.)
1983: Iron Formation: Facts and Problems; Elsevier, Amsterdam, 558 p.

Tuach, J.
1986: Metallogeny of Newfoundland granites-studies in the Western White Bay area and on the southwest coast; in Current Research; Newfoundland Department of Mines and Energy, Report 86-1, p. 27-38.

Tuach, J. Dean, P.J., Swinden, H.S., O'Driscoll, C.F., Kean, B.F., and Evans, D.T.W.
1988: Gold mineralization in Newfoundland: A 1988 review; in Current Research; Newfoundland Department of Mines and Energy, Report 88-1, p. 279-306.

van Staal, C.R. and de Roo, J.A.
In press: Mid-Paleozoic tectonic evolution of the Appalachian Central Mobile Belt in Northern New Brunswick, Canada: Collision, extensional collapse and dextral transpression; in New Perspectives in the Appalachian-Caledonian Orogen; Nuna Conference, Canadian Journal of Earth Sciences, Special Volume.

van Staal, C.R., Winchester, J.A., Brown, M., and Burgess, J.L.
1992a: A reconnaissance geotraverse through southwestern Newfoundland; in Current Research, Part D; Geological Survey of Canada, Paper 92-1D, p. 133-143.

van Staal, C.R., Burgess, J.L., Hall, L., Lee, C., Lin, S., and Schofield, D.
1992b: Geology of the Port aux Basques-Rose Blanche Area (NTS 110/10 and 110/11); Report of Activities, Geological Survey Branch, Government of Newfoundland and Labrador, p. 41-43.

van Staal, C., Dunning, G.R., Valverde, P., Burgess, J., and Brown, M.
1994: Arenig and younger evolution of the Gander margin: a comparison of the New Brunswick and Newfoundland segments; in New perspectives in the Appalachian-Caledonian orogen; Geological Association of Canada-Nuna Conference, Program with Abstracts, p. 28-29

Williams, H.
1979: Appalachian Orogen in Canada; Canadian Journal of Earth Sciences, v. 16, p. 792-807.

Williams, H. and Hatcher, R.D., Jr.
1983: Appalachian suspect terranes; in Contribution to the Tectonics of Moutain Chains, (ed.) R.D. Hatcher, Jr., H. Williams, and I. Leitz; Geological Society of Ameria, Memoir 158, p. 33-53.

Williams, H., Kennedy, M.J., and Neale, E.R.W.
1970: The Hermitage Flexure, the Cabot Fault, and the disappearance of the Newfoundland Central Mobile Belt; Geological Society of America Bulletin, v. 81, p. 1563-1568.

Williams, H., Colman-Sadd, S.P., and Swinden, H.S.
1988: Tectonic-stratigraphic subdivisions of central Newfoundland; in Current Research, Part B; Geological Survey of Canada, Paper 88-1B, p. 91-98.

Williams, S.H., Boyce, W.D., and Colman-Sadd, S.P.
1992: A new Lower Ordovician (Arenig) faunule from the Coy Pond Complex, central Newfoundland, and a refined understanding of the closure of the Iapetus Ocean; Canadian Journal of Earth Sciences, v. 29, p. 2046-2057.

Wilson, G.C. and Rucklidge, J.C.
1987: Mineralogy and microstructures of carbonaceous gold ores; Mineralogy and Petrology, v. 36, p. 219-239.

Wilton, D.H.C.
1983a: Metallogenic, tectonic and geochemical evolution of the Cape Ray Fault Zone, with emphasis on electrum mineralization; Ph.D. thesis, Memorial University, St. John's, Newfoundland, 618 p.
1983b: The geology and structural history of the Cape Ray Fault Zone in southwestern Newfoundland; Canadian Journal of Earth Sciences, v. 20, p. 1119-1133.
1984: The origin of ore metals and hydrothermal fluids in the Cape Ray gold deposits, Newfoundland, Canada; in Gold'82: The Geology, Geochemistry and Genesis of Gold Deposits, (ed.) R.P. Foster; Proceedings of the symposium Gold'82, University of Zimbabwe, May 1982, p. 507-519.
1985: Tectonic evolution of southwestern Newfoundland as indicated by granitoid petrogenesis; Canadian Journal of Earth Sciences, v. 22, p. 1080-1092.

Wilton, D.H.C. and Strong, D.F.
1986: Granite-related gold mineralization in the Cape Ray Fault Zone of southwestern Newfoundland; Economic Geology, v. 81, p. 281-295.

APPENDIX

Procedures in the Geochronology Laboratories of the Geological Survey of Canada

"...Potassium, for conventinal analyses, was analyzed by atomic absorption spectrometry on duplicate dissolutions of the samples. Conventional argon extractions were carried out using a radio frequency vacuum furnace with a multi-sample loading system capable of holding six samples. The extraction system is on-line to a modified A.E.I. MS-10 with a 0.18 tesla permanent magnet. An atmospheric Ar aliquot system is also incorporated to provide routine monitoring of mass spectrometer mass discrimination. Details of computer acquisition and processing of data are given in Roddick and Souther (1987). Decay constants recommended by Steiger and Jäger (1977) are used in the age calculations and errors are quoted at the 2 sigma level.

^{40}Ar-^{39}Ar Analyses

"In the ^{40}Ar-^{39}Ar step heating technique, the sample is irradiated in a nuclear reactor to convert some K atoms to ^{39}Ar. The ^{39}Ar is used as a measure of the K in the sample and a sample's age is determined by the measurement of the ^{40}Ar-^{39}Ar isotopic ratio (corrected for interfering isotopes and atmospheric Ar). By step-wise heating of a sample in a vacuum furnace ages can be calculated for Ar fractions released at incrementally higher temperatures. In general, ages determined from the higher temperature steps represent Ar released from more retentive sites in a mineral. For further analytical details see Roddick (1990) and for an explanation of the principles of the technique see McDougall and Harrison (1988) or Hanes (1991).

"The analyses reported consist of three heating steps, with the temperature of the first step selected to liberate most of the atmospheric argon but a minimum of the radiogenic argon from the sample. This step contains very little radiogenic Ar and usually is not reported. The next temperature step is selected to release about 50% of the radiogenic argon from the sample. A final fusion step releases any remaining Ar. The analyses are therefore essentially two age measurements and permit a comparative test of the consistency of the ages of argon released from a sample. If the ages of the two fractions are in agreement, it is assumed that a reliable age can be assigned to the sample. Should the ages differ then it is likely that there has been a disturbance to the K-Ar system in the sample.

"The results are presented in a format similar to the K-Ar reports but with an additional section detailing the ages of the steps and the preferred age of the sample. The first age given represents the weighted mean age of all three gas fractions, weighted and summed according to the amounts of ^{39}Ar in each fraction, and is indicated as an integrated age with 2 uncertainty limits. The error limit on the age includes uncertainty in irradiation calibration of the amount of K converted to ^{39}Ar (J factor, typically ± 0.5 - 1.0% 2σ) which must be considered when comparing the ages of different samples. The integrated age is equivalent to a conventional K-Ar age and, in samples that are not subject to recoil Ar loss (see McDougall and Harrison, 1988), is the age which would be determined by that technique. The percent atmospheric argon in the sample is given for this integrated age. The ages of the last two steps are given separately, along with their 2σ uncertainties and proportions of sample argon, as percentages of ^{39}Ar, in the fractions. The uncertainties of these ages do not include irradiation calibration error since it does not contribute to uncertainties between heating steps on a single sample. If these two ages agree within their error limits the preferred age is a weighted mean of these fractions weighted by the amounts of ^{39}Ar in the fractions. The error estimate for this age also includes uncertainty in the irradiation calibration. This is termed the plateau age. If these two ages do not agree then one of the steps may be designated as the preferred age. In many cases of known complex geological history the age of highest temperature gas fraction may be the best estimate of the age as the lower temperature release may record a partial ^{40}Ar loss induced by the most recent geological reheating of the sample. In some cases excess argon is present in the initial Ar released and in this case the highest temperature step is also the best estimate of the age of a sample.

"The potassium concentration of the sample is also given. This is determined from calibration of the mass spectrometer as a precise manometer, the conversion factor for ^{39}Ar production, and the weight of the sample. The precision of this K concentration is one to four per cent and is limited mainly by errors associated with weighing of the small (4 to 30 mg) samples used for analyses."

(from Hunt and Roddich, 1994, p. 126